Design and Development of Biocompatible Silk Fibroin Coatings for Breast Implant Applications

by

Emmanuel Joseph

AcSIR Enrollment No: 20EE16A26034

A thesis submitted to the

Academy of Scientific & Innovative Research

for the award of the degree of

DOCTOR OF PHILOSOPHY

in

ENGINEERING

Under the supervison of

Dr. Anuya Nisal

CSIR - National Chemical Laboratory, Pune

Academy of Scientific and Innovative Research

AcSIR Headquarters,CSIR-HRDC campus

Sector 19, Kamla Nehru Nagar,

Ghaziabad, U.P.–201 002, India

December 2021

DEDICATION

TO MY FAMILY
and the beautiful souls around me

Certificate

This is to certify that the work incorporated in this Ph.D. thesis entitled, *" Design and Development of Biocompatible Silk Fibroin Coatings for Breast Implant Applications"*, submitted by *Emmanuel Joseph* to the Academy of Scientific and Innovative Research (AcSIR) in fulfillment of the requirements for the award of the Degree of *DOCTOR OF PHILOSOPHY in ENGINEERING*, embodies original research work carried-out by the student. We, further certify that this work has not been submitted to any other University or Institution in part or full for the award of any degree or diploma. Research material(s) obtained from other source(s) and used in this research work has/have been duly acknowledged in the thesis. Image(s), illustration(s), figure(s), table(s) etc., used in the thesis from other source(s), have also been duly cited and acknowledged.

Emmanuel Joseph

(Signature with Date)

Dr. Anuya Nisal

(Signature with Date)

Statements Of Academic Integrity

I Emmanuel Joseph, a Ph.D. student of the Academy of Scientific and Innovative Research (AcSIR) with Registration No. 20EE16A26034 hereby undertake that, the thesis entitled "Design and Development of Biocompatible Silk Fibroin Coatings for Breast Implant Applications" has been prepared by me and that the document reports original work carried out by me and is free of any plagiarism in compliance with the UGC Regulations on "*Promotion of Academic Integrity and Prevention of Plagiarism in Higher Educational Institutions (2018)*" and the CSIR Guidelines for "*Ethics in Research and in Governance (2020)*".

Signature of the Student

Name: Emmanuel Joseph

Date:

Place: Pune

It is hereby certified that the work done by the student, under my/our supervision, is plagiarism-free in accordance with the UGC Regulations on "*Promotion of Academic Integrity and Prevention of Plagiarism in Higher Educational Institutions (2018)*" and the CSIR Guidelines for "*Ethics in Research and in Governance (2020)*".

Signature of the Supervisor

Name: Dr. Anuya Nisal

Date:

Place: Pune

Acknowledgements

It is my extreme pleasure to be acknowledging the contributions of some wonderful people to my PhD journey without whom the time spent at CSIR-NCL would be extremely bad. Often the key moments which bring out some key insights and help you move forward during a PhD are spent on brainstorming with your mentors, friends, colleagues and sometimes with family as well. I also went through a similar journey. Although I must confess my journey was a little less stressful, thanks to those wonderful people around me in achieving my degree.

First and foremost, I would like to thank the Almighty God for without his graces and blessings, this path would not be possible. To Jesus Christ for giving the wisdom, strength, support and knowledge in exploring things.

I would like to extend my sincerest gratitude to all my secondary and higher secondary school teachers for laying a strong foundation for me to be a good student in life. Without that foundation, I may not have chosen this path. I extend my gratitude to my higher secondary teacher, especially Celin teacher, Jaison sir, Sunil sir and also my B. Tech tutors helped me to choose research as a career.

I am forever indebted to my supervisor Dr. Anuya Nisal, for all her help, support and guidance with supervision at both professional and personal levels. Her way of mentoring has clearly helped me become more independent and confident in taking decisions, writing quality research papers and approaching a problem. The time spent with her for discussions for my work, over group meetings and other discussions, were truly the most intellectually enriching times of my PhD.

I would like to thank Dr Ashish Lele, Dr S. Chandrashekar, and Prof. Ashwini Nangia, (Current and Previous) Director, CSIR-National Chemical Laboratory for extending all

iv

students to expand their horizons beyond their routine PhD work. I thank my dynamic NCL-TEC team Dr. Aniket, Dr. Pravin, Dr Indravadan, Dr Vishwanath, Dr Ramendra, Vikash, Sheena, and Meenakshi for volunteering and conducting so many events together. Organizing the events together definitely made learning so much fun and improvements to the professional life. I would also like to thank Dr. Magesh Nandagopal for his support to NCL-TEC and to me . I would always keep the lessons learned from his professional development workshop while navigating my workspace in my career. I will always remain grateful to the efforts that Dr. Premnath, Dr. Guruswamy and Dr. Magesh had put for the betterment of the students at NCL. I was lucky to be associated with all of them. I thank them for their support and encouragement to NCL-TEC and the student community at NCL.

Lastly and most importantly, I am grateful to the family and friends which has motivated me to improve myself along this journey. I also thank my parents and wife Littymol Tomy for their love and affection. Also, they helped me in all the ups and downs with a strong inspiration. I am forever thankful to my mom for her guidance and motivation in all the steps I have taken in my life.

Emmanuel Joseph

Date:

Synopsis

Introduction and Statement of Problem

Breast cancer globally accounts for about 23% among all cancers[1]. Radiation and systemic therapies have been a conventional treatment methods. However, over last two decades, surgical procedures have also been significantly improved and have enhanced especially the cosmetic result for patients after breast cancer surgery[1]. This includes all types of breast surgery such as immediate breast reconstruction surgery (IBRS), lumpectomy and skin-sparing mastectomy. An important component of this surgery includes the use of a silicone breast implant.

A polydimethylsiloxane (PDMS) or silicone breast implant is frequently used in the breast surgery to reconstruct the shape and size of the breast. However, the safety of silicone based implantable medical devices has been a challenge since their introduction. The common clinical problems associated with silicone implants are autoimmune diseases, capsular contracture, biofilm formation, allergic reaction and recently there is also a presence of a rare type of cancer associated with patients implanted with silicone breast implants[2]. The primary reason for implant failure was due to poor biocompatibility of implant material, which results in a foreign body reaction. Another hypothesis suggests that the presence of bacteria results in the formation of a bacterial biofilm onto the implant surface and causes failure of the implants[3], [4].

This thesis is focused on development of material strategies to modify the surface of silicone implants so as to mitigate the risk of failure of these implants. Coating the surface of biomedical implants is a promising strategy to reduce the failure rate of implants[5]. In this

work, we propose to coat the surface of silicone implant using a biocompatible polymer silk fibroin (SF)[6]. SF is a protein polymer extracted from the cocoons of silkworm Bombyx mori. SF has excellent thermo-mechanical properties and it can be processed using environment friendly processing protocols. However, adhesion between the coating material and soft flexible substrates such as silicones is poorly understood[7]. Further, delamination and cracking/crazing of implant coatings is a problem. It is also desirable to functionalise these coatings with appropriate drug molecules and functional biomolecules that will reduce the risk of failure[6].

Objectives

The objectives of the work presented in the thesis are outlined in this section. This thesis is focused on the materials science aspect for development of mechanically robust coatings on silicone polymers using a natural biocompatible polymer like silk fibroin. Accordingly, there are three objectives for this work:

- Development of test methods to quantify the adhesion of SF coatings on PDMS and study their failure under mechanical loading

- Develop a process to successfully form a functional coating of SF on PDMS such that the coating has enhanced cracking and delamination resistance

- To develop novel blends of silk fibroin with other suitable polymers/ biomolecules that further improve performance of coatings

The activities as part of each objective have been defined below.

Methodology

1) Development of test methods to quantify the adhesion of SF coatings on PDMS and study their failure under mechanical loading

- Surface modification of PDMS to improve the hydrophilicity using different physical and chemical methods

- Development of SF coatings on surface activated PDMS substrates

- Evaluation of adhesion between the coating material and modified PDMS

2) Develop a process to successfully form a functional coating of SF on PDMS such that the coating has enhanced cracking and delamination resistance

- Development of a crack-resistant SF coating on surface activated PDMS

- Evaluation of mechanical stability of SF coatings

- Development of functional SF coatings with a novel anti-quorum sensing molecule

- Biological evaluation of SF coatings in preventing biofilm formation

3) To develop novel blends of silk fibroin with other suitable polymers/ biomolecules that further improve performance of coatings

- Development of hydrophilic SF coatings on PDMS upon blending with a model molecule such as PEO of different molecular weight and recombinant elastin

- Evaluation of mechanical stability of SF blend coatings on PDMS

- Biological evaluation of hydrophilic SF ELP blend coatings and comparison of properties with SF PEO blends

Summary

The work presented on SF coatings on PDMS in this thesis is experimental investigations to mitigate the risk of implant failure on breast implants. The summary and key conclusions of each of the objectives and the work done are summarized below:

Scheme-1: Development of test methods to quantify the adhesion of coating material and PDMS

In this work, we have measured the performance of nano-coatings of biocompatible protein polymer Silk Fibroin (SF) on pristine as well as modified PDMS surfaces. The PDMS surfaces have been modified using oxygen plasma treatment and 3-amino-propyl-triethoxy-silane (APTES) treatment. Interestingly, testing of the coated samples using a bulk technique such as tensile and bending deformation showed that the SF nano-coating exhibits improved crack resistance when the PDMS surface has been modified using APTES treatment as compared

to an oxygen plasma treatment. These results were validated at the microscopic and meso-scopic length scales through nano-scratch and nano-indentation measurements. Further, we developed a unique method using modified Atomic Force Microscopy to measure adhesive energy between treated PDMS surfaces and SF molecules. These measurements indicated that the adhesive strength of SF to APTES treated PDMS is 10 times more compared to oxygen plasma treated PDMS due to higher number of molecular linkages formed in this nano-scale contact. The Force Spectroscopy measurements also identified breaking of these discrete molecular bonds formed between the amine groups on APTES-PDMS and the SF molecules. Thus, APTES modification to PDMS substrate provides a higher number of interaction sites for a protein polymer like SF and results in improved adhesion of nano-coating to the substrate. This improved adhesion enhances the delamination and crack resistance of the nano-coatings.

Scheme-2: Development of crack-resistant SF coatings on PDMS

In this work, a novel process that results in the formation of a coating that is stable under mechanical stresses in tensile, torsion and bending modes. The coating process involves a combination of two conventional coating processes – namely dip coating and electro-spinning. The coating was also further functionalized using a green biomolecule - glycomonoterpene prepared using citronellal and glucose. These functional compounds are being touted as the next generation antibiofilm molecules on account of quorum sensing inhibitory activity. We have demonstrated that the quorum quenching activity of the biomolecule is retained during the processing steps and the coatings exhibited excellent antibiofilm activity against

common infection causing bacterium P. aeruginosa and S. epidermidis. These silk fibroin-glycomonoterpene coatings can be used for implants in biomedical applications such as breast implants and catheter tubings.

Scheme-3:To develop novel blends of silk fibroin with other suitable polymers/ biomolecules that further improve performance of coatings

3A: Blending of a hydrophilic polymer – polyethylene oxide

In this work, we report functional coatings of silk fibroin and its blends with biopolymers and the effect of molecular weight of PEO on mechanical properties and aqueous stability of SF/PEO blend coatings on PDMS surface. The formation of SF/PEO blend coatings on PDMS surface was confirmed using FTIR spectroscopy. This spectroscopic data was correlated with the aqueous stability of these coatings. Further, it was also interesting to note that PEO molecular weight played a significant role in not only aqueous stability of the coatings, but also in mechanical stability. Blending of PEO at 25% and 50% with SF resulted in the formation of crack resistant coatings on PDMS surface. The coatings were tested for stability under mechanical deformation in different modes of strain such as bending and tensile. SF/PEO blends showed a higher surface wettability as compared to SF coatings on PDMS surface, which was characterized using water contact angle. Hydrophilic contact angle of SF blend coatings reduces the non-specific adsorption of proteins, which results in improved biocompatibility of the coatings. Also, we are developing hydrophilic recombinant proteins to blend with silk fibroin to improve the crack resistant properties and
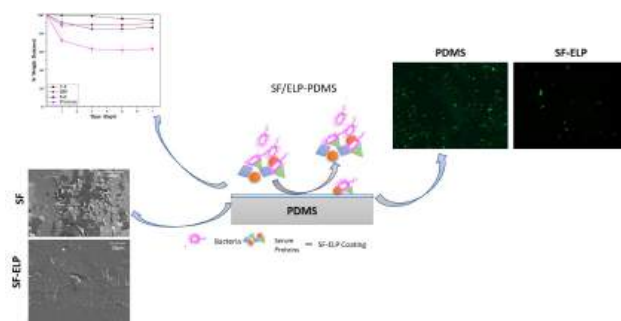
biocompatibility of blend coatings on biomedical implants.

Scheme 3B: Development of SF- recombinant elastin protein blend coatings on PDMS

This work is focused on the development of hydrophilic SF coatings upon blending with a novel polymers such as recombinantly produced elastin-like peptide (ELP), a class of polypeptide obtained from the primary sequence of mammalian elastin with a repeat unit of (GVGVP). The SF-ELP coatings were characterized for their physio-chemical and mechanical properties and their properties were compared with a selected molecular weight of PEO used for blending. The mechanical stability of SF-ELP blends shows more stable coatings than SF- PEO blends. This is due to the high elasticity of ELP molecules. The biological evaluation of these SF blends was performed by doing protein adsorption, accelerated degradation and cytotoxicity studies. The modified PDMS with SF, SF-PEO and SF-ELP coatings reduced Bovine Serum Albumin adsorption to 65%, 94% and 84%, respectively. Similarly, the Fibrinogen adsorption reduction on SF, SF-PEO and SF-ELP shows 47%, 80% and 82%, respectively. The actin staining and cell proliferation studies show that SF and SF blends have more spread morphology than PDMS, confirming the non-cytotoxicity of the coatings.

Future directions

The thesis focused on the material science aspect to mitigate the risk of implant failure. The biological studies performed using mouse fibroblast cell line with L929 cell line to evaluate the in-vitro cytotoxicity of the SF and SF blend coatings are a bare minimum. Advanced *in-vitro* studies of the coatings using various cell lines such as breast fibroblasts, breast

adipocytes and breast cancer cell lines is required to support the safety and biocompatibility data of implant coating. Further, the coated implants must also be studied for their non-immuogenic potential using advanced *in-vitro* techiniques. The biocompatibility evaluation of SF and SF blends coatings in the *in-vivo* studies using porcine models by implanting in the sub- mammary pockets of porcine for 13 weeks must be also completed. In this thesis, SF and SF blend coatings were prepared on either circular disc or rectangular block of PDMS by dip coating process to reduce implant failure. It would be more relevant to develop coatings on commercial implants and characterize their mechanical and biological performance, before taking these implants for clinical studies.

Publications

1. **Emmanuel Joseph**, Amrita Patil, Swarali Hirlekar,Abhijit Shete, Nimisha Parekh, Asmita Prabhune*, and Anuya Nisal*; Glycomonoterpene-Functionalized Crack- Resistant Biocompatible Silk Fibroin Coatings for Biomedical Implants, ACS Appl. Bio Mater 2019, 2, 2, 675–684.

2. Leena Thorat , **Emmanuel Joseph**, Anuya Nisal, Ekta Shukla, Ameeta Ravikumar, Bimalendu B. Nath ; Structural and physical analysis of underwater silk from housing nest composites of a tropical chironomid midge, International Journal of Biological Macromolecules 163 (2020) 934–942 (**Shared First Author**)

3. **Emmanuel Joseph**, Shatruhan Singh Rajput, Shivprasad Patil, Anuya Nisal*; Mechanism of adhesion of natural polymer coatings on chemically modified siloxane polymer, Langmuir 2021, 37, 9, 2974–2984

Contents

List of Figures

LIST OF ABBREVATIONS

AFM   Atomic Force Microscopy

ALCL   Anaplastic Large Cell Lymphoma

APTES   3-amino-propyl-triethoxy-silane

APTES-PDMS APTES Treated PDMS

ASTM   American Society for Testing and Materials

ATR-FTIR   Attenuated Total Reflection - Fourier Transform Infrared Spectroscopy

BIA-ALCL   breast implant associated anaplastic large cell lymphoma

DMEM   Dulbecco's Modified Eagle Medium

ELP   Elastin-like Peptide

FBGC   Foreign Body Giant Cells

FBR   Foreign Body Reaction

FBS   Fetal bovine serum

FDA   Food and Drug Administration

FTIR   Fourier Transform Infrared Spectroscopy

HFIP   Hexafluoroisopropanol

IBRS   Immediate Breast Reconstruction Surgery

IPA   Isopropyl Alcohol

ISO   International Organization for Standardization

KOH   Pottasium Hydroxide

Lc1	First Critical Load
Lc2	Second Critical Load
LiBr	Lithium Bromide
MAPLE	Matrix-Assisted Pulsed Laser Evaporation
MPC	2-Methacryloyloxyethyl phosphorylcholine
MRSA	Methicillin-resistant S. aureus
MTT	3-(4, 5-dimethylthiazol-2-yl)-2, 5-diphenyltetrazolium bromide
$NaHCO_3$	Sodium Bicarbonate
O_2-PDMS	Oxygen Plasma Treated PDMS
PBS	Phosphate Buffer Saline
PDMS	Polydimethylsiloxane
PEG	Polyethylene Glycol
PEO	Polyethylene Oxide
PMPC	Poly Methacryloxyethyl Phosphorylcholine
PU	Polyurethane
QSI	Quorum Sensing Inhibiting Molecules
RF	Radio Frequency
rpm	Rotations per minute
RTV	Room Temperature Vulcanized
SEM	Scanning Electron Microscopy
SF	Silk Fibroin
SF-APTES-PDMS	Silk Fibroin coated on APTES treated PDMS
SF-D	Silk Fibroin Dip coated PDMS
SF-DES	Silk Fibroin Dip and Electrospun PDMS
SF-O2-PDMS	Silk Fibroin coated on oxygen plasma treated PDMS
SFGC-DES	Silk Fibroin - G-Citron - Dip and Electrospun PDMS

SMA	Surface Modifying Addictive Amphiphiles
TDA	Toluenediamines
Tris-HCL	Tris(hydroxymethyl)aminomethane - Hydrochloric acid
US	United States
UVO	UV/ Ozone treatment
XPS	X-ray Photon Spectroscopy

List of Tables

Chapter 1

Introduction

Globally, breast cancer accounts for about 24.9% of all cancers in women, with more than 2.2 million new cases in 2020[8]. Similar trends are also seen in India, as shown in Figure 1.1. Radiation, surgical procedures and systemic therapies have been conventional treatment methods. Also, over the last two decades, surgical procedures have significantly improved and have enhanced, especially the cosmetic result for patients after breast cancer surgery. The breast reconstructive surgeries have been increasing every year with a 4-6% increase in primary reconstructive surgeries and a 6% increase in the revision surgeries across the US (Obtained from ASPS 2018 Annual Report). This includes all types of breast surgery, such as immediate breast reconstruction surgery (IBRS), lumpectomy and skin-sparing mastectomy. In lumpectomy, tumour cells and surrounding breast tissue are removed. In mastectomy, complete removal of breast tissue occurs. These surgical procedures results in the formation of a cavity. Prosthetics and tissue expanders are used to adjust the shape and size of breast tissue. Silicone based prosthesis have been used in the IBRS surgical procedures since these implants can be manufactured in a broad range of shapes, sizes, profiles and textures.

The breast implant consists of a soft silicone outer shell having flexibility. The inner gel consists of saline solution or silicone gel to recreate the aesthetic feel of natural breast tissue for the patients. However, the studies conducted on patients post implantation show a failure rate of 15-20%[9].
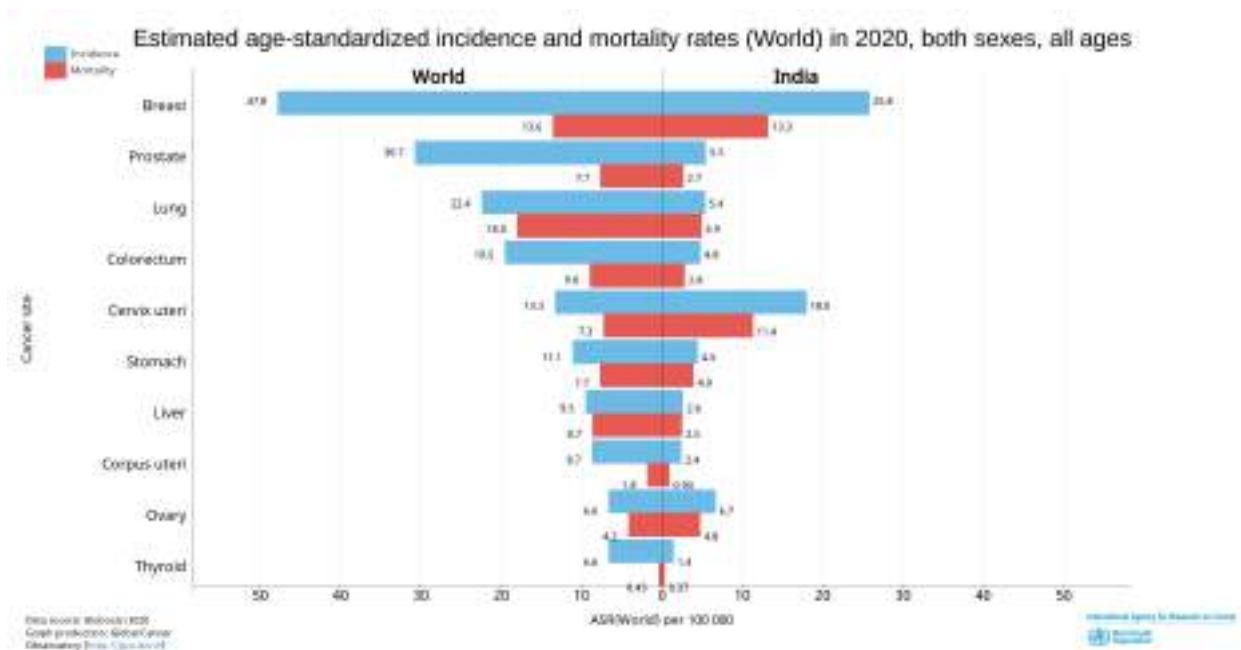
Figure 1.1: Estimated age-standardized incidence and mortality rates (World) in 2020, both sexes, all ages[10]

1.1 Silicone implant-based breast reconstruction surgeries

The most common problems associated with a breast implant are capsular contracture and biofilm formation around the implant. Capsular contracture is the abnormal formation of the fibrous scar tissue around the implant, causing pain, firmness, asymmetry and distortion. The extent of capsular contracture is classified as per the Baker grade I-IV, where Grade IV indicates the removal of breast implants due to severe pain and firmness of the patients. Capsular contracture may be triggered due to foreign body reaction, as discussed in the Section 1.1.1. Bacterial biofilm formation has also been associated with failure of breast implant (Section 1.1.2).

1.1.1 Foreign body reaction

The exact mechanism of host tissue response on silicone breast implants is poorly understood. The interaction of body fluids with silicone implants initiates foreign body reactions. Foreign body reaction consists of foreign body giant cells (FBGCs) and granulation tissue. The FBR starts with blood-biomaterial interaction followed by provisional matrix forma-

tion and acute inflammation. It is hypothetisized that irreversible and non-specific protein adsorption on the implant surface triggers the failure of breast implants. The extent of protein adsorption depends on a range of factors such as surface chemistry, surface topography, surface wettability and charge on the surface. Thus, altering the surface properties of silicone implants is a promising strategy to reduce the immune response, thereby reducing the failure of the implants. Researchers have been modifying the implant surface using various methods to improve the biocompatibility, such as micro or nanotexturing of implants outer shell surface, anti-adhesive modification, plasma-assisted surface modification and surface modification using anti-fibrosis drugs[5]. The surface roughness of the outer shell surface typically ranges from 10-100 μm after micro/nanotexturing. However, clinical trials show that surface textured implants cause a rare type of cancer known as anaplastic large cell lymphoma (ALCL).

1.1.2 Biofilm Formation

Biofilm is a dynamic biological structure that consists of adherent micro-organisms and other reactive polymeric saccharides. Like other medical devices, silicone breast implants surface could also be the victim of bacterial contamination and biofilm formation. The bacterial adhesion to medical devices or implantable devices highly depends on surface chemistry, hydrophobicity and surface topography or surface roughness. Several researchers have been investigating the pathogenesis of the biofilm formation and capsular contracture. The surface topography or roughness has been shown to affect the bacterial attachment and biofilm formation on silicone breast implants and leading to the development of textured surfaces for breast implants to reduce the risk of implant failure. The surface chemistry has also shown promising results in reducing bacterial attachment. However, the stability of these methods is poor.

This thesis focuses on developing material strategies to modify the surface of silicone implants to mitigate the risk of silicone implants. Coating the surface of biomedical implants is a promising strategy to reduce the failure rate of implants[11]–[13]. In this work, we propose to coat the surface of the silicone implant using a biocompatible polymer silk fibroin (SF). Silk fibroin (SF) is a natural polymeric protein extracted from cocoons of *Bombyx Mori* silkworm.

1.2 Motivation

Coating the surface of biomedical implants is a promising strategy to reduce the failure rate of implants. Recent literature on surface modification and surface coatings shows single or multi-layer coatings of collagen, hyaluronic acid, Poly Methacryloxyethyl Phosphorylcholine (PMPC), fibronectin, aggrecan. For silicone breast implants, the challenges for coating include the adhesion of the coating and the failure of coatings under mechanical stresses. However, adhesion between the coating material and soft, flexible substrates such as silicones is poorly understood. Delamination, flaking, crack formation are the common problems associated with surface coatings of biomedical implants when subjected to mechanical deformation during handling and in use. It is also desirable to functionalize these coatings with appropriate drug molecules and functional biomolecules that will reduce the risk of failure. The focus of this work is to develop material strategies to modify the surface of silicone implants using SF coatings to mitigate the risk of silicone implant failure.

SF is a protein polymer extracted from the cocoons of the silkworm *Bombyx mori*. SF has excellent thermo-mechanical properties, and it can be processed using environment-friendly processing protocols[14], [15]. SF protein has emerged as a promising biomaterial for various tissue engineering applications such as vascular, cartilage, bone, neural, ligament, skin, heart, ocular, intervertebral disc and spinal cord tissue regeneration.[13]–[18]. Also, SF has tunable degradation by controlling the crystallinity and secondary structure of SF protein. The native SF fibers show negligible hydrolytic degradation in an aqueous environment; however, SF shows enzymatic degradation under the influence of protease enzyme[19], [20].

1.3 Objectives

The polydimethylsiloxane (PDMS) has been extensively used as implant material due to its biocompatibility, mechanical properties and flexibility. Silicone implants show a failure rate of 15-20% upon implantation. Surface modification by coating is one of the simplest methods used to improve the biocompatibility of a biomedical implant. It allows tailoring the interactions of the implant surface with the surrounding tissue. The focus of this thesis is to develop a process to coat natural SF protein or its blend on PDMS substrates. Accordingly,

this thesis is divided into three parts as given below, and the objectives for each part have been outlined.

1: Development of test methods to quantify adhesion between coating materials and PDMS

Surface coatings play a significant role in improving the performance of biomedical implants. Surface coatings on PDMS show single/ multi-layer coatings of collagen, hyaluronic acid, PMPC, fibronectin, aggrecan etc. But adhesion of these coatings on implants has not been studied. Delamination, cracking, crazing, or flaking, of the coatings during surgical handling or during use can contribute to failure of implants.

The objective of this part of the work was to quantify the adhesion or interaction of nano-coatings of biocompatible protein polymer SF on pristine as well as modified PDMS surfaces. The PDMS surfaces have been modified using oxygen plasma treatment and 3-amino-propyl-triethoxy-silane (APTES) treatment. Interestingly, testing of the coated samples using a bulk technique such as tensile and bending deformation showed that the SF nano-coating exhibits improved crack resistance when the PDMS surface has been modified using APTES treatment as compared to an oxygen plasma treatment. These results were validated at the microscopic and mesoscopic length scales through nano-scratch and nano-indentation measurements. Further, we propose a unique method using modified Atomic Force Microscopy to measure adhesive energy between treated PDMS surfaces and SF molecules.

2: Development of novel process innovation for crack-resistant SF coatings on PDMS

In this work, we demonstrate a novel process that results in the formation of a coating that is stable under mechanical stresses in tensile, torsion and bending modes. The coating process involves a combination of two conventional coating processes – namely dip coating and electro-spinning. The coating was also further functionalized using a green biomolecule - glycomonoterpene prepared using citronellal and glucose. These functional compounds are being touted as the next generation antibiofilm molecules on account of quorum sensing inhibitory activity. We have demonstrated that the quorum quenching activity of the biomolecule is retained during the processing steps, and the coatings exhibited excellent antibiofilm activity against common infection causing bacterium *P. aeruginosa* and *S. epi-*

dermidis.

3: To develop novel blends of silk fibroin with other suitable polymers/biomolecules

The third objective invovles development of novel blends of SF blends with other suitable polymers/ biomolecules. Here, we evaluated the performance of a blend of SF with a popular hydrophilic polymer polyethyleneoxide and compared the performance of SF blend with recombinantly produced elastin. This work has been divided into two Sections as outlined below.

3A: Blending of a hydrophilic polymer − polyethylene oxide

This work focuses on blending of a popular hydrophilic polymer polyethylene oxide with SF for use in coating applications. These coatings exhibit excellent adhesion to the PDMS substrates and better performance in biological environments. Interestingly, blends of SF with PEO having molecular weights of 300 KDa and 600 KDa showed improved aqueous stability and also excellent resistance to cracking and delamination. FTIR spectroscopy provided crucial information about the secondary structure of the protein. Further, the 25% and 50% blends resulted in the formation of crack-resistant blend coatings on PDMS surface. The testing was done under mechanical deformation in different modes such as bending and tensile. SF/PEO blends also showed a higher surface wettability as compared to SF coatings on PDMS surface, which was characterized using water contact angle. The hydrophilic contact angle of SF blend coatings reduces the non-specific adsorption of proteins, which results in improved biocompatibility of the coatings.

3B: Development of SF- recombinant elastin protein blend coatings on PDMS

In this work, we discuss the development of hydrophilic SF coatings upon blending with a novel molecule such as recombinantly prepared elastin-like peptide (ELP). ELP is a polypeptide obtained from the primary sequence of mammalian elastin with a repeat unit of (GVGVP). We studied the physio-chemical and mechanical properties of SF/ELP blends and compared these properties with a selected molecular weight of PEO. As expected, the high elasticity of ELP molecule renders improved mechanical stability to the SF/ELP blend. The biological evaluation of these SF blends included protein adsorption studies, accelerated

degradation studies and cytotoxicity studies. The SF/ELP blends resulted in more than 80% reduction in the adsorption of proteins to the surface. The actin staining and cell proliferation studies showed that SF and SF blends have cells with better morphology than pure PDMS.

1.4 Thesis Outline

This Chapter highlights the problem, motivation and objectives of the thesis. It also briefly summarizes the work done. Chapter 2 presents a detailed literature review about silicone breast implants and their complications. It also outlines the unsolved challenges. Chapter 3 discusses the novel methods developed to measure the adhesion of the coating to the PDMS. It also discusses the crack resistance of coatings when subjected to tensile and bending mode deformation. Chapter 4 is focused on an innovative processing protocol that enhances the crack resistance of the SF coatings. Chapter 5 discusses blends of SF with 2 polymer - polyethylene oxide and recombinantly produced elastin. Chapter 6 is a summary of the work done and also details the future work that must be planned.

Chapter 2

Literature Review

The biocompatibility of medical devices is the key property determining proper functioning of medical devices. PDMS is the material of choice for more than 70% medical devices. This Chapter begins with literature review that outlines the problems associated with silicone breast implants. Section 2.2 focuses on the classification and general complications associated with biomedical devices. It also discusses proposed mechanism of implant failures and advances in breast implant design to reduce the failure rate. Section 2.5 discusses the material science strategies to mitigate the failure of breast implants, while Section 2.6 summarizes the unaddressed problems in silicone implants. Further, the Chapter outlines the objectives for the present work.

2.1   Medical implants

Medical devices are used in various applications, and their performance is directly linked to the patient's health. These devices are classified based on the risk associated. The risk is evaluated with respect to improper usage, complexity in design and the use characteristics. The US-FDA categorizes medical devices or implants into three classes. Class I devices are low-risk devices; Class II devices exhibit mild to moderate risk, and Class III are high risk medical devices. For example, toothbrush is a Class I device, while non-invasive blood pressure monitor is a Class II. A heart valve is an example of a Class III device. These devices can be in direct or indirect contact with the patient's body/body fluids at the time

of use. The time of use can range from few hours to as long as many years.

Medical implants have been used to replace the missing tissue, support the damaged tissue or organ function, or enhance the existing biological function. One such implant that is used to retrieve the shape, size and feel of the breast is a silicone breast implant. Silicone implants have been used for several decades in breast reconstruction and augmentation surgeries. The next Section provides an overview of this important medical device.

2.2   Silicone implants in breast reconstruction

Breast cancer is the second largest cancer globally with a rise of about 1.3 million cases every year. Radiotherapy, chemotherapy and surgical intervention are the treatment options for a cancer patient. After mastectomy, breast implants are used to recreate the size and shape of the breast. The material of choice for breast implant is a soft, flexible inorganic polymeric material known as polydimethylsiloxane (PDMS) or silicone polymer. PDMS is characterized with excellent chemical resistance, stable mechanical properties, high hydrophobicity and significant resistance to thermal degradation. The commercially available breast implants are categorized based on the inner shell material, i.e. they can either be silicone-filled or saline-filled. Saline filled implants are pre-filled or filled during the implantation process. Silicone gel filled implants have the advantage of real aesthetic feel of breast tissue. However risk due to leakage of fluids is higher for silicone-filled implants than the saline-filled implants.

2.3   History of silicone implants

The safety of silicone based medical devices has been a challenge since their introduction. The typical clinical problems associated with silicone implants are autoimmune diseases, capsular contracture, biofilm formation, allergic reaction, and recently there is a presence of a rare type of cancer associated with patients implanted with textured silicone breast implants[9]. The development of silicone breast implants have undergone five generations of manufacturing or design changes in response to clinical complications. The first-generation breast implants consisted of a thick, smooth-textured outer shell and a viscous gel filled in the inner shell for adherence to the chest wall[21]. However, the first generation implants, on account of their smooth surface resulted in problems such as dislocation of the implant.

Also, these implants resulted in significantly higher failure rates due to capsular contracture. This hardening due to calcification of fibrous tissue resulted in pain and discomfort to the patient. The second-generation of breast implants had a thinner outer shell and a low viscosity gel inside the outer shell. It was hypothesized that this design will reduce the calcification of breast implants[22]. However, second-generation breast implant resulted in implant rupture and leakage of the inner silicone gel. The third-generation silicone implants focused on improving the permeability and strength of the shell to overcome the bleed of silicone gel and thereby reduce the implant rupture and eventually gel migration of the silicone implants. This has been achieved by introducing a multilayered silicone surface and increasing the shell thickness to prevent the gel bleed with the help of a barrier layer. However, FDA imposed temporary restrictions on the third-generation silicone implants from the US market in 1992. Thus, it led to the development of fourth and fifth-generation silicone implants. The development of the fourth and fifth-generation emphasized the FDA criteria for silicone shell thickness and surface texture, resulting in reduced rates of implant failure.

2.4   Reasons for failure

Breast reconstruction surgeries often result in complications resulting a further corrective surgery. The clinical data of commercially available breast implants shows 20% - 50% failure rates on primary augmentation or reconstruction surgery. The reoperation rates of breast implant of Allergan and Mentor (trade name) are 28% and 20% for augmentation surgery and 52% and 34% for reconstruction surgeries, respectively, after six years of implantation[23]. In most cases, the failure mechanism is either capsular contracture, infection, gel bleed, shell rupture, wrinkling or sagging. Figure 2.1 shows the capsular contracture formation over an extended time of 10 years. The next Section discusses about failure of implant due to capsular contracture or a bacterial biofilm formation as these have been identified as primary reasons for failure of breast implants[24].

2.4.1   Foreign Body Reaction

The exact mechanism of host tissue response on silicone breast implants is poorly understood. The interaction of body fluids with silicone implants initiates foreign body reactions.
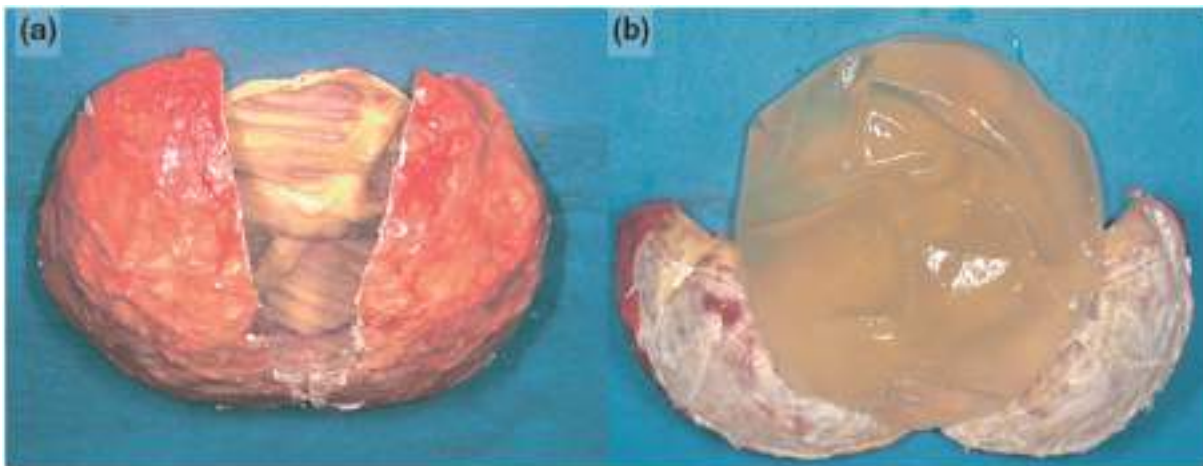
Figure 2.1: Calcified capsule of Breast implant (a) before (b) after removal surgery from the encased implant having distortion of the implant[25] "Reprinted from Infection in breast implants, Pittet, Brigitte and Montandon, Denys and Pittet, Didier, with permission from Elsevier"

Foreign body reaction consists of foreign body giant cells (FBGCs) and granulation tissue. The FBR starts with blood-biomaterial interaction followed by provisional matrix formation and acute inflammation. It is hypothesized that irreversible and non-specific protein adsorption on the implant surface triggers the failure of breast implants. The extent of protein adsorption depends on a range of factors such as surface chemistry, surface topography, surface wettability and charge on the surface. Thus, altering the surface properties of silicone implants is a promising strategy to reduce the immune response, thereby reducing the failure of the implants. Initially, albumin is bound to the implant surface and is being replaced by high-affinity proteins such as fibrinogen. This non-specific protein adsorption induces the formation of provisional matrix and results in acute inflammatory reaction followed by chronic inflammation over time. Acute inflammation occurs in a short time, from few hours to days and initiates the recruitment of macrophages, neutrophils and eosinophils and activates cell types through expression of various growth factors[26], [27]. Chronic inflammatory response occurs in the initial 2-3 weeks time after implantation and cytokines along with other cell types for fibrosis are recruited and activated. This cell activation step initiate fusion of macrophages into foreign body giant cells (FBGCs). These FBGCs have the potential to remove the foreign material through phagocytosis and cause cell activation. The FBGCs express various cytokines and other receptors to bind to interleukin surfaces[28], [29]. The expression of these factors modulate and control the fibrosis formation process.

Thus, fibrosis regulation depends on the biomaterial or implant material properties[29].

The wound healing process of human body could result in the formation of scar tissue around the implant. This scar formation is a normal healing mechanism for any type of implantation. In breast implants also, the healing process starts with the formation of scar formation around the implant. This scar tissue helps to prevent the slippage of the implant from the implant pocket. However, in some cases the thickness of the scar tissue increases over time and becomes unusually hard and is completely isolated from the rest of the body, causing pain, discomfort and irritation to patients. This results in implant failure, and this condition is called as capsular contracture (CC). The extent of pain and severity of CC was classified based on the baker grade I-IV grading system.

Grade I - the scar tissue formation around the implant does not affect the shape, size and texture of the breast tissue. Patients feels natural, and breast tissue remains soft.

Grade II - the scar tissue formation around the implant does affect the shape, size and texture of the breast tissue. But, patients feels natural and some firmness upon touch to breast tissue.

Grade III - the scar tissue formation around the implant does affect the shape, size and texture of the breast tissue. Patients feels firmness upon touch on breast tissue and abnormal in apprearence. The breast tissue will be round, hard, misshapen nipples but does not cause any forms of pain.

Grade IV - Similar to Garde III but more hard, pain, discomfort, and painful to touch.

The formation of capsular contracture is due to local foreign body reaction upon implantation. It is hypothesized that the inflammatory reaction around the implant causes fibrosis due to the production of collagen fibers around the implant[30], leading to the firmness and pain to the breast tissue[31]. The cellular composition of the capsule has been extensievly studied by several groups and concluded that capsular contracture is anticipated to be multifactorial. These studies suggest that the immune system plays a crucial role in the pathogenesis of CC. Macrophages, fibroblasts and lymphocytes are predominant cell types associated with capsule formation. Fibroblasts assemble at the interface of the implant and capsule[31]–[33]. It has been reported that baker grade IV capsule consists of higher

amount of fibroblast cells than grade I implants[34]. The fibroblast cell produce collagen and are associated with the initial scar formation. Histological analysis of capsular tissue revealed that capsular tissue majorly consists of uniformly arranged collagen fibers[30], [34]. The orientation and allignment of collagen fibers on implant changes with time and becomes hard and thicker, and results in pain and discomfort to the patients. Numerous studies have been performed and have shown that biofilm formation around the implant accelarates the capsular contracture, and this has been discussed in detail in the Section 2.4.2

2.4.2   Biofilm Formation

Another important reason for failure of breast implant is the formation of a biofilm on the surface of the implant. Biofilm is a dynamic biological structure that consists of adherent microorganisms and other reactive polymeric saccharides. The bacterial adhesion to medical devices or implantable devices depends on surface chemistry, hydrophobicity, surface topography, or surface roughness. Several researchers have been investigating the pathogenesis of biofilm formation. Figure 2.2 summarizes the list of the bacteria causing implant failure for breast implants. Multiple studies have confirmed the correlation between bacterial biofilm and acceralated capsular contracture on breast tissue. All these studies have used baker grading for their evaluation[35]. Human pathogens also can colonize the surface of silicone medical devices to initiate biofilm formation and infections. One of the pathogens, such as *P. aeruginosa*, is likely to adhere to hydrophilic, electrically neutral and smooth surfaces[36].Bacterial attachment and surface roughness have been closely linked. The implant surfaces have been classified into macro, micro, meso and nano-textured implant surfaces. Microtopography has served as a strategy for reducing biofilm formation on silicone implants. The microtopography of PDMS demonstrated by Chung et al. shows that biomimetic structure inspired by the skin of fast-moving sharks reduces the biofilm formation of S.aureus to an extent of 65% compared to smooth PDMS surfaces. This bacteria inhibition was due to surface nano topology than a chemical effect. These nanostructures improve the cell adhesion than smooth PDMS surface. However, the extent of bacterial adhesion depends on the strains of bacteria present in the implant pocket. Also, high surface textured implants showed increased bacterial contamination and biofilm formation. This description has now also been included in the revised thesis. A study also reported the CC for silicone implants
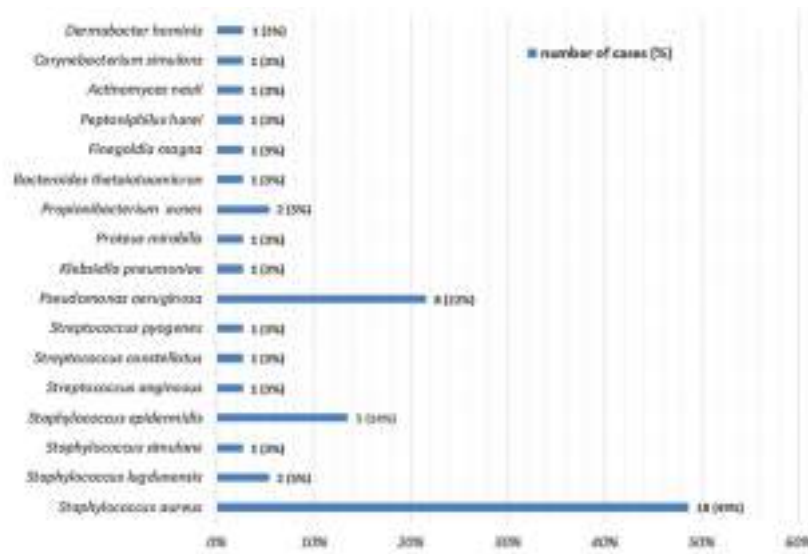
Figure 2.2: Various type of bacterial species found on breast implant infections[40]

implanted with implant pocket inoculated with *S. epidermidis* in varying concentrations. The histolgy analysis confirmed Baker the grade III-IV CC for implants inoculated with bacteria while control (without inoculating *S.epidermidis*) showed Baker grade I-II and similar results have been reported by other groups also[37]–[39].

2.5   Strategies to mitigate failure

Section 2.4.1 has described that capsular contracture, either due to foreign body response or due to bacterial biofilm are the two main causes for failure of implants. Here, we discuss about various material science strategies to reduce the risk of failure. Briefly, both physical and chemical modifications have been used to treat surface of implants. The surface modification of PDMS using physical methods includes plasma treatment using different gases, UV treatments or ozone treatments. These treatments result in a hydrophilic surface group on PDMS that helps prevent non-specific protein adsorption and eventually reduce capsular contracture. Other physical methods include surface texturing of silicone implants, as it has been reported that textured silicone implants show a reduced fibrotic tissue formation than smooth textured silicone implants. Also, strategies to improve biocompatibility include passive and active coatings, controlled release of antifouling agents, anti-inflammatory drugs, antimicrobial agents, anti-bacterial agents. The use of chemical methods includes
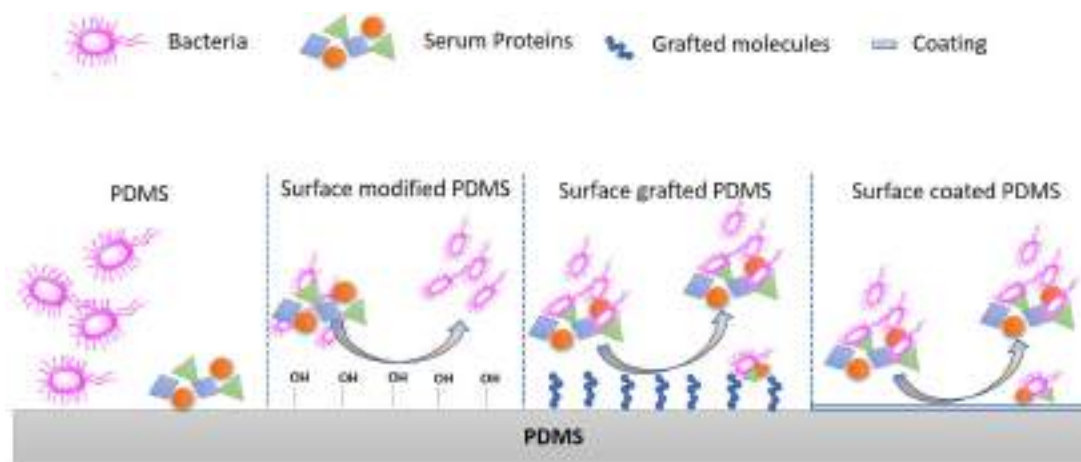
Figure 2.3: Overview of surface modification of silicone implants

surface grafting of antifouling agents on silicone implants. Other chemical methods include crosslinkers, fillers, nanoparticles, block copolymers, blends of PDMS. This Section provides a brief summary of these strategies.

2.5.1   Surface characteristics

Surface characteristics such as surface roughness have been shown to influence the performance of breast implants. There are several classification categories for a breast implant. The most widely accepted classification is International Organization for Standardization (ISO) 14607:2018. The surface roughness below 10 µm is categorized as smooth implants, 10 to 50 µm being microtextured, and above 50 µm as macro textured implants. Several studies have been performed to understand the effect of surface classification by roughness, wettability, surface area, fibroblast activity, macrophage polarization and bacterial attachment[4], [41]–[43]. These parameter have been shown to influence the implant failure.

Implant surfaces decorated with micro or nanopatterns can control cell types proliferation, differentiation, migration and attachment onto the implant surface. Scientific studies in biomedical devices and microfluidics show that the use of nanolayer patterns and design help improve cell growth and tissue engineering. Microtopography has served as a strategy for reducing biofilm on silicone implants. Bacterial attachment and surface roughness have been closely linked as bacterial cover increase with an increased surface roughness on electropolished steel[44]. One of the pathogens, such as *P. Aeruginosa*, is likely to adhere

to hydrophilic, electrically neutral, smooth surfaces[36]. The microtopography of PDMS demonstrated by Chung *et al.* shows that biomimetic structures inspired by the skin of fast-moving sharks reduces the biofilm formation of *S.aureus* to an extent of 65% compared to smooth PDMS surfaces[45]. Other biomimetic structure-inspired nanostructures such as nanopatterened cicida wing surfaces, also reduce bacterial attachment[46], [47]. This bacterial inhibition was due to surface nano topology than a chemical effect. Liu *et al.* demonstrated that nanotubular structures reduce bacterial function for *S.aureus* and *E.coli* with 79.2% and 57% inhibition after 48h of incubation, respectively, compared to smooth PDMS. These nanostructures improve the cell adhesion as compared to smooth PDMS surface[48]. Enchinas *et al.* demonstrated that irregular 3D nano topology drastically reduces with tailoring the surface chemistry of the nanostructure[49]. The other mechanism associated with implant failure was the formation of capsular contracture on the implant surface. Lei *et al.* demonstrated that C-ion implantation and microgrooves on silicone surfaces result in a lesser and weaker fibrous collagen matrix than unmodified silicone surfaces. Fibrosis was reduced for both C-ion and micro-grooved samples as compared to PDMS over 30 days of implantation[50]. Yoo *et al.* demonstrated a dual modification to suppress the capsular contracture formation of silicone implants. The study used micropatterns as a physical cue and a layer by layer poly-l- lysine coating as a chemical cue. This combined modification reduces fibrous collagen density secretion on poly l-lysine coated samples than pristine PDMS[51]. The electrospinning process results in the formation of aligned nanofibers with pore size in the range of 300-500 nm to support the differentiation and proliferation of stem cells. Thus, nanotechnology could be used to improve the biocompatibility of medical devices. Also, the biomimicry of the implant structures could reduce immune response when it is coated with patterns that mimic the host tissue.

In earlier days, breast implants available in the market for reconstruction surgeries were smooth textured in nature. The smooth textured design of breast implants is discontinued in clinical applications due to a poor understanding of the *in-vivo* immune response. The use of textured breast implants reduces inflammatory reaction upon implantation and physical stimulation[52], [53]. However, an increase in the frequency of capsular contracture on breast implants requires better implant design, minimizing foreign body reactions and thicker capsular contracture. The recent literature suggests the texturing of breast implants

reduces the capsular contracture using rat model[42], [54]. Initially, texturing of breast implants has been used to prevent the dislocation and malfunctioning of implants. However, these implants cause a reduction in the fibrotic tissue around the implant after few years of implantation. The 3-year follow-up studies on smooth and textured implants on randomized samples show that textured surface on implants reduces the capsular contracture from 59% to 11%[55]. However, textured implants are subjected to a higher bacterial attachment as compared to smooth textured implants[56]. Several groups have explored surface roughening strategies to implement surface texture ranging from 10μm - 500μm. One reason for reduced capsular contracture on textured implants is that the textured implant's grooves help the dermal fibroblast to grow in an orderly manner. It interferes with the migration of fibroblast and results in aligned collagen deposition. However, the mechanism of lesser capsular contracture and higher bacterial attachment on commercial breast implants is not well understood[57], [58]. The amount of inhibition of capsular contracture depends on the level of texture, based on texturing design with varying surface roughness[24], [41]. The stability of breast implants and their clinical data is not well understood, as these implants are next-generation designs of implants[59].

In 2019 US FDA recalled the textured breast implants that are currently available in the market. The long-term studies of textured implants show that texturing causes breast implant associated anaplastic large cell lymphoma (BIA-ALCL). There are no confirmed cases of BIA-ALCL on patients with smooth implants. The formation of BIA-ALCL on textured implants lead to the diffusion of gel from the inner shell of the implant. Patients have been diagnosed with ALCL irrespective of the saline or silicone used for filling inner shell. The formation of ALCL in saline-filled implants, therefore, confirms that silicone gel diffusion into body fluids is not the only mechanism that leads to BIA-ALCL[60]. Thus, a simple micro texturing/nano texturing of silicone implants is not an effective method to improve biocompatibility.

Surface activation

The PDMS has low surface energy and hydrophobic in nature. It is a chemically inert material, and this makes the material suitable for several biomedical applications. The hydrophobicity of PDMS is due to bulky methyl side groups limiting its chemical interactions

with other molecules. Thus, there is a need to activate the PDMS surface so that it becomes amenable to surface functionalization, grafting and surface coating. The changes in the surface properties have been characterized using water contact angle, SEM, FTIR-ATR and XPS analysis.

Plasma treatment is a widely accepted surface activation method, and it is rapid and effective as it forms a reactive silica layer on PDMS[61]. The surface wettability is vital in reducing non-specific plasma protein adsorption on silicone surface. Non-specific protein adsorption on the implant surface triggers foreign body reactions, resulting in implant failure. Altering the surface chemistry of the implant can reduce or prevent the failure of the implant by making the surface of the implant hydrophilic. This can be achieved with the help of plasma treatment using different gases such as oxygen, nitrogen, argon, hydrogen and helium[62]–[64]. The negatively charged ionized gas species are highly reactive. This reactive species cleave the methyl side chains of the PDMS. Upon hydrolysis, it forms a hydroxyl group when oxygen gas is used for plasma treatment; Similarly, nitrogen plasma results in the formation –NO, -NH$_2$ groups on the PDMS surface.

FTIR spectroscopy and XPS spectroscopy are used to characterize the changes in the surface chemistry after surface modification. Gas molecules used for plasma treatment determine the nature of functional groups formed on the polymer surface. Oxygen plasma treatment on PDMS results in hydroxyl groups, and the extent of functional group density depends on radio frequency (RF) power and exposure time.

The exposure of PDMS for a longer time results in improved surface wettability, with a water contact angle in the range of 20°-90° [65]. However, longer exposure time or high RF power results in physical damages such as micro-cracks on PDMS. Silicone implant surface exposed to oxygen plasma treatment show anti-bacterial property towards *P.aeroginosa*. The stability of plasma treatment is crucial since plasma treated samples exposed to air can cause hydrophobic recovery, and therefore, it is necessary to store these samples in water or polar solvents.

Exposure of oxygen plasma to silicone surface was limited as it causes physical damage to the silicone implant surface, eventually resulting in implant failure[5], [66]. Even though the plasma treatments on silicone implants reduce the implant failure upon implantation,

plasma-treated implants exposed to air result in the reversible recovery of hydrophobic surface groups, which increases the failure rate of the implant. Thus, alternative physical methods to improve the biocompatibility of the implants are also being studied.

Corona discharge

The corona discharge is a localized method used to tailor the surface properties of the polymer in atmospheric pressure conditions, while plasma treatment requires vacuum systems. After corona treatment, the density of functional groups is lesser than plasma-treated samples due to fewer ions getting ionized in the atmospheric pressure. Corona discharge produces a very high potential difference. Gas molecules get ionized and results in the formation of reactive particles, which are accelerated through a high electric voltage. The structural and chemical changes in corona and plasma treatments are reversible. A hydrophobic recovery due to low molecular weight oligomer migration on the PDMS surface is typically observed[67]. Stability and hydrophobic recovery after corona discharge could be controlled using secondary modifications methods such as surface grafting and surface coating using functional molecules[67]–[70], which improves the biological properties of PDMS.

UV/ Ozone Chamber

UV/ Ozone treatment (UVO) is a surface activation method that involves irradiating with UV light of different wavelengths using low-pressure mercury lamps. This method is also used to clean polymer surfaces, surface activation, improve hydrophilicity, and form polar groups using volatile molecules such as CO_2 and O_2 [71]. The surface activation using UVO is a two-step process and is time consuming as compared to plasma treatment. However, physical damage upon longer exposure time is less than plasma treatment. The UVO treatment on PDMS results in forming a hydroxyl group by reacting the ozone molecule with methyl side groups on the PDMS surface[71], [72]. The UVO exposure on PDMS generates –OH functional groups, which helps graft PMMA for the DNA extraction process. The surface oxidation on PDMS using UVO for the 30s resulted in a hydrophilic PDMS surface without any change in the bulk properties such as Young's modulus. However, PDMS requires a longer exposure time to achieve a comparable amount of hydrophilic functional group density[73].

2.5.2   Chemical modifications

The chemical modification of silicone implants to mitigate the risk of implant failure has been achieved by using various strategies such as incorporating filler molecules, developing blends of PDMS with hydrophilic molecules, synthesizing block copolymers and crosslinking systems. Developing organic-inorganic hybrid nanocomposite system using silicone macromer, hydrophilic monomers and inorganic nanoparticles such as SiO_2, AgNps, CuO, CTAB capped CuO, ZnO etc., without affecting the bulk properties of the nanoparticles and polymer systems to prevent fouling of biomedical implants and non-medical devices has also been demonstrated[74]–[77]. The extended use of nanoparticles, filler molecules and other additive substances depends on the chemicals toxicity. Yin *et al.* demonstrated the effect of laser-assisted surface modification on silicone nanocomposite hydrogel in inhibiting bacterial biofilm growth[78]. The hydrophilicity of silicone nanocomposite results in higher swelling behaviour. A second step surface modification using the MAPLE process followed by PEG coating results in a 40% reduction in BSA adsorption on silicone nanocomposite. The silicone nanocomposite incubated in *E.coli* and *S. aureus* shows a decrease of 56% and 54%, respectively[78]. Other chemical strategies to improve antifouling properties include developing antifouling silicones either using surface modifying additive amphiphiles (SMA) or copolymers of silicones. The SMA used in breast implant applications are typically diblock or triblock oligomers with a high affinity of the hydrophobic block to silicones or base polymer. Interestingly, SMA to prevent non-specific protein adsorption includes SMAs based on PEO having high surface concentration. The non-specific protein adsorption and hydrophilicity of PEO based SMAs are higher than RTV silicones bulk-modified with conventional PEO n - silanes (n = 3, 8 and 16)[79], [80]. The enhanced reduction in non-specific protein adsorption and hydrophilicity are due to the restructuring of PEO chains under different environments such as air or water. This restructuring of PEO chains is limited in conventional PEO n –silanes[81]–[84].

2.5.3   Surface coatings

Surface coatings is one of the easiest strategies to tailor the surface properties of the silicone breast implant. Coatings have the advantage of incorporating functional molecules, drugs,

anti-microbial agents and green molecules to prevent bacterial colony formation on implant surface. Coatings can also be used to control the release of the functional molecule or drugs into the media and help in reducing the biofilm formation and implant failure rate. The surface coatings method is categorized as passive coating and active/ functional coatings. This classification of passive and active coatings is based on the use of functional molecules, drugs, growth factors, nanoparticles, etc. that are incorporated in the coating process.

Passive Coatings

Recently, researchers are exploring various biomaterials such as biopolymers for coating applications. Table 2.1 summarizes the coating material and its effect on capsular contracture on silicone implants. Collagen coating is an interesting strategy to improve biocompatibility and reduce implant failure. It has been reported that the formation of collagen coating after plasma treatment on silicone implants significantly reduced the inflammatory cells surrounding the implant surface[85]. Collagen coating also helped in the neovascularization surrounding the silicone implant. Similar studies on plasma treated silicone implants coated with collagen-1 has also been evaluated and concluded that collagen coating results in enhanced cell adhesion and viability for mouse fibroblast cells. Thus, authors highlighted that collagen coatings on pretreated silicone surfaces enhance the biocompatibility and reduce the failure rate of the implant[86]. One of other strategy is use of spider silk coatings on silicone implants. Recombinantly prepared spider silk proteins were coated on silicone breast implants with few layers of protein using dip coating process. Spider silk coated on textured silicone implants shows 70% reduction in adhesion of BALB/3T3 fibroblast cells and compared to uncoated PDMS implants. The changes in the hydrophobicity of implants were characterized using a contact angle with a coating thickness of 1µm - 6µm. *In-vivo* experiments of uncoated and coated silicone implants show reduced proliferation of fibroblasts and decrease in formation of collagen I fibres. The cell abundance of chronic inflammatory cells shows a 1.5 to 3 fold decrease compared to uncoated silicone implants for 12 months[11]. Synthetic polymer coating has also been used to enhance biocompatibility of silicone implants. Park *et al.* have demonstrated that methacryloyloxyethyl phosphorylcholine (MPC) can be photopolymerized on silicone implants using UV irradiation. The authors show that PMPC coatings inhibit the adsorption of fibrinogen and albumin, the most abundant pro-

teins present in the blood. The coating also results in signitficant reduction in the fibroblast adhesion, which is the primary trigger for foreign body reaction as discussed in the Section 2.4.1. However, there is a possibility of the presence of unreacted monomers, which can cause toxicity upon implantation. The *in-vivo* implantation studies with PMPC coated silicone implants resulted in significant reduction in capsular contracture than pristine implants[87]. These coatings also show reduced collagen density, TGF-β expression, lower myoleoperoxidase and lesser α-actin muscle indicating reduced capsular contracture. Valencia–Lazcano *et al.* developed natural biopolymer SF (derived from *Bombyx Mori* cocoons) coatings on silicone implants[13]. The aqueous solution SF was blended with PEO and this blended solution was used for surface coating on silicone implants via electrospinning process. The SF/PEO blend coatings shows improved cell viability for mouse fibroblast cell lines. However, electrospinning coating of SF/PEO results in the formation of micropores on the coatings. The body fluids can diffuse through the micropores to the silicone surface and eventually non-specific protein adsorption followed by fibrosis formation may be triggered.

Functional coatings

In addition to the passive coatings discussed above, researchers have evaluated active or functional coatings for silicone implants. One of the most commonly employed methods includes loading of polymeric coatings with antimicrobial drug molecules. Physical blends can immobilize the drug molecule with the coating material or entrap it inside the polymeric matrix. The degradation of polymer matrix or application of an external stimulus can control the release of these active drugs. Literature reports suggests that the predominant bacterium associated with the subclinical infection on implants and is *staphylococcus epidermidis*. Figure 2.4 shows the SEM images of biofilm formation on the silicone implant surface.

Immersing the implant in anti-biotic solution is one of the surgical practice prior to implantation surgery. However, this method has not been found to be effective enough to prevent biofilm formation. Second approach to counter bacterial colony formation is administration of antibiotics in the perioperative pocket when infection is observed. But capsule formation around the implant prevent the penetration or diffusion of drug molecule to the target site.

Table 2.1: Summarizes the passive coatings used for breast implant applications

Polymer	Pre-treatment	Methodology	Remarks	References
Collagen	Plasma treatment of oxygen and argon gas mixture	Collagen coated silicone implants are implanted in the rats	The treated group shows few inflammatory cells penetrating the surrounding tissue	[85], [86]
Spider silk	Washed with 70% ethanol	Dip coated eADF4 spider silk on PDMS implants studies in rat model	The cell abundance of chronic inflammatory cells shows a 1.5 to 3 fold decrease as compared to uncoated silicone implants over 12 months	[11]
poly(2-methacryloyl oxyethyl phosphoryl-choline)	Covalently coated using the monomer of MPC	Polymerization was carried out on the surface of the implant, implantation in rat model	Peri-implant capsule thickness was reduced by 2 fold as compared to silicone implants	[87]
Polyethylene oxide/Silk fibroin	Electrospun PEO/SF was used to improve the biocompatibility	Surface coating of SF/PEO was employed to improve the cell viability and proliferation	No *in-vivo* analysis is performed	[13]

Standard cephalosporins such as cefazolin/gentamicin/bacitracin have been widely used to coat the surface prior to implantion. Baker *et al.* compared the efficacy of Doxycycline coated silicone implants and gentamycin/ cefazolin/ bacitracin wash. Doxycycline-coated silicone implants showed significant reduction in bacterial colony formation than control groups inoculated with *S. aureus* (MRSA) or *P. aeruginosa*[89].

Another strategy adopted by researchers includes loading an anti-microbial agent triclosan into PEG. This enables long-term stability and sustained release. McBride *et al.* demonstrated the use of grafted PEG chains with triclosan for prevention of biofilm [90]. The non-PEGylated silicone implant coated with triclosan showed short-term prevention of biofilm formation while PEGlyation resulted in prolonged antimicrobial property over a period of 70 days. The porcine model of polypropylene coated with minocycline and rifampicin impregnated effectively inhibited biofilm formation against *S.epidermidis*. The controlled re-
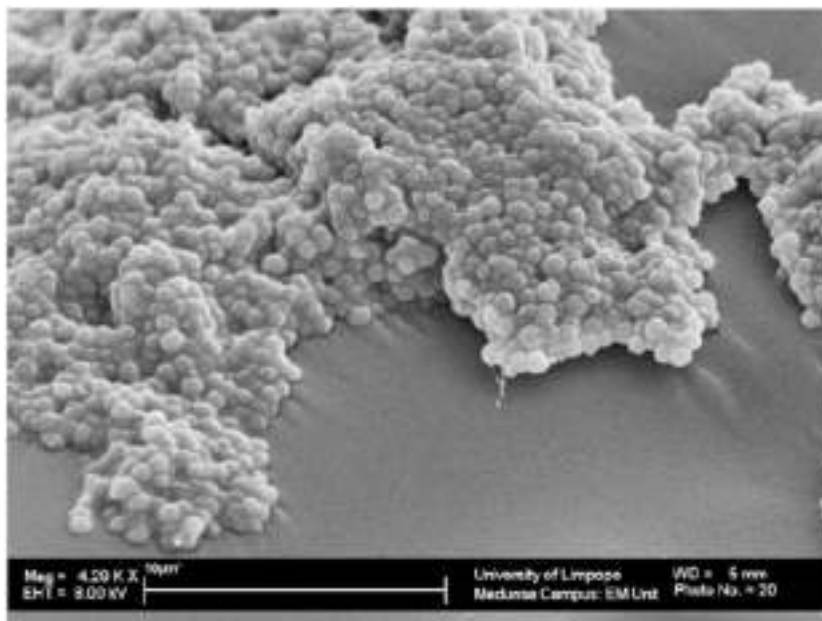
Figure 2.4: Biofilm formation on silicone implants due to *S.epidermidis* bacterium [88] Reprinted from Antimicrobial coating agents: can biofilm formation on a breast implant be prevented?, Van Heerden, J., Turner, M., Hoffmann, D., & Moolman, J. (2009). Journal of Plastic, Reconstructive & Aesthetic Surgery, 62(5), 610–617, with permission from Elsevier"

lease of impregnated drugs limits the shorter inhibition time only for a time period of 7-10 days[91].

Other strategies to reduce biofilm formation include incorporating nano drug depots by grafting ethyl (dimethylamino)propyl carbodiimide followed by encapsulation of drug molecules such as budesonide [92]. *In-vitro* analysis in the rat model shows that these drugs cause less Nitrous Oxide (NO) production and anti-inflammatory activity with and without drug molecules. However, the inhibition of anti-biofilm properties was not evaluated.

Also, antibiotics or antimicrobial drugs result in the development of multidrug resistance in these micro-organisms. Incorporating antimicrobial drugs alone or in combination is not effective in reducing the biofilm formation or inhibiting the biofilm formation. Thus, researchers have focused on developing polymers with anti-bacterial properties either by copolymerizing with PDMS or by surface modification. Salicyclic acid incorporated in poly(anhydride esters), poly(1,6-bis(o-carboxy-phenoxy)hexanoate) and polyurethane acrylate has been used as a coating material, and the hydrolytic degradation of polymer results in the release of salicylic acid, which inhibits biofilm formation[93], [94]. The ar-

gon plasma-deposited PEO-like thin films resulted in reduced bacterial attachment on samples coated with low molecular weight plasma pre-cursors[95]. The presence of hydrophilic groups on PEO reduces bacterial attachment. Similarly, Poly(ethylene glycol), hydrophilic polyurethanes (PU) also reduce the bacterial attachment and eventually biofilm due to the presence of hydrophilic groups on the coatings [95]–[99]. *In-vitro* studies show reduced bacterial attachment, but these coatings show significant degradation of the coating in a physiological environment[96], [100]. The polymeric coatings loaded with vancomycin on different polymers such as Poly(D, L - Lactide), poly (caprolactone) have also been explored to inhibit biofilm formation using layer-by-layer mechanism to incorporate drug molecules. Layer-by-layer enables multiple drug incorporation and sustained release to inhibit biofilm formation towards both strains of bacteria.

Surface coatings incorporated with anti-fibrotic drugs on silicone implants and their effect on bacterial attachment and fibrosis formation have been studied. The polyurethane coating on the silicone implant surface with multiple layers of coating has also shown to reduce the foreign body reaction. The clinical data at 4 year and 10-year studies show 10% and 25% of capsular contracture; this could be since PU coating is degraded over time and causes the release of toluenediamines (TDA) in the body fluids[97]. Scientific investigations confirm that TDA, a tumour promotor, enhances hepatic cells proliferation and cell mutation in rats[98], [99]. These studies suggested that the use of PU foam coated silicone implants may be susceptible to the development of breast cancer in women[100], [101]. The surface-coated silicone implants loaded with antifibrotic drugs show inhibition in collagen fibre density and macrophages formation. This reduction in fibrosis formation could be due to inhibition of TGF-β expression and results in the formation of thinner capsular contracture[101]. The 12 weeks of *in-vivo* data support that incorporating antifibrotic drugs coated on silicone implants inhibits the acute inflammatory response and reduces the foreign body reaction.

2.5.4   New materials

Since 2006, silicone is the only FDA approved material for the manufacturing of breast implants for the public use. As discussed in the Section 2.2, 15-20% of the patients post implantation experience various types of problems such as capsular contracture, biofilm formation, firmness, gel bleed and implant rupture results in revision surgery or corrective

surgery[23]. One of challenging and promising strategy is to develop new class of materials with mechanical properties similar to PDMS. However, these materials must have enhanced biocompatibility. Thermoplastic rubbers of branched polyisobutylene (PIB)-based block copolymer is one of the alternative for silicone implants. Linear poly(styrene-b-isobutylene-b-styrene) (SIBS) has similar stress at 100%, 200%, and 300% strain with 1.8 times higher ultimate tensile strength and 0.625 times lesser ultimate tensile strain as compared to PDMS. The histopathology studies, when implanted in rabbit model, confirms that SIBS has 20% lesser granulation tissue and 60% lesser giant cells[102]. Other alternative materials that are being developed for breast implant applications include co-polymers of silanes such as PEG-silane amphiphiles with variable PEO length, interpenetrating networks of P(HEMA) and glycosylated polymersomes[82], [103]–[105]. However, these studies are at a relatively early stage, and it will be several years untill these technologies are mature and are ready for products to be launched in the market.

2.6 Motivation

PDMS is one of the materials of choice for medical devices due to the low-cost fabrication, chemical inertness, non-toxicity, viscoelasticity with highly reversible deformability etc. The use of PDMS in various implantable devices is widely known. However, silicone breast implants result in 15-20% failure rates. The two main reasons causing capsular contracture are foreign body reaction and bacterial biofilm formation. Various strategies have been developed to modify the surface of silicone implants. Plasma treatment on the surface of PDMS is a widely used physical method to improve the wettability of the PDMS surface. Several groups working in droplet microfluidics have also been using plasma treatment to introduce hydrophilic functional groups using gases such as nitrogen, ammonia, hydrogen, argon, helium and oxygen[61], [106]–[109]. However, pretreatment of silicone implants by simple plasma treatment is not effective enough to prevent capsular contracture. An alternative to plasma treatment to reduce fibrosis in silicone implants is surface texturing. Clinical data suggests that texturing reduces fibrotic tissue capsule formation. However, patients who underwent reconstruction surgeries with textured implants have been diagnosed with a rare infection at six years and ten years follow up. Thus physical methods of the implants have

not been very successful in enhancing the biocompatibility of the silicone implants. Other alternatives to improve the biocompatibility of silicone implants include chemical methods such as grafting functional molecules, functional macromolecules/ polymers, passive and active surface coatings. Surface coatings are the easiest method to tailor the surface properties of the implants. They enable the incorporation of active molecule and sustained release of these functional molecules resulting in longer term stability.

Surface coatings are one of the most promising, and emerging area to improve the biocompatibility and reduce implant failure rate. Functional molecules can easily be incorporated in the coating material by blending the functional molecules results in sustained release. Coating without functional molecule has also been explored to improve the biocompatibility using biopolymer and proteins such as collagen, spider silk protein, PMPC and silk fibroin or its blends. However, surface coatings for silicone breast implants is an emerging field and several scientific and technical questions are unanswered. Various methods such as dip coating, electrospinning have been reported to coat the surface of silicone breast implants. However, the following considerations have not been taken into account for the development of stable coatings. SF has emerged as a promising biomaterial on account of easy availability, proven biocompatibility, biodegradability and aqueous processability. In addition, SF has several active chemical groups that have been modified to tune cell–scaffold interactions[110].SF surfaces can also be modified using simple layer by layer techniques to tune cell biomaterial interactions [111]. Therefore, it can be hypothesized that use of SF in coating of breast implants, can reduce failure rates. Although preliminary work has been done for SF coatings on PDMS, the following questions are unanswered.

(a) **Adhesion of the coating**: Adhesion of coating to the surface of PDMS implant has not been adequately studied in the literature. Recently, US-FDA has recalled few medical devices and the reason for recall was delamination of these coating. Delaminated coating material can diffuse into the body fluids causing serious health issues[112]. Thus, excellent adhesion of coating to the substrate is critical for enhancing the performance of PDMS implants. Adhesion of polymeric coatings to the substrate is typically measured by a peel test or lap shear test. These test methods provide poor accuracy and reproducibility for nano coatings[113]. Scratch tests is an active area of research for testing the adhesion. However,

this method is considered as an indirect method and provide only qualitative information about the adhesion[114]. Thus, there is a need to develop test methods to quantify the adhesion between PDMS and coating material.

(b) **Crack resistence of the coating**: Secondly, the mechanical properties of the coating and its ability to resist mechanical deformation has not been quantified. These coatings experience tensile, bending and compressive stress due to handling, transportation and also during use. Earlier study by Zeplin *et al.*[11] demonstrated that 180°bending test results in the formation of micro-cracks on the silk coated silicone substrates. Thus, there is a need for the development of crack resistant biocompatible surface coatings on silicone substrates using novel processing or blending strategies.

2.7   Conclusion

- Silicone breast implants are widely used in breast reconstruction and augmentation surgeries.

- These implants experience a failure rate of 15-20% . One of the major reasons for failure is capsular contracture (CC). CC can be triggered either due to FBR or bacterial biofilm formation.

- Various physical and chemical methods have been developed to modify the surface of silicone implants. Surface coatings using natural polymers has emerged as a promising strategy to modify the surface of silicone implants.

- Adhesion of coating to the PDMS substrate is a challenge. Also, conventional methods used to measure adhesion strength cannot be used to measure the adhesion of nano coatings to the implant surface. Secondly, failure of the coatings due to mechanical deformation has not been studied

- Thus it is an objective of the thesis

    1) Develop novel test methods to measure the adhesion of coating to the PDMS and the crack resistance of coatings when subjected to tensile and bending mode deformation.

2) Development of innovative processing protocol that enhances the crack resistance of the SF coatings.

3) Developemnt of SF blends that enhance the crack resistance and biological properties of the nano coatings.

Chapter 3

Adhesion of silk fibroin coating to PDMS

Molecular Measurement

Enhanced Crack Resistance

Emmanuel Joseph, Shatruhan Singh Rajput, Shivprasad Patil*, and Anuya Nisal*

3.1 Abstract

Polydimethylsiloxane (PDMS) is a commonly used material for biomedical implants, and surface-coated PDMS implants frequently face problems such as delamination or cracking of the coating. In this Chapter, we have measured the performance of nano-coatings of biocompatible protein polymer SF on pristine as well as modified PDMS surfaces. The PDMS surfaces have been modified using various physical and chemical treatment. Interestingly, testing of the coated samples using a bulk technique such as tensile and bending deformation showed that the SF nano-coating exhibits improved crack resistance when the PDMS surface has been modified using APTES treatment as compared to other modification. These results were validated at the microscopic and mesoscopic length scales through nano-scratch and nano-indentation measurements. Further, we developed a unique method using modified Atomic Force Microscopy (AFM) to measure adhesive energy between treated PDMS surfaces and SF molecules. These measurements indicated that the adhesive strength of SF to APTES treated PDMS is 10 times more compared to oxygen plasma treated PDMS due to higher number of molecular linkages formed in this nano-scale contact. The Force Spectroscopy measurements also identified breaking of these discrete molecular bonds formed between the amine groups on APTES-PDMS and the SF molecules. Thus, APTES modification to PDMS substrate provides a higher number of interaction sites for a protein polymer like SF and results in improved adhesion of nano-coating to the substrate. This improved adhesion enhances the delamination and crack resistance of the nano-coatings.

This Chapter begins with literature review that outlines the problems associated with surface coatings on silicone implants, experimental techniques to quantify adhesion, and physical and chemical modifications of PDMS to improve adhesion. Sections 3.2 discusses the gaps in the literature and describe the motivation and objectives of the present work. Section 3.3 provides detailed information about the experimental methods and material used. The Section 3.4 summarizes the key results of the present study. Section 3.5 concludes the Chapter.

3.2 Literature review

Medical devices play a crucial role to alleviate or minimize discomfort and pain to the patients and thereby contribute towards better quality of life in numerous ways. PDMS is a chemically inert silicon based inorganic polymer, that is used in various medical devices including breast implants, lenses, catheter tubing, [115], [116] etc. PDMS is processed using conventional polymer processing techniques. It has tunable mechanical properties, which suit a variety of applications. PDMS also has proven biocompatibility[117]. PDMS, however, exhibits lower surface wettability and high surface energy. This hydrophobicity, with a typical contact angle greater than 90°, has been recognized as one of the reasons behind failure of PDMS implants. The hydrophobic water contact angle leads to non-specific adsorption of proteins from the blood plasma, which triggers events such as fibrotic capsular contracture in breast implants and eventually results in its failure[118].

In order to reduce the failure rate of PDMS implants, they are coated with natural polymers and several researchers have explored this strategy[119]. However, the high surface energy of PDMS leads to poor adhesion of coatings to the PDMS surface and coating delamination poses multiple clinical problems and results in recall of products by regulatory bodies[112]. Recently, FDA had warned and recalled guided wire system containing PTFE coating, and the reason for the recall was due to the delamination of PTFE coatings to body fluids causing serious infections to the patients. Thus, excellent adhesion of coating to the substrate is critical for enhancing the performance of PDMS implants.

To improve surface wettability of PDMS, various physical and chemical treatments on PDMS surface have been proposed[118], [120], [121]. The physical methods of surface modification include plasma treatments using different gases such as oxygen, argon, nitrogen, hydrogen, helium. UV treatment and ozone treatment are other modes of physical treatments. These treatments result in the formation of hydrophilic groups such as -OH, -NH2, -NO2 and -COOH on the PDMS surface. In addition to these physical methods, various chemical modifications of the surface to produce hydrophilic groups have also been reported. Some chemical treatments include piranha treatment, 3-amino-propyl-triethoxy-silane (APTES) treatment and self-polymerization of dopamine. The piranha treatment produces a surface

with -OH groups, while APTES provides amino functional groups. The self-polymerization of dopamine on PDMS, results in stabilized stem cell adhesion, multipotency, improved hemo-compatibility and antimicrobial property[122], [123]. These treatments on PDMS surface result in the formation of hydrophilic functional groups[124]. Presumably, these functional groups interact with the coating material through non-covalent bonds such as hydrogen bonding and electrostatic interactions. However, the adhesion of natural polymers to PDMS surfaces after these treatments has not been thoroughly investigated. In particular, the mechanical strength of these coatings and its resistance to shear stresses is poorly understood. One of the approaches to compare the interaction of different surface treatments was to quantify the amount of coating material adsorbed using fluorescent dyes on the PDMS surface after surface modification[125].

There are various test methods to quantify the adhesion of thin films or coatings to the substrate. These test methods include peel test, scribe test, pull-off test, blister test, micro indentation test, small punch test, edge delamination test and four point bending test. One of the challenges in quantifying the strength of adhesion of natural polymers to the modified PDMS surface is that the PDMS is an elastomer and results in significant deformation of the bulk of PDMS material while performing tests such as peel test and lap shear[113], [126]. Thus, evaluation of adhesive strength using conventional methods results in artefacts in the measurement. The quantification of adhesive energy of stiff material on a soft substrate is therefore a challenge.

In this Chapter, we provide quantitative details of adhesion of natural polymer, SF to the modified PDMS surface. The silk fiber obtained from silkworms consists of 2 proteins - 70-75% of the silk fiber is madeup of Fibroin, while 25-30% of the fiber has sericin. Sericin is hydrophilic glue-like protein, while fibroin is the main structural protein responsible for excellent thermo-mechanical properties and lustrous appearance. SF has exceptional mechanical strength and toughness along with excellent high temperature thermal stability [127]. It has tunable degradation and proven biocompatibility[128].

The extraction of sericin protein or removal of sericin from silk cocoon is known as degumming process. Several protocols are reported in the literature for degumming process of mulbery silk including heat treatment, wet autoclaving and chemical treatments such as

urea solution, tartaric acid, soda ash - hydrogen peroxide, organic acids, sodium oleate assisted, alkaline solution and other methods include ultrasonication and microwave assisted removal[129]–[132]. The protocol helps in the dissolution of sericin into the media. The cottony mass obtained after degumming process consists of fibroin fibers. Several different protocols have been reported in the literature to convert the SF fibers to fibroin solution and the final solution obtained after dissolution process is termed as Regenerated Silk Fibroin. This RSF solution can be processed into various forms such as films, non-woven mats, gels, micro/nano particles, foams and coatings[15]. Fibroin, the structural protein of silk fiber has been used in various non-medical applications including semiconductor, optoelectronics and medical applications such as drug delivery, wound dressing and various tissue (bone, cartilage, nerve, intervertebral disc, etc) engineering applications. Thus, Silk fibroin, obtained from *Bombyx mori* silkworm is an excellent material for medical device coating application.

The PDMS discs were surface modified using various physical and chemical treatment method to make them hydrophilic. At a macroscopic level, we compared the adhesive strength of SF coating on PDMS modified by physical and chemical methods using peel test. We used mechanical tests such as bending and tensile loading and characterized the resulting surface morphology using microscopy. We performed nanomechanical measurements such as nano scratch and nanoindentation on SF coatings on PDMS. All these tests suggest that APTES treated PDMS is better suited for SF adhesion compared to O2-plasma treated PDMS. To gain insight into the molecular level mechanism of better adhesion in case of APTES treated PDMS, the interaction of SF with individual functional groups of physically and chemically modified PDMS was measured using Atomic Force Microscopy (AFM). The energy required to separate SF coated glass microsphere (20 μm) from the PDMS surface modified to produce hydrophilic groups was measured. The force spectroscopy measurements suggest that the APTES treated PDMS surface forms a greater number of bonds with SF compared to the oxygen plasma treated PDMS. Hence the energy required to separate SF coated glass bead from the former surface is 10 times more compared to later due to higher number of molecular linkages formed in this nano-scale contact. This molecular interaction results in excellent performance of the nano-coating in adhesion measurements performed at meso and bulk scales. To the best of our knowledge this is the first report about characterizing the SF-PDMS interface using mechanical tests and force spectroscopic measurements

which explains the results from these macroscopic tests. The experimental protocol developed in this work has a tremendous impact on enhancing the performance of implants.

3.3 Experimental Section - Materials and Methods

3.3.1 Preparation of PDMS Discs

Medical grade PDMS (Sylgard 184, Dow Corning) was cast on polystyrene Petri dishes to obtain a disc with a uniform thickness of 1mm. The prepolymer was thoroughly mixed with the curing agent for 5 minutes using a weight ratio of 10:1. It was then poured into the petri dish and degassed for 30 minutes. This mixture was kept in a convection oven at 40°C for 24h. PDMS discs of required dimension were then cut out, and isopropyl alcohol (IPA) treatment was performed to clean the samples, which were used for further experimentation. The treatment involved 30 minutes sonication in an IPA bath to remove dust particles before further experimentation. This process of cleaning was followed by a drying step (60°C for 4h in a vacuum oven) to remove any traces of the IPA solvent.

3.3.2 Surface treatments of PDMS Discs

Oxygen plasma treatment

Plasma treatment of PDMS surface after cleaning with IPA and drying at 60°C was done on both sides of the PDMS disc using Emitech 1050 plasma unit. The chambers were initially purged for 15 minutes with oxygen gas. The optimized plasma conditions of 50W RF power and 1 minute time duration were determined by measuring the contact angle on the surface and confirming no physical damage to the PDMS disc surface using optical microscopy. The plasma-treated discs were stored under DI water for a maximum of 1 week, before use for further experimentation.

Ammonia plasma treatment

The PDMS discs after surface treatment with IPA to remove the dust particles on the surface was used. The plasma treatment was done on both sides of the PDMS disc. The optimized plasma conditions of 250W RF power and 20 seconds duration were determined by measuring

the contact angle on the surface. The plasma treated discs were stored in DI water for further experimentation.

Piranha Treatment

Piranha solution is a mixture of H_2SO_4 and H_2O_2 in different ratios varying from 1:1 to 3:2. The treatment involved treating PDMS discs for an optimum time followed by treatment with 1M KOH for the same time. The PDMS discs after surface treatment with IPA to remove the dust particles on the surface was used. The discs were dipped in the piranha solution (3:2) for different time, followed by DI water wash. These discs were again dipped in the 1M KOH solution for the same time. After Piranha treatment, PDMS discs after piranha treatment were stored in the DI water for further experimentation.

Polydopamine coating on PDMS discs

The coating of polydopamine onto PDMS discs was done by dissolving dopamine hydrochloride at a concentration of 2 mg/ml in a 10mM Tris-HCL buffer at pH 8.5. PDMS elastomers, after curing were submerged in the dopamine solution immediately for 24h at 80°C, followed by DI water wash in DI water for 3 times. The washed PDMS discs were dried at 60°C for 6 h.

3-Aminopropyl-tri-ethoxy-silane (APTES) treatment

The chemical attachment of APTES to PDMS was performed after completing the oxygen plasma treatment as described earlier. This oxygen plasma treated PDMS disc was then kept in the 10% APTES solution in DI water for 20 minutes, followed by drying for 24h at 60|*degree* C temperature. APTES treated samples were stored at room temperature for further experiments.

3.3.3 Preparation of SF solution

The silk fibroin solution was prepared from *Bombyx mori* silkworm cocoons obtained from Central Sericultural Research and Training Institute, Mysore as per the protocol described elsewhere[133].

Briefly, the *B. mori* silk cocoons were boiled in 0.5w/v% solution of $NaHCO_3$ twice for

about 30 minutes to remove the sericin coating. The resulting mass of fibroin fibers was then washed with water and dried. The dissolution of the cottony mass of fibroin fibers was done using a chaotropic salt Lithium Bromide (LiBr) at 60°C for 4h. The cottony mass of fibroin fibres dissolved in 9.3M Lithium Bromide solutions using a ratio of 1gm of silk fibers in 10ml LiBr solution. This solution was then extensively dialyzed against deionized water for 51h at 8°C to ensure complete removal of the salt. The solution was centrifuged at 10000 rpm for 30 minutes at 4°C and the supernatant was collected and stored in a refrigerator for about 20 days. The solution had a concentration of 40mg/ml or 4wt%.

3.3.4 Coating of PDMS disc

Surface treated PDMS substrates were used for coating experiments with silk fibroin. The SF solution was diluted to 4mg/ml concentration or 0.4 (v/v) % using DI water. Surface treated PDMS discs were dipped in the diluted SF solution for 10 minutes followed by a drying step at 60°C for 8h. The SF coated PDMS discs were exposed to methanol vapor for 48h, to induce the secondary structure random coil to β-sheet structure. These discs after methanol treatment and drying process at 60°C for 8h under vacuum, to remove any entrapped methanol on the coatings was used for further experimentation.

3.3.5 Fourier Transform Infrared (FTIR) Spectroscopy − ATR

The uncoated and coated PDMS discs, before and after surface modification, coating process, and methanol treatment, were characterized using an ATR-FTIR Bruker Tensor II spectrophotometer equipped with a diamond crystal probe detector. The scan was recorded from 500-4000 cm^{-1} with a resolution of 4 cm^{-1}. The quantification of secondary structure of SF coating before and after methanol treatment was performed using peak fit software.

3.3.6 Contact Angle Measurement

Surface modification and surface coating on the PDMS surface was confirmed by 4μl sessile drop water contact angle in DI water. The equilibrium contact angle was reported as an average of four measurements done on each sample.

3.3.7 X-ray Photoelectron Spectroscopy (XPS)

The physical and chemical modifications on the PDMS surface were assessed by XPS with ambient pressure photoelectron spectrometer (M/s Thermo Fisher Scientific Instruments UK). The reference binding energy C1s was 284.8eV. XPS analysis of the sample was measured using anode Al K(α) X-ray generated at 72 W. The pressure in the analysis chamber was maintained in the range of 2x10E-9 mbar. The energy resolution of the spectrometer was pre-set at 0.5 eV at a pass energy of 50 eV and scanned binding energy from 0 to 1000 eV. The multiple peak fitting function of Peak fit software was used for peak fitting.

3.3.8 Tape Test (ASTM D 3359) / Cross Hatch Test

A 5x5 cm PDMS block having a thickness of 1.5 cm was coated with SF after different physical and chemical modifications. The cross-hatch was prepared using ASTM standard blade having sharp edges 1 mm apart. After peeling off with a scotch tape, the image was captured using a digital camera and the delaminated area was measured. The classification of the samples was done as per the ASTM standard, which says that rating 5B – 0%, 4B - <5%, 3B- $5^{-1}5\%$, 2B – 15-35%, 1B – 35-65%, where the numbers denote the percentage of the area where the coating is peeled off.

3.3.9 Scanning Electron Microscopy

The surface morphology of the SF-coated PDMS before and after mechanical deformation was characterized using a scanning electron microscope (SEM) Model – FEI Quanta 200 3D. Representative images at appropriate magnifications were recorded after sputter coating of gold on the samples to prevent charging on samples.

3.3.10 Atomic Force Microscopy - Imaging

The surface topography of the modified PDMS discs was performed in ambient conditions in tapping mode for a 50μm x 50μm area with a scanning probe microscope (JPK, NanoWizard II). Silicon cantilevers with a spring constant k of 60 N/m were used to perform experiments. The cantilever was oscillated at its free resonance frequency (250 - 350 kHz).

3.3.11 Bradford Assay

The quantification of the amount of proteins present on the surface modified PDMS surface was carried out using Bradford assay as reported earlier. Briefly, the SF coated unmodified and modified PDMS discs were immersed in 1.5 ml of Bradford reagent and incubated for 5 min. The absorbance of supernatant was measured at 595 nm.

3.3.12 Bending and Tensile Measurement

A simple bending test, followed by SEM imaging, was designed to characterize the crack resistance of the coating on the PDMS implant. The SF-coated PDMS strip without modification was used as a control. The crack resistance of the coating was measured using a 180°bending test with a rectangular block of 1 cm x 3 cm in size and a 0.15 cm thickness as per the protocol described by Borkner *et al.*[12]. The central 1cm portion of the PDMS strip was imaged in the SEM to validate the quality of coating before subjecting the strip to any mechanical deformation. Also, 1mm thick dumb-bell shaped specimens were prepared from the PDMS. These specimens were stretched to 50 and 100% strain at a stretching rate of 50mm/min using a Universal Tensile Machine, and SEM images of the central region were recorded after the release of the strain.

3.3.13 Nano-Scratch Test

The nano-scratch test on unmodified and modified coated PDMS discs was performed using a Rockwell C diamond, sphero-conical stylus having an initial load of 3μN to a final load of 10mN with a loading rate of 30mN/min over a length of 1mm with a speed of 3mm/min.

3.3.14 Nano-Indentation Test

Nano-indentation is a technique used to characterize the local elastic modulus and hardness of the surface coating. Nano-indentation of unmodified and modified SF coated PDMS was performed using a tip with a sphero-conical head. The sample was loaded with a maximum load of 20μN at a loading rate of 80μN/min for 30 seconds.

3.3.15   Atomic Force Microscopy -Force Spectroscopy

A 20 μm glass bead is attached to the end of a tipless-cantilever with spring constant   0.8 N/m (Micromasch, Bulgaria). A superglue (araldite) is used for the attachment, which makes a hard contact between cantilever and glass bead which avoids the unwanted deformation of bead-cantilever contact during the measurement. Cantilever-bead assembly is brought close to the SF solution, and only the bead is carefully dipped into it for   60 seconds. A thin layer of SF got coated on the bead. Cantilever-bead assembly is pulled out of the solution and kept in methanol vapour for   24 hours which prevents it from redissolving into the media where measurements are performed. Coating of SF on the glass bead was confirmed by fluorescence spectroscopy. Rhodamine - SF solution is used to confirm the formation of SF coating glass beads. When the SF coated cantilever is pressed against the physically/chemically terminated (O_2 or APTES) substrate, bonds form between SF molecules and the surface functional groups on the substrate. Adhesion energy between the two substrates is determined by measuring the force required to pull these two surfaces apart from each-other. This force experienced by the AFM cantilever during the pulling away from the substrate.

3.4   Results and Discussion

PDMS is a polymeric material routinely used in a variety of biomedical implants and devices. Owing to the hydrophobicity and low surface energy, the surface of PDMS is modified using various known physical and chemical treatments[118], [120], [121], [123], [124]. All these treatments reduce the hydrophobicity of the PDMS surface by forming –OH, -NH$_2$ functionalities. It has been hypothesized that these functionalities help in improving the surface energy of the PDMS surface, which helps in stable coatings that do not delaminate. In this work, PDMS discs of required sizes and shapes were prepared, and standardized protocols were used to modify their surface.

X-ray Photoelectron spectroscopy (XPS) and Fourier Transform Infrared (FTIR) spectroscopy techniques were used as the preliminary confirmatory tests for surface modification of PDMS surface using physical and chemical treatments. The formation of –OH groups after oxygen plasma treatment (Sample abbreviation: O_2-PDMS) was confirmed by char-
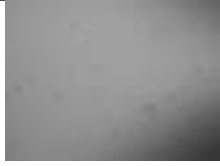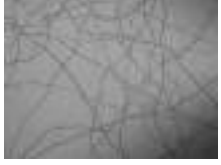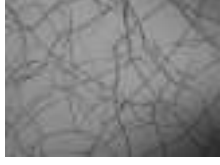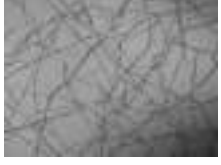
RF Power (W)	Exposure Time (min)	Representative image	RF Power (W)	Exposure Time (min)	Representative image
30	1		30	5	
30	10		30	15	
50	1		50	5	
50	10		50	15	
70	1		70	5	
70	10		70	15	

Table 3.1: Summarize the optical images of PDMS after oxygen plasma treatment at different power for different exposure time

acterizing the PDMS surface using XPS. The oxygen plasma treatment was optimized by varying the RF power for plasma treatment and the time for treatment. The surface of the PDMS disc was monitored using an optical microscope for any defects such as cracks or crazes or visible surface roughness. The results of this experiment have been summarized in Table 3.1. It was observed that increasing the RF value beyond 50W and the exposure time beyond 1 minute resulted in cracking on the PDMS surface. In the XPS spectrum, a shift in the binding energy of oxygen from 531 eV to 535 eV confirms the formation of –OH groups on the PDMS surface as shown in Figure 3.1. The oxygen plasma treatment was also corroborated by recording the change in contact angle.
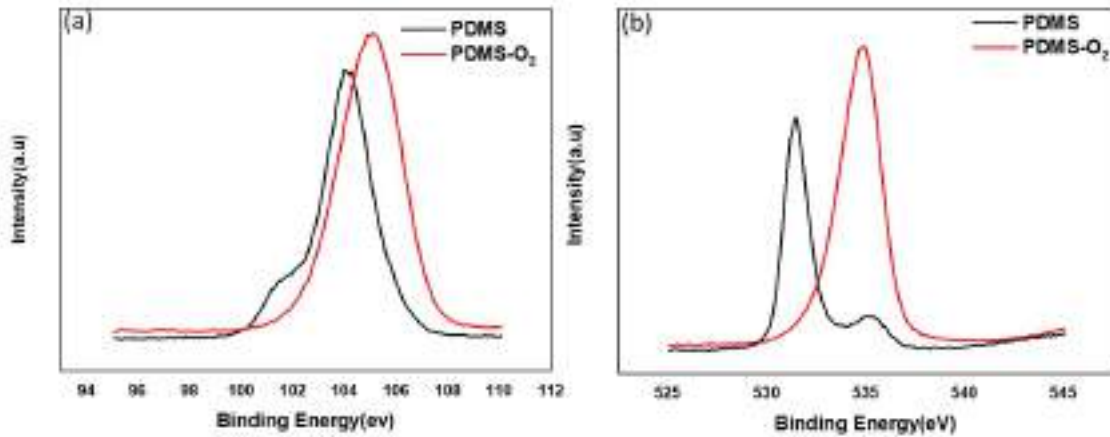
Figure 3.1: XPS spectra of oxygen before and after oxygen plasma treatment (a) Silicon (b) Oxygen

Figure 3.2 shows the FTIR-ATR spectra for all physical and chemically modified PDMS surfaces. The pristine PDMS surface shows characteristic symmetric and asymmetric stretching peaks at 2963 cm^{-1} and 2903 cm^{-1} and vibrational bending peaks at 1253 cm^{-1} that correspond to the methyl group[124]. There are no characteristic signals present beyond the 3000 cm^{-1} range[120]. The FTIR spectra for the oxygen plasma (Sample abbreviation: O2-PDMS) sample was found to be identical to that of pure PDMS. This is because the oxygen plasma treatment is done over the first few atomic layers of the PDMS surface. Thus, the bulk PDMS signals dominate the FTIR signal. A broad absorption peak at 3300cm^{-1} to 3700cm^{-1} for the piranha treated PDMS (Sample abbreviation:Piranha-PDMS) sample, confirms the formation of –OH groups on to the surface of the PDMS surface. The presence of amide peak at 1655cm^{-1} and a broad hydroxyl peak at 3100 to 3500 cm^{-1} confirms surface modification after ammonia plasma on PDMS (Sample abbreviation: Ammonia-PDMS). The APTES modification was validated through the absorption peak at 1576 cm^{-1} in the FTIR spectra (Figure 3.2 (d)) which is attributed to the vibrational stretching of –NH$_2$ groups[125]. The additional –NH stretching of APTES molecule on PDMS surface confirms the formation of amino terminated silane on PDMS. The board spectrum at 2800 cm^{-1} to 3300 cm^{-1} is due to overlapping of –CH stretching at 3000cm^{-1}, -NH stretching at 2800 cm^{-1} to 3200 cm^{-1}, -OH stretching at 3300cm^{-1}. The presence of –NH bending at 1650cm^{-1} to 1580 cm^{-1} also support the formation of a polydopamine (PDA-PDMS) coating on PDMS surface. The sharp peak at 1410 cm^{-1} and 1303 cm^{-1} is due –OH bending and presence of
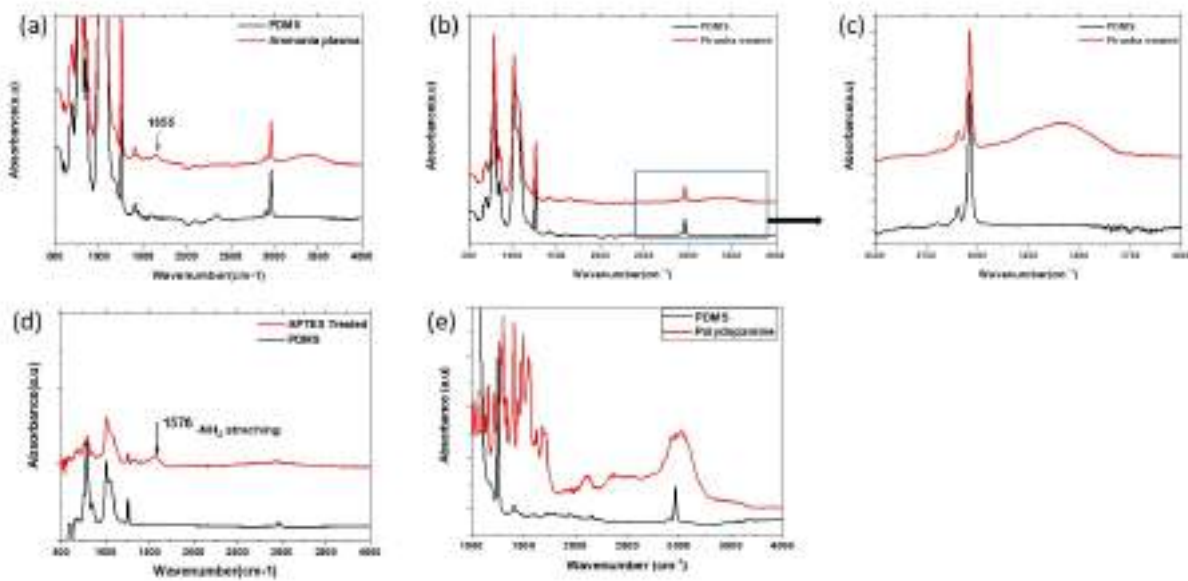
Figure 3.2: FTIR spectroscopy of unmodified and modified PDMS

aromatic amine respectively as shown in Figure 3.2 (e) The changes in the surface wettability of unmodified and modified PDMS is summarized in Table 3.2. The contact angle decreased from 112±5°for pristine PDMS surface to 55±3°for oxygen plasma treatment. This intermediate hydrophilicity is the optimum wettability possible with oxygen plasma treatment without any physical and visible damage to the PDMS surface. The reduction in the water contact angle from 112±50°to 60±50°confirmed the chemical oxidation of PDMS after piranha treatment for 4 min. longer exposure time does not results in any further improvement in hydrophilicity as summarized in the Figure 3.3. Piranha treatment followed by 1M KOH treatment results in reduced water contact angle. However, treatment above 4 min does not provide any reduction in water contact angle. This could be due to completion of reaction between piranha solution and PDMS surface. Das et.al. demonstrated that longer treatment time results in higher water contact angle value and this could be due to the hydrophobic recovery of PDMS and formation of irregular surface roughness. APTES - PDMS samples show complete surface wettability. This was attributed to the formation of a uniform layer of APTES with a large number of surfaces –NH$_2$ groups. These hydrophilic contact angles further confirm the modification of PDMS substrate using APTES molecules.

The surface-modified PDMS discs were used for SF coating experiments. The formation of the SF nano-coatings on PDMS substrate were also characterized using FTIR – ATR
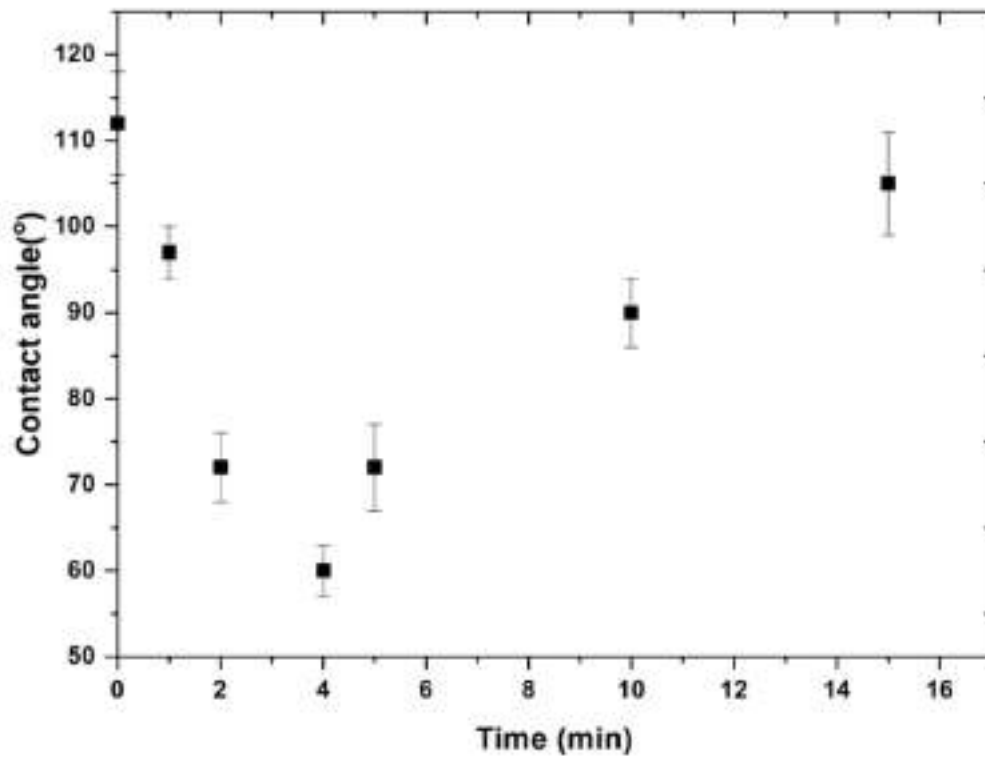
Figure 3.3: water contact angle as a function of treatment time for piranha solution on PDMS

Table 3.2: Water contact angle after surface modification on PDMS substrate

Sl.No	Modifications	Functional Groups	Optimized Conditions	Water contact angle
1	PDMS	-CH$_3$	Without any treatments	112°±5°
2	PDMS-O2	-OH	50W, 1 min	55°±3°
3	PDMS-Piranha	-OH	H$_2$SO$_4$:H$_2$O$_2$ (3:2), 4 min	62°±3°
4	PDMS-Ammonia	-NH, -NH$_2$	250W, 20 sec	60°±3°
5	PDMS-PDA	-OH, -NH$_2$	10mM of Tris-HCL, 8.5 pH, 2mg/ml, 24 h	65°±3°
6	PDMS-APTES	-NH2	Oxygen plasma followed by dip coating of PDMS discs in 10% APTES solution for 30 min.	less than 10°
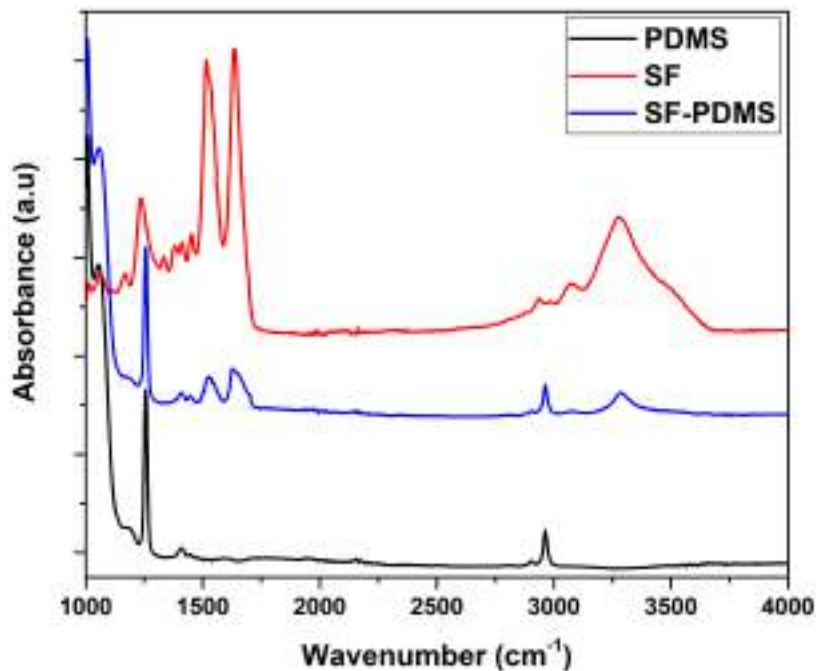
Figure 3.4: FTIR spectra of modified PDMS before and after SF dip coating process

spectroscopy. The presence of amide I and amide II peaks confirm the presence of SF, which was confirmed through a sharp peak at 1625 cm^{-1} and 1515 cm^{-1} respectively[134] as shown in the Figure 3.4

3.4.1 Tape Test (ASTM D 3359) / Cross Hatch test

ASTM standard Tape test B (ASTM D3359) or Cross Hatch test is a qualitative measure of coating adhesion at bulk scale and has been used to measure the adhesion between the coating and soft substrates such as PDMS, PU etc[113]. Here, a cross-hatch of 25 squares is made on the coated surface. The cross-hatch was prepared using ASTM standard blade having sharp edges 1 mm apart. After peeling off a scotch tape, the delaminated area was measured. Figure 3.5 summarizes the delamination of SF coatings on modified and unmodified PDMS using cross hatch test.

The pristine PDMS shows complete delamination of the coating and hence confirms that
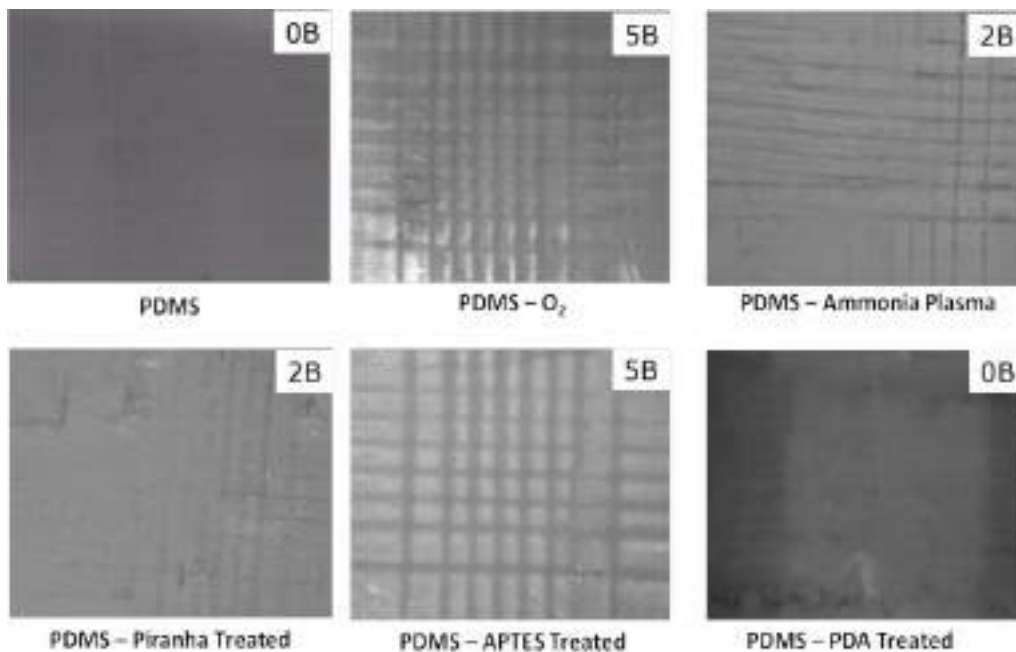
Figure 3.5: Processed digital images of unmodified and modified SF coated PDMS surface after cross-hatch test

surface modification of the PDMS is essential to coat the PDMS using SF. Polydopamine modified PDMS also shows complete delamination of the coating. We could not differentiate if the delamination was happened from polydopamine layer or top SF layer. Our hypothesis here is that, this delamination could be due to less interaction of polydopamine coating with PDMS surface. The piranha treated and ammonia plasma treated PDMS also showed some amount of delamination of the SF coating after tape test. Thus, these modifications are classified as intermediate adhesion. The oxygen plasma (SF-O2-PDMS) and APTES (SF-APTES-PDMS) surfaces showed no measurable delamination after tape test. The results are summarized in the Table 3.3. The qualitative measurement to compare the adhesion of coating on soft substrates is less effective since reproducibility of test results is a challenge. We did further quantitative tests at various length scales only for O2-PDMS and APTES-PDMS, since other modification method for PDMS didnot pass the cross hatch test. This indicates that these surface modification methods are less effective in improving the adhesion or interaction between modified substrate and SF. Further, we demosnstrated the effect of surface roughness and changes in the surface chemistry in detail using XPS, AFM, SEM and amount of SF protein present on modified PDMS using bradford assay.

Table 3.3: Scale of surface modified PDMS coated with SF after tape test

Sl.No	Modifications	Scale
1	PDMS	0B
2	PDMS-O2	5B
3	PDMS-Piranha	2B
4	PDMS-Ammonia	2B
5	PDMS-PDA	0B
6	PDMS-APTES	5B

3.4.2   X-ray Photon Spectroscopy (XPS) Analysis

Successful immobilization of surface groups such as –OH and –NH2 groups on PDMS surface were confirmed using XPS analysis. The XPS spectra of pristine PDMS exhibited a ratio of 1.08 between the Oxygen and Silicon. However, a O:Si ratio of 1.61 was observed for PDMS-O2, indicating that introduction of –OH groups on PDMS and a change in its chemical composition, introducing more oxygen content. The formation of –OH groups on the surface was confirmed by the shift in the binding energy of O1s from 532.3 eV to 533.1 eV. The incorporation of –OH on the surface of PDMS results in the broadening of XPS spectra. The deconvolution of O1s peak of PDMS-O2 suggests that binding energy of oxygen composed of 2 different environment Si-O-Si and Si-OH linkage. The quantification of XPS spectra confirms that 15% of oxygen is present in Si-OH linkages, and allowing these functional groups to interact with SF molecules results in better adhesion as compared to pristine PDMS. The XPS spectra of PDMS-APTES confirms the formation of NH_2 groups on the surface of PDMS surface. The survey scan of PDMS-APTES results in an additional peak at 399.9 eV, which corresponds to Nitrogen element and confirms the immobilization of APTES molecule on the surface of PDMS. The XPS spectra of PDMS-APTES shows 26% of oxygen, 49% carbon, 17% silicon and 7% nitrogen. This corresponds to the elemental composition of APTES molecule. Thus, elemental composition from XPS analysis confirms that immobilization of APTES molecule was successful. The XPS analysis of PDMS, PDMS-O2, PDMS-APTES is summarized in the Table 3.4

Table 3.4: The Elemental composition of PDMS, PDMS-O2, PDMS-APTES surfaces by XPS analysis

Element	PDMS-APTES	PDMS-O2	PDMS
Oxygen	26.38	29.24	27.54
Carbon	49.71	51.5	46.44
Silicon	17.13	18.73	26.01
Nitrogen	6.78		

3.4.3   Surface Morphology of modified PDMS before and after SF coating

The cross-sectional SEM image of the SF coated PDMS samples is summarized in the Figure 3.7. As can be seen from the images, the O_2-PDMS has an SF coating of 350 nm thickness while the APTES-PDMS sample exhibits a coating with a thickness that is more than double of O_2-PDMS. The surface morphology of PDMS after surface modification is also performed using AFM analysis as summarized in Figure 3.6. The surface roughness upon surface modification is quantified by calculating rms roughness on both samples. It can be concluded here that APTES-PDMS shows higher surface roughness with rms roughness of 18 nm, whereas O_2-PDMS shows a smooth textured surface with a rms roughness of 1 nm.

3.4.4   Bradford Assay

The amount of SF on PDMS was quantified using a Bradford assay, and these results have been summarized in Figure 3.8. As can be seen from these results, the amount of SF adsorbed on the APTES-PDMS is the highest. The lowest amount of SF adsorbs on the unmodified PDMS while the O_2-PDMS shows an intermediate adsorption of SF. This progressive change in adsorption of SF can be attributed to the number of interaction sites available on these surfaces for the SF protein to bind. It may therefore be hypothesized here that the modified PDMS offers more interaction sites as compared to the pristine PDMS discs. Also, the APTES-PDMS provides a significantly higher number of molecular sites as compared to O_2-PDMS and hence increases the amount of SF adsorbed. To validate the adhesion between SF and various PDMS substrates, the coated samples were used to perform mechanical tests.
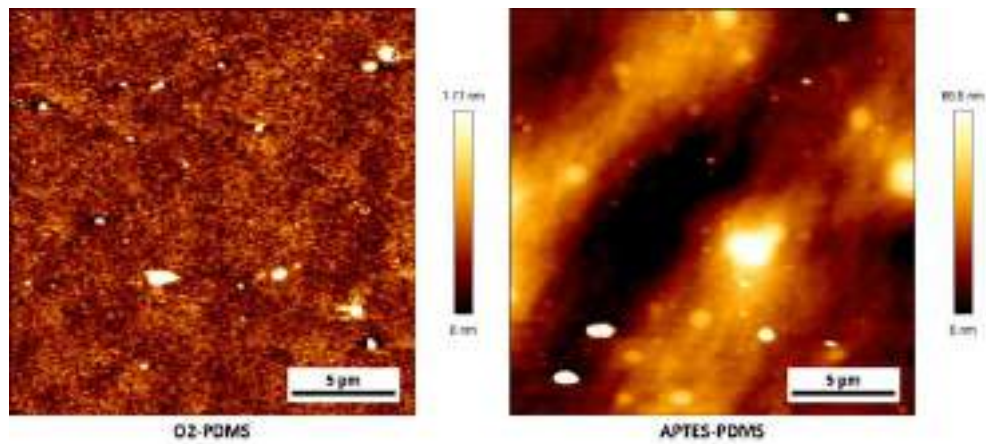
Figure 3.6: AFM images of PDMS surface after (a) O2-PDMS (b) APTES-PDMS
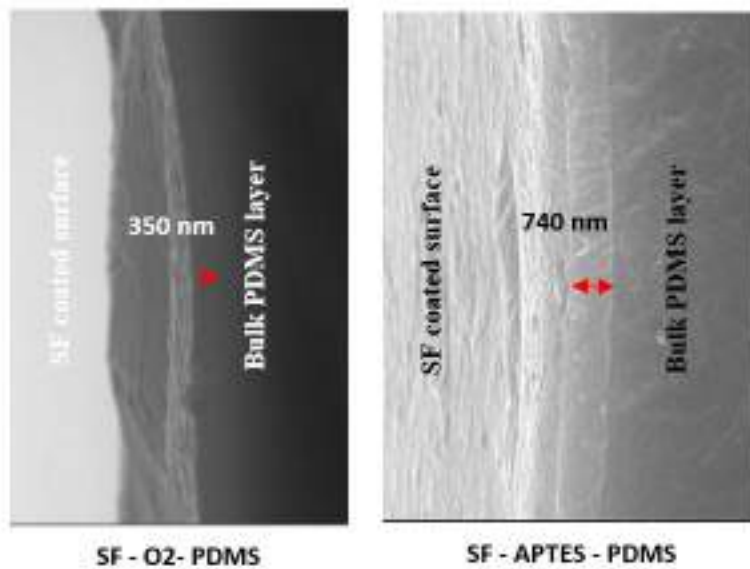
Figure 3.7: SEM cross-sectional micrographs of SF coated PDMS after surface modification
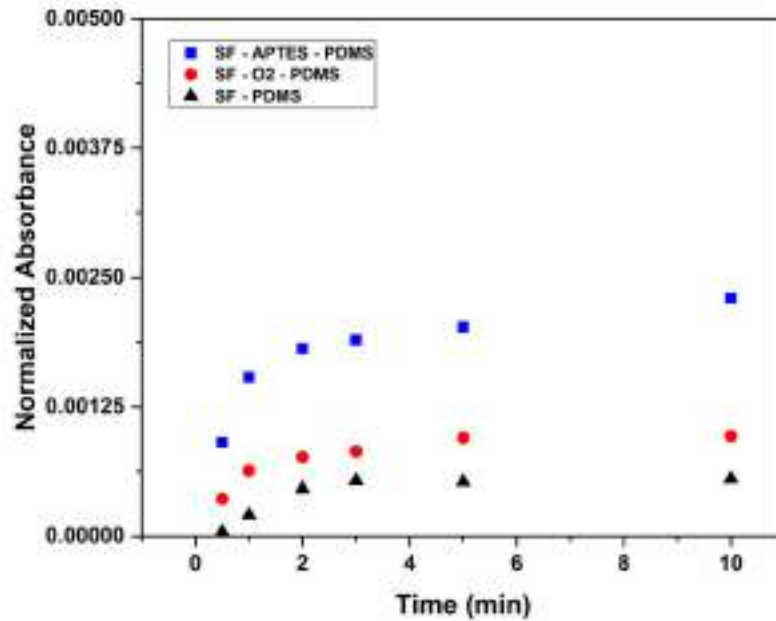
Figure 3.8: Quantification of SF coated onto modified PDMS surface with time using Bradford Assay

3.4.5   Bending and Tensile Analysis

A simple bending test, followed by SEM imaging, was designed to characterize the cracking resistance of the coating on the PDMS implant. A PDMS strip without modification was used as a control. The crack resistance of the coating was measured using 180°bending test as per the protocol described by Borkner *et al.*[12]. The central, 1 cm portion of the PDMS strip was imaged in the SEM. The PDMS sample has a smooth surface before bending test and does not exhibit any crack features even after mechanical deformation. The surface did not exhibit any changes in surface topology after the bending test, and this confirms that development of cracks on the SF coated PDMS is not initiated from the PDMS layer. The SF dip-coated disc also showed a uniform coating with a smooth surface on SF-O2-PDMS and SF-APTES-PDMS samples. However, post the bending test, large visible cracks were seen on the surface of the coating on SF-O2-PDMS discs. A similar test was conducted on recombinant spider silk coating on PDMS by Borkner *et al.*, and they too have observed cracking of the coating, although the cracking reported is not as severe as the one observed here[135]. The density of the crack formed after the 180°bending test shows a considerable
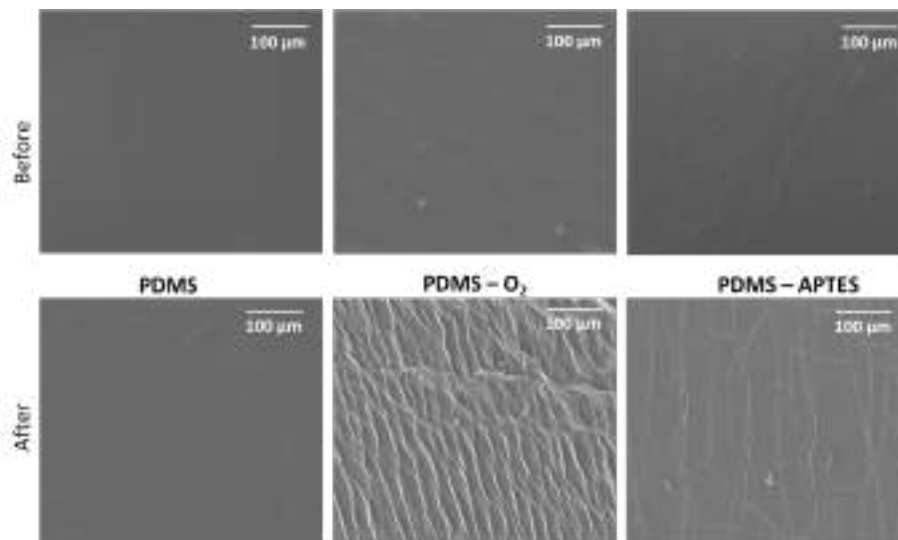
Figure 3.9: SEM images of unmodified and modified PDMS before and after bending test (a & d) PDMS without SF coating (b & e) SF dip-coated on oxygen plasma treated PDMS discs (c & f) SF dip-coated on APTES treated PDMS

difference between SF-O2-PDMS and SF-APTES-PDMS samples. The lower crack density of SF dip-coating after bending test confirms that mechanical stability of surface modification under mechanical deformation is better for SF-APTES-PDMS as compared to SF-O2-PDMS as can be seen from the Figure 3.9. Since the bending deformation can also introduce subjectivity in measurement, a more controlled tensile deformation test was done to validate these observations.

1 mm thick dumb-bell shaped specimens were prepared from the PDMS. These specimens were stretched to 50 and 100% strain at a stretching rate of 50 mm/min using a universal tensile testing machine and SEM images of the central region were recorded after the release of the strain. The schematic representation of tensile measurement is shown in Figure 3.10 (a).

Tensile measurements were performed on SF-O2-PDMS and SF-APTES-PDMS. The SF-APTES-PDMS surface shows lesser crack density as compared to SF-O2-PDMS discs, verifying the earlier data of the bending test. The SF-O2-PDMS shows delamination of the coating at 100% strain whereas few cracks were observed on SF-APTES-PDMS samples, which confirmed that APTES showed improved mechanical stability with SF coating, as shown in Figure 3.10 (b).
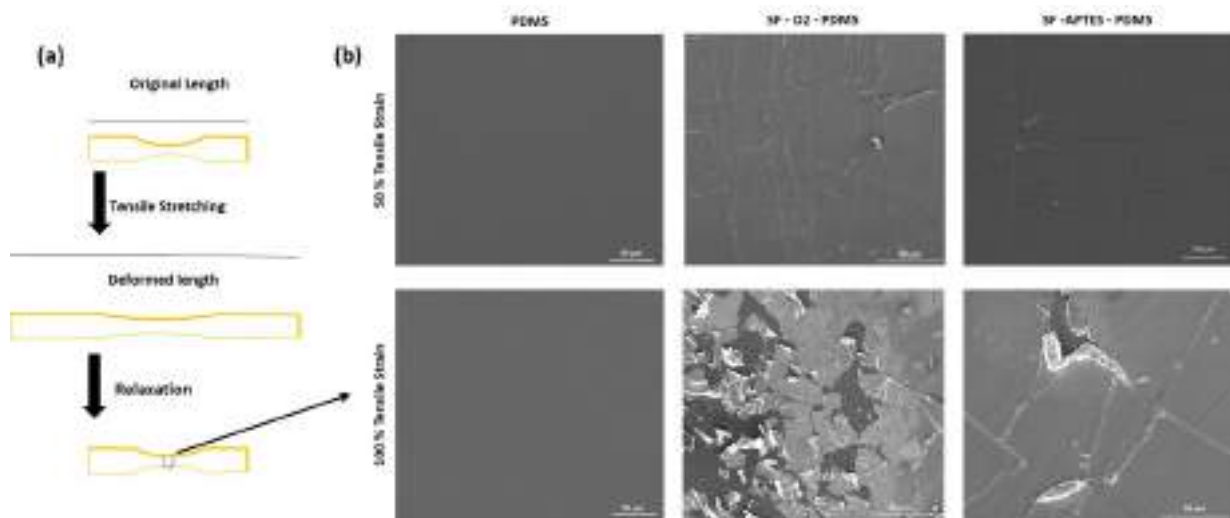
Figure 3.10: (a) Schematic representation of tensile deformation (b) SEM micrographs of SF coated PDMS after surface modification after tensile deformation

From the above bulk mechanical tests, it is clear that the APTES treatment provides better delamination resistance and cracking resistance to the SF coating as compared to oxygen plasma treatment.

3.4.6   Nano Scratch Test

The Nano-scratch test has emerged as a powerful tool to measure the adhesion of the coating to the substrate[136]. The method has been primarily used for metal/polymer coatings on hard substrates. There is no precedent for using this method on soft substrates such as PDMS as the substrate here would experience large scale elastic deformation. The cracking of coating and delamination of the coating are the two phenomena occurring simultaneously while performing nano-scratch tests. The lower load region is responsible for the tensile cracking of the coating, without the delamination of the coating from the substrate. The load at which the tensile cracking of the coating occurs is termed as the first critical load (Lc1). The delamination of the coating will occur at higher load corresponding to the second critical load (Lc2). The nano-scratch test was performed on PDMS, SF-O2-PDMS and SF-APTES-PDMS substrates, with a scanning load of 3μN and a scratch of 1 mm was done. Representative optical micrographs of these tests have been presented in Figure 3.11. For the unmodified PDMS substrate, complete delamination of SF coating was observed, while the SF-O2-PDMS and SF-APTES-PDMS samples showed negligible delamination. Cracks in
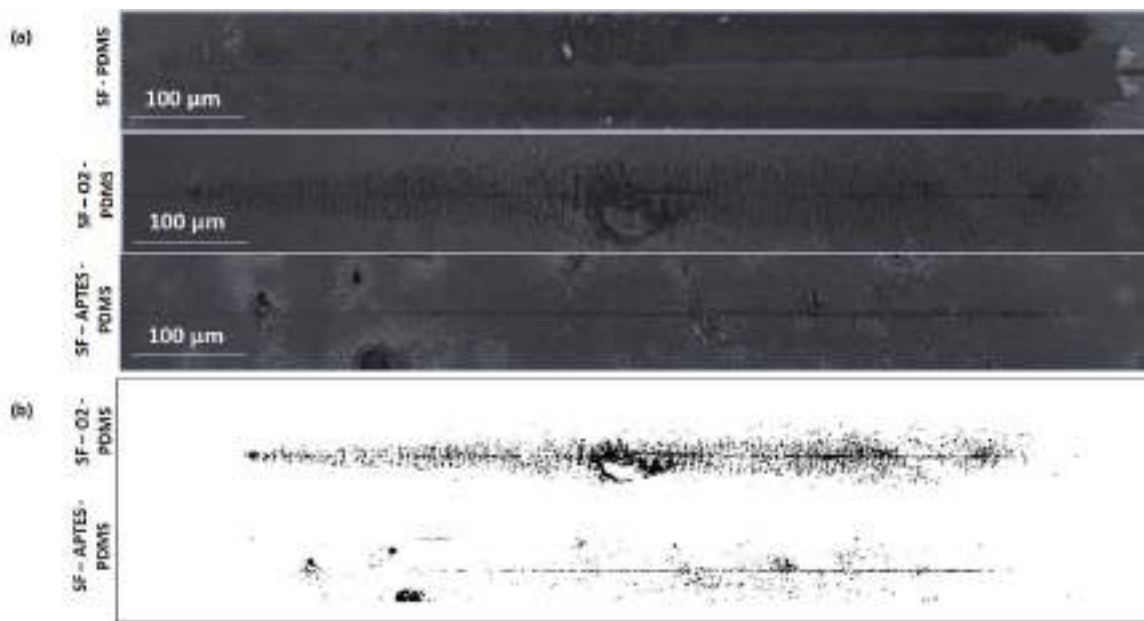
Figure 3.11: Optical images of unmodified and modified SF coated PDMS substrates after nano scratch test showing coating delamination and cracking in unmodified PDMS sample (b) processed images after nano scratch test showing negligible cracking in SF-APTES-PDMS samples

the coating were observed primarily for pristine PDMS and SF-O2-PDMS, and these cracks intensified with increase in the load. The cracks were observed not only on the test track but on a large area surrounding it for these samples. The PDMS showed a very low Lc1 compared to SF-APTES-PDMS and SF-O2-PDMS discs. For bare PDMS Lc1 was 0.9 mN and complete delamination occurred at 9.5 mN. The SF-APTES-PDMS and SF-O2-PDMS showed comparable Lc1 of 5.06 and 4.5 mN, respectively. But SF-APTES-PDMS and SF-O2-PDMS samples did not show any delamination of the coating from the PDMS substrate, and hence a Lc2 value could not be calculated for these samples. The optical images of the PDMS, SF-APTES-PDMS, SF-O2-PDMS are shown in the Figure 3.11 (a) and the amount of crack on the test track, and surrounding regions of both modified samples were determined using Image Processing software MATLAB 2018b by converting the RGB images into pixel points. The results have been summarized in Figure 3.11 (b). It is clear from the processed images that the cracks formed on the SF-APTES-PDMS are drastically less as compared to SF-O2-PDMS. The processed optical images of modified PDMS samples further confirm the results obtained in the bulk mechanical measurements under different tensile strains.
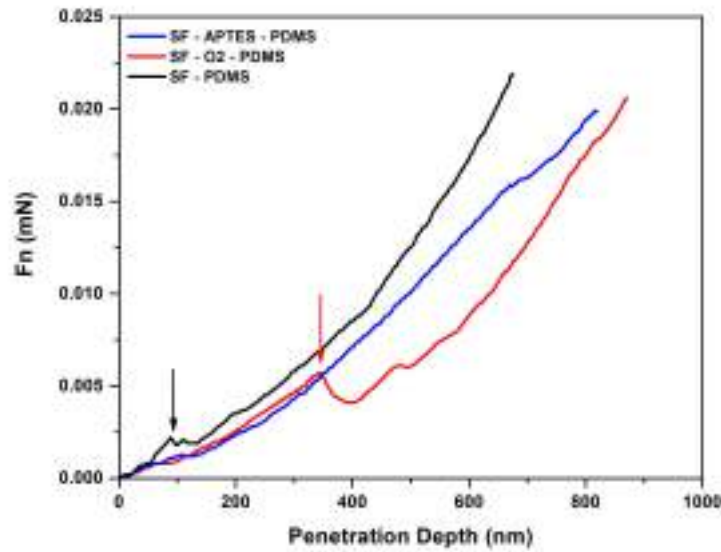
Figure 3.12: Force–displacement curves of the nanoindentation experiments performed on PDMS substrates coated with SF

3.4.7   Nano-Indentation

Nano-indentation is a technique used to characterize the local elastic modulus and hardness of the surface coating. Carroll *et al.* demonstrated the adhesive strength of thermoresponsive polymer coating on nitinol wire[114]. Charitidis *et al.* demonstrated that nano-indentation is used to measure nano-mechanical properties, creep behaviour, and adhesive forces of PDMS[137].

We performed the nano-indentation test using an established method where an indenter tip with a sphero-conical geometry is driven into a specific region of the material to be tested, by applying an incremental normal load. When reaching a predefined maximum load, the normal load was reduced until complete or partial relaxation occurs. This procedure was performed repeatedly, and at each stage of the experiment, the position of the indenter relative to the sample surface was precisely monitored with a differential capacitive sensor. The equipment precisely controlled the load while simultaneously measuring the penetration depth into the material and thus minimized the influence of the substrate on the resulting measurements.

Given the softness of the substrate and thickness of the top coating, the elastic modulus

of the coating/modified layer by itself could not be measured. Testing the coating only would require normal loads below the capabilities of the instrument. The load-displacement curve of unmodified PDMS in the Figure 3.12 shows a rupture at a load of 2 μN and a penetration depth of 100nm. The SF-O2-PDMS showed a slightly tougher coating with a rupture occurring at a load of 5μN and at a penetration depth of 350nm, which also matches with the overall thickness of the SF coating as shown in Figure 3.7 (a). This means that the rupture occurs at the SF-PDMS interface indicating poor adhesion between the SF coating and the O2-PDMS surface. A similar observation can also be made for the SF-PDMS sample, that has less than half of the coating thickness as compared to the SF-O2-PDMS sample. The SF-APTES-PDMS did not exhibit a rupture even at loads as high as 20μN. A mild change in slope is observed for this sample at 15μN and a penetration depth ranging from 650-750 nm. Here, too it must be noted that the coating has a thickness of 750 nm, as shown in Figure 3.7 (b). These results indicate that the SF-APTES-PDMS sample has an interface that exhibits excellent adhesion between the SF coated layer and the APTES-PDMS surface. The interface helps in efficient dissipation of the loads and prevents cracking and delamination of the nano-coating. These findings are in agreement with higher adsorption of SF on the APTES-PDMS substrate and improved crack resistance observed in the bulk tensile measurements and the nano-scratch test results reported earlier in Figure 3.11. This is in agreement with literature that the adsorption of fluorescently tagged protein molecules on APTES treated shows higher fluorescence intensity as compared to oxygen plasma treated PDMS samples[138].

3.4.8   Atomic Force Microscopy - Force Spectroscopy

From the macroscopic as well as microscopic tests, we conclude that the SF coating on APTES-PDMS is mechanically much more robust compared to SF coating on O2-PDMS substrates. It yields at much higher shear and normal stresses compared to SF coating on O2-PDMS. In the following, we address the molecular origin of robustness of SF on APTES-PDMS compared to the O2-PDMS using force spectroscopy experiments which is capable of measuring strengths of individual bonds in both chemistry and biology[139]. One of the challenges in using Atomic Force Microscopy methods is that the PDMS is an elastomer and deforms easily when surfaces are made to separate from each other. By carefully separating
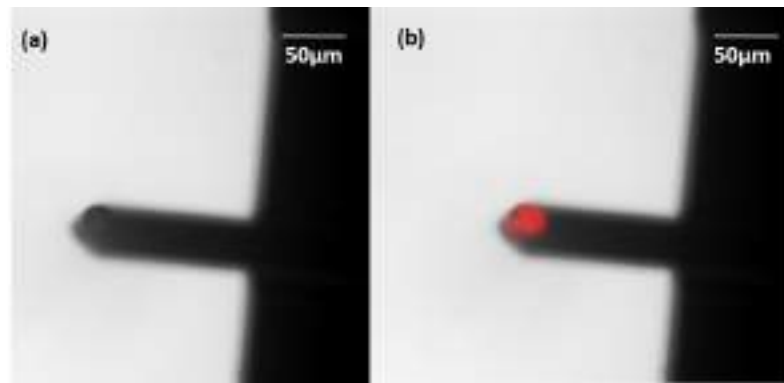
Figure 3.13: Fluorescence images (a) without and (b) with Rhodamine loaded silk fibroin coatings on glass beads attached to the cantilever confirms the presence of silk fibroin

the effects arising from this phenomenon, we were able to measure the adhesion energies required to separate the nano-scale contacts formed between the SF coated glass surface and the APTES-PDMS substrate. The 20 µm glass beads attached to a tipless AFM cantilevers are coated with SF. The glass beads are allowed to form contact with O2-PDMS as well as APTES-PDMS with help of servo-control in the AFM. The bead is then pulled away, and adhesive energy between surfaces is measured by recording the substrate movement and cantilever deflection. Figure 3.14 (a) shows a typical force curve with approach and retract of the entire process. The APTES-PDMS substrate is pressed with the bead with nN load, and then it is pulled away. The binding sites of SF and APTES-PDMS bends the cantilever downwards as the elastomer deforms to form a neck. The neck then relaxes, and the cantilever is almost in its zero-force equilibrium position. The further pulling of the substrate breaks these bonds sequentially, as seen in the schematic shown in the inset of Figure 3.14 (a). The process appears very similar to unfolding of protein domains observed using AFM. Here the SF chains are likely getting unraveled before the bonds are broken. In this force curve, the hysteresis caused by the plastic deformation of PDMS bulk largely dominates the measurement. The energy lost in forming the neck and its relaxation is much higher compared to the bond energies. In short, the energy required to break these bonds and separate these two surfaces is overwhelmed by the deformation of PDMS bulk. In Figure 3.14 (b) and (c), we remove the approach curve and part of the retract which is attributed to the formation and relaxation of the PDMS neck. The control experiment is performed using a bead without SF coating on it. In Figure 3.14 (b), the O2-PDMS substrate and SF

coated bead are pulled away from each other. The control (bead without SF) and SF coated bead show similar force curves and the bond breaking events are not significantly different. In figure 3.14 (c), we show force curves depicting separation of the bead and APTES-PDMS. There is a striking difference between O2-PDMS and APTES-PDMS adhesion to the SF-coated glass bead. There are multiple (10) bond breaking events. These bonds cost more energy to separate the SF-coated glass bead from APTES-PDMS compared to O2-PDMS. Figure 3.14 (d) shows energies required to separate SF coated glass bead from APTES-PDMS and O2-PDMS along with controls. The cost of energy for separating APTES-PDMS and O2-PDMS from SF-coated bead is $1.0 \pm 0.04 *10^{-1}5$ and $4.1 \pm 0.3 * 10^{-1}6$ J respectively. The adhesive strength of SF to APTES treated PDMS is 10 times more compared to O2-PDMS due to higher number of molecular linkages formed in this nano-scale contact. Force Spectroscopy experiments are also able to identify breaking of these discrete molecular bonds formed between the amine groups on APTES-PDMS and the SF on the glass beads. The end part of force displacement curve of force spectroscopy measurement is summarized in Figure 3.15

To summarizes, in this Chapter, we have measured the adhesion of SF nano-coatings on PDMS surfaces and have demonstrated using various techniques the mechanical and adhesive properties of these coatings. Our work confirms that APTES modification significantly improves the adhesion and mechanical performance of natural polymer coatings on PDMS as compared to only oxygen plasma treatment. Spectroscopic measurements using Infrared spectroscopy have confirmed that APTES treatment results in a surface that has amine functionalities, while the oxygen plasma produces a surface with hydroxyl groups as validated by the XPS measurement. The oxygen plasma treatment improves the hydrophilicity of the PDMS substrate only to a limited extent reducing the contact angle to 55±3°. Contrary to this, when a drop of water is placed on the APTES-PDMS substrate, the drop spreads completely, indicating a contact angle less than 10°. This implies that the APTES-PDMS treatment more effectively modifies the PDMS substrate. Further, the amount of SF protein attached to the APTES-PDMS substrate was also found to be at least two times that observed for O2-PDMS substrate, resulting in a coating that is double the thickness as compared to O2-PDMS. A bulk technique like peel test could not differenti-
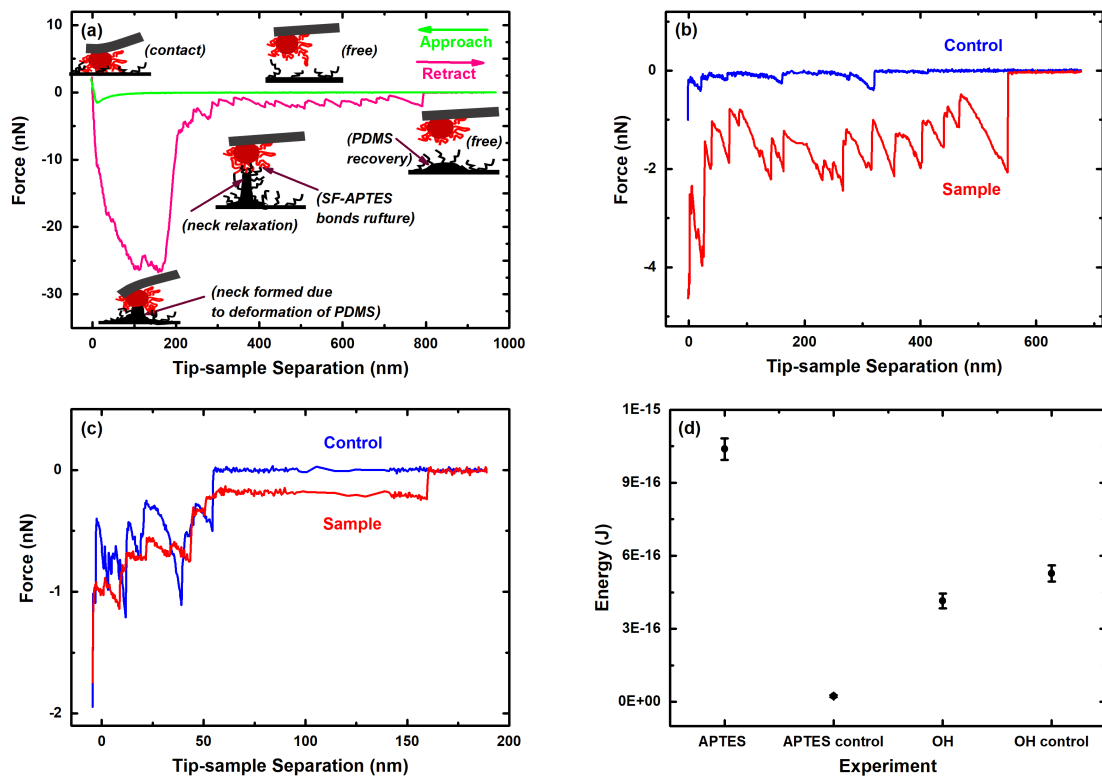
Figure 3.14: Figure 15:a) A typical force curve showing molecular level interaction of SF to PDMS surface modified with APTES treatment. A 20 um bead coated with SF is attached to a tipless AFM cantilever. The bead is lowered onto the APTES-PDMS substrate. The SF on the bead is shown in red and amine groups on the APTES-PDMS are shown in black. After the contact, the substrate is loaded slightly. The SF and amine groups on APTES-PDMS substrate form semi-covalent bonds and the bead is tightly adhered to the substrate. The cantilever is then pulled away leading to deformation in PDMS and formation of a neck. The neck is relaxed as the cantilever is pulled further away and the cantilever attains a near-equilibrium position. Finally, the individual bonds between the amine groups and SF break sequentially to produce a sawtooth-like pattern typically seen in protein unfolding experiments. The bead leaves the PDMS surface and the cantilever attains zero-force equilibrium position. (b-c) We remove part of the retract curve related to the deformation caused in the bulk of PDMS and focus on molecular-level interactions of SF with O2-PDMS and APTES-PDMS surface. The blue curves show control experiments wherein the glass bead is not coated with SF. The number of bonds formed between SF coated glass bead and O2-PDMS do not show a significant deviation from the control (glass bead without SF coating). In the case of APTES-PDMS there are considerably more number of bond-breaking events compared to control or O2-PDMS. These bonds between SF and amine groups require a much larger energy to separate the SF coated surface and the APTES-PDMS substrate. (d) The energy required to separate the SF coated surface from O2- PDMS and APTES-PDMS substrates along with controls. The number of force curves for each case were 200. The control experiments were performed with 30 force curves . The bars represent standard error. The energy needed to separate SF coated surface from APTES-PDMS surface is $1.0 \pm 0.04*10^{-1}5$ J and O2-PDMS surface is $4.1 \pm 0.3*10^{-1}6$ J
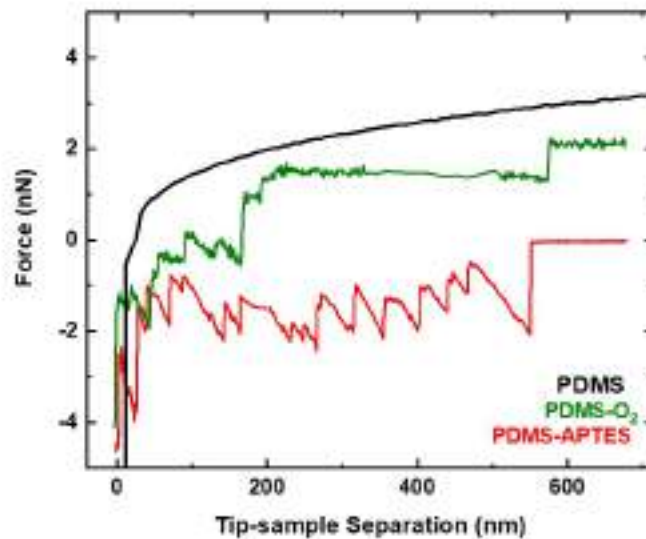
h!

Figure 3.15: Zoomed Force displacement curve showing molecular level interaction of SF to unmodified and modified PDMS

ate between the adhesion of SF protein to the O2-PDMS and APTES-PDMS treatment, most likely due to the deformation of the underlying elastomeric PDMS substrate. However, when these coated surfaces were subjected to tensile and bending deformation, the SF coating on APTES-PDMS was found to be more resistant to cracking and failure as compared to the O2-PDMS substrate. These observations were further validated in the nano-scratch and nano-indentation measurements. The optical micrograph of the Nano-scratch clearly showed increased cracking for the O2-PDMS substrate as compared to the APTES-PDMS sample. The nano-indentation measurement also showed a rupture at 5μN for the O2-PDMS substrate whereas the APTES-PDMS substrate did not exhibit any rupture even at loads as high as 20μN. These techniques further corroborated the findings of bulk mechanical measurements at a microscopic and mesoscopic length scale and validated the superior performance of the APTES-PDMS substrate. At the molecular level, the Atomic Force Microscopic technique showed that SF protein forms a higher number of molecular linkages with the APTES-PDMS surface as compared to the O2-PDMS surface. This improves the adhesion of the SF protein to the APTES-PDMS substrate. This is in agreement with the improved hydrophilicity and higher SF protein adsorption for APTES-PDMS surface, as discussed earlier.

Correlating the adhesive and nano-mechanical performance of these coatings it can therefore be concluded that APTES modification results in a more crack-resistant coating on the PDMS substrate as compared to an oxygen plasma modified surface due to improved adhesion between the coating and the substrate. Thus, APTES modification must be used to modify the surface for implants to improve their performance and reduce the rate of failure both during handling before surgery and also during use. This chemical modification strategy will help in development of improved implants with reduced risks of failure.

3.5   Conclusion

Surface coating of implants using natural protein polymers has emerged as a promising strategy to reduce the failure rate of implants. PDMS is a commonly used hydrophobic polymer for biomedical implants, and surface coated PDMS implants frequently face problems such as delamination or cracking of the coating, as discussed in the Section 3.2. In this Chapter, we evaluated the adhesion of SF coatings on PDMS surfaces that were modified using various physical and chemical treatment. At a macroscopic length scale, using conventional tensile and bending deformation, we demonstrated that the APTES treated PDMS surface shows enhanced crack resistance as compared to oxygen plasma treated PDMS surface. In both nanoindentation and nanoscratch tests, these observations were further validated, and we showed that cracking was minimal in the nanoscratch test for APTES-PDMS sample. In the nano-indentation measurements also no rupture was observed for the APTES-PDMS sample upto 20μN loads, whereas the O2-PDMS sample showed a rupture at loads as low as 5μN. This improved performance can be attributed to the higher number of molecular linkages formed between the SF protein and the APTES-PDMS substrate was shown in the Atomic Force Microscopy measurements. These increased molecular linkages result in better adhesion of SF protein to the PDMS substrate and this improved adhesion enhances the delamination and crack resistance of the nano-coatings. Therefore, this chemical modification strategy will assist in development of coated medical devices and implants, which in turn will mitigate the risk of coating delamination and medical device failure.

Chapter 4

Crack-resistant SF coatings on PDMS
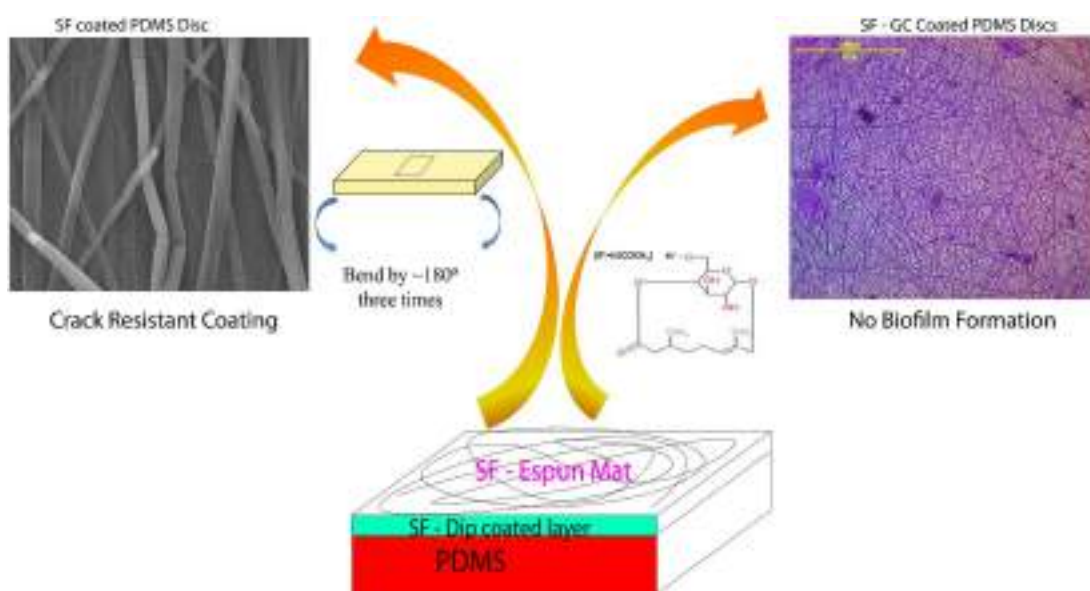
The content of this Chapter is published in, "*ACS Appl. Bio Mater. 2019, 2, 675-684*".
(Reproduced with permission from American Chemical Society)

Glycomonoterpene-Functionalized Crack-Resistant Biocompatible Silk Fibroin Coatings
for Biomedical Implants

Emmanuel Joseph, Amrita Patil, Swarali Hirlekar, Abhijit Shete, Nimisha Parekh,
Asmita Prabhune,* and Anuya Nisal*

4.1   Abstract

Surface coatings for biomedical implants have been used to prevent premature failure of implant due to bacterial biofilm formation and foreign body reaction. Delamination, cracking, crazing, etc., are frequent problems associated with coatings when implants are subjected to mechanical deformation either during surgical handling or during use. We demonstrate here, a novel process that results in the formation of a coating that is stable under mechanical stresses in tensile, torsion and bending modes. The coating process involves a combination of two conventional coating processes – namely dip coating and electro-spinning. Poly-dimethylsiloxane was selected as the substrate owing to its wide use in biomedical implants. Silk fibroin, a natural biocompatible protein polymer obtained from Bombyx mori silkworm, was used for demonstrating the process of coating. The coating was also further functionalized using a green biomolecule - glycomonoterpene prepared using citronellal and glucose. These functional compounds are being touted as the next generation antibiofilm molecules on account of quorum sensing inhibitory activity. We have demonstrated that the quorum quenching activity of the biomolecule is retained during the processing steps and the coatings exhibited excellent antibiofilm activity against common infection causing bacterium *P. aeruginosa* and *S. epidermidis.* These silk fibroin-glycomonoterpene coatings can be used for implants in biomedical applications such as breast implants and catheter tubings.

This Chapter begins with literature review that outlines the problems associated with surface coatings on silicone implants and failure mechanisms of silicone implants. Sections 4.2 discusses the unaddressed questions in the literature and describe the motivation and objectives of the present work. Section 4.4 provides detailed information about the experimental methods and material used. The Section 4.5 summarizes the key results and discussion of the present study. Section 4.6 concludes the Chapter.

4.2   Literature Review

Implantable medical devices are increasingly being used to diagnose, treat, cure a severe medical condition or repair and regenerate a damaged tissue. The failure of these implants has primarily been attributed to two factors - device-associated infection and foreign body

response[4]. More than 25% of the hospital-acquired infections (HAI) are directly linked to the implanted device, for example, in urinary catheters or even joint replacement procedures[140]–[142]. Biofilms have found to be a dominant problem in these infections[141]. Also, considering these scenarios and their consequences, surgeons frequently resort to oral doses of antibiotics during implantation in a patient. However, this has added and fuelled to the global problem of antibiotic resistance. The second most common reason for failure of implants is the foreign body reaction. Capsular contracture or implant failure due to fibrotic capsule formation has been reported in atleast 15-30% of the breast reconstruction and augmentation surgeries[42].

One of the approaches to solving both these problems is surface modification of the existing implant materials, as the inherent bulk properties of the implant remain unaltered. Surface coatings are, therefore, a rapidly evolving field[143]. There have also been recent efforts to modify the surface of the silicone breast implants using biocompatible polymers[11], [144], [145]. However, problems related to flaking, delamination, cracking and crazing of coatings are still an issue. Recently, FDA recalled polytetrafluoroethylene coated guidewires as separation of the coating may cause serious injuries to the patient both due to migration of coating to other body parts and exposure of underlying medical device surface which could trigger other undesirable events such as blood clots[112]. Researchers have also reported microcracks in coatings especially when subjected to mechanical deformation[12]. The failure of coatings may be attributed the mechanical stresses imposed on the implants due to handling either during manufacture and packaging and/or also during surgical intervention by the medical practitioners[135]. Some coatings may also fail after implantation as catheter tubes, for example, experience a variety of bending/tensile stresses when in use. Thus, it is an objective of this work to develop a novel process to form a stable coating on an elastomeric substrate such that the coating retains its integrity when subjected to mechanical deformation in tensile, bending or torsion modes while enhancing the biocompatibility of the implant surface. Medical grade PDMS is chosen as the substrate for this study as PDMS is extensively used in several medical devices such as breast implants and catheter on account of its easy processability into different shapes, ability to tune mechanical properties and biocompatibility[42], [140]. Natural silk fibroin (SF) obtained from *Bombyx mori* silkworm is chosen as the material for coating application. SF has emerged as a promising biomaterial on

account of easy availability, proven biocompatibility, biodegradability and aqueous process-ability[16]–[18]. Various techniques have been used to deposit SF coatings on both polymer as well as metal scaffolds[146]–[148]. However, the mechanical properties of the coating and its ability to resist mechanical deformation has not been quantified and studied. In this work, we demonstrate a novel sequential dip and electrospinning technique that results in an SF coating that is stable under tensile, torsion and bending loads.

As mentioned in the Section 2.2, antibiotic treatments for implant associated infections are leading to development of resistance in many pathogens. However, unlike antibiotics quorum sensing inhibiting molecules (QSI) do not put selective pressure by killing bacterial cells instead inhibit biofilm formation and pathogenesis by interrupting QS i.e. cell to cell communication. Therefore, bacteria are less likely to develop resistance to quorum sensing inhibitors in the future[149]. Along with this, upon administration of QSI the cells remain in planktonic form and they are available to be killed by phagocytic cells in the body, without affecting the normal flora. This also avoids infections by opportunistic pathogens and justifies QSIs as next generation molecules[150]. Thus, in present work we demonstrate the incorporation of a QSI biomolecule – G-citron (GC) to inhibit the bacterial biofilm formation on implants. GC is biosynthesized from citronellal and glucose by a non-pathogenic yeast *Candida bombicola.* GC molecule is considered to be a green molecule due to its biosynthesis and biodegradability. Citronellal was particularly chosen as a substrate for bio-modification, because it is a major component of many easily available essential oils. The modification with glucose results in a molecule with improved hydrophilicity and hence enhances its bioavailability[151]. Thus, it is an objective of this work to provide an innovative solution to simultaneously resolve multiple causes for failures of implant devices – biofilm formation, foreign body response and cracking/delamination of the coating.

4.3   Motivation and Objectives

Surface coatings is one of the promising strategy to improve the biocompatibility of silicone devices, as discussed in the Section 2.5.3. However, Spider silk coated PDMS under mechanical deformation results in microcracks on the coatings[12]. As shown in the Section 3.4, SF coatings on modified PDMS substrate also results in microcracks on the coatings under

mechanical deformation; however, density of microcracks have reduced on modified PDMS substrate. Thus, there is a need of alternative coating strategy to enhance the mechanical stability and crack resistance of the coatings on silicone substrate. Secondly, post implantation studies on patients demonstrated that one of the reason for implant failure was biofilm formation around the implant. Several strategies have been reported in the literature to prevent biofilm formation and implant failure. The advantage of surface coatings is that enhanced biocompatibility and antibacterial activity can be achieved simultaneously using functional molecules.

Thus, the objective of this part of the work was

- Development of a novel strategy to reduce cracking of coatings under mechanical loadings

- Use a novel molecule and evaluate the performance of coatings for antibacterial activity

4.4   Materials and Methods

4.4.1   Preparation of PDMS Discs

Medical grade PDMS (Sylgard 184, Dow Corning) was cast on polystyrene petridishes to obtain a disc with a uniform thickness of 1 mm. The prepolymer was thoroughly mixed with the curing agent for 5 minutes using a weight ratio of 10:1. It was then poured into the petridish and degassed for 30 minutes. This mixture was kept in a convection oven at 40°C for 24h. Circular PDMS discs of required diameters were then cut out and used for further experimentation. A cleaning process of 30 minutes sonication in isopropyl alcohol was followed to remove dust particles before further experimentation. This process of cleaning was followed by a drying step under vacuum at 60°C for 4h to remove any traces of the IPA solvent.

4.4.2   Oxygen plasma treatment

The plasma treatment was done on both sides of the PDMS disc using Emitech 1050 plasma unit. The chambers were initially purged for 15 minutes with oxygen gas. The optimized plasma conditions of 50W RF power and 1 minute time duration were determined by mea-

suring the contact angle on the surface and confirming no physical damage to the PDMS disc surface using optical microscopy. The plasma-treated discs were stored under DI water for a maximum of 1 week, before use for further experimentation. XPS spectra after one week of plasma treatment confirms the formation of stable –OH groups as shown in Figure 3.1.

4.4.3   Preparation of SF solution

The silk fibroin solution was prepared from *Bombyx mori* silkworm cocoons obtained from Central Sericultural Research and Training Institute, Mysore, as per the protocol described elsewhere[133]. Briefly, the cocoons were degummed using 0.5wt% sodium bicarbonate (NaHCO3) solution to remove the sericin protein. The dissolution of the cottony mass of fibroin fibers was done using a chaotropic salt Lithium Bromide (LiBr) at 60°C for 4h. The salt was then extensively dialysed out to obtain regenerated silk fibroin (RSF) solution with approximately 3-5 w/v% concentration. The RSF solution was then lyophilized at -55°C to obtain SF powder. This powder was stored at -20°C until further use. The powder was dissolved in Hexafluoroisopropanol (HFIP) at room temperature to obtain a 5 wt/v% solution, and this solution was then used for electrospinning[14].

4.4.4   Preparation of SF coating

The plasma-treated PDMS disc was used for coating experiments with SF. The RSF solution was diluted to 0.4 w/v% using DI water. The disc was immersed in this solution for 10 minutes to obtain a uniform SF coating. The PDMS disc was later air dried at room temperature and methanol vapor annealed as per the protocol described below. This SF coated PDMS disc is further referred to as the "SF-D disc". In another experiment, the PDMS disc was taken out of the SF solution and immediately mounted onto the collector plate of an electrospinning apparatus before drying. The electrospinning was done using 5 w/v% SF/HFIP solution as shown in Figure 4.1. The tip to collector plate distance was maintained at 10.5 cm and a voltage of 30 KV with a flow rate of 1 ml/h was used for electrospinning. After electrospinning, the discs were kept for drying at 40°C for 12 h to remove traces of the solvent. This was followed with a methanol vapor annealing treatment to introduce stable beta sheet conformation in the protein. The coated discs
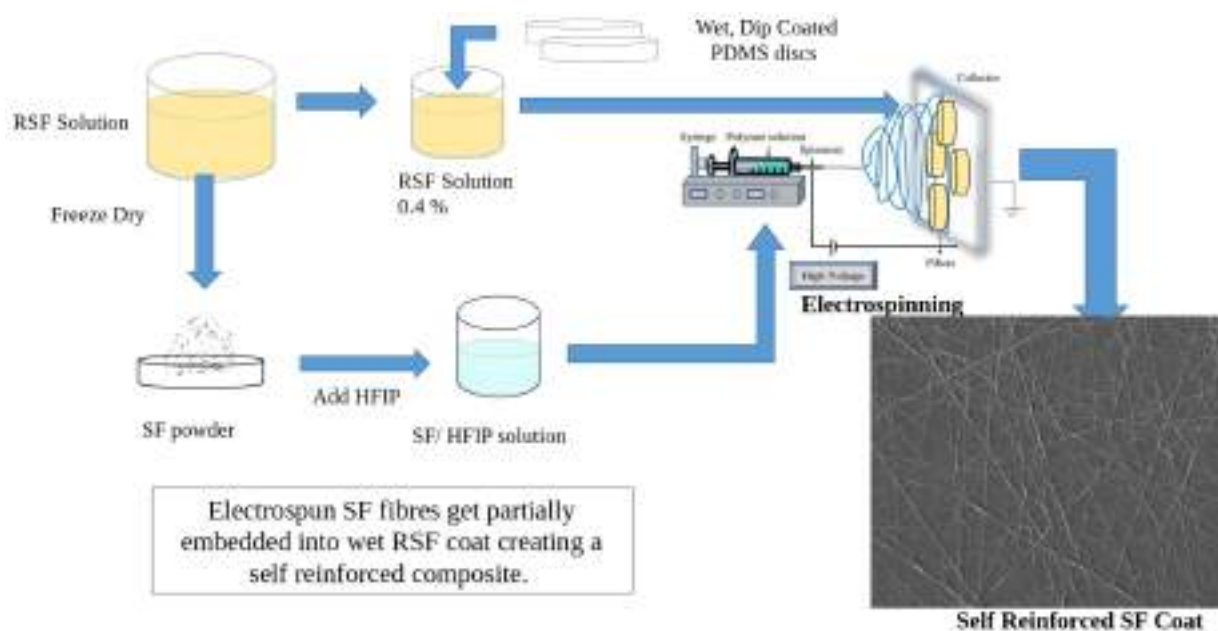
Figure 4.1: Schematic representation of the process innovation for coating of SF on PDMS discs

were incubated in a saturated methanol vapor closed chamber for 48h at room temperature. Further characterization was done after this treatment. These discs are further referred to as SF-DES (Dip + Electrospinning).The GC molecule was kindly gifted by Dr Ashmita Prabhune from Biochenical Division, CSIR-NCL. Also, blends of SF and GC (preparation described later) were made in 1:3 ratios to form 5 wt/v% solution in HFIP. This solution was then electrospun on the SF dip-coated PDMS disc, and these discs are further referred to as SFGC-DES.

4.4.5   Fourier Transform Infrared (FTIR) Spectroscopy

The uncoated and coated discs, before and after methanol treatment, were characterized using ATR-FTIR Perkin Elmer Q5000 Spectrum GX spectrophotometer equipped with a diamond crystal probe detector. Refer section 3.3.5

4.4.6   Contact Angle Measurement

The modification of PDMS and their coating was confirmed by 4μl stable sessile drop of DI water. The equilibrium contact angle was reported as the average of at least four measurements for each modification.

4.4.7   Scanning Electron Microscopy

The surface and cross-sectional morphology of the coated/uncoated PDMS discs was observed using scanning electron microscope (SEM) - Quanta 200 3D from FEI. Refer section 3.3.9

4.4.8   Atomic Force Microscopy

The surface topography of the uncoated/coated PDMS discs was performed in ambient conditions in tapping mode for a 40μm x 40μm area with a scanning probe microscope (JPK, NanoWizard II). Silicon cantilevers with a spring constant k of 60 N/m were used to perform experiments. The cantilever was oscillated at its free resonance frequency (250 - 350 kHz).

4.4.9   Aqueous stability of the coating

The aqueous stability of the SF-DES discs was determined by keeping the coated discs immersed in Phosphate Buffered Saline (PBS) solution for seven days at 37°C and UV-vis spectroscopy was done on the PBS solution to measure the amount of SF released at predefined time points. The concentration of SF released into PBS was estimated by recording the absorbance at 275 nm and using a Beer Lambert coefficient of 11.8 mol/L/cm. The experiment was carried out in triplicates.

4.4.10   Mechanical stability of the coating

The crack resistance of the coating was measured using 180°bending test with a rectangular block of 1cm x 3cm x 0.1 cm (thickness) as per the protocol described by Borkner *et al.*[12]. Refer section 3.3.12

4.4.11   Anti-quorum sensing activity of SF and GC coated PDMS discs

P. aeruginosa is one of the predominantly isolated pathogenic organisms from infected implants and it produces 3-oxo C12 HSL (long chain AHL molecule) therefore to assess inhibition of quorum sensing, we have used a reporter strain *E coli* pSB1142(a kind gift from Dr. Paul Williams, University of Nottingham) which exhibits luminescence in response to only

long-chain AHL molecules (C10-C14)). It was grown in Luria-Bertani (LB) medium supplemented with 10μg/ml tetracycline (Sigma Aldrich, India) at 37°C. SF-DES and SFGC-DES discs were dipped in PBS for 24h for releasing the active compound (GC), and anti-QS activity of released compound was checked using *E.coli* pSB1142 as per method described elsewhere[152]. Overnight grown culture of *E.coli* pSB1142 (OD 600nm: 0.1) was incubated along with GC released in PBS and 0.1 μg/ml of signal molecule (3-oxo-C12-HSL) (Sigma Aldrich, India). Reporter strain with and without signal molecule was considered as a positive and a negative control, respectively. All experimental sets were incubated at 37°C at 180 rpm for 6h. Luminescence was measured using micro plate reader (Spectra Max MSe molecular devices) and reported as relative light unit (RLU) normalized with OD at 600nm. Experiments were performed in triplicates, and percentage of (RLU/OD600) inhibition was calculated by using the formula:

$$
\%Luminsence\ inhibition(RLU/OD_{600}) =
$$
$$
(RLU/OD_{600})_{Positive\ control} - (RLU/OD_{600})_{test} * 100/(RLU/OD_{600})_{Positive\ control}
$$

(4.1)

4.4.12   Anti-biofilm activity of SF and SF-GC coated PDMS discs

Staphylococcus epidermidis and *Pseudomonas aeruginosa* are often associated with infections of implanted medical devices. And both organisms have high rates of antibiotic resistance due to their biofilm forming ability, which is one of the phenotypes mediated through quorum sensing. Therefore, the anti-biofilm activity of the uncoated/coated PDMS disc was evaluated using *P. aeruginosa* (NCIM 5029) and *S. epidermidis* (NCIM 5270) as test organisms. Initially, overnight grown cultures of *P. aeruginosa* and *S. epidermidis* were subcultured to petri plates (30 mm diameter) containing 2ml LB medium (OD600 nm was adjusted to 0.1). SF-DES and SFGC-DES PDMS discs were then added to these petriplates. After incubation of the plates for 24h at 37°C, biofilms formed on the discs were subjected to crystal violet staining. The stained biofilm was then visualized under light microscope at 400x magnification[151]. Biofilm formed on the PDMS discs were also visualized by SEM. For quantitative evaluation of anti-biofilm activity, the crystal violet stain was extracted from the discs using

30% acetic acid. OD of the extracted crystal violet was measured at 580 nm.

4.4.13   *In-vitro* cell proliferation and cytotoxicity study

L929 is a mouse fibroblast cell-line. It is recommended by ISO 10993 as the preferred cell-line for preliminary cytotoxicity testing of biomaterials. L929 (Purchased from NCCS, Pune, Maharashtra, India) mouse fibroblast cells were seeded on coated/uncoated PDMS discs in a 96 well flat bottomed non-adherent plate at a density of 5x103 cells/disc in 10µL of DMEM (Invitrogen) containing 10% FBS (Invitrogen). The plate was incubated at 37°C with 5% CO_2 for 10 minutes that allows the cells to settle on the scaffold, followed by the addtion of 250μL of DMEM with 10% FBS and further incubated. During incubation, on the 1st, 5th and 7th day, the media was replaced with filter sterilized MTT (3-(4, 5-dimethylthiazol-2-yl)-2, 5-diphenyltetrazolium bromide) (0.45 mg/mL) (Invitrogen) prepared in DMEM containing 10% FBS and incubated for 4h at 37°C with 5% CO_2. At the end of incubation, MTT was aspirated from the well and DMSO 200 μL/well was added to dissolve insoluble formazan crystals followed by incubation at 37ºC with 5% CO_2 for 10 minutes. The absorbance was measured at 550 nm using a microtitre plate reader (Multiskan EX, Thermo Scientific). Each absorbance was taken to be the mean of triplicate measurements.

4.4.14   Statistical analysis

Experiments were performed in triplicates, and the data obtained from the experiments were represented in the graph as mean ±standard deviation values. To determine significant differences from the control Tukey's Multiple Comparison Test was performed by using Graph pad prism 5 software.

4.5   RESULTS AND DISCUSSIONS

4.5.1   Formation and characterization of coating

PDMS is a polymer routinely used in a variety of biomedical devices and implants. PDMS implants are frequently coated with functional molecules/polymers to improve biocompatibility, add lubricity or antimicrobial functionality to the surface. The first Section of the Chapter 4, therefore, deals with development of a process to prepare a crack-resistant coat of
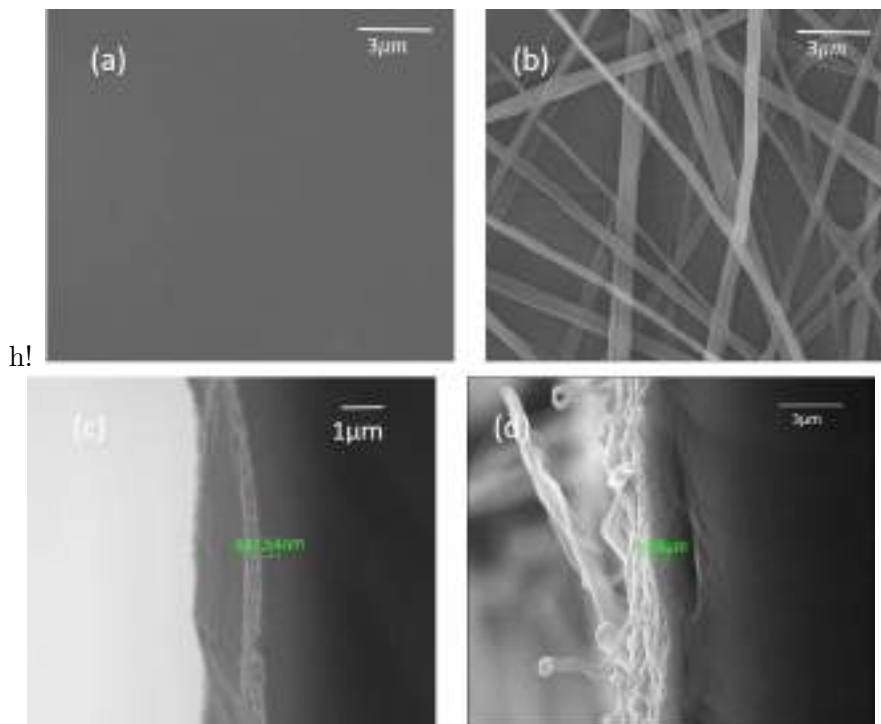
Figure 4.2: The SEM images of coatings (a) SF-D (b) SF –DES and cross section images of coatings (c) SF-D (d) SF-DES

SF on PDMS. Dip coating was the obvious first choice of process owing to the simplicity of the process. Figure 4.2 (a) shows the image of oxygen plasma treated PDMS substrate after dip coating with SF (Sample abbreviation: SF-D) and the cross-sectional image (Figure 4.2 (c)) confirms that the coating has a thickness of the order of 400-500nm. Dip coating of thin layers (<10nm) of SF on quartz substrates has been demonstrated earlier[148]. However, these coatings are too thin to achieve a sustained or prolonged release of a functional drug molecule, and the researchers later proposed another method of using silk barrier layer to suppress the initial burst release of functional molecule[153]. Thicker coatings typically will have poor cracking resistance under mechanical deformation. The authors did not comment on the mechanical stability of the coating, rightly so, considering that the substrate used here was a rigid quartz slide. However, when an elastomeric substrate like PDMS is coated with a thick layer of polymer like SF, it is necessary to understand the effect of mechanical deformation of the substrate on the coating. Thus, to improve the stability of coatings under mechanical deformation, an innovative coating process was used here. A combination of two conventional processing protocols - dip coating and electrospinning - was combined to form a
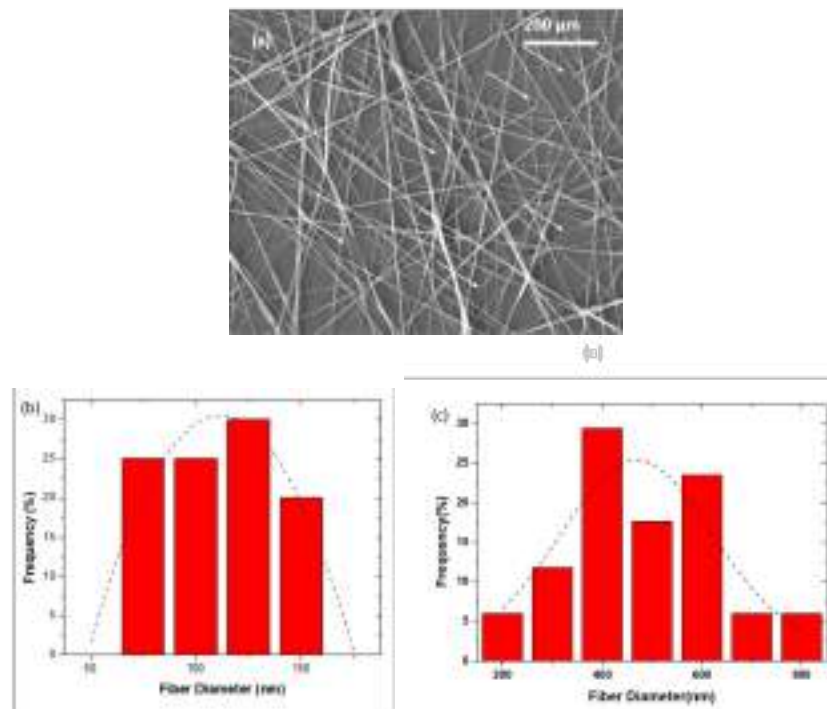
Figure 4.3: SEM images and Distribution of fiber diameter of (a& b)SF-DES group (c) SFGC-DES

self-reinforced coating. (Sample abbreviation: SF-DES). The coating was first characterized using SEM, and the results have been summarized in Figure 4.2 (b). Figure 4.3 (a) shows that the electro spun nanofibers are embedded in the dip coated matrix The diameter of the electrospun fiber was found to be in the range of 50-200 nm. Figure 4.3 (b) and (c) shows fiber distribution. The electrospun fibers are at least partially embedded in the dip coated SF matrix (Figure 4.2 (b)) and some fibers also appear to be on the surface of the coat. As can be seen in Figure 4.2 (d), the resultant SF coating has a total thickness of about 1μm. For thicker coatings, electrospinning of solutions can be done for longer duration, which might also be desirable for sustained drug release.

The surface topography of uncoated/coated PDMS discs was studied using scanning probe microscopy in tapping mode, and these results are summarized in Figure 4.4. The oxygen plasma treated PDMS disc exhibits a RMS surface roughness of 18 nm, as can be seen in Figure 4.4. After dip coating with SF, the surface is still found to have a very similar surface roughness. As expected, the disc with sequential dip and electrospun SF exhibits a surface roughness that is atleast an order of magnitude higher than the other two substrates. This increased surface roughness is desirable for biomedical applications. It
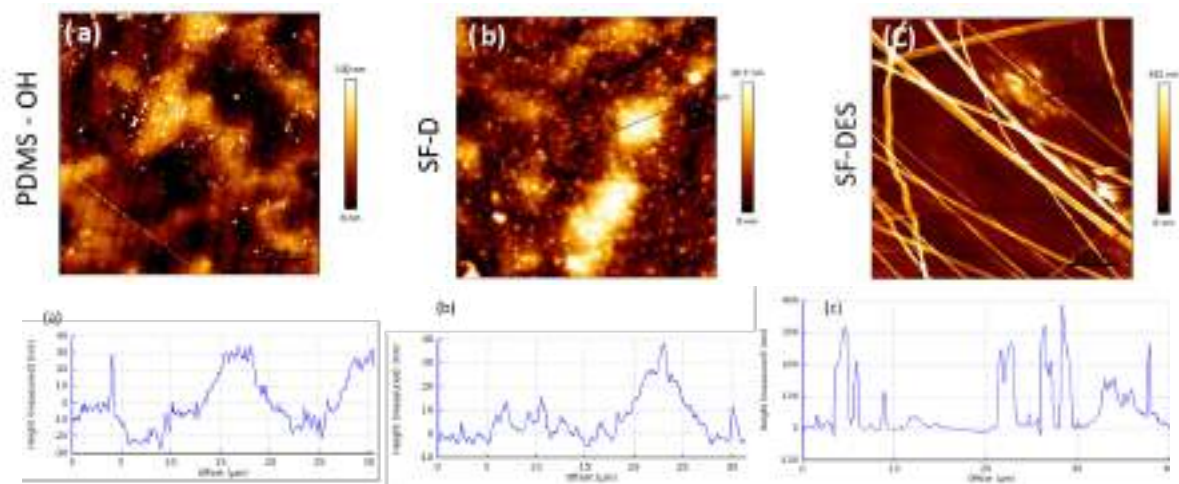
Figure 4.4: The AFM images of coatings (a) PDMS after oxygen plasma (b) SF-D (c) SF–DES

has been shown that the fibroblast attachment on textured breast implants was higher than smooth implants by Valencia-Lazcano *et al.*[42]. Researchers have also demonstrated that proliferation of fibroblast was better in electrospun mats as compared to SF films.

4.5.2   Mechanical stability of the coating

A simple bending test, followed by SEM imaging, was designed to characterize the cracking resistance of the coating on the PDMS implant. The PDMS strip subjected to oxygen plasma treatment was used as a control. As can be seen from the Figure 4.5(a), the PDMS disc has a smooth surface after the plasma treatment, and the surface did not exhibit any changes in surface morphology after the bending test. The SF-D disc also showed a uniform coating with smooth surface. Refer Figure 4.2(a). However, post the bending test; the coating did not retain its integrity. Large visible micro and macro-cracks were seen the surface of the coating (Figure 4.5(b)). This result is in agreement with prior literature which shows that after a similar test was conducted on recombinant spider silk coating on PDMS, the authors did observe cracking on the coating, although the cracking reported is not as severe as the one observed here[135]. The reason for this difference is the variation in the coating process, thickness of coatings and the material composition. Contrary to this observation, the surface morphology of the novel dip + Espun PDMS strip was comparable before and after the bending test (Figure 4.2(b) & Figure 4.5(c)). The electrospun fibers exhibit regions of stress whitening (marked with white arrows), indicating that the mechanical stress exerted
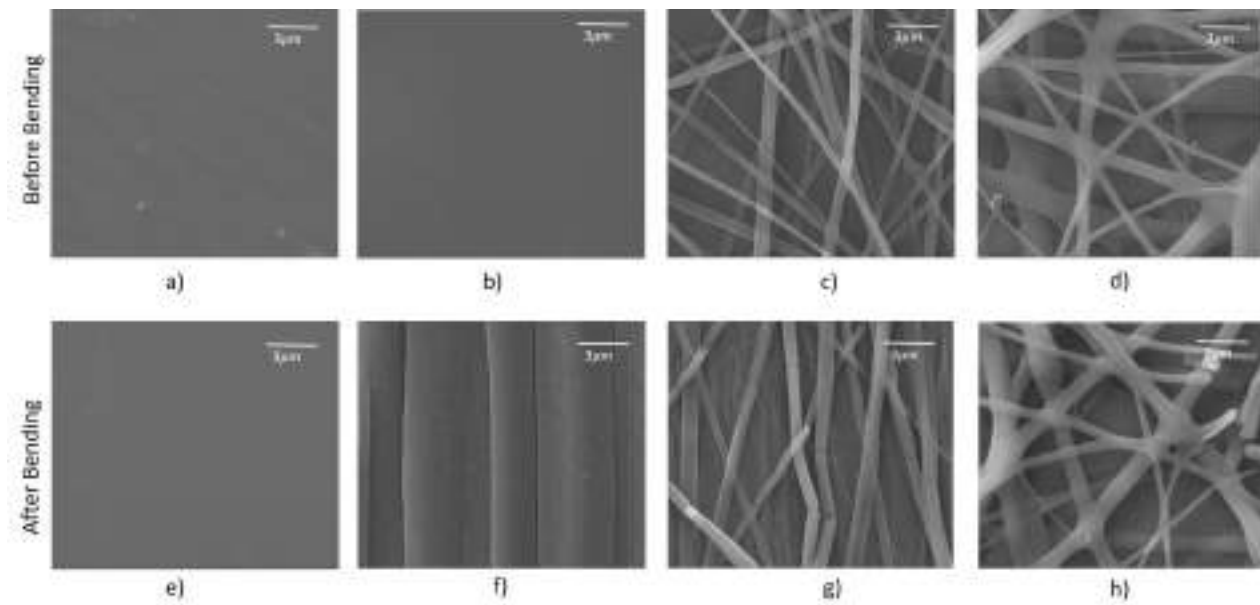
Figure 4.5: Scanning Electron Micrographs of the coated PDMS discs after bending test (a) Oxygen plasma treated PDMS (b) SF-D (c) SF-DES (d) SFGC-DES. The white arrows indicate extension of individual nano-fibers post mechanical loading.

on the samples is primarily taken up by the nano-fibers, and thus, the damage caused to the lower dip coated layer is minimum. Also, as discussed earlier, the electrospun nanofibers are partially embedded in the dip-coated layer. It may, therefore, be hypothesized that these embedded fibers act as reinforcement and improve the cracking resistance of the coating. Self-reinforcement of polymer matrices using nano/microfibers is a classical and proven technique to improve the toughness of the material[154], [155].

A similar result has also been reported by authors Mandal *et al.*[156].; the authors used SF microfibers to improve the mechanical toughness of SF scaffolds. However, the use of sequential dip and electrospinning process as a coating toughness enhancement mechanism is novel. The technique also worked perfectly after preparation of a blend of SF and GC, as shown in Figure 4.5 (d).

Further to the bending test, we have also performed tensile tests on our samples. These tests were performed on dogbone shaped PDMS substrates, coated with dip and thick electrospun layer of SF. Our results indicate that at strains of 100%, no physical damage to the SF nano-fibers is observed. At higher strains of 150 and 200%, some regions with stress whitening can be observed on the nanofibers, as shown in Figure 4.6 (a) – (c). However, no
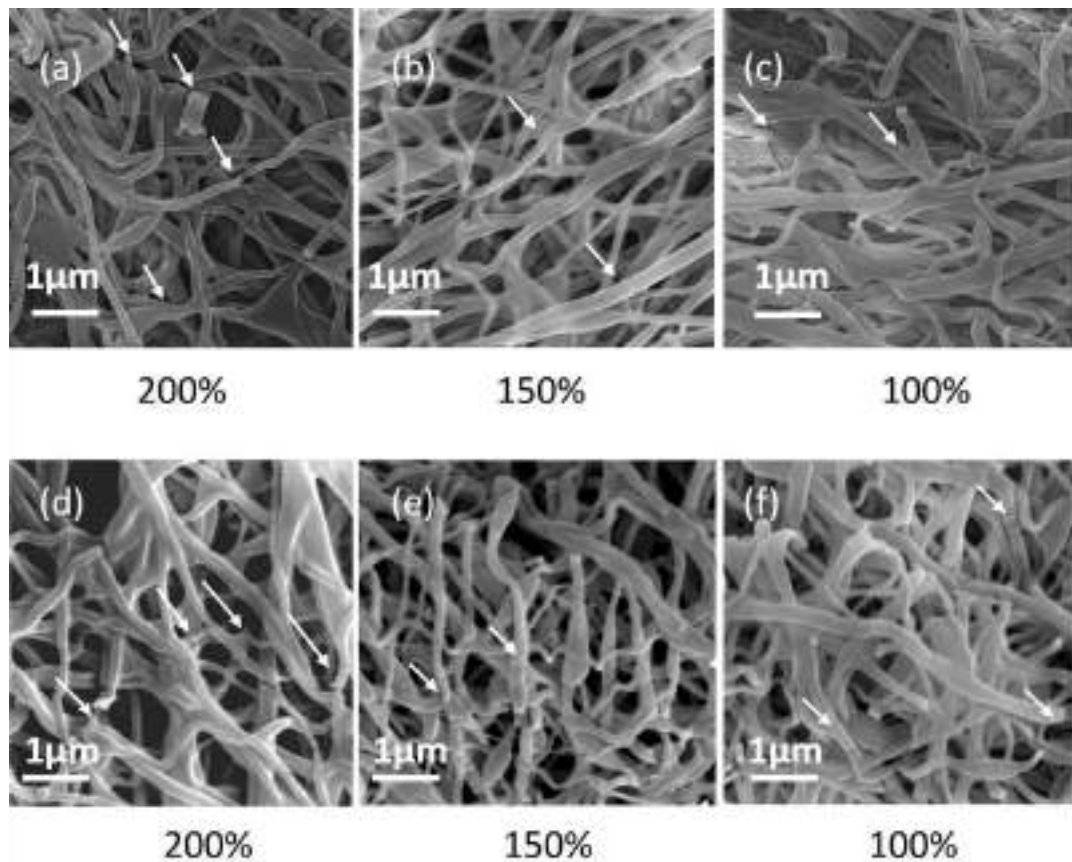
Figure 4.6: Scanning electron micrographs of SF-DES discs after tensile test (a) 100% (b) 150% (c) 200% strain in dry condition (d) 100% (e) 150% (f) 200% strain in wet condition The white arrows indicate extension of individual nano-fibers post mechanical loading.
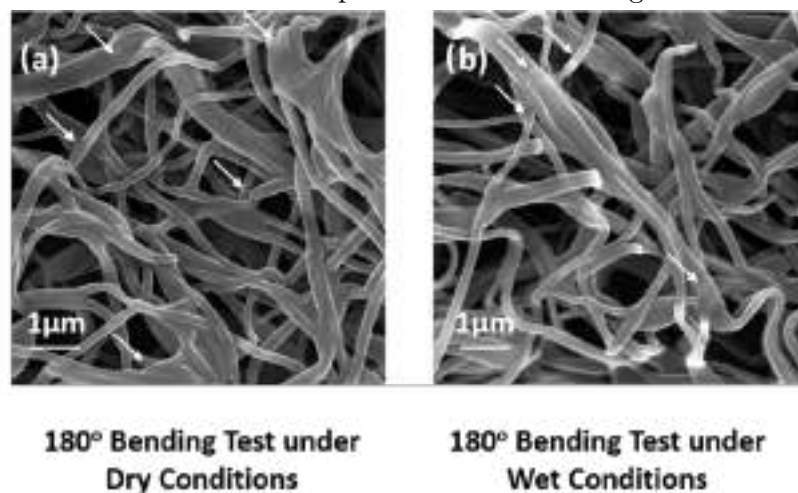
Figure 4.7: Scanning electron micrographs of SF-DES discs after 180°Bending test (a) under dry conditions and (b) under wet conditions

significant change in fiber morphology was observed. We also looked at the behavior of these samples under wet conditions when the coatings have been swollen to equilibrium weight. Here, we observed that when the strain is increased to 150% and 200%, some of the fibers showed a break as shown in Figure 4.6 (d) – (f). However, the damage is not significant and the integrity of the coating is still maintained. We have also observed that the SF coatings retain their physical integrity under torsional loads (as shown in Figure 4.7).

Thus, our results demonstrate that a novel combination of two conventional processes of coating – dip and electrospinning, significantly enhances the performance of the coating under mechanical loading both in the dry and wet state. This performance improvement is highly desirable considering that implants are subjected to a variety of mechanical stresses both during handling and in use. The experiments on the dry SF coating simulate the forces exerted on an implant primarily during storage and handling. Post implantation the SF coating is wetted by the bodily fluids and thus, the wet experiments demonstrate the stability to coating during use after implantation in the body.

The PDMS surface was characterized after each processing step using a simple instantaneous contact angle measurement to confirm successful modification. The pristine PDMS polymer surface is highly inert and unreactive and hence it is extremely challenging to have a coating adhere onto the PDMS surface. Oxygen plasma was the method of choice for PDMS surface modification since it has been reported that this treatment results in the formation of hydrophilic –OH groups on the surface and increases the wettability of the PDMS discs. As shown in Figure 4.8, oxygen plasma treated PDMS discs exhibited a contact angle of $55 \pm 5°$which was significantly lower than the contact angle of the discs before plasma treatment i.e. $115 \pm 5°$. After SF-D coating, the contact angle was found to increase to $95 \pm 5°$. Further SF-DES discs increased the contact angle to $128 \pm 3°$. This increase in contact angle post electrospinning can be attributed to presence of small air pockets between the electrospun nanofibers that resist the wetting of the surface[157]. The SFGC-DES discs had a contact angle of $85 \pm 5°$, which is much lower that the SF-DES mat. Glycolipids are hydrophillic molecules and hence improve the wettability of a surface. Thus, the change in contact angle after each processing step provides sufficient evidence to corroborate the modification of the PDMS surface and it successful coating.
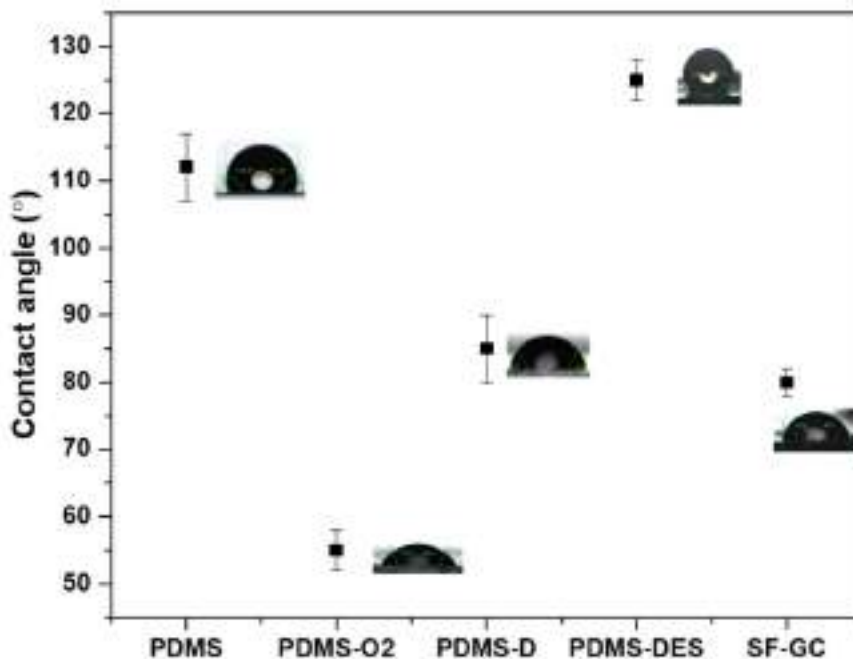
Figure 4.8: Contact angle measurement on coated/uncoated PDMS discs

The modification of the PDMS substrate after coating was also characterized using ATR-FTIR spectroscopy to gain insights into the conformation of the SF protein. The data has been summarised in Figure 4.9. The control samples used here were pure PDMS substrate, SF degummed fibers and as synthesized GC molecule. The pristine PDMS has no signal beyond the 3000 cm^{-1} range. The symmetric and asymmetric streching of CH$_3$ shows peaks at 2963 cm^{-1} and 2906 cm^{-1}, along with CH$_3$ bending vibration at 1258 cm^{-1}. The peak in the range 1200cm^{-1} to 800cm^{-1} confirms the presence of Si-O-Si groups of PDMS[158]. G-citron shows a peak at 3063 cm^{-1} to 3640 cm^{-1} corresponds to –OH streching from glucose. The asymmertric and symmetric streching of CH$_2$ gives a peak at 2857 cm^{-1}. The prescence of C=O streching in glucose gives a peak at 1720 cm^{-1} due to saturated aliphatic 6 membered ring of glucose. After SF-DES of PDMS with SF, a broader peak from 3300 cm^{-1} to 3700cm^{-1} is observed, and this corresponds to –OH groups present in the system. The random coil conformation of silk fibroin shows a peak at 1650 cm^{-1} and 1540 cm^{-1} for amide I and amide II peak, respectievly[14]. The SF coated PDMS exhibited peaks from both pure SF and the PDMS substrate below. This is anticipated since the IR beam is known to penetrate the first few microns of the surface. Since the coating is only 1μm in thickness, the spectrum also shows peaks corresponding to the below PDMS substrate.
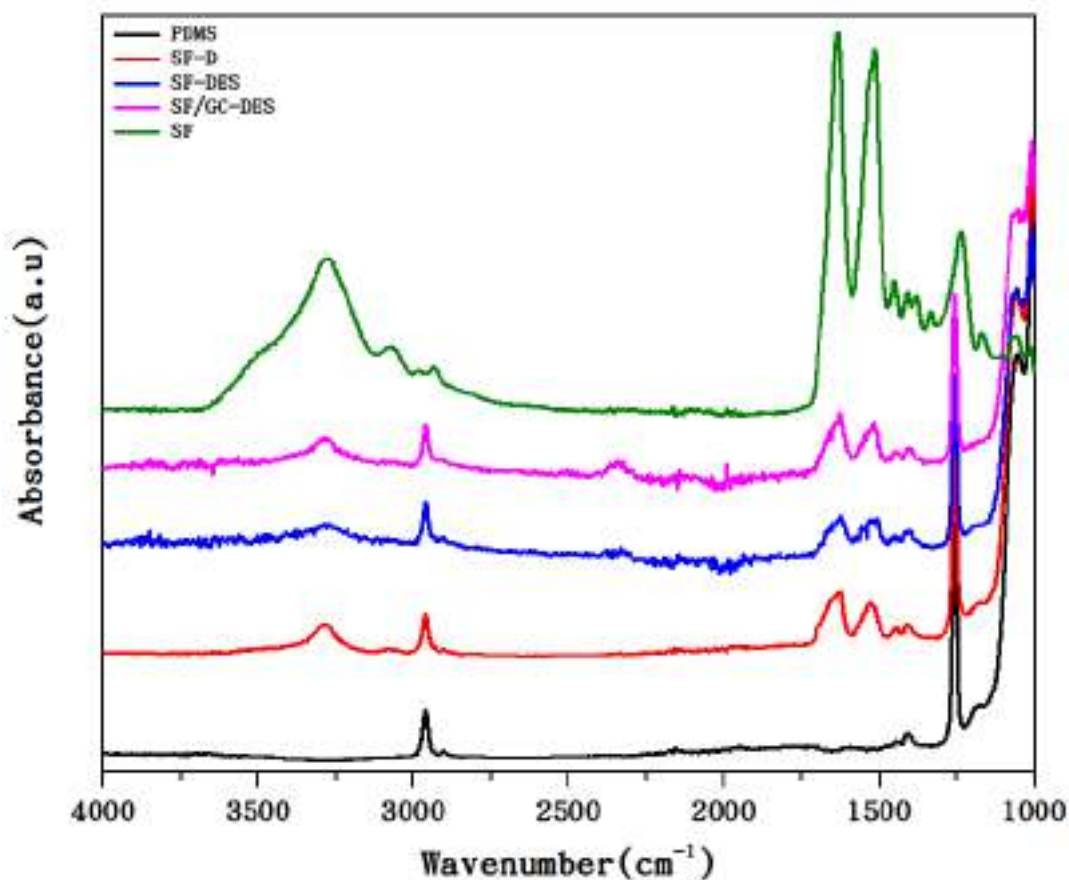
Figure 4.9: FTIR analysis of before and after silk fibroin coatings

The Amide I stretching peak at 1623cm^{-1} indicates that the protein has predominantly beta sheet conformation. Earlier reports suggest that SF after electrospinning displays lower beta sheet content. However, the methanol vapor post treatement results in the change in protein conformation. (as shown in Figure 4.10). The IR spectrum displays a prominent Amide I peak at the lower wavenumber of 1623 cm^{-1}. Correspondingly, an high beta sheet content of 40% was also observed after deconvolution of the Amide I spectra as shown in Chapter 3. The SFGC-DES sample did show the peaks for PDMS and also for SF. However, the GC peaks were too weak to be discerned and quantified. However, the change in contact angle observed between the SF-DES and SFGC-DES sample, can be considered to be a sufficient proof of the presence of GC in the coatings. Further, we also show that when the SFGC-DES mat is incubated in PBS solution, the GC is released into the aqueous medium
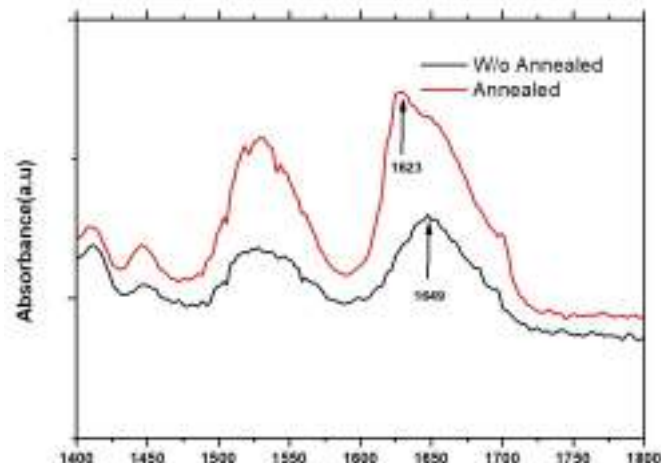
Figure 4.10: FTIR analysis of before and after silk fibroin coatings

4.5.3   Aqueous stability of the coatings

The aqueous stability of the SF coating was determined using UV-vis spectroscopy. Since no significant weight loss or SF release was observed after a 3 day period, the experiment was terminated after 7 days. The test was performed on the SF-DES discs before and after methanol vapor treatment. The release of SF into the PBS solution was monitored using UV-vis spectroscopy and the data has been summarized in Figure 4.11. The SF protein in aqueous solutions shows an absorbance at 275 nm and this absorbance was used to estimate the amount of SF released from the coating[153]. The total amount of SF present on each disc can be estimated to be about 0.34 mg. The amount of silk fibroin released before annealing was around 50 - 60% of the total SF. The amount of SF released from the coating after the methanol vapor treatment was negligible and below the measurable limit. Thus, it may be concluded here that the methanol treatment results in a stable coating of SF for use in biomedical applications.

After completion of the mechanical and physico-chemical characterization of the coatings, the coatings were further evaluated for their biological activity. As discussed in the Section 2.4.2, one of the primary reasons for failure of implants is formation of a bacterial biofilm. Also, growth of microorganisms in biofilms shows high resistance to antimicrobial agents. This is probably due to decreased penetration of antibiotics and decreased growth rate or metabolism of the bacterial cells present in biofilm. Antibiotic gives selective pressure to
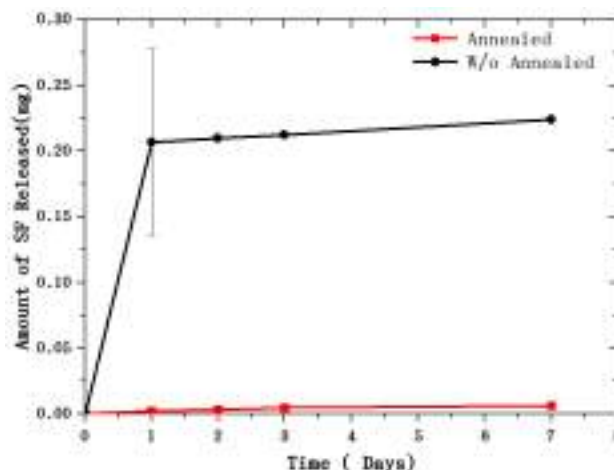
Figure 4.11: Stability of the SF-DES before and after methanol treatment

bacteria and thus, they indeed find ways of resisting the newly developed antibiotics. High doses of antibiotic are required to be administered, which in turn affects the normal flora of the host body as well. Quorum sensing inhibition provides a promising alternative to antibiotic resistance by altering bacterial communication, without putting selective pressure on bacteria as well by inhibiting biofilm formation[159]. It is a means of communication between the bacterial cells using certain diffusible signal molecules called as auto-inducers specific to their species. These molecules aid bacteria to sense their population density and to regulate the expression of various genes in response to the density[160]. Quorum sensing controls expression of genes for virulence, motility and biofilm formation etc. which play crucial role in the pathogenesis[159]. Thus, molecules, which target QS in the bacterial population, automatically also, inhibit biofilm formation, the resultant of QS.

Reports suggest that plant derived essential oils act as quorum sensing inhibitors[161]. But this biological activity cannot be exploited fully due to their hydrophobicity. It has already been demonstrated by our earlier papers that addition of glucose moiety to these hydrophobic molecules improves their bioavailability[151]. GC is a molecule that has been demonstrated to exhibit antibiofilm and quorum quenching activity.

4.5.4   Antiquorum sensing activity

E. coli pSB1142 was used to check the inhibition of quorum sensing mediated through long-chain AHL signal molecule. The strain possesses lasR and las promoter of *P. aeruginosa* fused

to the luxCDABE cassette from Photorhabdus luminescens which responds to long-chain AHLs (C10-C14) to produce luminescence. This reporter strain does not synthesize AHL molecules but exhibits luminescence in the presence of external AHL signal molecule. In this experiment, the external signal molecule selected was N-(3-oxo-dodecanoyl)-L-homoserine lactone, one of the signal molecules produced by *P aeruginosa*. Decrease in the luminescence of the cells (compared to positive controls) in presence of coating confirms its anti-QS activity35. To exclude growth-dependent effects, OD measurements were recorded in order to normalize luminescence production to cell density. Using PDMS discs with and without coating, QSI activity of released compound was checked when the 3-oxo-C12 HSL signal molecule was added externally. Active compund released from disc coatings with GC SF showed significant quorum sensing inhibition, which is more than 50% when compared to PDMS discs without coatings. Refer Figure 4.12.
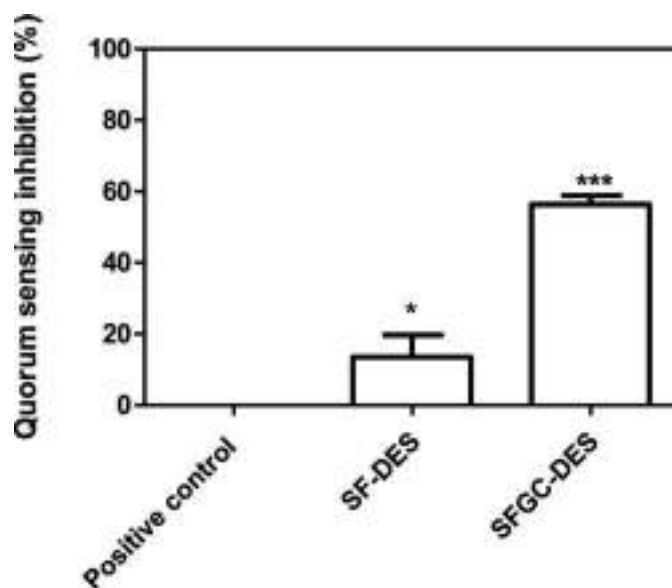
Figure 4.12: Antiquorum sensing activity of coated and uncoated PDMS discs: * and *** indicates significant differences from the control with P< 0.05 and P<0.001 respectively and the error bars indicates standard deviation

4.5.5 Antibiofilm activity

The formation of bacterial biofilms is one of the major phenomenon controlled by quorum sensing. Impeding bacteria's capacity to form biofilm is a major challenge in treating chronic infections. In this study, the antibiofilm activity of SF-DES and SFGC-DES PDMS disc was

evaluated by using *P. aeruginosa* (NCIM 5029), *Staphylococcus epidermidis* (NCIM 5270) as test organisms. The PDMS disc containing GC in the coating showed significant antibiofilm activity when observed after 24h. Around 85% biofilm inhibition when tested against *P. aeruginosa* was observed whereas same coating showed nearly 70% biofilm inhibition when tested against *S. epidermidis*. These results have been summarized in Figure 4.13 (a), (b) and (c).
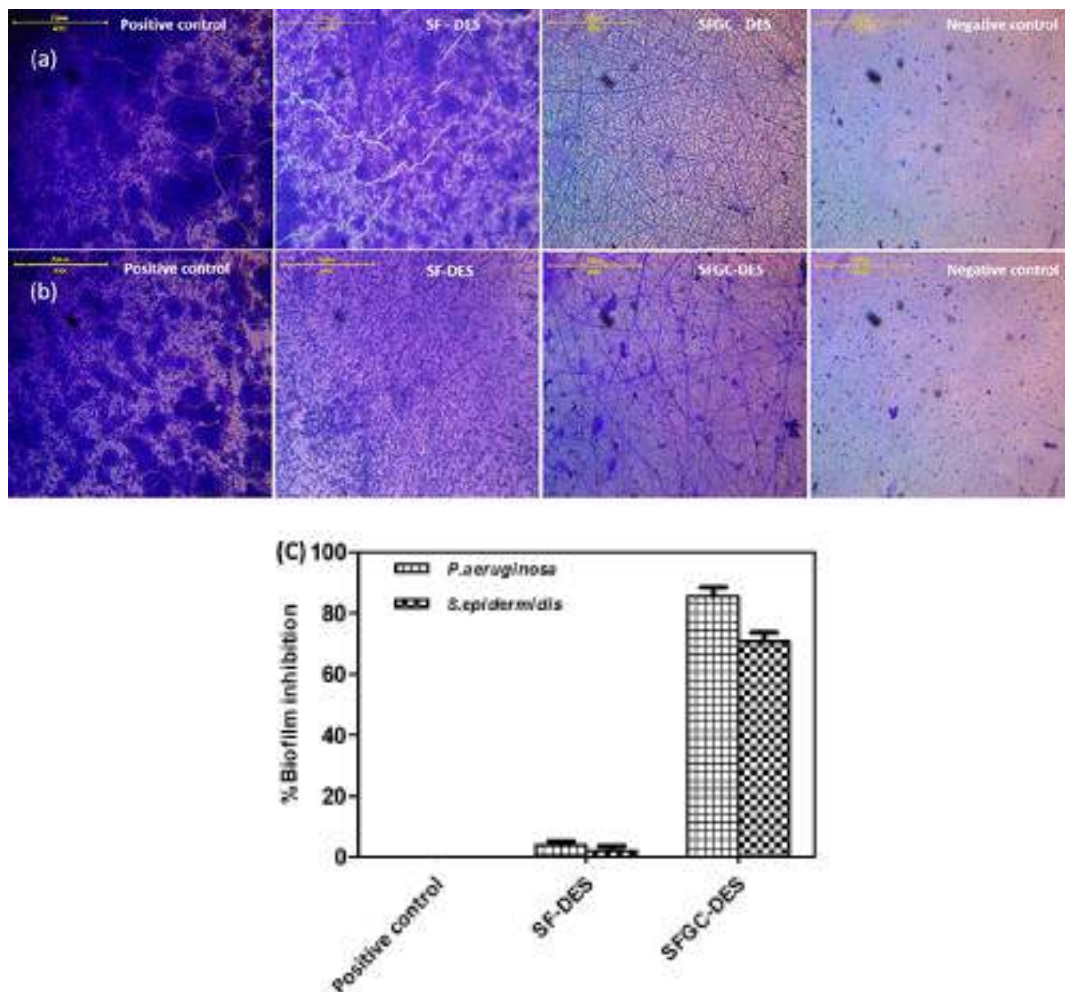
Figure 4.13: Optical microscopy images of biofilm inhibition observed on coated and uncoated PDMS discs stained with crystal violet (a) *P. aeruginosa* (b) *S.epidermidis* (c) *S.epidermidis* and *P.aeruginosa* biofilm inhibition quantified by extracting crystal violet stain from the coated/uncoated PDMS discs (ns and *** indicates significant differences from the control with P>0.05 and P<0.001 respectively and the error bars indicates standard deviation))

4.5.6 *In-vitro* cell proliferation and cytotoxicity

The coated and/or uncoated PDMS discs were evaluated for cytotoxicity using *in-vitro* cell culture studies with mouse fibroblast cell line L929. Cell proliferations were evaluated by performing MTT test. MTT data in Figure 4.14 shows increase in absorbance on day 1 in SF-DES as compare to SF-D and PDMS that indicates greater biocompatibility was achieved with electro-spinning technique. Higher cell viability with respect to all three groups was observed in SFGC-DES discs on day 1, confirming the non-cytotoxicity of GC. Similar cell viability trend was observed on 5th and 7th day that is sufficient to prove the biocompatibility of the modified discs.
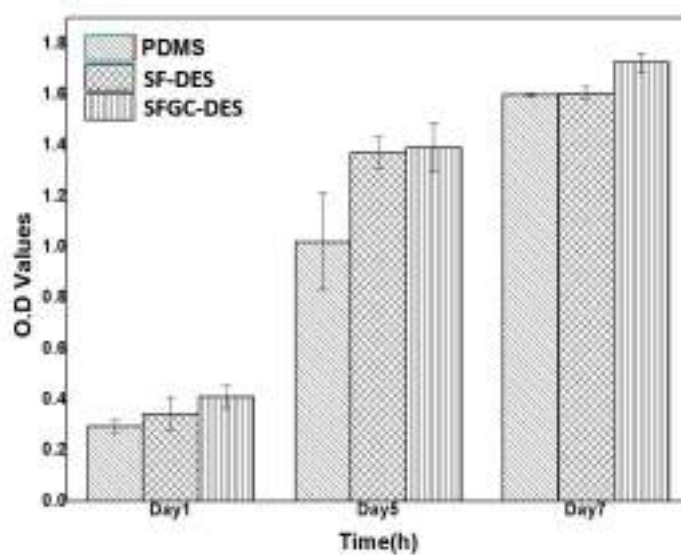
Figure 4.14: MTT Assay using L929 cells on PDMS, SF-DES and SFGC-DES samples for 7 days (ns, * and ** indicates significant differences from the control (PDMS) with P>0.05, P<0.05, and P<0.01 respectively and the error bars indicates standard deviation)

4.6 Conclusion

Surface coatings have emerged as promising alternative to reduce implant failure due to both foreign body response and device associated infections. Failure of coatings due to cracking, delamination, flaking is also a concern for successfull use of implants. Here, we report a process innovation – sequential dip and electrospinning process, that results in the formation of self-reinforced coating of silk fibroin on an elastomeric substrate like PDMS. These new

coatings have shown to be crack resistant under mechanical deformations in tensile, bending and torsional modes. Silk Fibroin improves the biocompatibility of the PDMS substrate thus, mitigating the risk of implant failure due to foreign body response. Further, we have blended in a next generation quorum-quenching antibiofilm molecule into the coating. This molecule not only retains its quorum sensing activity throughout the processing steps, but also inhibits biofilm formation of two of the most notorious infection causing bacterium - *P aeruginosa* and *S epidermidis.* All these functions have been achieved while retaining the inherent biocompatibility of these materials. Thus our work demonstrates an innovative solution to simultaneously resolve multiple causes for failures of implant devices – biofilm formation, foreign body response and cracking of the coating.

Chapter 5

Novel blends of silk fibroin for coating of silicone implants

5.1 Abstract

In this work, we report coatings of silk fibroin and its blends with two biopolymers. The first polymer chosen for blending with SF is a well known hydrophilic material - Polyethylene oxide (PEO). The second biopolymer has now emerged as a promising material for tissue engineering and drug delivery applications - recombinantly produced elastin-like peptide (ELP).

This Chapter has been divided into two parts. Part I focuses on SF/PEO blends in Section 5.2. This Section begins with a literature review of SF/PEO blends. This is followed by Section 5.3 that discusses about the experimental methods and materials. The key results have been summarized and discussed in the Section 5.4.

Part II is focused on SF/ELP blends. It uses SF/PEO as a model system and then compare its performance with SF/ELP system. Section 5.7 provide detailed information about the experimental methods and material used. Section 5.8 summarize the key results and discussion of the present study. Section 5.9 concludes part I and part II of the Chapter.

Part I

Blending of a hydrophilic synthetic polymer – polyethylene oxide

5.2 Literature Review

Surface coatings is a promising approach to tailor the surface properties of the implant surface. Polymer based coatings enhance the biocompatibility of medical devices. These surface coatings can serve the purpose of biomimetic biological structures. Drugs and functional molecules can also be incorporated to improve the biological performance of the medical devices. SF has emerged as a promising biopolymer for several coating applications. However, as discussed in Chapter 3, SF coatings on elastic PDMS substrates are not resistant to cracking. The objective of this Chapter is to develop blends of SF so as to improve the crack resistance of SF coatings formed using a simple dip coating method. Further, the objective of this Chapter is to enhance the biological performance of the SF coatings. Also, as described in Section 2.4, one of the primary reasons for failure of implants is irreversible adsorption of non-specific proteins. This triggers the events, which further lead to failure of implant due to formation of a fibrotic capsule. The hypothesis in this Chapter is therefore, to blend SF with a hydrophilic polymer such that this hydrophilic polymer will plasticize the SF biopolymer and improve the crack resistence. Further, it will reduce non-specific adsorption of proteins. This Chapter begins with a literature review that summarises various strategies to prepare blends of SF to achieve the above mentioned mechanical and biological properties.

SF has been blended with various other polymers and proteins for tissue engineering applications such as polyethylene oxide, chitosan, agarose, sodium alginate, gelatin, polyvinyl alcohol, polyurethane, polycaprolactone, and poly l-lactic acid-co-caprolactone[162]–[167]. Among these polymers, PEO has been extensievly used to prepare SF blends. Since PEO is also one of the highly proven antifouling polymers, we have restricted our further discussion to only SF/PEO blends. Initially, PEG macromer was used in the synthesis of semi-interpenetrating networks and results in improved tensile strength and elongation at break[168]. Later, PEG macromer was blended with SF in different amount, followed by SO_2 plasma to enhance the blood compactibility of SF. SF has intermediate hydrophilicity and this can be improved by blending with PEO molecule[169]. The SF/ PEO blend films have also been demonstrated to introduce porosity in the SF films by etching out the lower molecular weight PEO molecule from SF/PEO blend films. Nong *et al.* demonstrated aerogels prepared from pure SF solution using free-drying method. The authors show that,

the process results in low elasticity and high brittleness. However, SF blended with PEG molecule helped in improving the elasticity due to the formation of hydrogen bonding with SF chains. This inhibits the formation of intramolecular-β sheets in SF chains and resulted in the aerogels with enhanced elasticity as compared to pure SF aerogels[170]. Similar observations have also been reported by Wang *et al.*, and results confirms that incorporation of PEG molecule enhances the elongation at break to 20 - 35 times higher than pure SF films [171]. Anne *et al.* demonstrated SF blended with PEO enhances the processing properties, and PEO acts as plasticizing molecule for SF for fabricating SF non-woven mats[172]. Low molecular weight PEG blended with SF improves the water-stability of the scaffold, and it has notable wettablity and reduced protein adsorption[173]. Although SF has been extensievly blended with PEO for various applications, a systematic and detailed study about effect of PEO molecular weight on the physical, chemical and mechanical properties of SF/PEO blends has not been reported. Therefore the objective of the work described in Section 5.3 and 5.4 is to evaluatevthe SF/PEO blends by varying molecular weight of PEO. Here, we have prepared SF/PEO blend using 4 different molecular weight of PEO. The blends were characterized for their ability to form stable crack-resistant coatings on PDMS implants. The aqueous stability of these blends was also evaluated. Interestingly, we observed that PEO with molecular weight comparable to SF molecular weight result in composition that provide excellent crack resistance.

5.3   Experimental Section

5.3.1   Preparation of PDMS Discs

Medical grade PDMS (Sylgard 184, Dow Corning) was cast on polystyrene petri dishes to obtain a disc with a uniform thickness of 1.5 mm. The preparation of PDMS film with a uniform thickness has been described in the Chapter 3. Briefly, the prepolymer was thoroughly mixed with the curing agent for 5 minutes using a weight ratio of 10:1. It was then poured into the petri dish and degassed for 30 minutes. This mixture was kept in a convection oven at 40°C for 24h. PDMS discs of the required dimension were then cut out, and isopropyl alcohol (IPA) treatment was performed to clean the samples before using them for further experimentation. The treatment involved 30 minutes of sonication in an IPA bath

to remove dust particles. This cleaning process was followed by a drying step (60°C for 4h in a vacuum oven) to remove any IPA solvent traces.

5.3.2 Plasma treatment

The oxygen plasma treatment was used to introduce hydroxyl groups on the surface of PDMS on both sides of the disc using an RF plasma from Quorum Technologies (K1050X), a solid-state RF plasma barrel reactor. The oxygen gas was purged for 15 min at 100W to remove the impurities. The optimized plasma conditions were found to be RF power of 50W for time period of 1 minute. The conditions were determined by measuring the contact angle on the surface and using optical microscopy as a tool to confirm no physical damage.

5.3.3 Preparation of SF solution

The SF solution was prepared from silkworm cocoons as per protocols described earlier[6]. Silkworm cocoons were degummed to remove the sericin protein present in the silkworm cocoons. The dissolution of SF fibers was done using a chaotropic salt – Lithium Bromide (LiBr), followed by dialysis with DI water for 51h, which resulted in a regenerated SF solution with a concentration of typically 4-5wt%.

5.3.4 Preparation of Polyethylene Oxide (PEO) solution

The Polyethylene Oxide with a molecular weight ranging from 20000-2000000 g/mol, purchased from Sigma Aldrich was used as-is for experimentation. The PEO powder was dissolved in DI water to prepare a solution with a concentration of 0.4 % (w/v), and the solution was stirred using a magnetic needle at a low rpm of 300 for 120 minutes at 25°C to ensure complete dissolution of PEO.

5.3.5 Preparation of SF blend coating

The oxygen plasma-treated PDMS discs were used for dip coating. 5 wt% RSF solution was diluted to a concentration of 0.4 wt% using DI water. The PEO solution of a concentration of 0.4 wt% was prepared using DI water at 25°C and was used for blending. The solutions were blended to achieve final weight ratios of 50:50 and 75:25 for SF and PEO, respectively.

The PDMS discs were completely immersed in the blend solution for 10 minutes to get the required thickness of the uniform coating. After drying, the disc was exposed to a saturated methanol vapor treatment at room temperature for 2h. Further, the coated and methanol treated discs were dried at 60°C for 12 h to remove the traces of methanol vapor. All characterization on the coated discs was done after the completion of this drying treatment.

5.3.6   FTIR Analysis

The disc samples before and after SF and SF blend coatings were characterized using an ATR-FTIR Bruker TENSOR II instrument equipped with a diamond crystal probe detector. The samples were scanned from 500 cm^{-1} to 4000 cm^{-1} with a resolution of 4 cm^{-1}. The spectra was baseline corrected using a two-point linear correction. The spectra was smoothened using a 10-point Savitski-Golay smoothening function. Further, the FTIR spectrum in the Amide I region (1580-1720cm^{-1}) was deconvoluted using the Peak fit v 4.12 software. The second derivative method was used to identify the peaks, and the spectrum was smoothened till 12 peaks in the Amide I region (1595–1605, 1605-1615, 1616-1621, 1622- 1627, 1628-1637, 1638-1646, 1647-1655, 1656-1662, 1663-1670, 1671-1685, 1686- 1696, 1696-1703cm^{-1}) could be fit. These peak positions have been defined as per the protocol described by Hu *et al.* (Hu *et al.* 2006). A Gaussian amplitude fit with fixed peak width was used for automatic curve fitting till an R^2 value of 0.999 was obtained. The % areas under the 12 peaks were used to calculate total beta sheet content, the intra-molecular beta sheet content, and intermolecular beta sheet content in the samples. Also, the amount of random coil, beta sheet with and without the incorporation of PEO having different molecular weights was quantified from the second derivative deconvolution analysis.

5.3.7   Contact Angle Measurement

The changes in the surface wettability of uncoated PDMS and coated PDMS discs with SF and SF blend was monitored by stable sessile drop method (Kruss DSA25S, Advance), using 4μl of DI water. Refer section 3.3.6

5.3.8 X-ray Diffraction

The crystalline structure analysis of the SF and SF/PEO blends were performed on a powder X-ray diffractometer, (Rigaku) with Ni-filtered Cu-K α radiation. The voltage and current of the X-ray source were 40kV and 20mA, respectively. The wavelength (λ) was 0.15406 nm. The samples were mounted on glass frames and scanned from 2°to 50°(2θ) at a speed of 10°/min.

5.3.9 Testing for crack resistance

The crack resistance of the coating was measured by subjecting the samples to a 180°bending test. The test was performed on a rectangular block of 1cm x 3cm with 0.1 cm thickness. A tensile test with dumb-bell shaped specimens was also done as per the protocol described earlier[12]. Representative images of the center of the sample, before and after the mechanical deformation were recorded using Scanning Electron Microscopy (Model: Quanta 200 3D from FEI). The micrographs were used to evaluate the cracking resistance of the coating.

5.3.10 Aqueous stability of films

The *in-vitro* stability studies were performed on SF or SF blend films instead of coatings. The stability experiment includes monitoring the weight loss of a sample over time, where the sample is incubated in an appropriate media. Since it is difficult to accurately and precisely monitor the weight loss of nanocoatings, we used SF and SF blend films for this experiment. Silk fibroin blends films without any post treatment were used for this experiment. SF/PEO blend films were accurately weighed (20±5 mg) and incubated in 2ml PBS solution for 7 days at 37°C in 24-well cell culture plate. The mass loss was calculated by measuring the weight of the blend film at various time points of incubation. The samples were vaccum dried at 60° C for 24h. All experiments were performed in triplicate.

5.4 RESULTS AND DISCUSSION

The SF and SF blend films cast from 3 w/v% SF or SF/PEO solution were optically transparent. SF films were post-treated with methanol vapour annealing protocol described in Section 3.3.4. SF/ PEO blend films were used as-is for further experimentation. The physic-

ochemical properties of SF with and without post treatments and SF/PEO blends were evaluated using FTIR-ATR and XRD. These measurements were done to quantify the changes in secondary structure with different molecular weights and amounts of PEO present in each composition. Water contact angle measurements were done to understand the differences in surface wettability of the SF blend coating on PDMS. Further, weight loss measurements were performed to evaluate the stability of SF blends in aqueous media. Finally, SEM images were recorded after mechanical deformation of coated PDMS discs to evaluate the crack resistance of the coatings.

5.4.1 FTIR Analysis

Firstly, we report the chemical characterization of SF and SF/ blend coatings on PDMS. The FTIR data has been compiled in Figure 5.1. The PDMS has no signal beyond the 3000 cm^{-1} range. The peaks at 2963 cm^{-1} and 2903 cm^{-1} correspond to symmetric and asymmetric CH_3 streching vibration. The signal in the range of $1200-800$ cm^{-1} confirms the presence of Si-O-Si linkages of PDMS. PDMS, PEO powder of different molecular weights, and SF films were used as control samples. The pure PEO shows sharp absorptions peaks at 2875 cm^{-1} corresponding to the intrinsic band of asymmetric stretching of (C-H) in the CH_2 of the PEO chain. Peak at 1465 cm^{-1} and 1345 cm^{-1} correspond to swing vibrations of the C-H group, while peak at 1090 cm^{-1} corresponds to the C-O-C vibrational stretching of PEO chain. The C-H swing vibrations and C-O-C vibrational stretch confirm the amorphous nature of PEO chain. The absorption peaks at 950 cm^{-1} and 845 cm^{-1} correspond to the C-H strech of the CH_3 group's rocking vibrations and the PEO chain's helical structure, as shown in Figure 5.1. The Amide I peak of SF in the region of 1600-1700 cm^{-1} corresponds to the C=O stretching vibration of amide bonds in the SF protein. The Amide II peaks in the 1500-1600 cm^{-1} correspond to the N-H bending vibration of SF protein. The shift in the wavenumber of Amide I and Amide II can be attributed to changes in the secondary structure of SF protein.

The SF shows absorbance at 1635 cm^{-1} in the Amide I region. This corresponds to the co-existence of both random coil and β-sheet conformation from the second derivative analysis. The SF/ PEO blend coatings show a shift in the wavenumber towards 1620 cm^{-1} irrespective of the molecular weight and composition of PEO in the coatings. The second
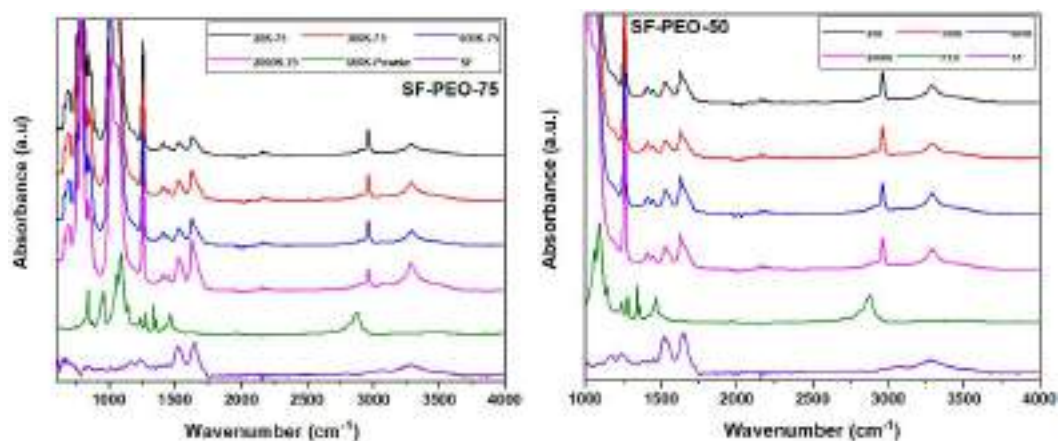
Figure 5.1: FTIR spectra of SF/ PEO blends coated on modified PDMS substrates

derivative of SF/ PEO is summarized in Figure 5.2.

The SF/PEO blends of 20k show slightly lower beta sheet content on a 75:25 blended ratio than other SF/PEO blends groups. Also, there is no drastic change in the beta sheet content of SF/PEO blends of 50:50 composition. This confirms that the PEO molecule induces beta sheet formation in SF chains in SF/PEO blends. The intermolecular and intramolecular beta sheet content of different blend compositions and molecular weights are summarized in Table 5.1 and Figure 5.3 . The intermolecular beta-sheets for 20k PEO of 75:25 blend ratio is 26.5%. This content further increases to 28.2 % for 2000k. Intermolecular beta-sheets of SF/PEO of 50:50 blends have a higher beta sheet content of 29.4% and does not vary with an increase in molecular weight of PEO.

5.4.2 XRD Analysis

The structural and conformational changes of SF and SF/PEO blends with different molecular weights of PEO is summarized in the Figure 5.5. The SF film show a diffraction at 20.4 and 24.3°indicating coexistence of both random coil and β-sheet. This data is in agreement with the FTIR second derivative analysis. This diffraction peaks corresponds to the silk I and silk II peaks of SF. The pure PEO shows a diffraction peak at 19.1 and 23.3°indicating the crystalline nature of PEO. The intensity of PEO peaks is reduced for 20k and 300k whereas similar intensity of peaks is observed for 600k and 2000k. The spectra of SF/PEO
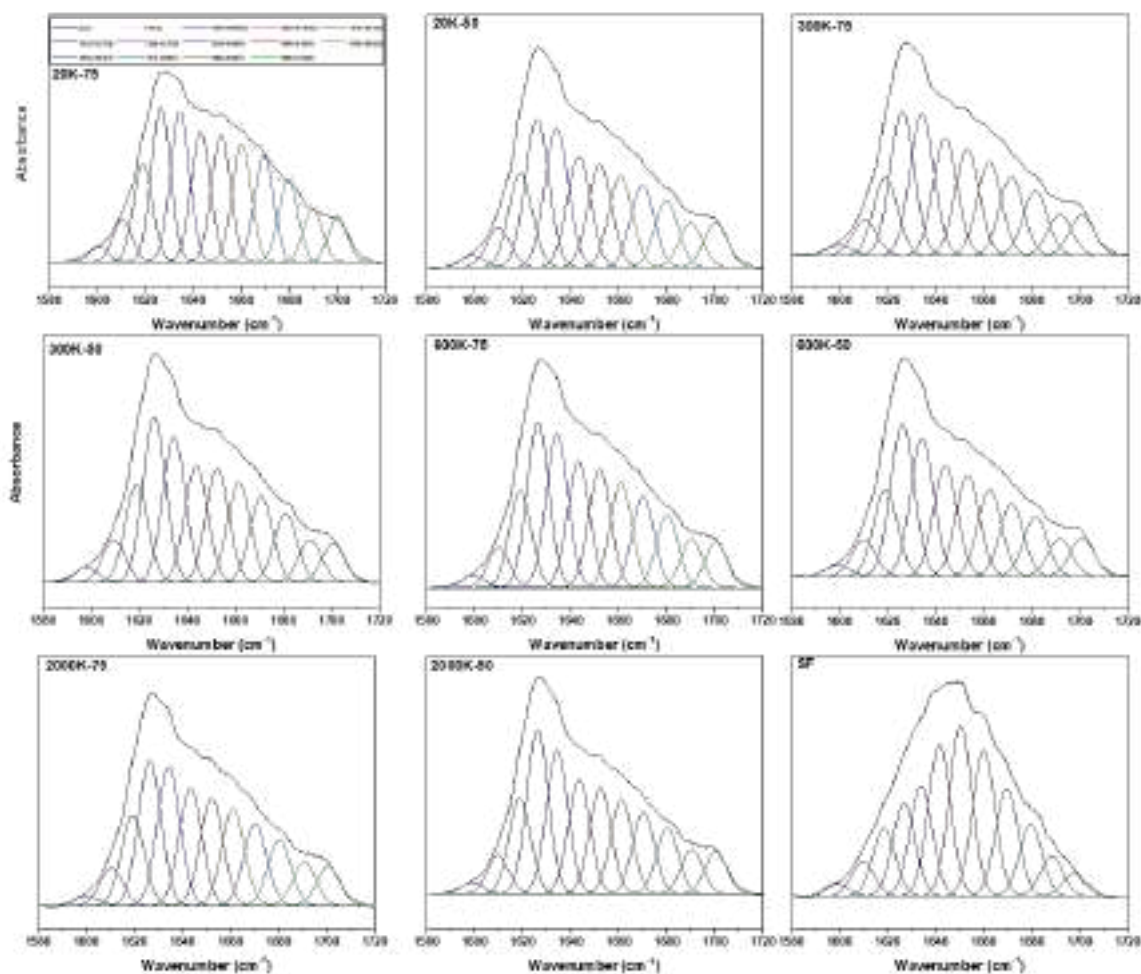
Figure 5.2: Second derivative analysis of SF, SF/PEO-20k, SF/PEO-300k, SF/PEO-600k and SF/PEO-2000 in 25 and 50 composition without any post-treatment
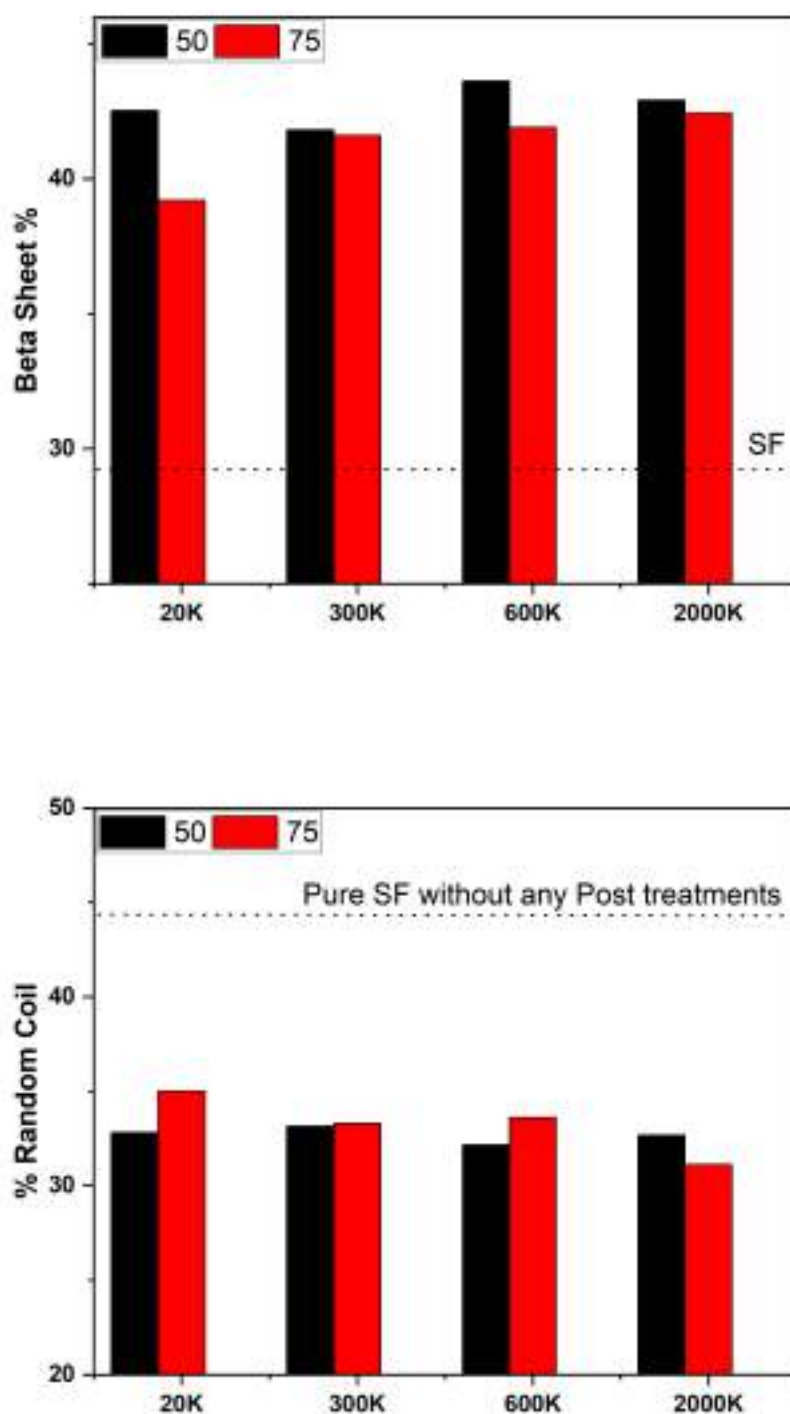
Figure 5.3: Comparison of β-sheet content and random coil content of untreated SF and SF/ PEO blends

Table 5.1: Second derivative analysis of SF, SF/PEO-20k, SF/PEO-300k, SF/PEO-600k and SF/PEO-2000k in 25 and 50 compositions without any post-treatment

SF/PEO-50						
Sample	% Area Intermolecular beta-sheets			Total % Area of inter-molecular beta-sheets	Total % area of In-tramolec-ular beta-sheets	Total % Area of beta-sheets
Molecular Weight	1616-1621 cm^{-1}	1622-1627 cm^{-1}	1696-1703 cm^{-1}		1628-1637 cm^{-1}	
20k	9.6	15.2	4.5	29.4	14.2	43.6
300k	9.4	15.9	3.7	29.2	14.0	43.2
600k	9.3	16.3	4.1	29.8	14.8	44.6
2000k	9.5	16.3	4.2	30.0	14.3	44.3
SF/PEO-75						
20k	8.6	13.7	4.0	26.4	13.3	39.7
300k	8.2	15.2	4.2	27.6	14.9	42.5
600k	9.0	15.3	4.2	28.5	14.2	42.8
2000k	9.2	15.0	4.0	28.2	14.2	42.4

blends with molecular weights of 20k and 300k shows co-existence of silk fibroin and PEO chains in the blend film. However, 600k and 2000K molecular weight shows dominant PEO peaks, indicating formation of aggregates of PEO in SF/PEO with this composition. Similar observations are observed on SF/ PEO blend with higher amount of PEO content irrespective of molecular weight used.

5.4.3 Water Contact Angle

The water contact angle of any thin film or coatings correlates to the hydrophilic or hydrophobic nature of the coating material. The water contact angle depends on various factors such as micropores, surface chemistry, and the interaction of water. The surface wettability of the SF/PEO blend coated surface with respect to the molecular weight of PEO is summarized in the Figure 5.6. The water contact angle of SF coating on PDMS is 75°± 5°. The water contact was found to correlate non-monotonically with molecular weight. The 20k SF/PEO blend shows a water contact angle of 50°and the 300k blend shows a reduction in contact angle to 35°. The higher molecular weight PEO blended with SF, however, re-
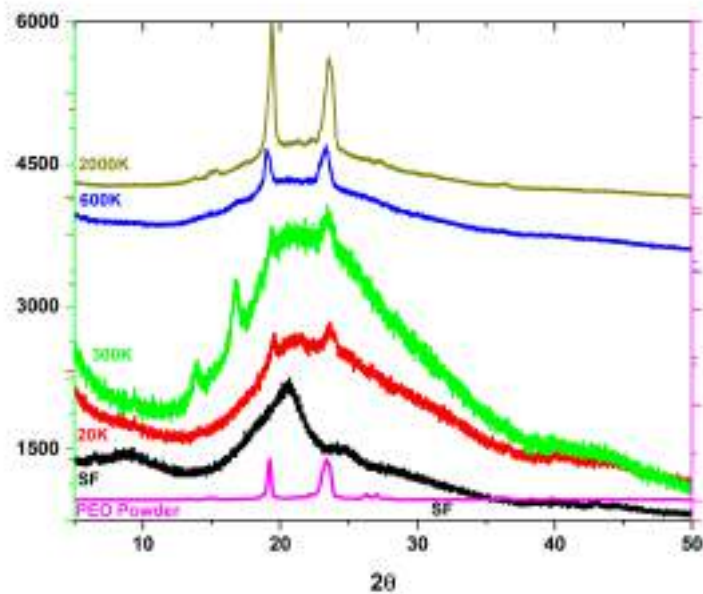
Figure 5.4: XRD analysis of SF, SF/PEO-20k, SF/PEO-300k, SF/PEO-600k and SF/PEO-2000K blends
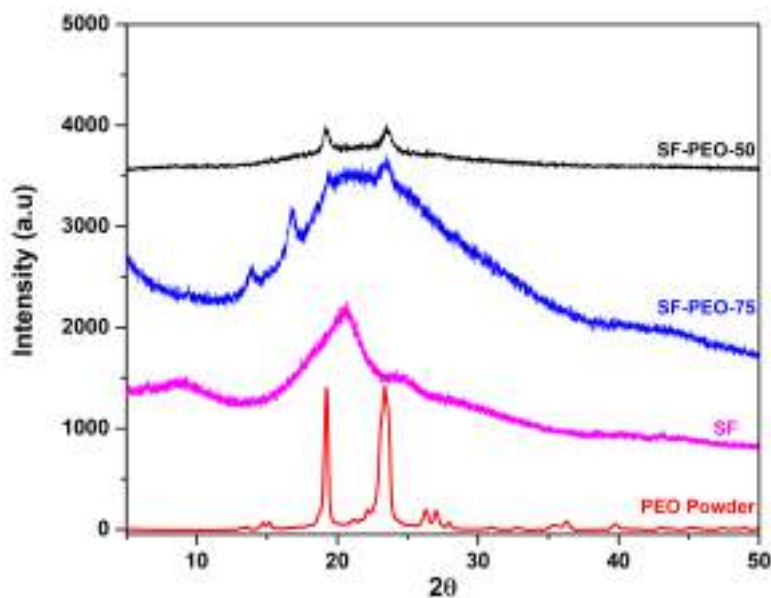
Figure 5.5: XRD analysis of SF and SF/PEO-300k in 25 and 50 compositions
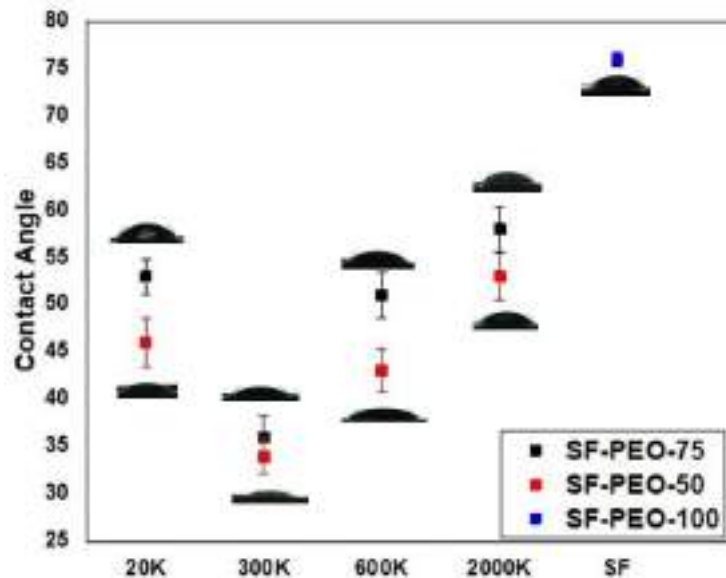
Figure 5.6: Water contact angle analysis of SF, SF/PEO-20k, SF/PEO-300k, SF/PEO-600k and SF/PEO-2000k in 25 and 50 compositions

sults in an increase in contact angle for both compositions for 600k and 2000K blends. This non-monotonic change in water contact angle w.r.t to change in molecular weight cannot be completely understood and needs to be studied further.

5.4.4 Aqueous stability of the coating

The PEO has been used in tissue engineering as a sacrificial material to fabricate pores in the 3D scaffold fabrication process. However, here we have used PEO as a plasticizing agent to improve crack resistance of the coating under mechanical deformation. Stability of PEO in SF/PEO blend coating is important as it also plays a vital role in reducing non-specific protein adsorption on coated substrate to prevent fibrosis. The stability studies have been performed by incubating SF/PEO blend films in PBS at 37°C for 7 days followed by drying process to quantify the release of PEO molecule. The 20k PEO molecule show a weight loss of 14%, and other molecular weights show a weight loss of 6-7% in 50:50 SF:PEO blend. The 20k PEO molecule shows a weight loss of 5%, and other PEO moecules show a release of less than 1% in 75:25 SF:PEO blends. The higher weight loss in 20k molecular weight in both compositions is due to the diffusion of PEO molecules to media. The low molecular weight of PEO allows faster diffusion of PEO chains. The PEO chains of higher molecular weight are entrapped between the SF chains preventing the release of high molecular weight PEO
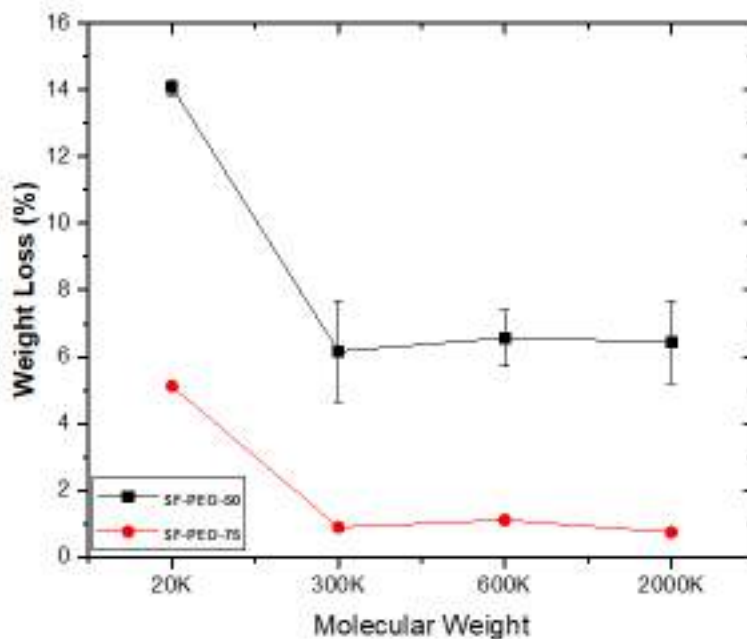
Figure 5.7: Aqueous stability analysis of SF/PEO-20k, SF/PEO-300k, SF/PEO-600k and SF/PEO-2000k in 25 and 50 compositions

chains. The amount of SF present is lower in 50:50 compositions causing diffusion of higher number of chains of PEO into the media and resulting in higher weight loss. However, the weight loss for 75:25 blend compositions for higher molecular weight PEO is acceptable for blending purposes from the point of view of aqueous stability.

5.4.5 Testing for crack resistance

The crack resistance of surface coating of implants plays a vital role in preventing implant failure due to limited interaction between the coating material and body fluids. Crack resistance of SF and SF/PEO coating on PDMS was characterized by subjecting these coated PDMS strips to a mechanical deformation. An SEM micrograph was captured at the centre of these coated strips after they relaxed back to their original position post the mechanical deformation. Using a Universal Tensile Testing Machine, these strips were stretched to 100% strain at a stretching rate of 50mm/min. The SEM images of SF/PEO coating is summarized in Figure 5.8. The SEM images of SF and SF/PEO blends showed a uniform coating with a smooth surface. However, post tensile test, the coating did not retain its integrity for SF
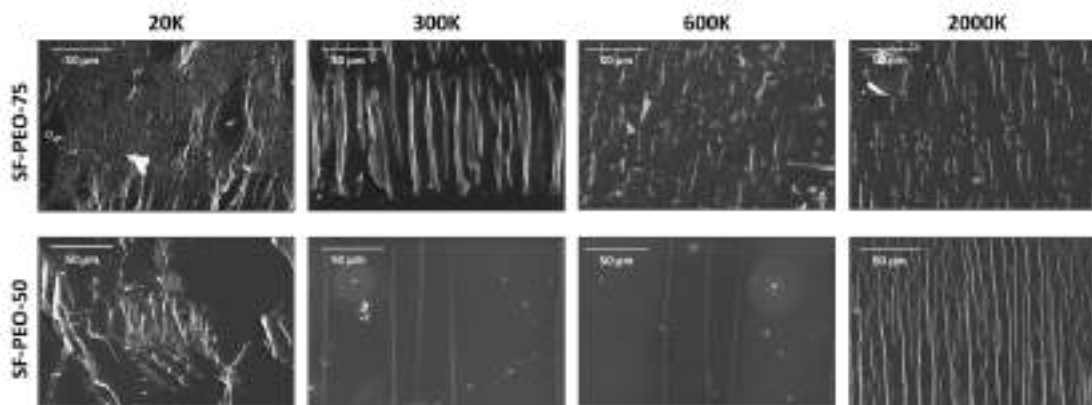
Figure 5.8: Mechanical stability analysis of SF/PEO-20k, SF/PEO-300k, SF/PEO-600k and SF/PEO-2000k in 25 and 50 compositions

coating. The SF/PEO blends maintain the integrity of coating. It depends on the molecular weight of PEO used. The low molecular weight 20k PEO at 75:25 compositions reduces the crack density than pure SF coating. The extent of crack formation upon mechanical deformation decreases and reaches a minimum amount of cracks for high molecular weight PEO. A similar observation was also observed on SF/PEO blends having a blending ratio of 50:50. However, SF/PEO blends above 2000K showed higher crack density than 300k and 600k PEO.

The PEO molecule is known for plasticizing molecules for SF. PEO has been used in the different fabrication processes to improve the viscosity of the solution. Low molecular PEO has been used in the electrospinning process to fabricate SF nanofibers. The low molecular weight of PEO has also been used to develop micropores on the SF film for tissue engineering applications. However, the effect of molecular weight on crack resistance of SF/PEO blends has not been reported in the earlier literature. This is the first study that shows that use of comparable molecular weight of PEO drastically improves the crack resistance of SF blend coatings.

5.5   Conclusion

Surface coatings have emerged as a promising alternative to reduce implant failure due to both foreign body response and device-associated infections. Here we demonstrate crack

resistant and mechanical stable hydrophilic SF/PEO blend nano coatings. Also, the effect of molecular weight of PEO on crack resistance and stability of coatings has been studied. The water contact angle, aqueous stability, crack resistance under mechanical deformation confirms that comparable molecular weight of PEO blended with SF results in enhanced mechanical stability and aqueous stability with negligible amount of PEO being release into aqueous media. All these functions have been achieved while retaining the inherent biocompatibility of these materials. The next Chapter uses this SF/PEO blends as a model system and compares the performance of SF-blends with a newer promising biopolymer-recombinantly produced elastin.

Part II

Blending of a recombinant elastin protein
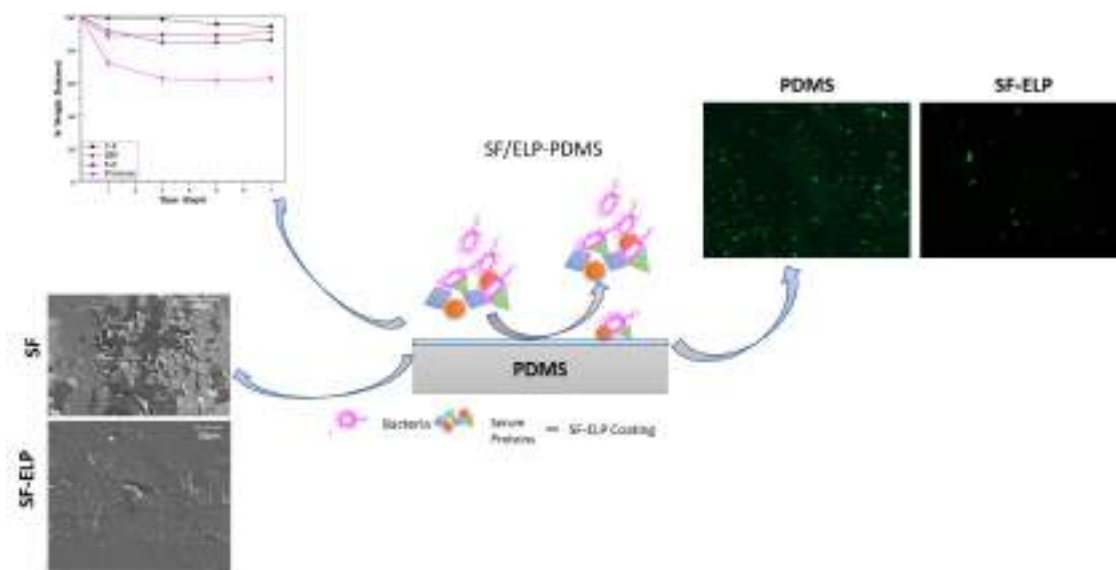
5.6   Literature Review

5.6.1   Silk Fibroin - Elastin like polypeptide Blends

Silk fibroin protein, extracted from the cocoons of *B. Mori* silkworm, has shown encouraging results for implants coating applications. However, as discussed in Chapter 4, SF coatings prepared using simple dip coating techniques exhibit poor crack resistance and therefore fail under nominal mechanical deformation. Section 5.4.5, we have shown that addition of a hydrophilic polymer like PEO to the SF coatings results in coatings that exhibit improved cracking resistance. Further, these coatings are also stable in aqueous environments. However, recent literature suggests that PEO induces an immune response that can hamper the biological performance of coatings. More specifically, it has been demonstrated by researcher that conjugation of PEG molecule has been widely used in biomedical applications such as bioconjugation, drug delivery, imaging, biosensing, and tissue engineering. PEGylated drugs results in the formation anti-PEG antibodies and immune response. Multiple doses of PEGylated drugs resulted in reduced efficacy of therapeutic agents. PEGylated graphene oxide interfacing macrophage membrane showed induced immunological responses resulted in the activation of macrophages and formation of anti-PEG antibodies[174]. Another study by caliceti *et al.* demonstrated the immunological response of mPEG conjugated uricase with multiple doses. The adminstration of PEGylated uricase resulted in the formation of low levels of anti-PEG IgM[175]. Similar results has been reported in the patients exposed to

PEG resulted in the anti-PEG IgM in the body fluids prior to the administration of PEGylated drugs or nanoparticles[176]. Thus, it is an objective of this study to identify blends of SF thathave similar hydrophilic properties like PEO. It is also important that the SF blend coatings exhibit improved cracking resistance. Elastin like polypeptides are being evaluated for their potential in various biomedical applications like drug delivery, tissue engineering, and regenerative medicine.

ELastin is a 68 KDa human protein found in the skin, ligament, and in specialized cartillages. It is characterized with high strength and elastisity. Elastin-like polypeptides (ELPs) are biopolymers composed of short repeating peptide motifs, mostly the pentapeptide VPGXG, where X is a guest residue, which can be any amino acid except proline. ELPs can be produced either by DNA recombination or chemical synthesis. Several ELPs have been reported to be light and pH-sensitive[177]. In addition, ELPs have gained most interest due to their thermo-responsiveness, particularly for targeted drug delivery applications[178]. Similar to tropoelastin, ELPs can exhibit thermo-responsive LCST phase-transition behaviour. They have been shown to be soluble at temperatures below a characteristic cloud-point temperature, denoted as T_t (also known as the inverse phase transition temperature). Above the T_t, they aggregate into larger structures. This aggregation has been associated with a change in the ELP secondary structure, as ELPs have been shown to undergo a substantial transformation from a random coil to type II β-turns (also known as β-spirals) upon heating to temperatures above the T_t. The secondary structure transformation is reversible and can take place in a temperature window as narrow as 3°C [179]–[182]. These materials have potential applications such as sensors, drug delivery devices, tissue engineering platforms, and other applications[183]. Recombinant ELP has been used as a biomaterial for tissue engineering and drug therapeutics applications[184]. The incorporation of bioactive agents in hydrogels and their release at the target site are mediated by several factors. Several groups have demonstrated that ELP is a non-immunogenic molecule with high elasticity and hydrophilic. Thus, ELP has been selected as a novel molecule to blend with SF to improve crack resistance and the biological properties of SF coatings on PDMS. Janorkar *et al.* demonstrated that collagen-ELP hydrogels provide high elasticity due to the presence of ELP molecules[185].

Researchers have also prepared blends and copolymers of elastin and silk fibroin that combine the excellent properties of SF with elastin. Hu *et al.* prepared a series of SF-tropoelastin physical blends, which represent a new class of biomaterials. The authors observed improved mechanical properties and cell proliferation[186]. Liu *et al.* reported the blends of SF/tropoelastin for elecrospinning of non-woven mats. The results showed that incorporation of tropoelastin into silk scaffolds reduced both the acute and chronic inflammatory response following sub-cutaneous implantation for up to 3 weeks. Hybrid SF/tropoelastin materials are promising candidates for highly tunable implantable materials for a range of tissue repair applications[187]. White *et al.* showed SF–tropoelastin protein films for nerve guidance. SF–tropoelastin blends in film form supported peripheral neuron and Schwann cell growth. Since, SF–tropoelastin films are transparent and flexible, they provide additional options for utility as biomaterials for neural repairs[183]. Very recently, Luo *et al.* synthesized diblocks of ELP-Collagen like peptide (CLP) conjugates and studied their self-assembly. They found that these materials formed vesicular structured nanoparticles and the size of the vesicles decreased with increasing temperature. The results suggest a bilayer structure of the vesicle walls, with collapsed ELP domains in the center and CLP triple helical domains at both interior and exterior surfaces[184], [188]. silk-elastin like protein polymer (SELPs) are copolymers of silk fibroin protein and elastin. The physical properties of SELP depends on the number and sequence of the silk and elastin protein[189].

However, use of SF/ELP blends to make coatings for medical implants has not been evaluated. The objective of this work is to develop SF/ELP blend coatings for silicone implants. It is hypothesized that the SF/ELP blend coating will exhibit better cracking resistance as compared to pure SF coatings. It is also an objective of this work to evaluate the biological performance of their blend coatings, especially their aqueous stability, their ability to control non-specific protein adsorption, and support cell adhesion and proliferation. The performance of SF/ELP coating is also compared with SF/PEO coatings, as discussed in Section 5.4.

5.7 Experimental Section

5.7.1 Preparation of PDMS Discs

Medical grade PDMS (Sylgard 184, Dow Corning) was cast on polystyrene petri dishes to obtain a disc with a uniform thickness of 1.5 mm. The preparation of PDMS thin film with a uniform thickness has been described previously. Briefly, the prepolymer was thoroughly mixed with the curing agent for 5 minutes using a weight ratio of 10:1. It was then poured into the petri dish and degassed for 30 minutes. This mixture was kept in a convection oven at 40°C for 24h. PDMS discs of the required dimension were then cut out, and isopropyl alcohol (IPA) treatment was performed to clean the samples used for further experimentation. The treatment involved 30 minutes of sonication in an IPA bath to remove dust particles before further experimentation. This cleaning process was followed by a drying step (60°C for 4h in a vacuum oven) to remove any IPA solvent traces.

5.7.2 Plasma treatment of PDMS Disc

The oxygen plasma treatment was used to introduce hydroxyl groups on the surface of PDMS on both sides of the disc using an RF plasma from Quorum Technologies (K1050X), a solid-state RF plasma barrel reactor. The oxygen gas is purged for 15 min at 100W to remove the impurities. The optimized plasma conditions were found to be RF power of 50W for time period of 1 minute. The conditions were determined by measuring the contact angle on the surface and using optical microscopy as a tool to confirm no physical damage.

5.7.3 Preparation of SF solution

The silk fibroin solution was prepared from silkworm cocoons as per protocols described earlier. Silkworm cocoons were degummed to remove the sericin protein present in the silkworm cocoons. The dissolution of silk fibroin was done using a chaotropic salt – Lithium Bromide (LiBr), followed by dialysis with DI water for 51h, which results in a regenerated silk fibroin solution with a concentration of typically 4-5wt%.

5.7.4 Preparation of elastin-like polypeptide (ELP) solution

The elastin-like polypeptide with a primary sequence of $(GVGVP)_{120}$ was prepared using *E.coli* suspension culture as per the detailed procedure described in the earlier work. Briefly, the suspension culture of *E.coli* at 37°C for 24h. The lysed cells were then centrifuged and purified using inverse phase transition method and in PBS saline solution. The obtained solution was lyophilized and stored at -4°C. The lyophilized ELP is dissolved in DI water and is used for coating process.

5.7.5 Preparation of Polyethylene Oxide (PEO) solution

The Polyethylene Oxide with a molecular weight of 300000 g/mol purchased from Sigma Aldrich (CAS Number 25322-68-3) was used as-is for experimentation. The PEO powder was dissolved in DI water to prepare a solution with a concentration of 0.4 % (w/v), and the solution was stirred using a magnetic needle at a low rpm of 300 for 120 minutes at 25°C to ensure complete dissolution of PEO.

5.7.6 Preparation of SF blend coating

The oxygen plasma-treated PDMS discs were used for dip coating. 5 wt% RSF solution was diluted to a concentration of 0.4 wt% using DI water. The ELP solution of a concentration of 0.4 wt% was prepared using DI water at 25°C. Similarly, the prepared PEO solution of 0.4 wt% was used for blending. The solutions were blended to achieve final weight ratios of 50:50 and 75:25 for SF and ELP/PEO, respectively. The PDMS discs were completely immersed in the blend solution for 10 minutes to get the required thickness of the uniform coating. After drying, the disc was exposed to a saturated methanol vapor treatment at room temperature for 2h. Further, the coated and methanol treated discs were dried at 60°C for 12h to remove the traces of methanol vapor. All characterization on the coated discs was done after the completion of this drying treatment.

5.7.7 FTIR Analysis

The disc samples, before and after SF and SF blend coatings, were characterized using an ATR-FTIR Bruker TENSOR II instrument equipped with a diamond crystal probe detec-

tor. The samples were scanned from 500 cm^{-1} to 4000 cm^{-1} with a resolution of 4 cm^{-1}. The spectra was baseline corrected using a two-point linear correction. The spectra was smoothened using a 10-point Savitski-Golay smoothening function. Further, the FTIR spectrum in the Amide I region (1580-1720cm^{-1}) was deconvoluted using the Peak fit v 4.12 software. The second derivative method was used to identify the peaks, and the spectrum was smoothened till 12 peaks in the Amide I region (1595–1605, 1605-1615, 1616-1621, 1622-1627, 1628-1637, 1638-1646, 1647-1655, 1656-1662, 1663-1670, 1671-1685, 1686- 1696, 1696-1703cm^{-1}) could be fit. These peak positions have been defined as per the protocol described by Hu *et al.* (Hu *et al.* 2006). A Gaussian amplitude fit with fixed peak width was used for automatic curve fitting till an R^2 value of 0.999 was obtained. The % areas under the 12 peaks were used to calculate total beta sheet content, the intra-molecular beta sheet content, and intermolecular beta sheet content in the samples. Also, the amount of random coil, beta sheet with and without the incorporation of PEO having different molecular weights was quantified from the second derivative deconvolution analysis.

5.7.8 Contact angle measurement

The changes in the surface wettability of uncoated PDMS and coated PDMS discs with SF and SF blend coatings was monitored by stable sessile drop method (Kruss DSA25S, Advance), using 4µl of DI water. Four measurements were taken at various locations of the sample after the drop reached equilibrium and the average of these measurements has been included in the results.

5.7.9 Testing for crack resistance

The crack resistance of the coating was measured by subjecting the samples to a 180°bending test. The test was performed on a rectangular block of 1cm x 3cm with 0.1 cm thickness. A tensile test with dumb-bell shaped specimens was also done as per the protocol described earlier[12]. Representative images of the center of the sample, before and after the mechanical deformation were recorded using Scanning Electron Microscopy (Model: Quanta 200 3D from FEI). The micrographs were used to evaluate the cracking resistance of the coating.

5.7.10 *In-vitro* degradation studies of films

The *in-vitro* degradation of SF blends was carried out on SF blend films (75:25). The experiment was performed on a film instead of the coated samples as it is difficult to accurately measure the mass loss in the thin nano coatings. The 5 wt% RSF solution was diluted to a concentration of 3 wt% using DI water. The ELP solution of a concentration of 3 wt% was prepared using DI water at 25°C. Similarly, a 3 wt% PEO solution was used for blending. The solutions were blended to achieve final weight ratios of 75:25 for SF and ELP/PEO, respectively. The blended films were cast on polystyrene petri dish, and drying was carried out at 60°C for 6h under vacuum. The Protease Type XIV enzyme from *streptomyces griseus* (CAS # P5147), purchased from Sigma Aldrich was used for the study. The SF/ELP and SF/PEO films were incubated at 37°C for 7 days in a 2U/ml Protease solution prepared in PBS buffer and freshly prepared protease solution were replaced on 1st, 3rd, and 5th day. Similarly, SF/ELP and SF/PEO films were incubated in simulated body fluid for a period of 7 days. The simulated body fluid was prepared using the protocol as reported earlier[190]. The weight loss was calculated after drying at 60°C under vacuum for 6h to remove the unbounded water. The stability of SF/ELP and SF/PEO film at different pH was quantified by incubating these films at different pH ranging from 5.0 – 9.0 for 7 days, and weight loss was calculated after drying at 60°C under vacuum for 6h to remove the unbounded water.

% Weight Loss = W_f*100/W_0..(1)

W_0 and W_f are respectively, the initial and final dry weight of the SF blend film.

5.7.11 *In-vitro* cell proliferation study

Cell culture

L929 (Mouse fibroblast) cell line was purchased from National Centre for Cell Science (NCCS), Pune, Maharashtra, India. Cells were maintained in DMEM (Gibco, Cat no: 12320032) with 10% FBS (Gibco, Cat no: 10082139) at 37°C with 5% CO_2 atmosphere.

Cell proliferation

Cell proliferation of L929 cells was determined with the help of MTT (3-(4,5-dimethylthiazol-2-yl)-2,5-diphenyltetrazolium bromide) assay. MTT is tetrazolium bromide yellow dye, which is used to determine cytotoxicity. It is reduced by cellular enzymes to form a purple formazan product. Direct contact method was used to determine cell viability, as mentioned in our earlier protocol [12]. In brief, L929 cells were seeded on coated/uncoated PDMS discs in a 96 well flat-bottomed non-adherent plate with a density of 5×10^3 cells/disc in 20 μL of DMEM (Gibco) containing 10% FBS (Gibco). The plate was incubated at 37°C with 5% CO_2 for 15 mins to allow the cells to settle on the scaffold. This was followed by the addition of 200 μL of DMEM with 10% FBS for further cell growth uptoup to 7 days. On the required time points, i.e. the third and seventh day, growth medium was replaced with filter sterilized 10% working MTT (3-(4,5-dimethylthiazol-2-yl)-2,5-diphenyltetrazolium bromide) (0.45 mg/mL) (Invitrogen) solution, which was prepared in DMEM+10% FBS. The plate was incubated for 4h at 37°C with 5% CO_2. At the end of incubation, MTT solution was replaced with 100 μL of DMSO to dissolve the formazan crystals that were formed. The plate was then incubated at 37°C with 5% CO_2 for 10 min. The absorbance was measured at 550 nm using a microtiter plate reader (Multiskan EX, Thermo Scientific). Each absorbance was taken to be the mean of triplicate measurements. The relative % cell viability was calculated by using the equation: Relative percent cell viability $= A_{test}/A_{control} \times 100\%$ (A_{test} is the absorbance of the sample treated cells, and $A_{control}$ is the absorbance of the untreated cells).

Cell morphology by Actin cytoskeleton staining

L929 cells were seeded on uncoated and coated PDMS scaffolds with a density of 5 x 10^3 cells/100 μl of complete media (DMEM+10% FBS) in a 96 well flat bottomed non-adherent plate. Cells were incubated at 37°C with 5% CO_2 up to 7 days. On 7th day, actin cytoskeleton staining was performed as mentioned in our previous report [13]. In brief, all scaffolds were gently washed with PBS followed by fixation of cells with 4% paraformaldehyde for 15 minutes at room temperature. PBS wash was given twice to the cells, followed by the addition of 0.1% Triton X-100 (Sigma-Aldrich) and incubated for 5 minutes at room temperature. After washing twice with PBS, cells were incubated with 5% BSA for 20 minutes at room

temperature to avoid non-specific binding. Actin filaments of L929 cells were stained by Alexa Fluor 488 phalloidin (Thermo Fisher Scientifc) (1:100 dilution) prepared in PBS. The scaffolds were incubated in dark for 30 minutes at room temperature. Nucleus of L929 cells was counter stained with DAPI at a concentration of 300 nM, for 5 minutes at room temperature and washed with PBS. Images were captured by epi-fluorescence microscopy with the help of Axio Observer Z1 Carl Zeiss Microscope (Model: Axio Observer.Z1, objective 20X, Filter sets: 49 DAPI shift free EX G 365, Alexa Fluor® 488).

5.7.12 Statistical analysis

All cell culture experiments were performed in triplicates, and the data obtained from the experiments were represented graphically with mean $\pm$ standard deviation values. To determine significant differences within samples, Tukey's post hoc interaction test was performed with the help of PAST software.

5.7.13 Fluorescence microscopy

The adsorption of proteins on uncoated and coated PDMS discs was carried out using fluorescently labelled (Alexa fluor) 488 bovine serum albumin (Cat# A13100) and fibrinogen (Cat# F13191) proteins procured from M/s Thermo-fisher. The PDMS discs were incubated in the labelled proteins solutions of 1mg/ml concentration for a predetermined time interval ranging from 1 – 30 minutes. After incubation, the discs were washed with DI water to remove the unbounded protein molecules present on uncoated and coated PDMS surface. The representative images of the surface of these discs were captured on a fluorescence microscope (Axio Observer Z1 microscope (Carl Zeiss)) at a magnification of 10X. 10 images per sample per time point were used for the quantification of percentage fluorescent area per sample. The ImageJ software was used to calculate the fluorescent intensity of the images captured by converting the RGB images into grayscale.

5.8 RESULTS AND DISCUSSION

PDMS is an extensively used material in the manufacture of medical devices. The chemical and biological inertness of this material makes it highly suitable for use in these healthcare

applications. Breast implants based on PDMS have been used for several decades to reconstruct the shape and size of the breast. However, these implants are hydrophobic in nature, and this results in non-specific adsorption of plasma proteins on the implant surface. This adsorption has been shown to adversely affect the biocompatibility of the implant, and it increases the failure rate of implants. Surface coatings have emerged as a promising methodology for mitigating this risk of failure. However, medical devices frequently exhibit a failure due to cracking, crazing, and delamination of the surface coating. In this work, we have modified the surface of PDMS implant using coating of a biocompatible natural polymer silk fibroin. However, as shown in Chapter 4, SF coating prepared using simple dip coating techniques have poor cracking resistance. Hence, we have developed novel formulations based on hydrophilic polypeptide and compared its performance with a model anti-fouling molecule polyethylene oxide (PEO). The coatings of SF and its blends with ELP/PEO have been characterized using various spectroscopic and microscopic techniques, and the crack resistance of these coatings has been studied under mechanical deformation.Further, the stability of these coatings in an aqueous environment has also been studied. The coatings have also been evaluated for their biological performance in protein adsorption and their ability to support cell attachment and cell proliferation.

5.8.1 Surface Modification and Coating on PDMS

The surface coating of SF and SF blends was characterized using water contact angle and FTIR-ATR spectroscopy. Pristine PDMS shows a water contact angle of $112°\pm5°$ due to hydrophobic methyl groups on the surface. The drop in the contact angle from hydrophobic to the intermediate water contact angle of $65°\pm5°$confirms the modification of PDMS surface with SF. SF films have been shown to exhibit a water contact angle in the range of $58°$ to $75°$[191]. Our observations are thus in agreement with the reported literature. SF/PEO and SF/ELP blend coatings show a further reduction in the water contact angle to $45°\pm3°$and $53°\pm3°$respectively. ELP is a hydrophilic protein predominantly consisting of a repetitive sequence of GVGVP. The proline and valine amino acids are responsible for the hydrophilicity of the ELP protein. ELP protein by itself is shown to exhibit a water contact angle in the range from $25°$- $66°$. The silk elastin copolymers where the ratio of silk to elastin is 75:25 exhibit a contact angle of $52\pm4°$and is dependent on the ratio of the two proteins used and
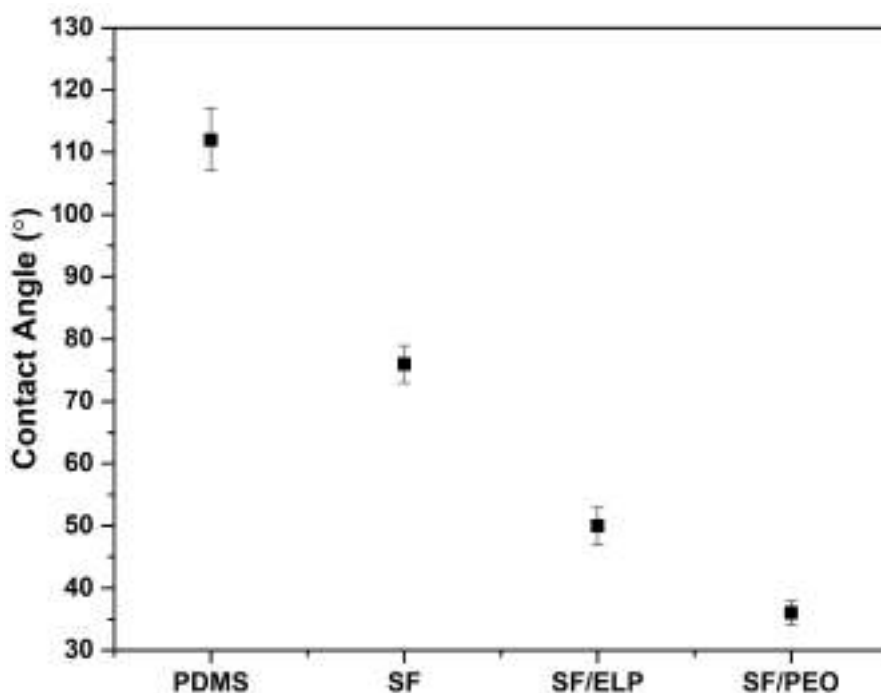
Figure 5.9: Contact angle measurements of uncoated and coated on PDMS discs

their molecular weights selected[192]. The contact angle for the SF/ELP blend was found to be in-line with these earlier reports. Also, the presence of hydrophilic functional groups on PEO results in the hydrophilic water contact angle. The SF/PEO (900 kg/mol) blends fabricated using the electrospinning technique have been shown to have a contact angle ranging from 25°to 48°. The water contact of PEO depends on molecular weight of PEO used for blending with SF. Also, the low molecular weight PEO shows higher contact angle, and it reduces with further increase in molecular weight[193], [194].

The modification of the PDMS surface with SF and SF blend coatings was also studied using FTIR-ATR spectroscopy, and this data has been summarized in Figure 5.10. The PDMS has no signal beyond the 3000 cm^{-1} range. The peaks at 2963 cm^{-1} and 2903 cm^{-1} correspond to symmetric and asymmetric CH_3 stretching vibration. The signal in the range of $1200 - 800$ cm^{-1} confirms the presence of Si-O-Si linkages on PDMS. PDMS, PEO, Elastin, and SF were used as control samples. The pure PEO sample shows sharp absorptions peaks at 2875 cm^{-1} corresponding to the intrinsic band of asymmetric stretching of (C-H) bond in the CH_2 moeity of the PEO chain. The peaks at 1465 cm^{-1} and 1345 cm^{-1} corresponds to swing vibrations of the C-H group, while the peak at 1090 cm^{-1} corresponds to the C-
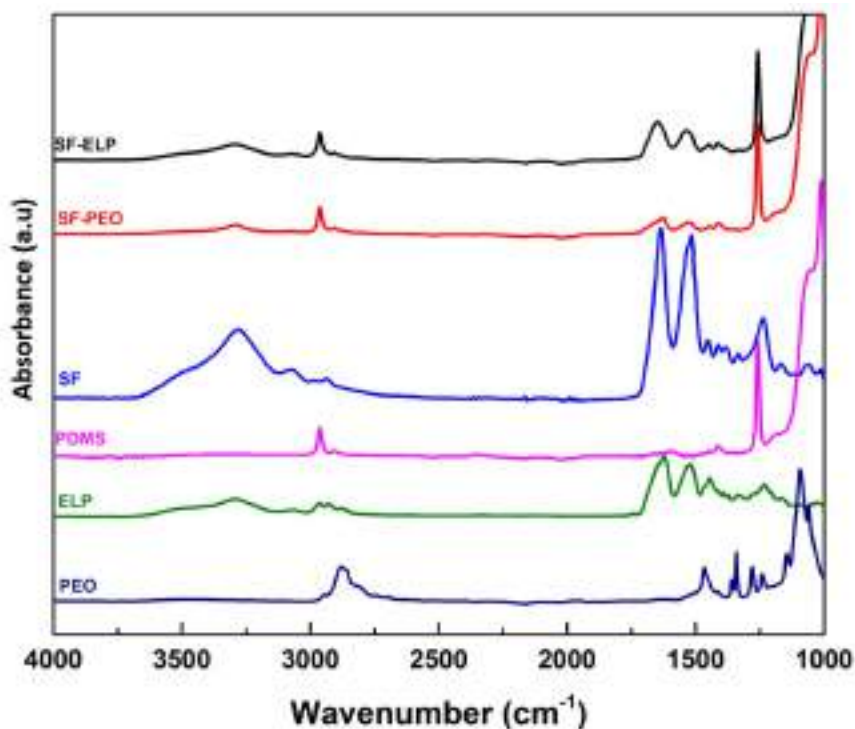
Figure 5.10: FTIR spectra of uncoated and coated PDMS substrates

O-C vibrational stretching of PEO chain. The C-H swing vibrations and C-O-C vibrational stretch confirm the amorphous nature of PEO chain[193]. The absorption peaks at 950 cm^{-1} and 845cm^{-1} correspond to the C-H stretch of the CH$_3$ group's rocking vibrations and the PEO chain's helical structure, as shown in Figure 5.10. ELP shows characteristic peaks at wavenumbers 3300 cm^{-1} corresponding to the N-H and O-H stretching vibration. The CH$_3$ stretching vibrations are seen at 2965 cm^{-1} and 2954 cm^{-1}. The Amide I and Amide II peaks of ELP were present at 1622 cm^{-1} and 1522 cm^{-1}, respectively[192]. The addition of ELP to the SF coating does not alter any of the signature peaks seen in the spectra. This is expected since the ELP protein does not have any other functional groups dominating the ATR-IR signals. However, blending with SF causes a shift in the Amide I to 1645 cm^{-1}, and this shift point towards the presence of both SF and ELP.

The stability of SF and its blends depends on the crystallinity and amount of β sheet content of the SF chain. The changes in SF's secondary structure upon blending with ELP and PEO were characterized by deconvoluting the Amide I peak in the range from 1600 cm^{-1} to 1700 cm^{-1}. The SF protein without any post-treatment after a simple dip coating process

has a beta sheet content of 36% and a random coil content of 30 %. Thus, post-treatments such as methanol vapor annealing are required to increase the β sheet content and improve the aqueous stability of SF coatings. The SF/PEO blends show a higher beta sheet content of 40% without any post-treatment than pure SF, resulting in more stable coatings without any post-treatment. Similarly, the quantification of β sheet content on SF/ELP shows lower beta sheet content of 22% than pure SF and SF/PEO blends. The crystallinity reduction is due to the co-existence of random coil conformation for both SF and ELP chains. Also, the changes in SF's secondary structure of SF/ELP blend is due to the predominant random coil conformation of ELP. As can be seen in the Figure 5.10 b, SF/ELP blend shows a peak at $1646 cm^{-1}$ (Amide I) and 1532 cm^{-1} (Amide II) assigned to random coil conformation[192]. Also, methanol treatment induces a molecular reorganization, and crystallinity of SF/ELP blend increases from 23 to 36%. This results in a more insoluble SF blend coating on PDMS. Similar increase in β sheet content upon treatment with methanol has also been observed for silk-elastin like (SELP) copolymers[195]. Thus,our observations are in agreement with the reported literature.

5.8.2 Crack resistance of coatings

Crack resistance of SF, SF/PEO, and SF/ELP coating on PDMS was characterized by subjecting these coated PDMS strips to a mechanical load. An SEM micrograph was captured at the center of these coated strips after they relaxed back to original position post the mechanical loading. The Chapter 3 and 4 showed that this method can be reproducibly used to quantify the cracking resistance of the coatings.

The surface morphology of SF and SF blend coatings, before and after mechanical deformation using tensile elongation at 100% strain and central region of the samples is summarized in Figure 5.11 (a-c). SF, SF/ELP and SF/PEO shows smooth and uniform surface morphology before mechanical deformation. This indicates the formation of an uniform coating on the PDMS samples. After mechanical deformation, SF coated PDMS results in complete delamination of SF layer from the PDMS substrates. When SF is blended with a plasticizing molecule such as PEO an enhancement in crack resistance was observed. The mechanical improvement of SF/PEO is shown in the Figure 5.11 (e). SEM images show minor amount of folds on the surface. However, there is no indication of delamination of

the coating from the PDMS substrate. Interestingly, SF/ELP blend coatings show better enhancement in the crack resistance of the coatings as evident by the SEM images after mechanical deformation. Thus, it can be concluded that the incorporation of elastin-like molecules reduces the mechanical failure of SF coatings on PDMS surfaces. These observations are inline with the literature. The mechanical stability of rigid polymer films can be enhnaced by blending with plasticizing molecules or polymers such as PEG and glycerol. In an earlier report, it has been shown that SF/PEO blends exhibit an improvement in elongation at break. Similar improvement in elongation at break has also been observed for composite films of starch blended with glycerol, sorbitol, or combination of glycerol and sorbitol [196]. Hydroxypropyl methylcellulose (HPMC) blended with PEG also showed similar improvement of elongation at break[197]. This improvement in elongation at break can be correlated to the enhancement in crack resistance.

It is also important to note here that improvement in crack resistance for SF/PEO blend is mechanically different than the SF/ELP blend. PEO act as a plasticizer and enables better chain mobility. On the other hand, elastin like polypeptides are molecules with excellant elongation to break. Elastin hydrogels has the potential to stretch to about 400 – 1500% tensile strains as demonstrated by Desai *et al.*. The extent of elongation depends on the chain length of the ELP repeat sequnce. ELP, used in our study, has the potential to withstand tensile deformation of 100% without any failure[198]. Thus, SF/ELP blend results in formation of coatings with enhanced crack resistance.

5.8.3 *In-vitro* degradation studies of SF blend films

The *in-vitro* degradation studies of the SF/ELP and SF/PEO films were carried out using the protease Type XIV enzyme from *streptomyces griseus* enzyme. The weight loss of SF/ELP and SF/PEO was measured at various time intervals and was calculated after drying at 60°C under vacuum for 6h to remove the water. The weight loss was calculated using equation 1 to understand the extent of weight retention or bioerosion.

The stability of surface coatings in aqueous environments ia an important performance parameter determining the failure of device. Our study focussed on the stability of SF and SF blends films under different biological environments. The proteolytic degradation of SF
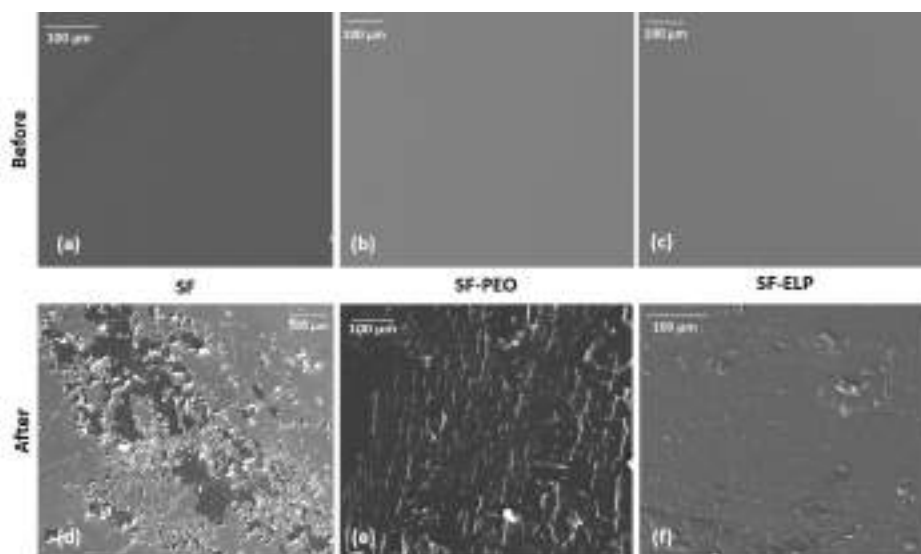
Figure 5.11: (a): SEM images of (a&d)SF (3:1), (b&e) SF/PEO (3:1) and (c&f)SF/ELP, before and after tensile deformation at 100% strain

SF/PEO   **SF/ELP**
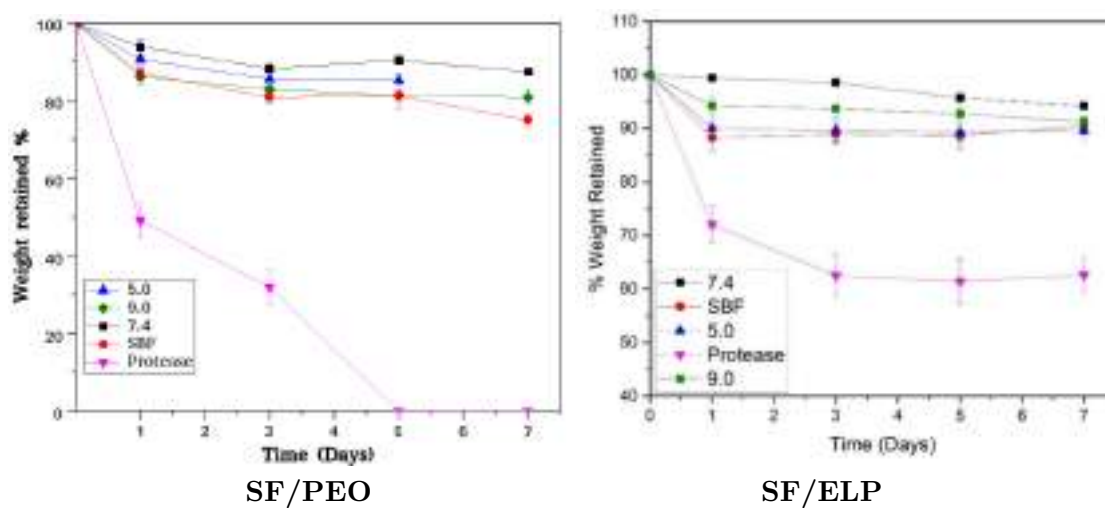
Figure 5.12: Degradation of SF/PEO and SF/ELP blend films in PBS at 37°C for 7 days

blends is summarized in the Figure 5.12. The stability of SF in aqueous environment is governed by various physical and chemical factors such as the porosity of the material, pore size, and secondary structure of the SF chains. The SF films incubated in protease enzyme result in a weight loss of 10-30 % on day 3, depending on the post treatment process. The degradation process starts with degradation of hydrophilic amorphous domains of the silk chains followed by the hydrophobic crystalline domains of the silk chains [199]. The proteolytic degradation of SF/PEO films shows accelerated degradation as compared to SF/ELP and SF. The PEO is a hydrophilic molecule and has a high affinity towards the water. Thus, the films quickly swell with water. Remya *et al.* demonstrated that, when PEO having molecular weight 100 kg/mol is blended with PCL, it also shows a higher weight loss and the extend of degradation depends on the PEO content[200]. The proteolytic degradation of SF/ELP results in a weight loss of 36% after 3rd day, and no further weight loss was observed. The weight loss observed on SF/ELP blend was due to the degradation of hydrophilic amorphous chain present on both SF and ELP. This indicates that that SF/ELP results in slower degradation as compared to SF/PEO blends. The SF/ELP shows more stable coatings on the PDMS surface, and this could be due to the higher β-sheet of SF after post-treatment of SF/ELP blend films. Vasconcelos *et al* demonstrated that *in-vitro* degradation studies of SF/ELP blend using porcine pancreatic elastase enzyme shows a weight loss of 36% on methanol treated SF/ELP samples and 28% on methanol treated genipin crosslinked SF/ELP samples. Degradation rate depends on extent of β-sheet content and amount of elastin in SF/ELP blends. Thus, our observations are in agreement with reported literature[201]. The stability of SF blend films at different pH was also performed. As can be seen from Figure 5.13, at physiological pH of 7.4 in PBS shows a less than 10% weight loss is observed for SF/PEO and SF/ELP. The mass loss is due to the random coil conformation of SF in both blends. In the case of PEO, it shows a higher amount of mass loss as compared to SF/ELP. The mass loss at pH 7.4 is 10% after 7 days for SF/PEO, while SF/ELP shows only 2% mass loss.

Similarly, the mass loss in the simulated body fluid for SF/PEO is close to 20 %, while SF/ELP shows only 10% weight loss. Similar trends are seen at pH 5.0 and 9.0. Thus, it is concluded that SF blended with ELP will result in more stable and robust coatings on
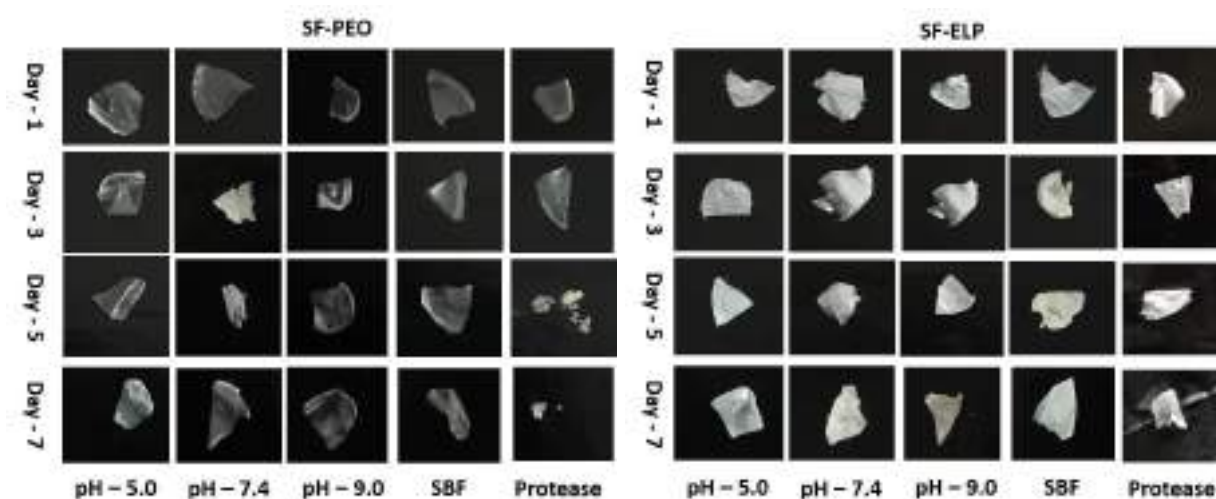
Figure 5.13: Digital images of SF/PEO and SF/ELP blend films after incubation and drying

PDMS, as compared to SF/PEO blends.

5.8.4 *In-vitro* cell proliferation study

The coated and uncoated PDMS discs were evaluated for cell proliferation with the help of *in-vitro* cell culture studies. Mouse Fibroblast cell line (L929) was chosen for this study. Figure 5.14 shows that all four types of uncoated and coated PDMS discs support the growth of cells, and cell proliferation was significantly higher on 7th day with respect to 3rd day. (Significance between day 3 and 7 for PDMS $p < 3.78e-3$; PDMS-SF $p < 6.70e-7$; PDMS-SF/ELP $p < 2.47e-3$ and PDMS-SF/PEO $p < 5.38e-5$). Thus, it can be concluded coated and uncoated PDMS discs are non-toxic to cells and support the cells to grow and proliferate.

5.8.5 Cell morphology by actin cytoskeleton staining

Further, to confirm morphology of grown L929 cells on different discs, F-actin cytoskeleton staining was performed with the help of Alexa Fluor 488 phalloidin probe. The behavior of cells on scaffolds is directly related the substrate or the material to which they attach while growing. The cell morphology observations are relatable to MTT results that have been obtained. Figure 5.15 shows the actin cytoskeleton of L929 cells grown on coated and uncoated PDMS discs. From the images it can be inferred that there is significant cell growth on all the discs. Elongated cell morphology is clearly visible for PDMS-SF and
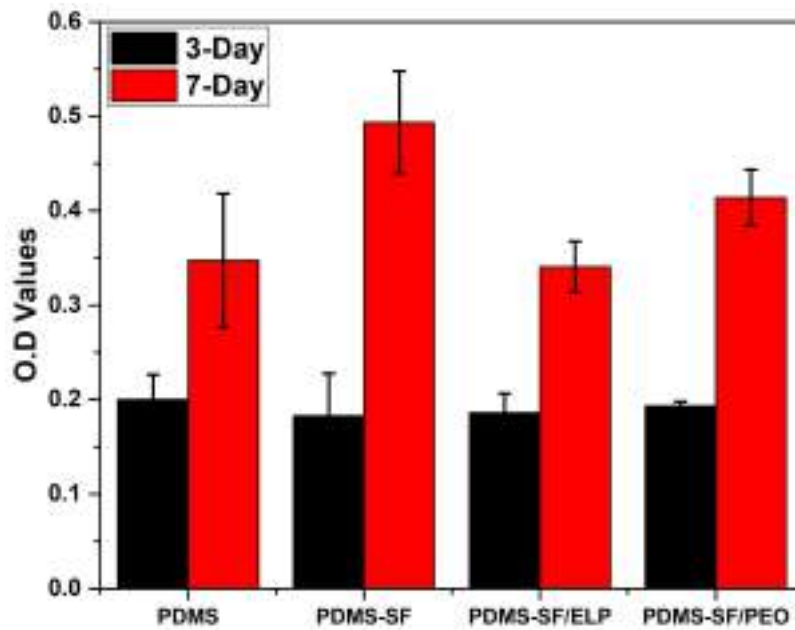
Figure 5.14: Cell proliferation assay (MTT assay) of L929 cells cultured on PDMS, PDMS-SF, PDMS-SF/PEO and PDMS-SF/ELP
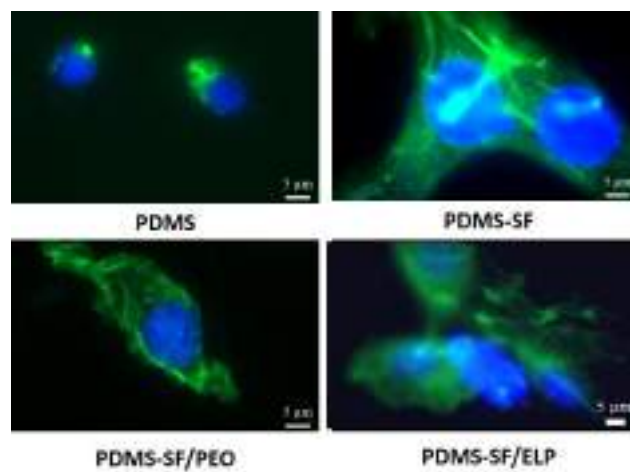
Figure 5.15: Staining of Actin filaments of L929 cells seeded on PDMS, PDMS-SF, PDMS-SF/ELP and PDMS-SF/PEO

PDMS-SF/PEO and PDMS-SF/ELP discs. For PDMS discs elongated morphology of cells was not observed. The variations in cell morphology can be due to type of material used to coat PDMS discs.

5.8.6 Protein adsorption of fluorescently labelled blood plasma protein on uncoated and coated PDMS discs

The non-specific protein adsorption on uncoated and coated PDMS was studied using serum proteins abundantly present in the body fluids such as albumin and fibrinogen. Flourescently labelled Bovine Serum Albumin (BSA) and Fibrinogen (FGN) were chosen as the model proteins. The fluorescent intensity of FITC-BSA and FITC-FGN strongly adsorbed on uncoated and coated PDMS surfaces was monitored as a function of time. The flourescent intensity was calculated from the micrographs captured at different time points. This data has been shown in Figure 5.17. The fluorescent intensity of adsorbed proteins was found to increase with time. A maximum intensity after 10 minutes was observed for most samples. An average of 10 images was used to quantify the flourescent intensity for each sample at each time point. The data has been summarized in Figure 5.16. The SF coated PDMS discs reduce the BSA adsorption at 10 minutes. Also, at 30 minutes the BSA protein adsorption has not saturated. Blending SF, with both PEO and ELP significantly reduces the adsorption of the protein. The extent of BSA adsorption on SF/PEO and SF/ELP samples was found to be comparable. The reduction in the protein adsorption on these samples could be attributed to the presence of hydrophilic functional groups. At 30 minute time point, the SF, SF/PEO and SF/ELP coatings reduce the BSA adsorption by 65%, 94% and 84%, respectively as comapred to pure PDMS surface.

Similar protein adsorption trends were also seen for the fibrinogen protein. The fluorescent intensity was found to increase with time. It reaches a maximum intensity after 10 minutes. Here, the SF, SF/PEO and SF/ELP coatings were found to be comparable in their ability to inhibit adsorption of fibrinogen. The FGN adsorption on SF, SF/PEO and SF/ELP was found to be reduced by 55%, 60% and 58%, respectively.

The extent of FGN protein adsorption is higher on PDMS, SF/ELP and SF/PEO as compared to BSA adsorption. Srokowski *et al.* demonstrated fibrinogen adsorption process

Bovine Serum Albumin (BSA)

Fibrinogen (FGN)
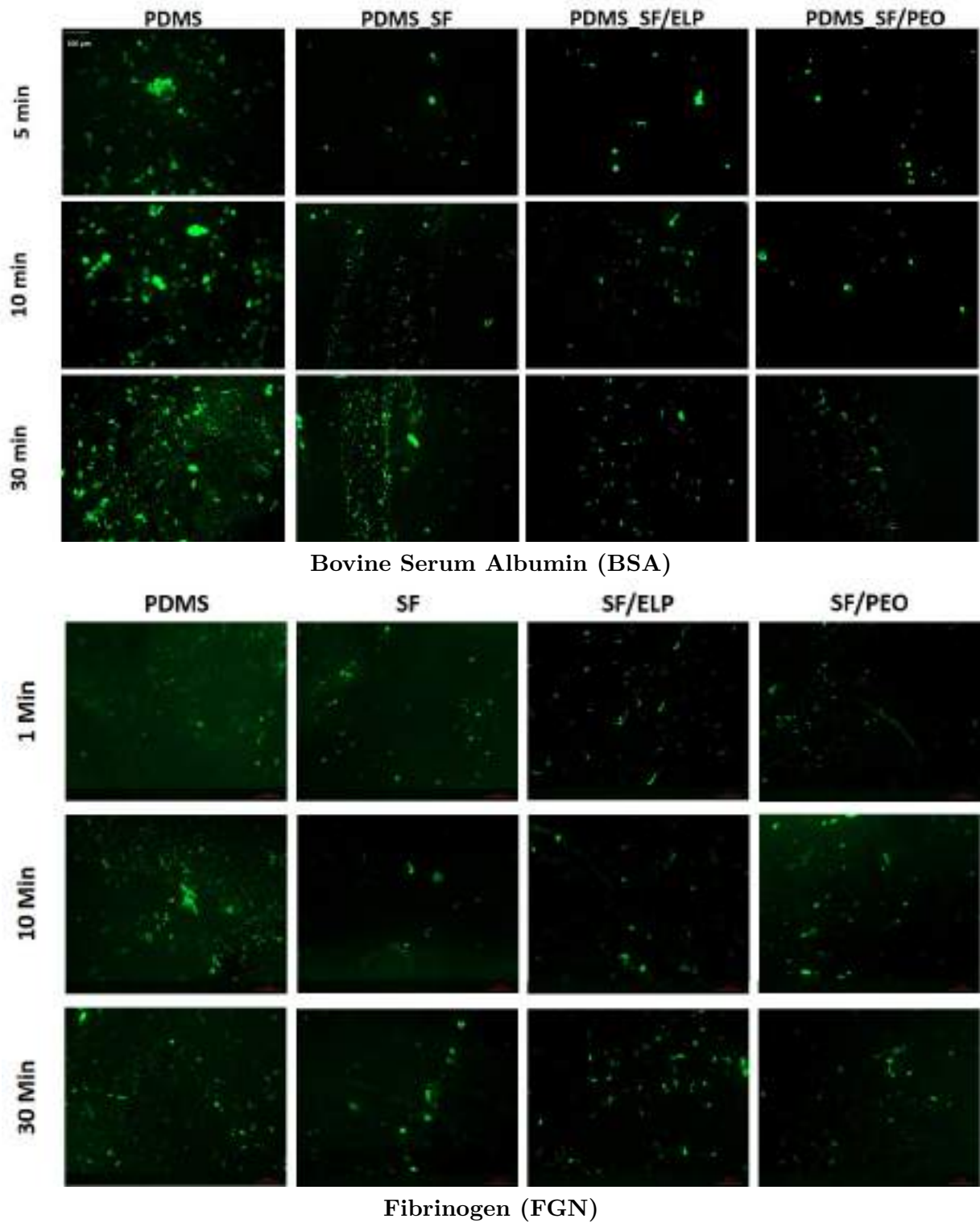
Figure 5.16: Fluorescence microscopy images of (a) BSA and (b) FGN on uncoated and coated PDMS discs

Bovine Serum Albumin (BSA)   **Fibrinogen (FGN)**
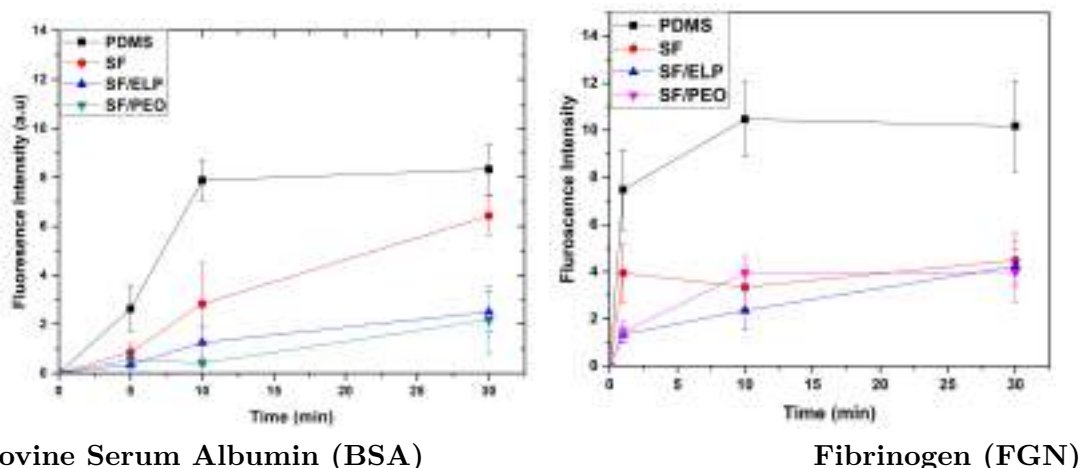
Figure 5.17: Quantification of protein adsorption of (a) BSA and (b) FGN on uncoated and coated PDMS discs

on various ELP. The authors reported extremely low adsorption on ELP surfaces compared to commercial hydrophobic Mylar. The extent of fibrinogen adsorption also depends on the chain length of ELP. The shorter chain has higher adsorption than larger ELP chains[202]. Similar studies on ELP nanoparticles suggest one order of magnitude reduction on ELP nanoparticles compared to thermoresponsive gelling hydrogels and bioactive glass. Therefore, it is maybe concluded that coating implant surface with hydrophilic molecules can drastically reduce the protein adsorption and eventually mitigate the risk of implant failure to a large extent.

5.9   Conclusion

Surface coatings have emerged as a promising alternative to reduce implant failure due to foreign body response and device associated infections. Failure of coatings due to cracking, delamination, flaking is also a concern for successfully using implants. Here, we report a blending of a hydrophilic molecule such as PEO and ELP with SF. Dip-coating these blends results in a mechanically stable coating on an elastomeric substrate like PDMS. These coatings are crack-resistant under mechanical deformations in tensile and bending modes. Further, we have evaluated the protein adsorption on SF and SF blend coating; SF/ELP has the potential to prevent or reduce protein adsorption for BSA and fibrinogen. Also, SF/ELP

coating has excellent aqueous stability. The stability of the formulations was evaluated in various biological environments. All these functions have been achieved while retaining the inherent biocompatibility of these materials. Thus, our work demonstrates an innovative solution to simultaneously resolve multiple causes for failures of implant devices – foreign body response and cracking of the coating.

Chapter 6

Conclusion and Future Work

A PDMS or silicone breast implant is frequently used in breast cancer patients post mastectomy to reconstruct the shape and size of the breast. However, the safety of silicone based implantable medical devices has been a challenge since their introduction. The primary reasons for implant failure are foreign body reaction and biofilm formation. The primary focus of this work is to reduce the rate of failure of silicone breast implants by coating the implants with a biocompatible polymer-silk fibroin The work has been divided into three Sections:

- Development of test methods to improve the adhesion of SF to PDMS substrates

- Development of crack-resistant SF coating on modified PDMS using an innovative coating process

- development of crack-resistant SF blend coatings.

The detailed objectives of each Section have been summarized in Chapter 1 and 2. Chapter 3, 4 and 5 describe in detail the work done and highlight the key experimental results. This Chapter summarizes the key conclusions of work and define the path forward for future studies.

6.1 Summary: Promising strategies for further evaluation

The work presented on SF coatings on PDMS in this thesis is experimental investigations to mitigate the risk of implant failure on breast implants. The summary and key conclusions

of each of the objectives and the work done are summarized below:

6.1.1 Adhesion of silk fibroin coating to PDMS

Surface coatings are one of the most promising strategy to reduce implant failure rate. Adhesion of coating to the surface of PDMS implant has not been adequately studied in the literature. Recently, US-FDA has recalled few medical devices and the reason for recall was delamination of these coatings. Delaminated coating material can diffuse into the body fluids causing serious health issues. Thus, excellent adhesion of coating to the substrate is critical for enhancing the performance of surface coated silicone implants. The first objective of this work has been focused on developing test methods to quantify the adhesion of modified PDMS substrates and SF. Various techiniques, both microscopic and mesoscopic such as Cross-hatch test, Tensile test, nano-scratch, AFM force spectroscopy and nanoindentation measurements have been used to develop an understanding about adhesion of SF to modified and unmodified PDMS substrates. The surface modification of soft PDMS substrate results in a more hydrophilic surface with the formation of –OH or –NH_2 groups. These hydrophilic surface groups can interact with SF during the dip-coating process through secondary interactions and eventually result in enhanced adhesion between modified PDMS and SF. The bulk scale mechanical measurements on SF coating on modified and unmodified PDMS indicates resistance to delamination on modified PDMS than unmodified. Image analysis of cross-hatch test showed a drastic enhancement in adhesion for oxygen plasma-treated and APTES treated PDMS samples. The nanomechanical measurement on these samples also supports the bulk scale measurements. The optical images of SF coated PDMS substrates after nano scratch measurements showed complete delamination on unmodified PDMS. However, SF-O_2-PDMS and SF-APTES-PDMS treated samples did not suggest delamination, but micro-cracks are orthogonal to the test track. The crack density on SF-O2-PDMS samples was higher than SF-APTES-PDMS, indirectly supporting better adhesion for APTES treated samples. Further, nanoindentation measurements were performed to understand the interfacial behavior of the coating on SF coated PDMS substrates. The SF-PDMS samples exhibit a mechanical failure at a very low load with less than 100 nm penetration depth. However, SF-O2-PDMS indicates a mechanical failure at a load of 5µN with a penetration depth of 350nm. This penetration corresponds to the thickness of the SF coating on oxygen

plasma treatment, indicating failure occurs at SF coating and the modified surface layer of PDMS. Similar measurements were performed on SF-APTES-PDMS. Interestingly, there is no indication of mechanical failure at the interface and beyond even with load as high as 20μN. The cross-sectional SEM images of SF coated on modified substrate suggest that the amount of SF present or thickness of the SF coatings depends on the interaction between SF and functional groups present on each modification. Thus, mesoscale and microscale measurements conclude that APTES treated PDMS has higher interaction than O2-PDMS and PDMS. The mechanism of enhanced adhesion on APTES-PDMS was probed using modified AFM-Force Spectroscopy. The force-displacement curve of force spectroscopy provides information about the number of interacting sites on each modification and energy to break the interaction. The Force-displacement curve suggests that unmodified PDMS did not have any interaction site for interacting with the SF chain. Oxygen plasma-treated PDMS show 3-5 interacting sites in a 10x10 nm area, but APTES treated PDMS shows 12-16 interacting sites in the same area. Thus, it is concluded that the enhanced adhesion of SF coating with APTES treated PDMS is due to a higher number of interaction sites and higher pull off energy. This study explains the surface modification of PDMS using physical and chemical methods, followed by test methods to quantify the adhesion between the coating material and substrate.

6.1.2   Crack-resistant SF coatings on PDMS

In Chapter 3, the work focused on the surface modification of PDMS using physical and chemical methods, followed by test methods to quantify the adhesion between the coating material and substrate. The work also demonstrated that modofying the surface of PDMS using APTES results in improved adhesion of coating to the substrate. However, SEM images of SF coatings on APTES-PDMS show a minor amount of micro-cracks on the surface coatings. Thus, body fluids can diffuse into the PDMS layer through these micro-cracks and accelarate implant failure. Here, we focused on developing crack-resistant SF coatings on modified PDMS and incorporating a functional anti-quorum sensing molecule to reduce the biofilm formation. This work demonstrates a novel coating process using a combination of two conventional processing protocols - dip coating and electrospinning - to form a self-reinforced coating. Regenerated SF solution was used for dip-coating, and SF-HFIP so-

lution using lyophilized SF powder was used for the electrospinning process. The SF coating was characterized using water contact angle, FTIR, SEM, AFM and UV spectroscopy. The electrospun SF nanofibers were embedded in the dip-coated layer. The results show that SF coating prepared using a novel coating process retains it integrity inspite of mechanical deformation at different strains in bending, tensile and torsion modes in wet and dry conditions. The electrospun fibres exhibit regions of stress whitening, indicating that the nanofibers primarily take up the mechanical stress exerted on the samples. Thus, the damage caused to the lower dip-coated layer is minimal. These coatings were further functionalized using a G-citron green molecule obtained from a glycomonoterpene. The coatings exhibited resistance to biofilm formation on the implant surface. The G-citron molecule was incorporated in the electrospinning step without affecting the mechanical performance of the SF nanofibers. The molecule also retains its quorum sensing activity throughout the processing steps and inhibits biofilm formation of two of the most notorious infection-causing bacterium - P aeruginosa and S epidermidis. This is characterized using crystal violet assay and SEM images after incubation in the bacterial culture. All these functions have been achieved while retaining the inherent biocompatibility of silk. Thus, our study demonstrates an innovative solution to simultaneously resolve multiple causes for failures of implant devices – biofilm formation, foreign body response and cracking of the coating.

6.1.3 Development of novel blends of silk fibroin with other suitable polymers/ biomolecules that further improve performance of coatings

6.2 Proposed future work of the study

The learnings from this work have the potential to be developed into a technology. However, to translate the protocols developed into a technology requires further studies. This Section outlines the important future work identified. It involves development of suitable prototypes of breast implants which must be evaluated for advanced biological studies.

6.2.1 Proteomic studies

Our studies in Chapter 5 have shown that coating the PDMS using SF or SF blends, results in significant reduction in Protein adsorption. However, it is important to evaluate these

observations in an experiment by use of actual human blood samples. The human blood plasma typically contains more than 200 different proteins. Serum albumin and fibrinogen are the two proteins that are present in the highest amount. We did a preliminary experiment to evaluate the different plasma proteins that adsorb on a PDMS discs. The data suggests 83 proteins have high affinity to PDMS substrates. It would be interesting to see which proteins and in what quantites adsorb on the PDMS discs coated with SF and SF blends

6.2.2 Advanced *in-vitro* studies

The biological studies performed using mouse fibroblast cell line with L929 cell line to evaluate the *in-vitro* cytotoxicity of the SF and SF blend coatings confirmed that these materials are non-cytotoxic. However, advanced *in-vitro* studies using various cell lines such as breast fibroblasts, breast adipocytes and breast cancer cell lines must be completed to establish the biocompatibility of implant coating. Further, it is also necessary to see the effect of these coating materials on various primary cells procured from breast cancer patients. In addition to this, it is also important to study the immune response of various coating materials. The priliminary *in-vitro* studies using macrophage cell lines must be performed to monitor expression of inflammatory markers like Tumor necrosis factor (TNF-α), Interleukin 1 beta (IL-1β), Interleukin 16 (IL-16). Advanced immunlogical studies using dendritic cells also enable to determine immunological characteristics for these materials.

6.2.3 Coating methandologies on commercial breast implants

n this study, SF and SF blend coatings were prepared on either a circular disc or rectangular block of PDMS by dip-coating and electrospinning process. These specimens shapes and sizes were selected so as to enable measurement of various factors like adhesion of coating to substrate, hydrophilicity, spectroscopy,crack resistance, cell culture studies, etc. However, the coating protocols must be scaled up and the process must be developed to coat silicone implants that are mainly spherical or elliptical 3D structures. The performance of surface coatings depends on the uniformity of the coating thickness. The surface coating must be characterized spectroscopically and morphologically. This developed prototype can then be used for advanced *in-vitro* studies.
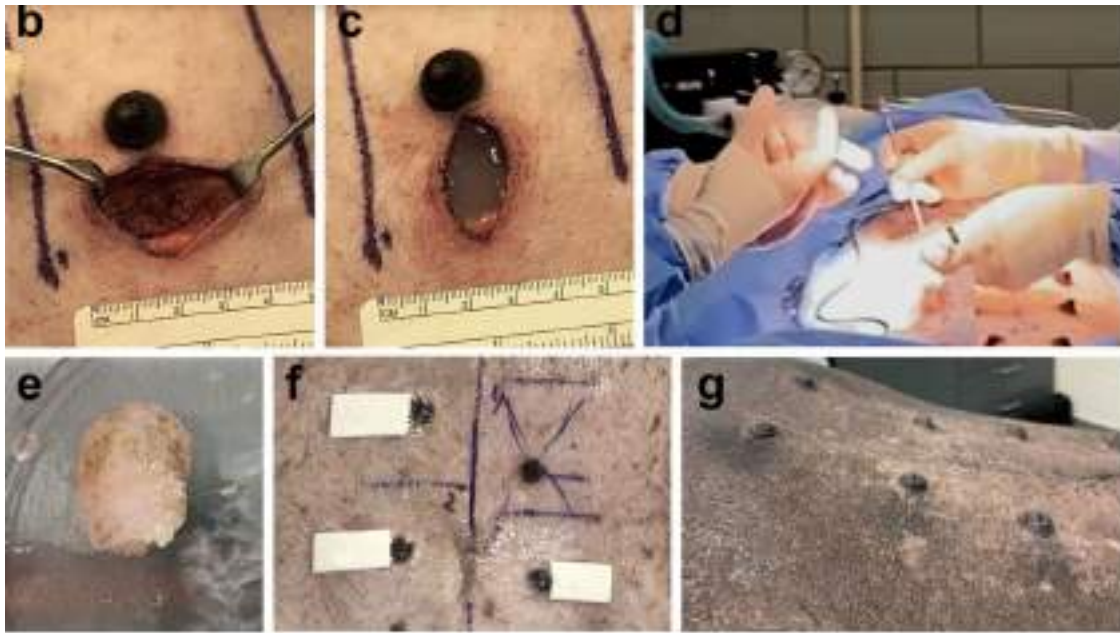
Figure 6.1: Overview of simulated lumpectomy procedures in guinea pig[203] Reproduced with

6.2.4   Simulated breast reconstruction in porcine model

The femaie mini-pigs are the most preferred animal model that has been used in translational studies due to their anatomical and physicological similarities to human breast tissue. Also, porcine model has 12 breast tissue and no of animals required for each study is less than rat model. The pig breast have variable volume, consistency and compsotion with in and between individual which is similar to human tissue as shown in the figure 6.1. The prototypes of coated implants developed in Section 6.2.3 can then be implanted in this porcine model. The histopathology studies at various time points can provide crucial insights about fibrotic tissues formed around the implant. If these studies show promising results, the technology can be developed towards commercialization.

ABSTRACT

Name of the Student: Emmanuel Joseph   **Registration No. : 20EE16A26034**

Faculty of Study: Engineering Sciences   **Year of Submission: 2021**

AcSIR academic centre/CSIR Lab: CSIR-NCL   **Name of the Supervisor(s): Dr. Anuya Nisal**

Title of the thesis: Design and Development of Biocompatible Silk Fibroin Coatings for Breast Implant Applications

---

Globally, Breast cancer accounts for about 23% of all cancers. PDMS or silicone breast implant is used in the breast reconstruction surgery to recreate the original shape and size of the breast post mastectomy. However, the safety of silicone based implantable medical devices has been a challenge since their introduction. The common clinical problems associated with silicone implants are autoimmune diseases, capsular contracture, biofilm formation, allergic reaction and recently there is also a presence of a rare type of cancer. Coating the surface of biomedical implants is a promising strategy to reduce the failure rate of implants. In this work, we coat the surface of silicone implant using a biocompatible natural protein polymer silk fibroin (SF). The PDMS surfaces have been modified using oxygen plasma treatment and 3-amino-propyl-triethoxy-silane (APTES) treatment. Interestingly, testing of the coated samples using a bulk technique such as tensile and bending deformation showed that the SF nano-coating exhibits improved crack resistance when the PDMS surface has been modified using APTES treatment as compared to oxygen plasma treatment. These results were validated at the microscopic and mesoscopic length scales through nano-scratch and nano-indentation measurements. Further, the work demonstrates that a novel process combining conventional dip coating with electrospinning results in the formation of a crack-resistant coating. The coating was also further functionalized using a green biomolecule – glycomonoterpene prepared using citronellal and glucose. These functional compounds are being touted as the next generation antibiofilm molecules on account of quorum sensing inhibitory activity. Also, we report functional coatings of silk fibroin and its blends with biopolymers and the effect of molecular weight of PEO on mechanical properties and aqueous stability of SF/PEO blend coatings on PDMS surface. Further, SF coatings have also been developed by blending with a novel polymers such as recombinantly produced elastin-like peptide (ELP), a class of polypeptide obtained from the primary sequence of mammalian elastin with a repeat unit of (GVGVP). The SF-ELP coatings were characterized for their physio-chemical and mechanical properties and their properties were compared with a selected molecular weight of PEO used for blending. The mechanical stability of SF-ELP blends shows more stable coatings than SF-PEO blends. The biological evaluation of these SF blends was performed by doing protein adsorption, accelerated degradation and cytotoxicity studies. Thus, this study shows various material science strategies that can be used to mitigate the risk of silicone implant failure.

Bibliography

[1] I. Oberhauser, J. Zeindler, M. Ritter, *et al.*, "Impact of oncoplastic breast surgery on rate of complications, time to adjuvant treatment, and risk of recurrence," *Breast Care*, pp. 1–9, 2020.

[2] M. Mempin, H. Hu, D. Chowdhury, A. Deva, and K. Vickery, "The a, b and c's of silicone breast implants: Anaplastic large cell lymphoma, biofilm and capsular contracture," *Materials*, vol. 11, no. 12, p. 2393, 2018.

[3] J. M. Anderson, "Biological responses to materials," *Annual review of materials research*, vol. 31, no. 1, pp. 81–110, 2001.

[4] V. Nandakumar, S. Chittaranjan, V. M. Kurian, and M. Doble, "Characteristics of bacterial biofilm associated with implant material in clinical practice," *Polymer journal*, vol. 45, no. 2, pp. 137–152, 2013.

[5] M. Lam, V. Migonney, and C. Falentin-Daudre, "Review of silicone surface modification techniques and coatings for antibacterial/antimicrobial applications to improve breast implant surfaces," *Acta Biomaterialia*, 2020.

[6] E. Joseph, A. Patil, S. Hirlekar, *et al.*, "Glycomonoterpene-functionalized crack-resistant biocompatible silk fibroin coatings for biomedical implants," *ACS Applied Bio Materials*, vol. 2, no. 2, pp. 675–684, 2019.

[7] C. Cha, E. Antoniadou, M. Lee, *et al.*, "Tailoring hydrogel adhesion to polydimethylsiloxane substrates using polysaccharide glue," *Angewandte Chemie International Edition*, vol. 52, no. 27, pp. 6949–6952, 2013.

[8] *Breast cancer india*, www.breastcancerindia.net. [Online]. Available: `https://www.breastcancerindia.net/`.

[9]   E. Swanson and E. Hall-Findlay, "Banning textured implants is a rational decision to elim-
        inate the risk of breast implant–associated anaplastic large-cell lymphoma (bia-alcl)," *Aes-
        thetic Surgery Journal*, vol. 40, no. 8, NP474–NP477, 2020.

[10]   "Global cancer observatory: Cancer tomorrow." (2020), [Online]. Available: `https://gco.
        iarc.fr/tomorrow`.

[11]   P. H. Zeplin, N. C. Maksimovikj, M. C. Jordan, *et al.*, "Spider silk coatings as a bioshield
        to reduce periprosthetic fibrous capsule formation," *Advanced Functional Materials*, vol. 24,
        no. 18, pp. 2658–2666, 2014.

[12]   C. B. Borkner, M. B. Elsner, and T. Scheibel, "Coatings and films made of silk proteins,"
        ACS Applied Materials & Interfaces, vol. 6, pp. 15 611–15 625, Jul. 2014. DOI: `10.1021/
        am5008479`. (visited on 06/13/2021).

[13]   A. Valencia–Lazcano, R. Román–Doval, E. De La Cruz–Burelo, E. Millán–Casarrubias, and
        A. Rodríguez–Ortega, "Enhancing surface properties of breast implants by using electro-
        spun silk fibroin," *Journal of Biomedical Materials Research Part B: Applied Biomaterials*,
        vol. 106, no. 5, pp. 1655–1661, 2018.

[14]   A. Nisal, R. Sayyad, P. Dhavale, *et al.*, "Silk fibroin micro-particle scaffolds with superior
        compression modulus and slow bioresorption for effective bone regeneration," *Scientific re-
        ports*, vol. 8, no. 1, pp. 1–10, 2018.

[15]   C. Vepari and D. L. Kaplan, "Silk as a biomaterial," *Progress in Polymer Science*, vol. 32,
        pp. 991–1007, Aug. 2007. DOI: `10.1016/j.progpolymsci.2007.05.013`. (visited on
        09/02/2019).

[16]   N. Kasoju and U. Bora, "Silk fibroin in tissue engineering," *Advanced healthcare materials*,
        vol. 1, no. 4, pp. 393–412, 2012.

[17]   G. Gronau, S. T. Krishnaji, M. E. Kinahan, *et al.*, "A review of combined experimental
        and computational procedures for assessing biopolymer structure–process–property rela-
        tionships," *Biomaterials*, vol. 33, no. 33, pp. 8240–8255, 2012.

[18]   B. Kundu, R. Rajkhowa, S. C. Kundu, and X. Wang, "Silk fibroin biomaterials for tissue
        regenerations," *Advanced drug delivery reviews*, vol. 65, no. 4, pp. 457–470, 2013.

[19]   N. Minoura, M. Tsukada, and M. Nagura, "Physico-chemical properties of silk fibroin mem-
        brane as a biomaterial," *Biomaterials*, vol. 11, no. 6, pp. 430–434, 1990.

[20]   R. L. Horan, K. Antle, A. L. Collette, *et al.*, "In vitro degradation of silk fibroin," *Bioma-
        terials*, vol. 26, no. 17, pp. 3385–3393, 2005.

[21] S. A. Braley, "The use of silicones in plastic surgery: A retrospective view," *Plastic and reconstructive surgery*, vol. 51, no. 3, pp. 280–288, 1973.

[22] J. L. Thomsen, L. Christensen, M. Nielsen, *et al.*, "Histologic changes and silicone concentrations in human breast tissue surrounding silicone breast prostheses.," *Plastic and reconstructive surgery*, vol. 85, no. 1, pp. 38–41, 1990.

[23] J. E. Puskas and M. T. Luebbers, "Breast implants: The good, the bad and the ugly. can nanotechnology improve implants?" *Wiley Interdisciplinary Reviews: Nanomedicine and Nanobiotechnology*, vol. 4, no. 2, pp. 153–168, 2012.

[24] Y. Bachour, C. A. Bargon, C. J. de Blok, J. C. Ket, M. J. Ritt, and F. B. Niessen, "Risk factors for developing capsular contracture in women after breast implant surgery: A systematic review of the literature," *Journal of Plastic, Reconstructive & Aesthetic Surgery*, vol. 71, no. 9, e29–e48, 2018.

[25] B. Pittet, D. Montandon, and D. Pittet, "Infection in breast implants," *The Lancet infectious diseases*, vol. 5, no. 2, pp. 94–106, 2005.

[26] C. A. Feghali, T. M. Wright, *et al.*, "Cytokines in acute and chronic inflammation," *Front Biosci*, vol. 2, no. 1, pp. d12–d26, 1997.

[27] C. N. Serhan and J. Savill, "Resolution of inflammation: The beginning programs the end," *Nature immunology*, vol. 6, no. 12, pp. 1191–1197, 2005.

[28] J. M. Anderson, A. Rodriguez, and D. T. Chang, "Foreign body reaction to biomaterials," in *Seminars in immunology*, Elsevier, vol. 20, 2008, pp. 86–100.

[29] Z. Sheikh, P. J. Brooks, O. Barzilay, N. Fine, and M. Glogauer, "Macrophages, foreign body giant cells and their response to implantable biomaterials," *Materials*, vol. 8, no. 9, pp. 5671–5701, 2015.

[30] W. Siggelkow, A. Faridi, K. Spiritus, U. Klinge, W. Rath, and B. Klosterhalfen, "Histological analysis of silicone breast implant capsules and correlation with capsular contracture," *Biomaterials*, vol. 24, no. 6, pp. 1101–1109, 2003.

[31] W. Dolores, R. Christian, N. Harald, P. Hildegunde, and W. Georg, "Cellular and molecular composition of fibrous capsules formed around silicone breast implants with special focus on local immune reactions," *Journal of autoimmunity*, vol. 23, no. 1, pp. 81–91, 2004.

[32] K. Tan, D. Wijeratne, B. Shih, A. Baildam, and A. Bayat, "Tumour necrosis factor-α expression is associated with increased severity of periprosthetic breast capsular contracture," *European Surgical Research*, vol. 45, no. 3-4, pp. 327–332, 2010.

[33] L. Prantl, P. Angele, S. Schreml, D. Ulrich, N. Pöppl, and M. Eisenmann-Klein, "Determination of serum fibrosis indexes in patients with capsular contracture after augmentation with smooth silicone gel implants," *Plastic and reconstructive surgery*, vol. 118, no. 1, pp. 224–229, 2006.

[34] J. Brazin, S. Malliaris, B. Groh, *et al.*, "Mast cells in the periprosthetic breast capsule," *Aesthetic plastic surgery*, vol. 38, no. 3, pp. 592–601, 2014.

[35] J. Q. Owsley Jr and R. A. Peterson, "Symposium on aesthetic surgery of the breast," *Plastic and Reconstructive Surgery*, vol. 64, no. 2, pp. 255–256, 1979.

[36] M. Pasmore, P. Todd, S. Smith, *et al.*, "Effects of ultrafiltration membrane surface properties on pseudomonas aeruginosa biofilm initiation for the purpose of reducing biofouling," *Journal of Membrane Science*, vol. 194, no. 1, pp. 15–32, 2001.

[37] Z. Shah, J. A. Lehman Jr, and J. Tan, "Does infection play a role in breast capsular contracture?" *Plastic and reconstructive surgery*, vol. 68, no. 1, pp. 34–42, 1981.

[38] N. Kossovsky, J. P. Heggers, R. W. Parsons, and M. C. Robson, "Acceleration of capsule formation around silicone implants by infection in a guinea pig model.," *Plastic and reconstructive surgery*, vol. 73, no. 1, pp. 91–98, 1984.

[39] H. Tamboto, K. Vickery, and A. K. Deva, "Subclinical (biofilm) infection causes capsular contracture in a porcine model following augmentation mammaplasty," *Plastic and reconstructive surgery*, vol. 126, no. 3, pp. 835–842, 2010.

[40] P. Seng, S. Bayle, A. Alliez, F. Romain, D. Casanova, and A. Stein, "The microbial epidemiology of breast implant infections in a regional referral centre for plastic and reconstructive surgery in the south of france," *International Journal of Infectious Diseases*, vol. 35, pp. 62–66, 2015.

[41] S. Barr, E. Hill, and A. Bayat, "Functional biocompatibility testing of silicone breast implants and a novel classification system based on surface roughness," *Journal of the mechanical behavior of biomedical materials*, vol. 75, pp. 75–81, 2017.

[42] A. A. Valencia-Lazcano, T. Alonso-Rasgado, and A. Bayat, "Characterisation of breast implant surfaces and correlation with fibroblast adhesion," *Journal of the mechanical behavior of biomedical materials*, vol. 21, pp. 133–148, 2013.

[43] P. Jones, M. Mempin, H. Hu, *et al.*, "The functional influence of breast implant outer shell morphology on bacterial attachment and growth," *Plastic and reconstructive surgery*, vol. 142, no. 4, pp. 837–849, 2018.

[44] E. Medilanski, K. Kaufmann, L. Y. Wick, O. Wanner, and H. Harms, "Influence of the surface topography of stainless steel on bacterial adhesion," *Biofouling*, vol. 18, no. 3, pp. 193–203, 2002.

[45] K. K. Chung, J. F. Schumacher, E. M. Sampson, R. A. Burne, P. J. Antonelli, and A. B. Brennan, "Impact of engineered surface microtopography on biofilm formation of staphylo-coccus aureus," *Biointerphases*, vol. 2, no. 2, pp. 89–94, 2007.

[46] J. Hasan, R. J. Crawford, and E. P. Ivanova, "Antibacterial surfaces: The quest for a new generation of biomaterials," *Trends in biotechnology*, vol. 31, no. 5, pp. 295–304, 2013.

[47] S. Pogodin, J. Hasan, V. A. Baulin, *et al.*, "Biophysical model of bacterial cell interactions with nanopatterned cicada wing surfaces," *Biophysical journal*, vol. 104, no. 4, pp. 835–840, 2013.

[48] L. Liu, B. Ercan, L. Sun, K. S. Ziemer, and T. J. Webster, "Understanding the role of polymer surface nanoscale topography on inhibiting bacteria adhesion and growth," *ACS Biomaterials Science & Engineering*, vol. 2, no. 1, pp. 122–130, 2016.

[49] N. Encinas, C.-Y. Yang, F. Geyer, *et al.*, "Submicrometer-sized roughness suppresses bacteria adhesion," *ACS applied materials & interfaces*, vol. 12, no. 19, pp. 21 192–21 200, 2020.

[50] Z.-y. Lei, T. Liu, W.-j. Li, X.-h. Shi, and D.-l. Fan, "Biofunctionalization of silicone rubber with microgroove-patterned surface and carbon-ion implantation to enhance biocompatibil-ity and reduce capsule formation," *International journal of nanomedicine*, vol. 11, p. 5563, 2016.

[51] B. Y. Yoo, B. H. Kim, J. S. Lee, *et al.*, "Dual surface modification of pdms-based silicone implants to suppress capsular contracture," *Acta biomaterialia*, vol. 76, pp. 56–70, 2018.

[52] C. Wang, J. Luan, A. C. Panayi, D. P. Orgill, and M. Xin, "Complications in breast augmen-tation with textured versus smooth breast implants: A systematic review protocol," *BMJ open*, vol. 8, no. 4, e020671, 2018.

[53] A. Pajkos, A. K. Deva, K. Vickery, C. Cope, L. Chang, and Y. E. Cossart, "Detection of subclinical infection in significant breast implant capsules.," *Plastic and reconstructive surgery*, vol. 111, no. 5, pp. 1605–1611, 2003.

[54] S. Fischer, C. Hirche, M. A. Reichenberger, *et al.*, "Silicone implants with smooth surfaces induce thinner but denser fibrotic capsules compared to those with textured surfaces in a rodent model," *PLoS One*, vol. 10, no. 7, e0132131, 2015.

[55] C. M. Malata, L. Feldberg, D. J. Coleman, I. T. Foo, and D. T. Sharpe, "Textured or smooth implants for breast augmentation? three year follow-up of a prospective randomised controlled trial," *British journal of plastic surgery*, vol. 50, no. 2, pp. 99–105, 1997.

[56] A. M. Munhoz, M. W. Clemens, and M. Y. Nahabedian, "Breast implant surfaces and their impact on current practices: Where we are now and where are we going?" *Plastic and Reconstructive Surgery Global Open*, vol. 7, no. 10, 2019.

[57] D. Ajdic, Y. Zoghbi, D. Gerth, Z. J. Panthaki, and S. Thaller, "The relationship of bacterial biofilms and capsular contracture in breast implants," *Aesthetic surgery journal*, vol. 36, no. 3, pp. 297–309, 2016.

[58] T. Brown, "Surface areas of textured breast implants: Implications for the biofilm theory of capsule formation," *Plastic and Reconstructive Surgery Global Open*, vol. 6, no. 3, 2018.

[59] M. Sforza, R. Zaccheddu, A. Alleruzzo, *et al.*, "Preliminary 3-year evaluation of experience with silksurface and velvetsurface motiva silicone breast implants: A single-center experience with 5813 consecutive breast augmentation cases," *Aesthetic surgery journal*, vol. 38, no. suppl_2, S62–S73, 2018.

[60] A. Loch-Wilkinson, K. J. Beath, R. J. W. Knight, *et al.*, "Breast implant–associated anaplastic large cell lymphoma in australia and new zealand: High-surface-area textured implants are associated with increased risk," *Plastic and reconstructive surgery*, vol. 140, no. 4, pp. 645–654, 2017.

[61] A. Mata, A. J. Fleischman, and S. Roy, "Characterization of polydimethylsiloxane (pdms) properties for biomedical micro/nanosystems," *Biomedical microdevices*, vol. 7, no. 4, pp. 281–293, 2005.

[62] S. M. Hong, S. H. Kim, J. H. Kim, and H. I. Hwang, "Hydrophilic surface modification of pdms using atmospheric rf plasma," in *Journal of physics: conference series*, IOP Publishing, vol. 34, 2006, p. 108.

[63] D. Bodas and C. Khan-Malek, "Formation of more stable hydrophilic surfaces of pdms by plasma and chemical treatments," *Microelectronic engineering*, vol. 83, no. 4-9, pp. 1277–1279, 2006.

[64] N. Gomathi, I. Mishra, S. Varma, and S. Neogi, "Surface modification of poly (dimethyl-siloxane) through oxygen and nitrogen plasma treatment to improve its characteristics towards biomedical applications," *Surface Topography: Metrology and Properties*, vol. 3, no. 3, p. 035 005, 2015.

[65] S. H. Tan, N.-T. Nguyen, Y. C. Chua, and T. G. Kang, "Oxygen plasma treatment for reducing hydrophobicity of a sealed polydimethylsiloxane microchannel," *Biomicrofluidics*, vol. 4, no. 3, p. 032 204, 2010.

[66] F. Heno, Z. Azoulay, B. Khalfin, *et al.*, "Comparing the antimicrobial effect of silver ion-coated silicone and gentamicin-irrigated silicone sheets from breast implant material," *Aesthetic Plastic Surgery*, pp. 1–10, 2021.

[67] K. Liu, P. Gu, K. Hamaker, and Z. H. Fan, "Characterization of bonding between poly (dimethylsiloxane) and cyclic olefin copolymer using corona discharge induced grafting polymerization," *Journal of colloid and interface science*, vol. 365, no. 1, pp. 289–295, 2012.

[68] P. Gu, K. Liu, H. Chen, T. Nishida, and Z. H. Fan, "Chemical-assisted bonding of thermoplastics/elastomer for fabricating microfluidic valves," *Analytical chemistry*, vol. 83, no. 1, pp. 446–452, 2011.

[69] C. Ciobanu, A. Groza, S. Iconaru, *et al.*, "Antimicrobial activity evaluation on silver doped hydroxyapatite/polydimethylsiloxane composite layer," *BioMed research international*, vol. 2015, 2015.

[70] T. Furuzono, A. Kishida, and J. Tanaka, "Nano-scaled hydroxyapatite/polymer composite i. coating of sintered hydroxyapatite particles on poly (γ-methacryloxypropyl trimethoxysilane)-grafted silk fibroin fibers through chemical bonding," *Journal of Materials Science: Materials in Medicine*, vol. 15, no. 1, pp. 19–23, 2004.

[71] K. Efimenko, W. E. Wallace, and J. Genzer, "Surface modification of sylgard-184 poly (dimethyl siloxane) networks by ultraviolet and ultraviolet/ozone treatment," *Journal of colloid and interface science*, vol. 254, no. 2, pp. 306–315, 2002.

[72] A. E. Özçam, K. Efimenko, and J. Genzer, "Effect of ultraviolet/ozone treatment on the surface and bulk properties of poly (dimethyl siloxane) and poly (vinylmethyl siloxane) networks," *Polymer*, vol. 55, no. 14, pp. 3107–3119, 2014.

[73] K. Efimenko, J. A. Crowe, E. Manias, D. W. Schwark, D. A. Fischer, and J. Genzer, "Rapid formation of soft hydrophilic silicone elastomer surfaces," *Polymer*, vol. 46, no. 22, pp. 9329–9341, 2005.

[74] K. Prasad, R. Zhou, R. Zhou, D. Schuessler, K. K. Ostrikov, and K. Bazaka, "Cosmetic reconstruction in breast cancer patients: Opportunities for nanocomposite materials," *Acta biomaterialia*, vol. 86, pp. 41–65, 2019.

[75]   M. S. Selim, S. A. El-Safty, M. A. El-Sockary, *et al.*, "Modeling of spherical silver nanoparti-
       cles in silicone-based nanocomposites for marine antifouling," *RSC advances*, vol. 5, no. 78,
       pp. 63 175–63 185, 2015.

[76]   Q. Guo, Y. Zhao, X. Dai, *et al.*, "Functional silver nanocomposites as broad-spectrum an-
       timicrobial and biofilm-disrupting agents," *ACS applied materials & interfaces*, vol. 9, no. 20,
       pp. 16 834–16 847, 2017.

[77]   G. G. Sankar, P. S. Murthy, A. Das, *et al.*, "Polydimethyl siloxane based nanocomposites
       with antibiofilm properties for biomedical applications," *Journal of Biomedical Materials
       Research Part B: Applied Biomaterials*, vol. 105, no. 5, pp. 1075–1082, 2017.

[78]   P. Yin, G. Huang, W. Tse, Y. Bao, J. Denstedt, and J. Zhang, "Nanocomposited silicone
       hydrogels with a laser-assisted surface modification for inhibiting the growth of bacterial
       biofilm," *Journal of Materials Chemistry B*, vol. 3, no. 16, pp. 3234–3241, 2015.

[79]   M. A. Rufin, B. K. D. Ngo, M. E. Barry, *et al.*, "Antifouling silicones based on surface-
       modifying additive amphiphiles," *Green materials*, vol. 5, no. 1, pp. 4–13, 2017.

[80]   H. Chen, M. A. Brook, Y. Chen, and H. Sheardown, "Surface properties of peo–silicone com-
       posites: Reducing protein adsorption," *Journal of Biomaterials Science, Polymer Edition*,
       vol. 16, no. 4, pp. 531–548, 2005.

[81]   M. A. Rufin, M. E. Barry, P. A. Adair, M. L. Hawkins, J. E. Raymond, and M. A. Grunlan,
       "Protein resistance efficacy of peo-silane amphiphiles: Dependence on peo-segment length
       and concentration," *Acta biomaterialia*, vol. 41, pp. 247–252, 2016.

[82]   M. L. Hawkins and M. A. Grunlan, "The protein resistance of silicones prepared with a
       peo-silane amphiphile," *Journal of Materials Chemistry*, vol. 22, no. 37, pp. 19 540–19 546,
       2012.

[83]   H. Chen, Z. Zhang, Y. Chen, M. A. Brook, and H. Sheardown, "Protein repellant silicone
       surfaces by covalent immobilization of poly (ethylene oxide)," *Biomaterials*, vol. 26, no. 15,
       pp. 2391–2399, 2005.

[84]   H. Chen, M. A. Brook, and H. Sheardown, "Silicone elastomers for reduced protein adsorp-
       tion," *Biomaterials*, vol. 25, no. 12, pp. 2273–2282, 2004.

[85]   A. Ring, S. Langer, D. Tilkorn, *et al.*, "Induction of angiogenesis and neovascularization in
       adjacent tissue of plasma-collagen–coated silicone implants," *Eplasty*, vol. 10, 2010.

[86] J. Hauser, J. Zietlow, M. Köller, *et al.*, "Enhanced cell adhesion to silicone implant material through plasma surface modification," *Journal of Materials Science: Materials in Medicine*, vol. 20, no. 12, p. 2541, 2009.

[87] J. U. Park, J. Ham, S. Kim, *et al.*, "Alleviation of capsular formations on silicone implants in rats using biomembrane-mimicking coatings," *Acta biomaterialia*, vol. 10, no. 10, pp. 4217–4225, 2014.

[88] J. van Heerden, M. Turner, D. Hoffmann, and J. Moolman, "Antimicrobial coating agents: Can biofilm formation on a breast implant be prevented?" *Journal of plastic, reconstructive & aesthetic surgery*, vol. 62, no. 5, pp. 610–617, 2009.

[89] J. E. Baker, R. M. Boudreau, A. P. Seitz, E. Gulbins, M. Edwards, and R. M. Gobble, "Doxycycline-coated silicone breast implant reduces surgical site infections compared with standard gentamycin/cefazolin/bacitracin wash," *Journal of the American College of Surgeons*, vol. 227, no. 4, S206–S207, 2018.

[90] M. C. McBride, R. K. Malcolm, A. D. Woolfson, and S. P. Gorman, "Persistence of antimicrobial activity through sustained release of triclosan from pegylated silicone elastomers," *Biomaterials*, vol. 30, no. 35, pp. 6739–6747, 2009.

[91] A. Jacombs, J. Allan, H. Hu, *et al.*, "Prevention of biofilm-induced capsular contracture with antibiotic-impregnated mesh in a porcine model," *Aesthetic surgery journal*, vol. 32, no. 7, pp. 886–891, 2012.

[92] J. Mokkaphan, W. Banlunara, T. Palaga, P. Sombuntham, and S. Wanichwecharungruang, "Silicone surface with drug nanodepots for medical devices," *ACS applied materials & interfaces*, vol. 6, no. 22, pp. 20 188–20 196, 2014.

[93] G. Vazquez and A. Pellon, "Polyurethane-coated silicone gel breast implants used for 18 years," *Aesthetic plastic surgery*, vol. 31, no. 4, pp. 330–336, 2007.

[94] M. L. Cunningham, J. Foley, R. R. Maronpot, and H. Matthews, "Correlation of hepatocellular proliferation with hepatocarcinogenicity induced by the mutagenic noncarcinogen: Carcinogen pair—2, 6-and 2, 4-diaminotoluene," *Toxicology and applied pharmacology*, vol. 107, no. 3, pp. 562–567, 1991.

[95] E. Johnston, B. Ratner, and J. Bryers, "Rf plasma deposited peo-like films: Surface characterization and inhibition of pseudomonas aeruginosa accumulation," *NATO ASI Series E Applied Sciences-Advanced Study Institute*, vol. 346, pp. 465–476, 1997.

[96]   P. Kingshott, J. Wei, D. Bagge-Ravn, N. Gadegaard, and L. Gram, "Covalent attachment
       of poly (ethylene glycol) to surfaces, critical for reducing bacterial adhesion," *Langmuir*,
       vol. 19, no. 17, pp. 6912–6921, 2003.

[97]   A. Roosjen, H. J. Kaper, H. C. Van Der Mei, W. Norde, and H. J. Busscher, "Inhibition of
       adhesion of yeasts and bacteria by poly (ethylene oxide)-brushes on glass in a parallel plate
       flow chamber," *Microbiology*, vol. 149, no. 11, pp. 3239–3246, 2003.

[98]   K. D. Park, Y. S. Kim, D. K. Han, *et al.*, "Bacterial adhesion on peg modified polyurethane
       surfaces," *Biomaterials*, vol. 19, no. 7-9, pp. 851–859, 1998.

[99]   A. Roosjen, J. de Vries, H. C. van der Mei, W. Norde, and H. J. Busscher, "Stability and
       effectiveness against bacterial adhesion of poly (ethylene oxide) coatings in biological fluids,"
       *Journal of Biomedical Materials Research Part B: Applied Biomaterials: An Official Journal
       of The Society for Biomaterials, The Japanese Society for Biomaterials, and The Australian
       Society for Biomaterials and the Korean Society for Biomaterials*, vol. 73, no. 2, pp. 347–354,
       2005.

[100] I. C. S. Fernández, H. C. van der Mei, M. J. Lochhead, D. W. Grainger, and H. J. Busscher,
       "The inhibition of the adhesion of clinically isolated bacterial strains on multi-component
       cross-linked poly (ethylene glycol)-based polymer coatings," *Biomaterials*, vol. 28, no. 28,
       pp. 4105–4112, 2007.

[101] B. H. Kim, B. K. Huh, W. S. Lee, *et al.*, "Silicone implant coated with tranilast-loaded
       polymer in a pattern for fibrosis suppression," *Polymers*, vol. 11, no. 2, p. 223, 2019.

[102] G. T. Lim, S. A. Valente, C. R. Hart-Spicer, *et al.*, "New biomaterial as a promising alterna-
       tive to silicone breast implants," *Journal of the mechanical behavior of biomedical materials*,
       vol. 21, pp. 47–56, 2013.

[103] S. L. Steffensen, M. H. Vestergaard, E. H. Møller, *et al.*, "Soft hydrogels interpenetrating
       silicone—a polymer network for drug-releasing medical devices," *Journal of Biomedical Ma-
       terials Research Part B: Applied Biomaterials*, vol. 104, no. 2, pp. 402–410, 2016.

[104] L. Martin, P. Gurnani, J. Zhang, *et al.*, "Polydimethylsiloxane-based giant glycosylated
       polymersomes with tunable bacterial affinity," *Biomacromolecules*, vol. 20, no. 3, pp. 1297–
       1307, 2019.

[105] N. H. Manimaran, H. Usman, K. L. Kamga, S.-L. Davidson, E. Beckman, and T. H. Niepa,
       "Developing a functional poly (dimethylsiloxane)-based microbial nanoculture system using

dimethylallylamine," *ACS Applied Materials & Interfaces*, vol. 12, no. 45, pp. 50 581–50 591, 2020.

[106]   L. Wang, B. Sun, K. S. Ziemer, G. A. Barabino, and R. L. Carrier, "Chemical and physical modifications to poly (dimethylsiloxane) surfaces affect adhesion of caco-2 cells," *Journal of Biomedical Materials Research Part A: An Official Journal of The Society for Biomaterials, The Japanese Society for Biomaterials, and The Australian Society for Biomaterials and the Korean Society for Biomaterials*, vol. 93, no. 4, pp. 1260–1271, 2010.

[107]   B. Thallinger, M. Brandauer, P. Burger, *et al.*, "Cellobiose dehydrogenase functionalized urinary catheter as novel antibiofilm system," *Journal of Biomedical Materials Research Part B: Applied Biomaterials*, vol. 104, no. 7, pp. 1448–1456, 2016.

[108]   A. L. Cordeiro, S. Zschoche, A. Janke, M. Nitschke, and C. Werner, "Functionalization of poly (dimethylsiloxane) surfaces with maleic anhydride copolymer films," *Langmuir*, vol. 25, no. 3, pp. 1509–1517, 2009.

[109]   V. Jokinen, P. Suvanto, and S. Franssila, "Oxygen and nitrogen plasma hydrophilization and hydrophobic recovery of polymers," *Biomicrofluidics*, vol. 6, no. 1, p. 016 501, 2012.

[110]   A. R. Murphy and D. L. Kaplan, "Biomedical applications of chemically-modified silk fibroin," *Journal of materials chemistry*, vol. 19, no. 36, pp. 6443–6450, 2009.

[111]   S. Das, D. Pati, N. Tiwari, A. Nisal, and S. Sen Gupta, "Synthesis of silk fibroin–glycopolypeptide conjugates and their recognition with lectin," *Biomacromolecules*, vol. 13, no. 11, pp. 3695–3702, 2012.

[112]   A. M. Chopra, M. Mehta, J. Bismuth, *et al.*, "Polymer coating embolism from intravascular medical devices—a clinical literature review," *Cardiovascular Pathology*, vol. 30, pp. 45–54, 2017.

[113]   F. Lewis and D. Mantovani, "Methods to investigate the adhesion of soft nano-coatings on metal substrates - application to polymer-coated stents," *Macromolecular Materials and Engineering*, vol. 294, pp. 11–19, Jan. 2009. DOI: `10.1002/mame.200800229`. (visited on 05/29/2020).

[114]   M. Burke, B. Clarke, Y. Rochev, A. Gorelov, and W. Carroll, "Estimation of the strength of adhesion between a thermoresponsive polymer coating and nitinol wire," *Journal of Materials Science: Materials in Medicine*, vol. 19, pp. 1971–1979, Oct. 2007. DOI: `10.1007/s10856-007-3274-4`. (visited on 06/13/2021).

[115] B. Rolfe, B. Zhang, G. Campbell, *et al.*, *The fibrotic response to implanted biomaterials: implications for tissue engineering.* Citeseer, 2011.

[116] L. E. L and T. I. G, "Materials for urinary catheters: A review of their history and development in the uk," *Medical Engineering and Physics*, vol. 27, pp. 443–453, Jul. 2005. DOI: `10.1016/j.medengphy.2004.12.013`. [Online]. Available: `https://www.sciencedirect.com/science/article/pii/S1350453305000068` (visited on 03/2021).

[117] N. Gomathi, I. Mishra, S. Varma, and S. Neogi, "Surface modification of poly(dimethylsiloxane) through oxygen and nitrogen plasma treatment to improve its characteristics towards biomedical applications," *Surface Topography: Metrology and Properties*, vol. 3, p. 035 005, Sep. 2015. DOI: `10.1088/2051-672x/3/3/035005`. (visited on 06/14/2021).

[118] S. Kuddannaya, Y. J. Chuah, M. H. A. Lee, N. V. Menon, Y. Kang, and Y. Zhang, "Surface chemical modification of poly(dimethylsiloxane) for the enhanced adhesion and proliferation of mesenchymal stem cells," *ACS Applied Materials & Interfaces*, vol. 5, pp. 9777–9784, Sep. 2013. DOI: `10.1021/am402903e`. (visited on 06/14/2021).

[119] P. H. Zeplin, N. C. Maksimovikj, M. C. Jordan, *et al.*, "Spider silk coatings as a bioshield to reduce periprosthetic fibrous capsule formation," *Advanced Functional Materials*, vol. 24, pp. 2658–2666, Jan. 2014. DOI: `10.1002/adfm.201302813`. (visited on 01/26/2021).

[120] L. Wang, B. Sun, K. S. Ziemer, G. A. Barabino, and R. L. Carrier, "Chemical and physical modifications to poly(dimethylsiloxane) surfaces affect adhesion of caco-2 cells," *Journal of Biomedical Materials Research Part A*, vol. 9999A, NA–NA, 2009. DOI: `10.1002/jbm.a.32621`. (visited on 06/14/2021).

[121] I. Wong and C.-M. Ho, "Surface molecular property modifications for poly(dimethylsiloxane) (pdms) based microfluidic devices," *Microfluidics and Nanofluidics*, vol. 7, Apr. 2009. DOI: `10.1007/s10404-009-0443-4`. (visited on 07/13/2019).

[122] Q. Zeng, Y. Zhu, B. Yu, *et al.*, "Antimicrobial and antifouling polymeric agents for surface functionalization of medical implants," *Biomacromolecules*, vol. 19, pp. 2805–2811, May 2018. DOI: `10.1021/acs.biomac.8b00399`. (visited on 06/13/2021).

[123] P. Xue, Q. Li, Y. Li, *et al.*, "Surface modification of poly(dimethylsiloxane) with polydopamine and hyaluronic acid to enhance hemocompatibility for potential applications in medical implants or devices," *ACS Applied Materials and Interfaces*, vol. 9, pp. 33 632–33 644, Sep. 2017. DOI: `10.1021/acsami.7b10260`. (visited on 06/2021).

[124] Y. J. Chuah, Y. T. Koh, K. Lim, N. V. Menon, Y. Wu, and Y. Kang, "Simple surface engineering of polydimethylsiloxane with polydopamine for stabilized mesenchymal stem cell adhesion and multipotency," *Scientific Reports*, vol. 5, Dec. 2015. DOI: 10.1038/srep18162. (visited on 03/09/2021).

[125] Z. Qian, D. Ross, W. Jia, Q. Xing, and F. Zhao, "Bioactive polydimethylsiloxane surface for optimal human mesenchymal stem cell sheet culture," *Bioactive Materials*, vol. 3, pp. 167–173, Jun. 2018. DOI: 10.1016/j.bioactmat.2018.01.005.

[126] C. Cha, E. Antoniadou, M. Lee, *et al.*, "Tailoring hydrogel adhesion to polydimethylsiloxane substrates using polysaccharide glue," *Angewandte Chemie*, vol. 125, pp. 7087–7090, May 2013. DOI: 10.1002/ange.201302925. (visited on 06/14/2021).

[127] Z. Shao and F. Vollrath, "Surprising strength of silkworm silk," *Nature*, vol. 418, no. 6899, pp. 741–741, 2002.

[128] G. H. Altman, F. Diaz, C. Jakuba, *et al.*, "Silk-based biomaterials," *Biomaterials*, vol. 24, no. 3, pp. 401–416, 2003.

[129] T.-T. Cao, Y.-J. Wang, and Y.-Q. Zhang, "Effect of strongly alkaline electrolyzed water on silk degumming and the physical properties of the fibroin fiber," *PLoS One*, vol. 8, no. 6, e65654, 2013.

[130] M. Gulrajani, R. Purwar, R. K. Prasad, and M. Joshi, "Studies on structural and functional properties of sericin recovered from silk degumming liquor by membrane technology," *Journal of applied polymer science*, vol. 113, no. 5, pp. 2796–2804, 2009.

[131] S. K. Vyas and S. R. Shukla, "Comparative study of degumming of silk varieties by different techniques," *The Journal of The Textile Institute*, vol. 107, no. 2, pp. 191–199, 2016.

[132] L. S. Wray, X. Hu, J. Gallego, *et al.*, "Effect of processing on silk-based biomaterials: Reproducibility and biocompatibility," *Journal of Biomedical Materials Research Part B: Applied Biomaterials*, vol. 99, no. 1, pp. 89–101, 2011.

[133] D. N. Rockwood, R. C. Preda, T. Yücel, X. Wang, M. L. Lovett, and D. L. Kaplan, "Materials fabrication from bombyx mori silk fibroin," *Nature Protocols*, vol. 6, pp. 1612–1631, Sep. 2011. DOI: 10.1038/nprot.2011.379. [Online]. Available: https://www.ncbi.nlm.nih.gov/pmc/articles/PMC3808976/ (visited on 09/14/2019).

[134] S.-W. Ha, A. E. Tonelli, and S. M. Hudson, "Structural studies of bombyx mori silk fibroin during regeneration from solutions and wet fiber spinning," *Biomacromolecules*, vol. 6, pp. 1722–1731, May 2005. DOI: 10.1021/bm050010y. (visited on 06/15/2021).

[135] C. B. Borkner, S. Wohlrab, E. Möller, G. Lang, and T. Scheibel, "Surface modification of polymeric biomaterials using recombinant spider silk proteins," *ACS Biomaterials Science and Engineering*, vol. 3, pp. 767–775, Aug. 2016. DOI: `10.1021/acsbiomaterials.6b00306`. (visited on 06/2021).

[136] J. Tomastik and R. Ctvrtlik, "Nanoscratch test — a tool for evaluation of cohesive and adhesive properties of thin films and coatings," *EPJ Web of Conferences*, vol. 48, M. Šulc, V. Kopecký, V. Lédl, R. Melich, and M. Škereň, Eds., p. 00 027, 2013. DOI: `10.1051/epjconf/20134800027`. (visited on 06/2021).

[137] S. Kassavetis, S. Logothetidis, and I. Zyganitidis, "Nanomechanical testing of the barrier thin film adhesion to a flexible polymer substrate," *Journal of Adhesion Science and Technology*, vol. 26, pp. 2393–2404, May 2012. DOI: `10.1163/156856111x599526`. (visited on 06/13/2021).

[138] A. Siddique, T. Meckel, R. W. Stark, and S. Narayan, "Improved cell adhesion under shear stress in pdms microfluidic devices," *Colloids and Surfaces B: Biointerfaces*, vol. 150, pp. 456–464, Feb. 2017. DOI: `10.1016/j.colsurfb.2016.11.011`. (visited on 06/13/2021).

[139] P. Hinterdorfer and Y. F. Dufrêne, "Detection and localization of single molecular recognition events using atomic force microscopy," *Nature Methods*, vol. 3, pp. 347–355, Apr. 2006. DOI: `10.1038/nmeth871`. (visited on 06/2021).

[140] P. Singha, J. Locklin, and H. Handa, "A review of the recent advances in antimicrobial coatings for urinary catheters," *Acta biomaterialia*, vol. 50, pp. 20–40, 2017.

[141] Z. K. Zander and M. L. Becker, *Antimicrobial and antifouling strategies for polymeric medical devices*, 2018.

[142] Z. Zhang, Y. Qu, X. Li, *et al.*, "Electrophoretic deposition of tetracycline modified silk fibroin coatings for functionalization of titanium surfaces," *Applied surface science*, vol. 303, pp. 255–262, 2014.

[143] K. Dunn, P. Hall, and C. Khoo, "Breast implant materials: Sense and safety," *British journal of plastic surgery*, vol. 45, no. 4, pp. 315–321, 1992.

[144] S. Amin, S. Rajabnezhad, and K. Kohli, "Hydrogels as potential drug delivery systems," *Scientific Research and Essays*, vol. 4, no. 11, pp. 1175–1183, 2009.

[145] S. Shi, Y. Liu, and L. Wang, *Methods and compositions for improved tissue regeneration by suppression of interferon-gamma and tumor necrosis factor-alpha*, US Patent App. 14/114,070, Jun. 2014.

[146] P. Petrini, C. Parolari, and M. C. Tanzi, "Silk fibroin-polyurethane scaffolds for tissue engineering," *Journal of Materials Science: Materials in Medicine*, vol. 12, no. 10, pp. 849–853, 2001.

[147] P. Arpaçay and U. Türkan, "Development of antibiotic-loaded silk fibroin/hyaluronic acid polyelectrolyte film coated cocrmo alloy," *Biomedical Engineering/Biomedizinische Technik*, vol. 61, no. 5, pp. 463–474, 2016.

[148] X. Wang, H. J. Kim, P. Xu, A. Matsumoto, and D. L. Kaplan, "Biomaterial coatings by stepwise deposition of silk fibroin," *Langmuir*, vol. 21, no. 24, pp. 11 335–11 341, 2005.

[149] J. P. Gerdt and H. E. Blackwell, "Competition studies confirm two major barriers that can preclude the spread of resistance to quorum-sensing inhibitors in bacteria," *ACS chemical biology*, vol. 9, no. 10, pp. 2291–2299, 2014.

[150] T. Bjarnsholt and M. Givskov, "Quorum sensing inhibitory drugs as next generation antimicrobials: Worth the effort?" *Current infectious disease reports*, vol. 10, no. 1, pp. 22–28, 2008.

[151] A. Patil, K. Joshi-Navre, R. Mukherji, and A. Prabhune, "Biosynthesis of glycomonoterpenes to attenuate quorum sensing associated virulence in bacteria," *Applied biochemistry and biotechnology*, vol. 181, no. 4, pp. 1533–1548, 2017.

[152] P. B. Flynn, A. Busetti, E. Wielogorska, *et al.*, "Non-thermal plasma exposure rapidly attenuates bacterial ahl-dependent quorum sensing and virulence," *Scientific reports*, vol. 6, no. 1, pp. 1–13, 2016.

[153] X. Wang, X. Hu, A. Daley, O. Rabotyagova, P. Cebe, and D. L. Kaplan, "Nanolayer biomaterial coatings of silk fibroin for controlled release," *Journal of Controlled release*, vol. 121, no. 3, pp. 190–199, 2007.

[154] Á. Kmetty, T. Bárány, and J. Karger-Kocsis, "Self-reinforced polymeric materials: A review," *Progress in Polymer Science*, vol. 35, no. 10, pp. 1288–1310, 2010.

[155] M. C. Lucchetta, J. P. Morales Arias, M. Mollo, and C. R. Bernal, "Self-reinforced composites based on commercial pp woven fabrics and a random pp copolymer modified with quartz," *Polymers for Advanced Technologies*, vol. 27, no. 8, pp. 1072–1081, 2016.

[156] B. B. Mandal, A. Grinberg, E. S. Gil, B. Panilaitis, and D. L. Kaplan, "High-strength silk protein scaffolds for bone repair," *Proceedings of the National Academy of Sciences*, vol. 109, no. 20, pp. 7699–7704, 2012.

[157] H. Li, J. Zhu, S. Chen, L. Jia, and Y. Ma, "Fabrication of aqueous-based dual drug loaded silk fibroin electrospun nanofibers embedded with curcumin-loaded rsf nanospheres for drugs controlled release," *Rsc Advances*, vol. 7, no. 89, pp. 56 550–56 558, 2017.

[158] J. Zhou, D. A. Khodakov, A. V. Ellis, and N. H. Voelcker, "Surface modification for pdms-based microfluidic devices," *Electrophoresis*, vol. 33, no. 1, pp. 89–104, 2012.

[159] V. C. Kalia, *Quorum sensing vs quorum quenching: a battle with no end in sight.* Springer, 2015.

[160] P. Williams, "Quorum sensing, communication and cross-kingdom signalling in the bacterial world," *Microbiology*, vol. 153, no. 12, pp. 3923–3938, 2007.

[161] R. Mukherji and A. Prabhune, "A new class of bacterial quorum sensing antagonists: Glycomonoterpenols synthesized using linalool and alpha terpineol," *World Journal of Microbiology and Biotechnology*, vol. 31, no. 6, pp. 841–849, 2015.

[162] S. L. Ang, B. Shaharuddin, J.-A. Chuah, and K. Sudesh, "Electrospun poly(3-hydroxybutyrate-co-3-hydroxyhexanoate)/silk fibroin film is a promising scaffold for bone tissue engineering," *International Journal of Biological Macromolecules*, vol. 145, pp. 173–188, Feb. 2020. DOI: `10.1016/j.ijbiomac.2019.12.149`. (visited on 10/30/2021).

[163] E. Yu, J. Zhang, J. A. Thomson, and L.-S. Turng, "Fabrication and characterization of electrospun thermoplastic polyurethane/fibroin small-diameter vascular grafts for vascular tissue engineering," *International Polymer Processing*, vol. 31, pp. 638–646, Nov. 2016. DOI: `10.3139/217.3247`. (visited on 03/15/2021).

[164] L. Bai, Q. Li, X. Duo, *et al.*, "Electrospun pcl-pibmd/sf blend scaffolds with plasmid complexes for endothelial cell proliferation," *RSC Advances*, vol. 7, pp. 39 452–39 464, 2017. DOI: `10.1039/c7ra06253b`. (visited on 10/30/2021).

[165] Y. P. Singh, A. Bandyopadhyay, and B. B. Mandal, "3d bioprinting using cross-linker-free silk–gelatin bioink for cartilage tissue engineering," *ACS Applied Materials and Interfaces*, vol. 11, pp. 33 684–33 696, Aug. 2019. DOI: `10.1021/acsami.9b11644`. (visited on 10/30/2021).

[166] K. A. Luetchford, J. B. Chaudhuri, and P. A. De Bank, "Silk fibroin/gelatin microcarriers as scaffolds for bone tissue engineering," *Materials Science and Engineering: C*, vol. 106, p. 110 116, Jan. 2020. DOI: `10.1016/j.msec.2019.110116`. (visited on 03/24/2020).

[167] T. Cha, A. Guo, Y. Jun, D. Pei, and X.-Y. Zhu, "Immobilization of oriented protein molecules on poly (ethylene glycol)-coated si (111)," *Proteomics*, vol. 4, no. 7, pp. 1965–1976, 2004.

[168] H. Y. Kweon, S. H. Park, J. H. Yeo, Y. W. Lee, and C. S. Cho, "Preparation of semi-interpenetrating polymer networks composed of silk fibroin and poly(ethylene glycol) macromer," *Journal of Applied Polymer Science*, vol. 80, pp. 1848–1853, 2001. DOI: `10.1002/app.1281`. (visited on 10/30/2021).

[169] H.-J. Jin, J. Park, P. Cebe, and D. L. Kaplan, "Engineered films of bombyx mori silk with poly (ethylene oxide)," *MRS Online Proceedings Library (OPL)*, vol. 735, 2002.

[170] Y. Nong, Y. Ren, P. Wang, *et al.*, "A facile strategy for the preparation of photothermal silk fibroin aerogels with antibacterial and oil-water separation abilities," *Journal of Colloid and Interface Science*, vol. 603, pp. 518–529, 2021.

[171] Y. Wang, Z. Zheng, Q. Cheng, D. L. Kaplan, G. Li, and X. Wang, "Ductility and porosity of silk fibroin films by blending with glycerol/polyethylene glycol and adjusting the drying temperature," *ACS Biomaterials Science & Engineering*, vol. 6, no. 2, pp. 1176–1185, 2019.

[172] A. J. Meinel, K. E. Kubow, E. Klotzsch, *et al.*, "Optimization strategies for electrospun silk fibroin tissue engineering scaffolds," *Biomaterials*, vol. 30, no. 17, pp. 3058–3067, 2009.

[173] F. Selmin, C. G. Gennari, P. Minghetti, *et al.*, "Enhanced hydration stability of bombyx mori silk fibroin/peg 600 composite scaffolds for tissue engineering," *Polymers for advanced technologies*, vol. 25, no. 5, pp. 532–538, 2014.

[174] N. Luo, J. K. Weber, S. Wang, *et al.*, "Pegylated graphene oxide elicits strong immunological responses despite surface passivation," *Nature communications*, vol. 8, no. 1, pp. 1–10, 2017.

[175] P. Caliceti, O. Schiavon, and F. M. Veronese, "Immunological properties of uricase conjugated to neutral soluble polymers," *Bioconjugate chemistry*, vol. 12, no. 4, pp. 515–522, 2001.

[176] B. W. Neun, Y. Barenholz, J. Szebeni, and M. A. Dobrovolskaia, "Understanding the role of anti-peg antibodies in the complement activation by doxil in vitro," *Molecules*, vol. 23, no. 7, p. 1700, 2018.

[177] J. A. MacKay, D. J. Callahan, K. N. FitzGerald, and A. Chilkoti, "Quantitative model of the phase behavior of recombinant ph-responsive elastin-like polypeptides," *Biomacromolecules*, vol. 11, no. 11, pp. 2873–2879, 2010.

[178] S. R. MacEwan and A. Chilkoti, "Applications of elastin-like polypeptides in drug delivery," *Journal of Controlled Release*, vol. 190, pp. 314–330, 2014.

[179] J. Reguera, A. Fahmi, P. Moriarty, A. Girotti, and J. C. Rodríguez-Cabello, "Nanopore formation by self-assembly of the model genetically engineered elastin-like polymer [(vpgvg)

2 (vpgeg)(vpgvg) 2] 15," *Journal of the American Chemical Society*, vol. 126, no. 41, pp. 13 212–13 213, 2004.

[180] S. G. Wise, G. C. Yeo, M. A. Hiob, *et al.*, "Tropoelastin: A versatile, bioactive assembly module," *Acta biomaterialia*, vol. 10, no. 4, pp. 1532–1541, 2014.

[181] S. G. Wise and A. S. Weiss, "Tropoelastin," *The international journal of biochemistry & cell biology*, vol. 41, no. 3, pp. 494–497, 2009.

[182] G. C. Yeo, F. W. Keeley, and A. S. Weiss, "Coacervation of tropoelastin," *Advances in colloid and interface science*, vol. 167, no. 1-2, pp. 94–103, 2011.

[183] J. D. White, S. Wang, A. S. Weiss, and D. L. Kaplan, "Silk–tropoelastin protein films for nerve guidance," *Acta biomaterialia*, vol. 14, pp. 1–10, 2015.

[184] T. Luo, M. A. David, L. C. Dunshee, *et al.*, "Thermoresponsive elastin-b-collagen-like peptide bioconjugate nanovesicles for targeted drug delivery to collagen-containing matrices," *Biomacromolecules*, vol. 18, no. 8, pp. 2539–2551, 2017.

[185] P. Pal, Q. C. Nguyen, A. H. Benton, M. E. Marquart, and A. V. Janorkar, "Drug-loaded elastin-like polypeptide–collagen hydrogels with high modulus for bone tissue engineering," *Macromolecular bioscience*, vol. 19, no. 9, p. 1 900 142, 2019.

[186] X. Hu, X. Wang, J. Rnjak, A. S. Weiss, and D. L. Kaplan, "Biomaterials derived from silk–tropoelastin protein systems," *Biomaterials*, vol. 31, no. 32, pp. 8121–8131, 2010.

[187] H. Liu, S. G. Wise, J. Rnjak-Kovacina, *et al.*, "Biocompatibility of silk-tropoelastin protein polymers," *Biomaterials*, vol. 35, no. 19, pp. 5138–5147, 2014.

[188] T. Luo and K. L. Kiick, "Noncovalent modulation of the inverse temperature transition and self-assembly of elastin-b-collagen-like peptide bioconjugates," *Journal of the American Chemical Society*, vol. 137, no. 49, pp. 15 362–15 365, 2015.

[189] J. L. Frandsen and H. Ghandehari, "Recombinant protein-based polymers for advanced drug delivery," *Chemical Society Reviews*, vol. 41, no. 7, pp. 2696–2706, 2012.

[190] T. Kukubo, H. Kushitani, S. Sakka, T. Kitsugi, and T. Yamamuro, "Solutions able to reproduce in vivo surface-structure changes in bioactive glass-ceramic aw," *J Biomed Mater Res*, vol. 24, pp. 721–734, 1990.

[191] K. Cai, K. Yao, S. Lin, *et al.*, "Poly (d, l-lactic acid) surfaces modified by silk fibroin: Effects on the culture of osteoblast in vitro," *Biomaterials*, vol. 23, no. 4, pp. 1153–1160, 2002.

[192] Z. Chen, Q. Zhang, H. Li, Q. Wei, X. Zhao, and F. Chen, "Elastin-like polypeptide modified silk fibroin porous scaffold promotes osteochondral repair," *Bioactive materials*, vol. 6, no. 3, pp. 589–601, 2021.

[193] H. Long, C. Lai, and C.-K. Chung, "Polyethylene glycol coating for hydrophilicity enhancement of polydimethylsiloxane self-driven microfluidic chip," *Surface and Coatings Technology*, vol. 320, pp. 315–319, 2017.

[194] M. Meran, P. D. Akkus, O. Kurkcuoglu, *et al.*, "Noncovalent pyrene-polyethylene glycol coatings of carbon nanotubes achieve in vitro biocompatibility," *Langmuir*, vol. 34, no. 40, pp. 12 071–12 082, 2018.

[195] W. Teng, J. Cappello, and X. Wu, "Recombinant silk-elastinlike protein polymer displays elasticity comparable to elastin," *Biomacromolecules*, vol. 10, no. 11, pp. 3028–3036, 2009.

[196] M. L. Sanyang, S. M. Sapuan, M. Jawaid, M. R. Ishak, and J. Sahari, "Effect of plasticizer type and concentration on tensile, thermal and barrier properties of biodegradable films based on sugar palm (arenga pinnata) starch," *Polymers*, vol. 7, no. 6, pp. 1106–1124, 2015.

[197] F. Laboulfie, M. Hémati, A. Lamure, and S. Diguet, "Effect of the plasticizer on permeability, mechanical resistance and thermal behaviour of composite coating films," *Powder Technology*, vol. 238, pp. 14–19, 2013.

[198] M. S. Desai, E. Wang, K. Joyner, T. W. Chung, H.-E. Jin, and S.-W. Lee, "Elastin-based rubber-like hydrogels," *Biomacromolecules*, vol. 17, no. 7, pp. 2409–2416, 2016.

[199] C. Guo, C. Li, and D. L. Kaplan, "Enzymatic degradation of bombyx mori silk materials: A review," *Biomacromolecules*, vol. 21, no. 5, pp. 1678–1686, 2020.

[200] K. Remya, S. Chandran, S. Mani, A. John, and P. Ramesh, "Hybrid polycaprolactone/polyethylene oxide scaffolds with tunable fiber surface morphology, improved hydrophilicity and biodegradability for bone tissue engineering applications," *Journal of Biomaterials science, Polymer edition*, vol. 29, no. 12, pp. 1444–1462, 2018.

[201] A. Vasconcelos, A. C. Gomes, and A. Cavaco-Paulo, "Novel silk fibroin/elastin wound dressings," *Acta biomaterialia*, vol. 8, no. 8, pp. 3049–3060, 2012.

[202] E. Srokowski, P. Blit, W. McClung, J. Brash, J. Santerre, and K. Woodhouse, "Platelet adhesion and fibrinogen accretion on a family of elastin-like polypeptides," *Journal of Biomaterials Science, Polymer Edition*, vol. 22, no. 1-3, pp. 41–57, 2011.

[203] T. J. Puls, C. S. Fisher, A. Cox, *et al.*, "Regenerative tissue filler for breast conserving surgery and other soft tissue restoration and reconstruction needs," *Scientific reports*, vol. 11, no. 1, pp. 1–17, 2021.

Appendix

```matlab
clear all
set(0,'defaulttextinterpreter','latex');
a=imread('A-3.png');
figure,imshow(a)
b=rgb2gray(a);
figure, imshow (b)
c = b<120;
figure, imshow (a)
%warning('off', 'Images:initSize:
    adjustingMag');
count=0;
for i=1:167
for j=1:1453
d=c(i,j);
if d==0
count = count + 1;
end
end
end
total_pixels = 167*1453;
crack_density = count/total_pixels;
```

1) List of publication(s).

1. **Emmanuel Joseph**, Amrita Patil, Swarali Hirlekar,Abhijit Shete, Nimisha Parekh, Asmita Prabhune*, and Anuya Nisal*; Glycomonoterpene-Functionalized Crack- Resistant Biocompatible Silk Fibroin Coatings for Biomedical Implants, ACS Appl. Bio Mater 2019, 2, 2, 675–684.

2. **Emmanuel Joseph**, Shatruhan Singh Rajput, Shivprasad Patil, Anuya Nisal*; Mechanism of adhesion of natural polymer coatings on chemically modified siloxane polymer, Langmuir 2021, 37, 9, 2974–2984.

2) List of Papers with abstract presented (oral/poster) at national/ international conferences/seminars with complete details.

- **Emmanuel Joseph**, Neeraja J, Pashupati Gupta, Anuya Nisal , "**Crack resistant biocompatible silk fibroin and blend coatings for biomedical Implants**", WBC 2020, Proceedings of the World Biomaterials Congress, 2020, Glasgow, UK.

- **Emmanuel Joseph**, Shatruhan S Rajput, Shivprasad Patil, Anuya Nisal "**Adhesion of biocompatible silk fibroin coatings on surface modified Polydimethylsiloxane surfaces** ", NCL Science Day 2019

- **Emmanuel Joseph**, Amrita Patil, Abijit Shete, Swarali Hirlekar, Ashmitha Prabhune, Anuya Nisal, "**Glycomonoterpene-Functionalized Crack-Resistant Biocompatible Silk Fibroin Coatings for Biomedical Implants**" Annual Students Conference National Chemical Laboratory – Research Foundation, 2019.

- **Emmanuel Joseph**, Shatruhan S Rajput, Shivprasad Patil, Anuya Nisal "**Adhesion of biocompatible silk fibroin coatings on surface modified Polydimethylsiloxane surfaces** ", CompFlu 2019, December 2019

- **Emmanuel Joseph**, Amrita Patil, Abijit Shete, Swarali Hirlekar, Ashmitha Prabhune, Anuya Nisal, "**Silk fibroin-sophorolipid based multi-functional biocompatible coatings exhibiting improved crack resistance, excellent anti-biofilm and quorum quenching activity** ", CompFlu 2018, December 2018

- **Emmanuel Joseph**, Amrita Patil, Abijit Shete, Swarali Hirlekar, Ashmitha Prabhune,

Anuya Nisal, "**Silk fibroin-sophorolipid based multi-functional biocompatible coatings exhibiting improved crack resistance, excellent anti-biofilm and quorum quenching activity**", BioMET 2018

- **Emmanuel Joseph**, Amrita Patil, Abijit Shete, Swarali Hirlekar, Ashmitha Prabhune, Anuya Nisal, "**Functional biocompatible implant coatings based on silk fibroin and glycomonoterpene exhibiting improved crack resistance, excellent anti-biofilm and quorum quenching activity**", NCL Science Day 2018.

- **Emmanuel Joseph**, Amrita Patil, Abijit Shete, Swarali Hirlekar, Ashmitha Prabhune, Anuya Nisal, "**Silk fibroin-sophorolipid based multi-functional biocompatible coatings exhibiting improved crack resistance, excellent anti-biofilm and quorum quenching activity**", Compflu-2017, December 2017

3) A copy of all SCI publication(s).

Glycomonoterpene-Functionalized Crack-Resistant Biocompatible Silk Fibroin Coatings for Biomedical Implants

Emmanuel Joseph,[†,§] Amrita Patil,[‡,§] Swarali Hirlekar,[‡] Abhijit Shete,[†] Nimisha Parekh,[†] Asmita Prabhune,*,[‡,§] and Anuya Nisal*,[†,§]

[†]Polymer Science and Engineering Division, CSIR-NCL, Pune 411008, India
[‡]Biochemical Sciences Division, CSIR-NCL, Pune 411008, India
[§]Academy of Scientific and Innovative Research (AcSIR), Ghaziabad 201002, India

S *Supporting Information*

ABSTRACT: Surface coatings for biomedical implants have been used to prevent premature failure of the implant due to bacterial biofilm formation and foreign body reaction. Delamination, cracking, crazing, etc. are frequent problems associated with coatings when implants are subjected to mechanical deformation either during surgical handling or during use. We demonstrate here a novel process that results in the formation of a coating that is stable under mechanical stresses in tensile, torsion, and bending modes. The coating process involves a combination of two conventional coating processes, namely, dip coating and electrospinning. Polydimethylsiloxane was selected as the substrate owing to its wide use in biomedical implants. Silk fibroin, a natural biocompatible protein polymer obtained from the *Bombyx mori* silkworm, was used for demonstrating the process of coating. The coating was also further functionalized using a green biomolecule , glycomonoterpene prepared using citronellal and glucose. These functional compounds are being touted as the next-generation antibiofilm molecules on account of quorum sensing inhibitory activity. We have demonstrated that the quorum-quenching activity of the biomolecule is retained during the processing steps and that the coatings exhibited an excellent antibiofilm activity against common infection-causing bacteria, *Pseudomonas aeruginosa* and *Staphylococcus epidermidis*. These silk fibroin-glycomonoterpene coatings can be used for implants in biomedical applications such as breast implants and catheter tubings.

KEYWORDS: *silk fibroin, glycomonoterpene, crack resistance, antiquorum sensing, antibiofilm, implant coating*

INTRODUCTION

Implantable medical devices are increasingly being used to diagnose, treat, cure or repair, and regenerate a severe medical condition. The failure of these implants has primarily been attributed to two factors: device-associated infection and foreign body response.[1] More than 25% of hospital-acquired infections (HAI) are directly linked to the implanted device, for example, in urinary catheters or even joint replacement procedures.[2−4] Biofilms have found to be a dominant problem in these infections.[3] Also, considering these scenarios and their consequences, surgeons frequently resort to oral doses of antibiotics during implantation in a patient. However, this has added and fuelled to the global problem of antibiotic resistance. The second most common reason for failure of implants is the foreign body reaction. Capsular contracture or implant failure due to fibrotic capsule formation has been reported in at least 15−30% of the breast reconstruction and augmentation surgeries.[5]

One of the approaches to solving both these problems is surface modification of the existing implant materials, as the inherent bulk properties of the implant remain unaltered. Surface coatings are, therefore, a rapidly evolving field.[6] There have also been recent efforts to modify the surface of the silicone breast implants using biocompatible polymers.[7−9]

However, problems related to flaking, delamination, cracking, and crazing of coatings are still an issue. Recently, FDA recalled polytetrafluoroethylene-coated guidewires as separation of the coating may cause serious injuries to the patient both due to migration of coating to other body parts and exposure of underlying medical device surfaces, which could trigger other undesirable events such as blood clots.[10] Researchers have also reported microcracks in coatings especially when subjected to mechanical deformation.[11] The failure of coatings may be attributed the mechanical stresses imposed on the implants due to handling either during manufacture and packaging and/or also during surgical intervention by the medical practitioners.[12] Some coatings may also fail after implantation as catheter tubes, for example, experience a variety of bending/tensile stresses when in use.
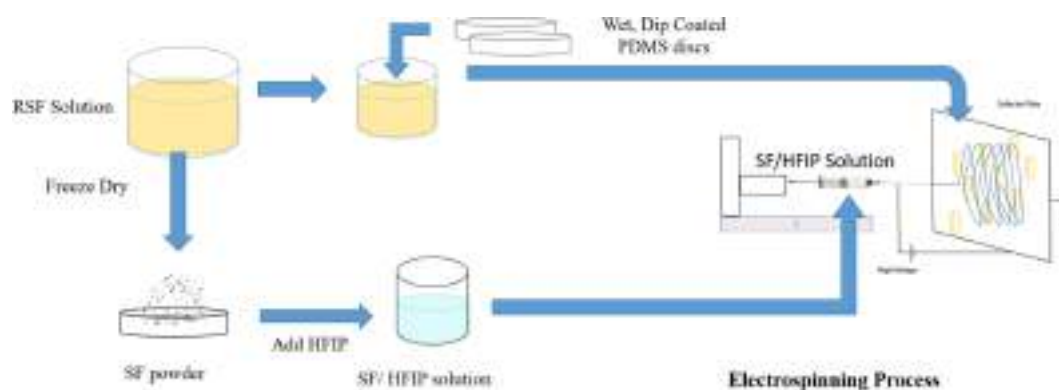
Figure 1. Schematic representation of the process innovation for coating of SF on PDMS discs.

Thus, it is an objective of this work to develop a novel process to form a stable coating on an elastomeric substrate such that the coating retains its integrity when subjected to mechanical deformation in tensile, bending, or torsion modes, while enhancing the biocompatibility of the implant surface. Medical grade polydimethylsiloxane (PDMS) is chosen as the substrate for this study as PDMS is extensively used in several medical devices such as breast implants and catheter on account of its easy processability into different shapes, ability to tune mechanical properties, and biocompatibility.[2,5] Natural silk fibroin (SF) obtained from *Bombyx mori* silkworm is chosen as the material for coating application. SF has emerged as a promising biomaterial on account of easy availability, proven biocompatibility, biodegradability, and aqueous processability.[13−15] Various techniques have been used to deposit SF coatings on both polymer as well as metal scaffolds.[16−18] However, the mechanical properties of the coating and its ability to resist mechanical deformation have not been quantified and studied. In this work, we demonstrate a novel sequential dip and electrospinning technique that results in an SF coating that is stable under tensile, torsion, and bending loads.

As mentioned earlier, antibiotic treatments for implant-associated infections are leading to the development of resistance in many pathogens. However, unlike antibiotics, quorum sensing inhibiting molecules (QSI) do not put selective pressure by killing bacterial cells, instead inhibit biofilm formation and pathogenesis by interrupting QS, i.e., cell to cell communication. Therefore, bacteria are less likely to develop resistance to quorum sensing inhibitors in the future.[19] Along with this, upon administration of QSI, the cells remain in planktonic form and they are available to be killed by phagocytic cells in the body, without affecting the normal flora. This also avoids infections by opportunistic pathogens and justifies QSIs as next-generation molecules.[20]

Thus, in the present work, we demonstrate the incorporation of a QSI biomolecule, G-citron (GC), to inhibit the bacterial biofilm formation on implants. GC is biosynthesized from citronellal and glucose by a nonpathogenic yeast, *Candida bombicola*. A GC molecule is considered to be a green molecule due to its biosynthesis and biodegradability. Citronellal was particularly chosen as a substrate for biomodification because it is a major component of many easily available essential oils. The modification with glucose results in a molecule with improved hydrophilicity and hence enhances its bioavailability.[21] Thus, it is an objective of this work to provide an innovative solution to simultaneously

resolve multiple causes for failures of implant devices: biofilm formation, foreign body response, and cracking/delamination of the coating.

MATERIALS AND METHODS

Preparation of PDMS Discs. Medical grade PDMS (Sylgard 184, Dow Corning) was cast on polystyrene Petri dishes to obtain a disc with a uniform thickness of 1 mm. The prepolymer was thoroughly mixed with the curing agent for 5 min using a weight ratio of 10:1. It was then poured into the Petri dish and degassed for 30 min. This mixture was kept in a convection oven at 40 °C for 24 h. Circular PDMS discs of required diameters were then cut out and used for further experimentation. A cleaning process of 30 min sonication in isopropyl alcohol was followed to remove dust particles before further experimentation. This process of cleaning was followed by a drying step under a vacuum at 60 °C for 4 h to remove any traces of the IPA solvent.

Oxygen Plasma Treatment of the PDMS Disc. The plasma treatment was done on both sides of the PDMS disc using an Emitech 1050 plasma unit. The chambers were initially purged for 15 min with oxygen gas. The optimized plasma conditions of 50 W RF power and 1 min time duration were determined by measuring the contact angle on the surface and confirming no physical damage to the PDMS disc surface using optical microscopy. The plasma-treated discs were stored under DI water for a maximum of 1 week, before use for further experimentation. XPS spectra after 1 week of plasma treatment confirms the formation of stable OH groups as shown in Figure S1.

Preparation of SF Solution. The silk fibroin solution was prepared from *Bombyx mori* silkworm cocoons obtained from Central Sericultural Research and Training Institute, Mysore as per the protocol described elsewhere.[22] Briefly, the cocoons were degummed using 0.5 wt % sodium bicarbonate (NaHCO$_3$) solution to remove the sericin protein. The dissolution of the cottony mass of fibroin fibers was done using a chaotropic salt lithium bromide (LiBr) at 60°C for 4 h. The salt was then extensively dialyzed out to obtain regenerated silk fibroin (RSF) solution with approximately 3−5 w/v % concentration. The RSF solution was then lyophilized at −55°C to obtain SF powder. This powder was stored at −20°C until further use. The powder was dissolved in hexafluoroisopropanol (HFIP) at room temperature to obtain a 5 w/v % solution, and this solution was then used for electrospinning.[23]

Preparation of Silk Fibroin Coating. The plasma-treated PDMS disc was used for coating experiments with SF. The RSF solution was diluted to 0.4 w/v % using DI water. The disc was immersed in this solution for 10 min to obtain a uniform SF coating. The PDMS disc was later air-dried at room temperature and methanol vapor annealed as per the protocol described below. This SF-coated PDMS disc is further referred to as the "SF-D disc". In another experiment, the PDMS disc was taken out of the SF solution and immediately mounted onto the collector plate of an electrospinning apparatus before drying. The electrospinning was done using 5 w/v % SF/HFIP
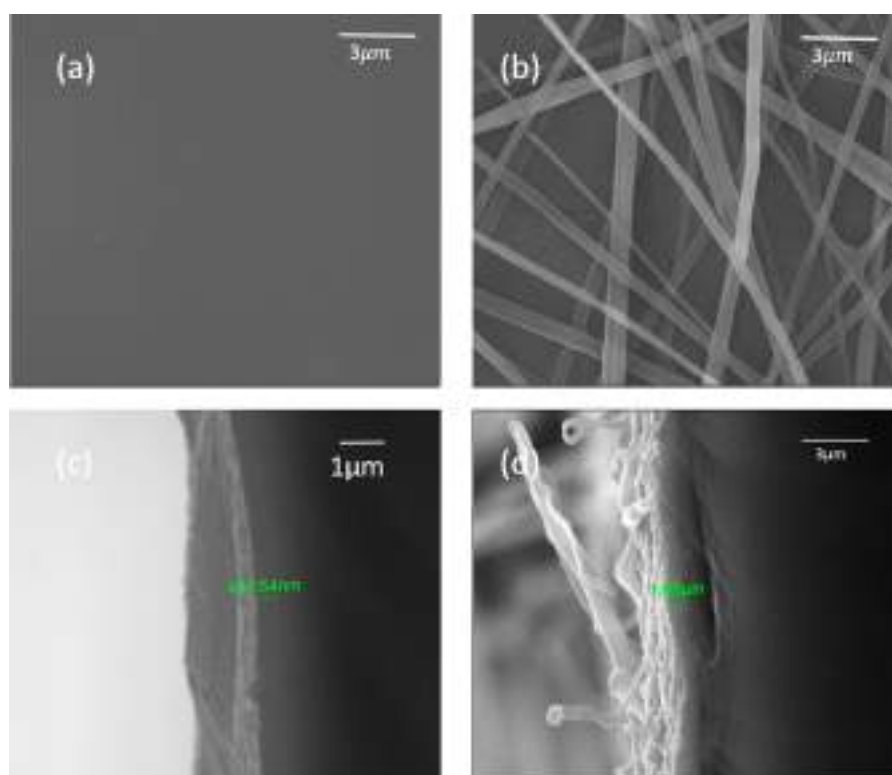
Figure 2. SEM images of coatings (a) SF-D and (b) SF-DES and cross-sectional images of coatings (c) SF-D and (d) SF-DES.

solution as shown in Figure 1. The tip to collector plate distance was maintained at 10.5 cm, and a voltage of 30 kV with a flow rate of 1 mL/h was used for electrospinning. After electrospinning, the discs were kept for drying at 40°C for 12 h to remove traces of the solvent. This was followed with a methanol vapor annealing treatment to introduce a stable β sheet conformation in the protein. The coated discs were incubated in a saturated methanol vapor closed chamber for 48 h at room temperature. Further characterization was done after this treatment. These discs are further referred to as SF-DES (dip + electrospinning). Also, blends of SF and GC (preparation described later) were made in 1:3 ratios to form 5 w/v % solution in HFIP. This solution was then electrospun on the SF dip-coated PDMS disc, and these discs are further refereed to as SFGC-DES.

Fourier Transform Infrared (FTIR) Spectroscopy. The uncoated and coated discs, before and after methanol treatment, were characterized using an ATR-FTIR PerkinElmer Q5000 Spectrum GX spectrophotometer equipped with a diamond crystal probe detector. The scan was recorded from 500 to 4000 cm^{-1} with a resolution of 4 cm^{-1}.

Contact Angle Measurement. The modification of PDMS and its coating was confirmed by 4 μL of a stable sessile drop of DI water. The equilibrium contact angle was reported as the average of at least four measurements for each modification.

Scanning Electron Microscopy. The surface and cross-sectional morphology of the coated/uncoated PDMS discs was observed using a scanning electron microscope (SEM), Quanta 200 3D from FEI. Representative images at appropriate magnifications were recorded after sputter coating the samples with a thin coating of gold to prevent sample charging.

Atomic Force Microscopy. The surface topography of the uncoated/coated PDMS discs was performed in ambient conditions in tapping mode for a 40 μm × 40 μm area with a scanning probe microscope (JPK, NanoWizard II). Silicon cantilevers with a spring constant (k) of 60 N/m were used to perform experiments. The cantilever was oscillated at its free resonance frequency (250−350 kHz).

Aqueous Stability of Coating. The aqueous stability of the SF-DES discs was determined by keeping the coated discs immersed in phosphate buffered saline (PBS) solution for 7 days at 37 °C, and UV−vis spectroscopy was done on the PBS solution to measure the amount of SF released at predefined time points. The concentration of SF released into PBS was estimated by recording the absorbance at 275 nm^{-1} and using a Beer−Lambert coefficient of 11.8 mol/L/cm. The experiment was carried out in triplicates.

Mechanical Stability of the Coating. The crack resistance of the coating was measured using the 180° bending test with a rectangular block of 1 cm × 3 cm × 0.1 cm (thickness) as per the protocol described by Borkner et al.[11] The central portion of the coated and uncoated PDMS strip was imaged in the SEM. Also, 1 mm thick dumbbell-shaped specimens were prepared from the coated/uncoated PDMS slabs. These specimens were stretched to 100, 150, and 200% strain at a stretching rate of 0.1 mm/sec using a universal tensile testing machine, and SEM images of the central region were recorded after release of the strain.

Synthesis of Glycomonoterpene. Glycomonoterpene (GC) was synthesized as per the method reported previously.[21] Briefly, *Candida bombicola* ATCC 22214 nonpathogenic yeast cells were grown in MGYP broth for 48 h at 28 °C. The yeast cells were then transferred to a production medium containing 10% glucose and citronellal (monoterpene). The cells were incubated in this medium at 28 °C for 6 days, and the product formed at the end of 6 days was harvested by ethyl acetate solvent extraction.

Antiquorum Sensing Activity of SF- and GC-Coated PDMS Discs. *Pseudomonas aeruginosa* is one of the predominantly isolated pathogenic organisms from infected implants, and it produces 3-oxo C12 HSL (long-chain AHL molecule); therefore, to assess inhibition of quorum sensing, we have used a reporter strain *Escherichia coli* pSB1142 (a kind gift from Dr. Paul Williams, University of Nottingham), which exhibits luminescence in response to only long-chain AHL molecules (C10−C14)). It was grown in Luria−Bertani (LB) medium supplemented with 10 μg/mL tetracycline (Sigma-Aldrich, India) at 37 °C. SF-DES and SFGC-DES discs were
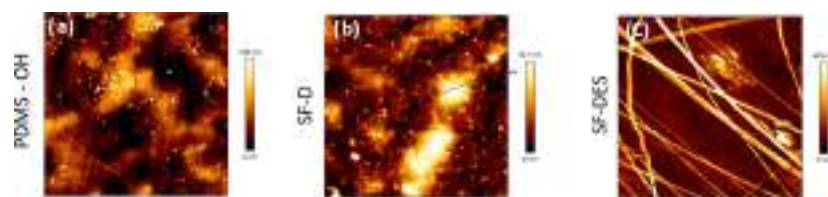
Figure 3. Surface topography of the (a) oxygen plasma-treated PDMS disc, (b) SF-D disc, and (c) SF-DES disc.
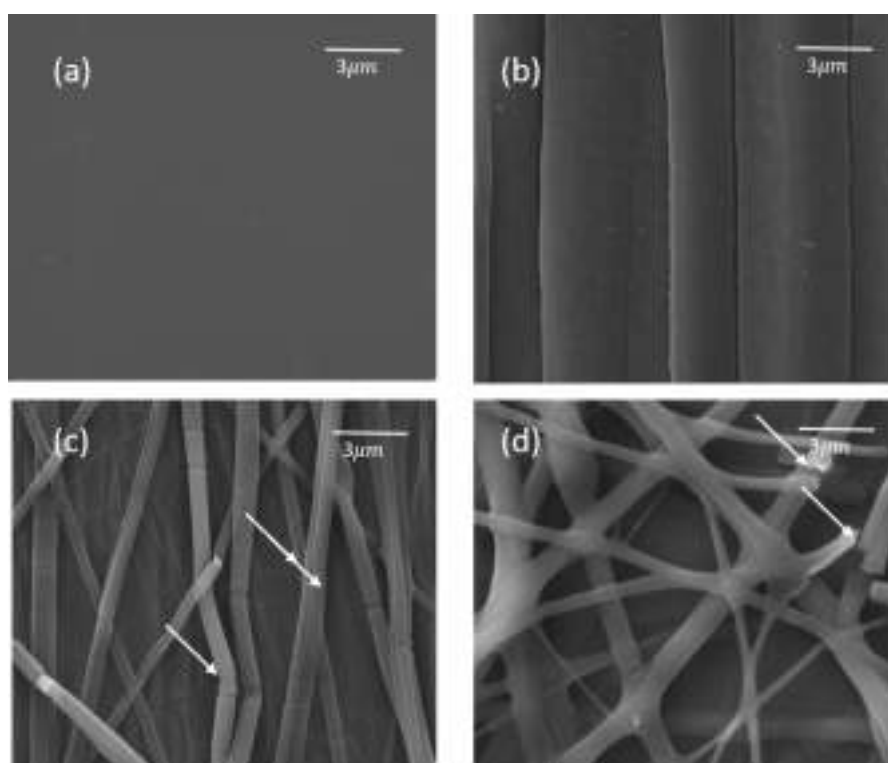
Figure 4. Scanning electron micrographs of the coated PDMS discs after the bending test of (a) oxygen plasma-treated PDMS, (b) SF-D, (c) SF-DES, and (d) SFGC-DES. The white arrows indicate extension of individual nanofibers post mechanical loading.

dipped in PBS for 24 h for releasing the active compound (GC), and the anti-QS activity of released compound was checked using *E. coli* pSB1142 as per the method described elsewhere.[24] An overnight grown culture of *E. coli* pSB1142 (OD_{600nm} = 0.1) was incubated along with GC released in PBS and 0.1 μg/mL of the signal molecule (3-oxo-C12-HSL) (Sigma-Aldrich, India). The reporter strain with and without a signal molecule was considered as a positive and a negative control, respectively. All experimental sets were incubated at 37 °C at 180 rpm for 6 h. Luminescence was measured using a micro plate reader (Spectra Max MSE molecular devices) and reported as relative light unit (RLU) normalized with OD at 600 nm. Experiments were performed in triplicates, and the percentage of (RLU/OD_{600}) inhibition was calculated by using the following formula:

$$\text{luminescence inhibition } (RLU/OD_{600}) \%$$
$$= [\text{positive control } (RLU/OD_{600}) - \text{test } (RLU/OD_{600})$$
$$/\text{positive control } (RLU/OD_{600})] \times 100$$

Antibiofilm Activity of SF- and SF-GC-Coated PDMS Discs. *Staphylococcus epidermidis* and *Pseudomonas aeruginosa* are often associated with infections of implanted medical devices, and both organisms have high rates of antibiotic resistance due to their biofilm forming ability, which is one of the phenotypes mediated through quorum sensing. Therefore, the antibiofilm activity of the uncoated/coated PDMS disc was evaluated using *P. aeruginosa* (NCIM 5029) and *S. epidermidis* (NCIM 5270) as test organisms. Initially, overnight grown cultures of *P. aeruginosa* and *S. epidermidis* were subcultured to Petri plates (30 mm diameter) containing 2 mL of LB medium (OD_{600} was adjusted to 0.1). SF-DES and SFGC-DES PDMS discs were then added to these Petri plates. After incubation of the plates for 24 h at 37 °C, biofilms formed on the discs were subjected to crystal violet staining. The stained biofilm was then visualized under a light microscope at 400× magnification.[21] Biofilms formed on the PDMS discs were also visualized by SEM. For the quantitative evaluation of antibiofilm activity, the crystal violet stain was extracted from the discs using 30% acetic acid. OD of the extracted crystal violet was measured at 580 nm.

In Vitro Cell Proliferation and Cytotoxicity Study. L929 is a mouse fibroblast cell line. It is recommended by ISO 10993 as the preferred cell line for preliminary cytotoxicity testing of biomaterials. L929 (Purchased from NCCS, Pune, Maharashtra, India) mouse fibroblast cells were seeded on coated/uncoated PDMS discs in a 96-well flat-bottomed nonadherent plate at a density of 5×10^3 cells/disc in 10 μL of DMEM (Invitrogen) containing 10% FBS (Invitrogen). The plate was incubated at 37 °C with 5% CO_2 for 10 min that allows the cells to settle on the scaffold followed by the addition of 250 μL of DMEM with 10% FBS and further incubated. During incubation, on the first, fifth, and seventh day, the medium was replaced with filter-
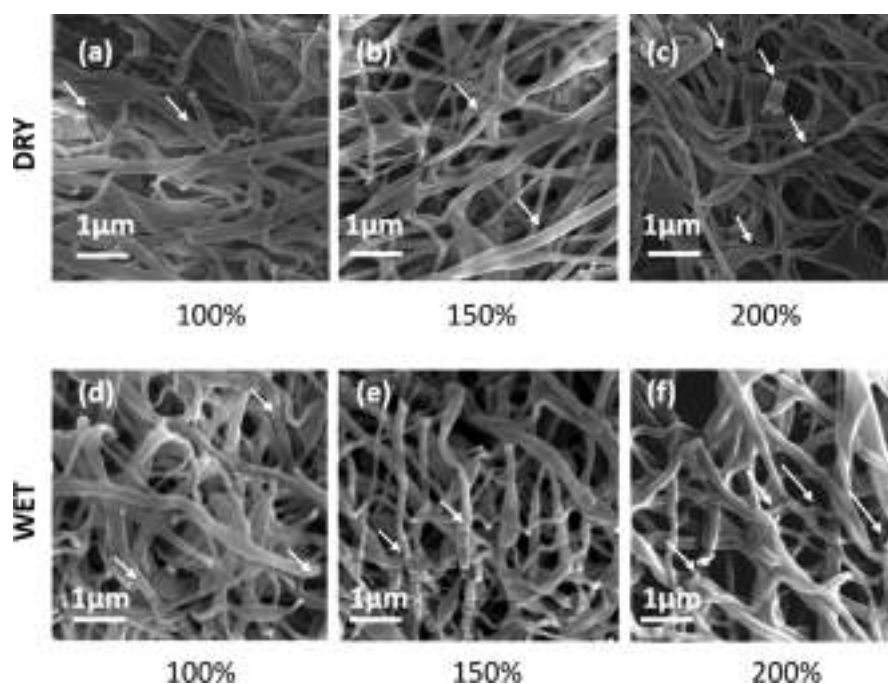
Figure 5. Scanning electron micrographs of SF-DES discs after the tensile test at (a) 100%, (b) 150%, and (c) 200% strain in dry conditions and (d) 100%, (e) 150%, and (f) 200% strain in wet conditions. The white arrows indicate extension of individual nanofibers post mechanical loading.

sterilized MTT (3-(4,5-dimethylthiazol-2-yl)-2,5-diphenyltetrazolium bromide) (0.45 mg/mL) (Invitrogen) prepared in DMEM containing 10% FBS and incubated for 4 h at 37 °C with 5% CO_2. At the end of incubation, MTT was aspirated from the well, and DMSO 200 μL/well was added to dissolve insoluble formazan crystals followed by incubation at 37 °C with 5% CO_2 for 10 min. The absorbance was measured at 550 nm using a microtiter plate reader (Multiskan EX, Thermo Scientific). Each absorbance was taken to be the mean of triplicate measurements.

Statistical Analysis. Experiments were performed in triplicates, and the data obtained from the experiments were represented in the graph as mean ± standard deviation values. To determine significant differences from the control Tukey's multiple comparison test was performed by using Graph Pad Prism 5 software.

■ RESULTS AND DISCUSSION

Formation and Characterization of Coating. PDMS is a polymer routinely used in a variety of biomedical devices and implants. PDMS implants are frequently coated with functional molecules/polymers to improve biocompatibility and add lubricity or antimicrobial functionality to the surface. The first section of the paper, therefore, deals with development of a process to prepare a crack-resistant coat of silk fibroin on PDMS. Dip coating was the obvious first choice of process, owing to the simplicity of the process. Figure 2a shows the image of an oxygen plasma-treated PDMS substrate after dip coating with SF (sample abbreviation: SF-D) and the cross-sectional image (Figure 2c) confirms that the coating has a thickness of the order of 400−500 nm. Dip coating of thin layers (<10 nm) of SF on quartz substrates has been demonstrated earlier.[18] However, these coatings are too thin to achieve a sustained or prolonged release of a functional drug molecule, and the researchers later proposed another method of using a silk barrier layer to suppress the initial burst release of functional molecule.[25] Thicker coatings typically will have a poor cracking resistance under mechanical deformation.
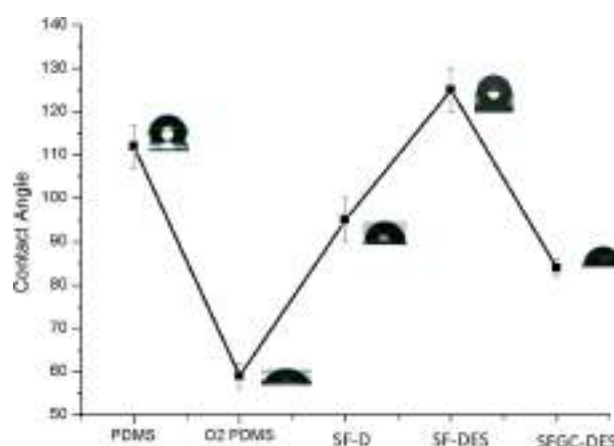
Figure 6. Contact angle measurement on coated/uncoated PDMS discs.

The authors did not comment on the mechanical stability of the coating, rightly so, considering that the substrate used here was a rigid quartz slide. However, when an elastomeric substrate like PDMS is coated with a thick layer of polymer like SF, it is necessary to understand the effect of mechanical deformation of the substrate on the coating. Thus, to improve the stability of coatings under mechanical deformation, an innovative coating process was used here. A combination of two conventional processing protocols, dip coating and electrospinning, was combined to form a self-reinforced coating. (sample abbreviation: SF-DES). The coating was first characterized using SEM, and the results have been summarized in Figure 2b. Figure S2a shows that the electrospun nanofibers are embedded in the dip-coated matrix. The diameter of the electrospun fiber was found to be in the range 50−200 nm. Figure S2b,c shows fiber distribution. The
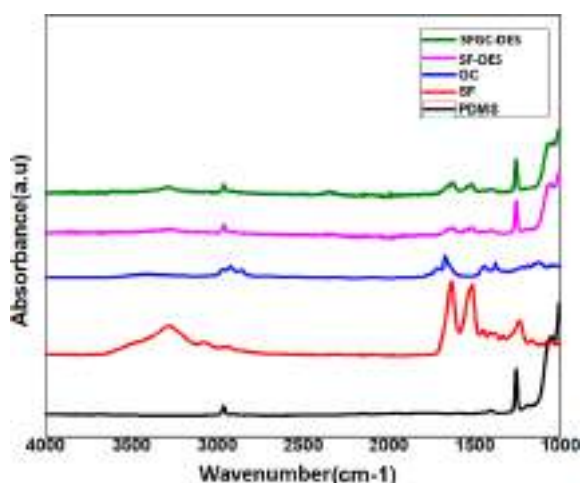
Figure 7. FTIR analysis of before and after silk fibroin coatings.

Figure 9. Antiquorum sensing activity of coated and uncoated PDMS discs, where * and *** indicate significant differences from the control with $P < 0.05$ and $P < 0.001$, respectively. The error bars indicate the standard deviation.

electrospun fibers are at least partially embedded in the dip-coated SF matrix (Figure 2b), and some fibers also appear to be on the surface of the coat. As can be seen in Figure 2d, the resultant SF coating has a total thickness of about 1 μm. For thicker coatings, electrospinning of solutions can be done for a longer duration, which might also be desirable for sustained drug release.

The surface topography of uncoated/coated PDMS discs was studied using scanning probe microscopy in tapping mode, and these results are summarized in Figure 3. The oxygen plasma-treated PDMS disc exhibits a RMS surface roughness of 18 nm, as can be seen in Figure S3. After dip coating with SF, the surface is still found to have a very similar surface roughness. As expected, the disc with a sequential dip and electrospun SF exhibits a surface roughness that is at least an order of magnitude higher than the other two substrates. This increased surface roughness is desirable for biomedical applications. It has been shown that the fibroblast attachment on textured breast implants was higher than smooth implants

by Valencia-Lazcano et al.[5] Researchers have also demonstrated that proliferation of fibroblasts was better in electrospun mats as compared to SF films.

Mechanical Stability Measurements. A simple bending test, followed by SEM imaging, was designed to characterize the cracking resistance of the coating on the PDMS implant. The PDMS strip subjected to oxygen plasma treatment was used as a control. As can be seen from Figure 4a, the PDMS disc has a smooth surface after the plasma treatment and the surface did not exhibit any changes in surface morphology after the bending test. The SF-D disc also showed a uniform coating with a smooth surface (Figure 2a). However, after the bending test, the coating did not retain its integrity. Large visible micro- and macro-cracks were seen on the surface of the coating (Figure 4b). This result is in agreement with prior literature, which shows that, after a similar test was conducted on a recombinant spider silk coating on PDMS, the authors did observe cracking on the coating, although the cracking reported is not as severe as the one observed here.[12] The reason for this difference is the variation in the coating process,
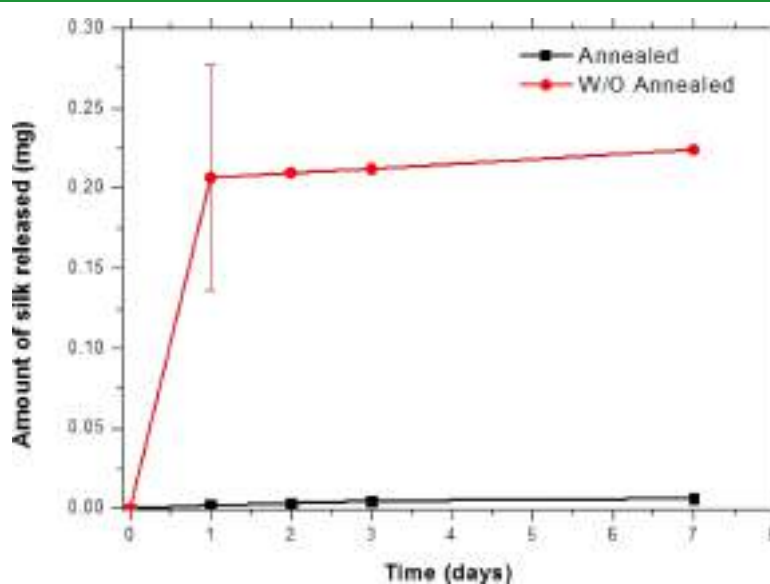
Figure 8. Stability of the SF-DES before and after methanol treatment.
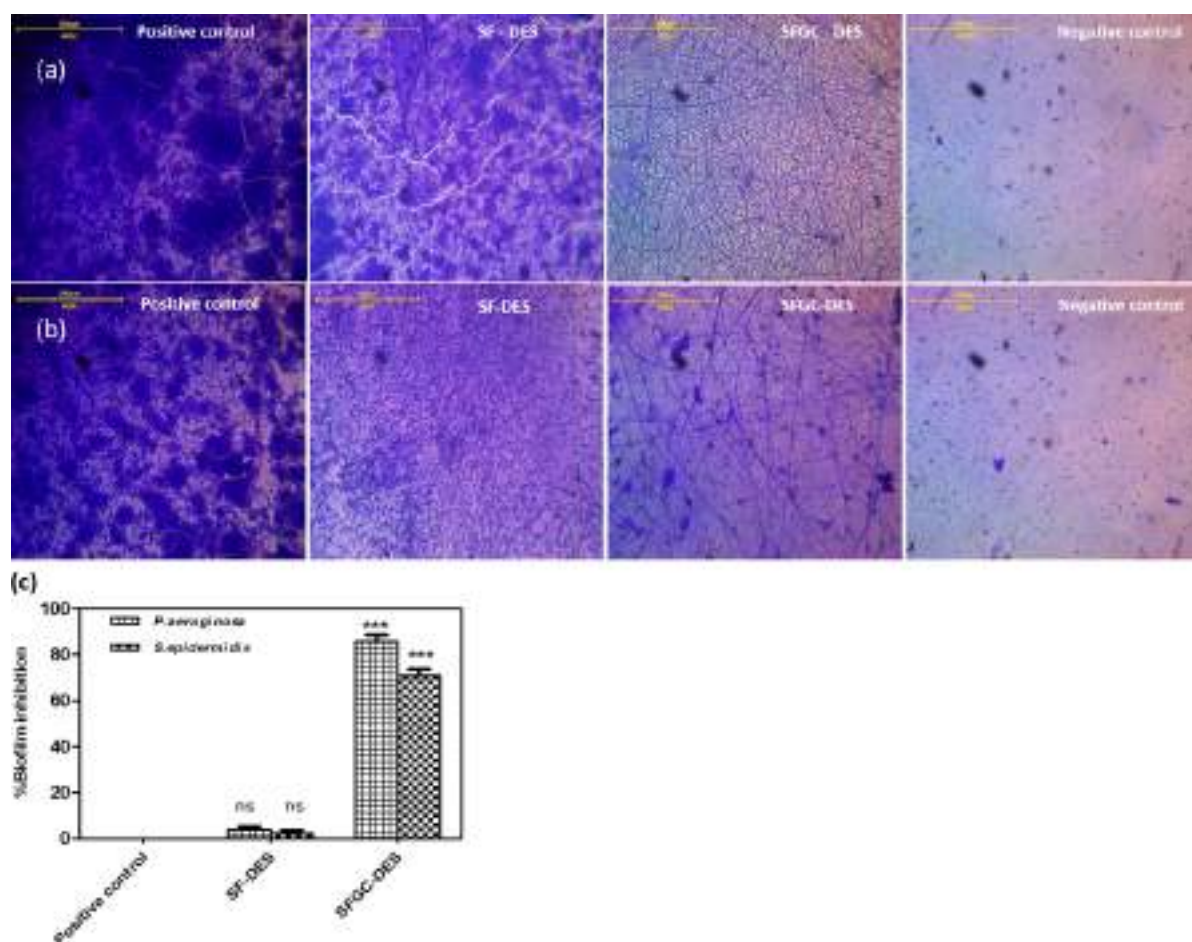
Figure 10. Optical microscopy images of biofilm inhibition observed on coated and uncoated PDMS discs stained with crystal violet. (a) *P. aeruginosa*, (b) *S. epidermidis*, (c) *S. epidermidis*, and *P. aeruginosa* biofilm inhibition quantified by extracting crystal violet stain from the coated/uncoated PDMS discs (where ns and *** indicate significant differences from the control with $P > 0.05$ and $P < 0.001$, respectively, and the error bars indicate the standard deviation).
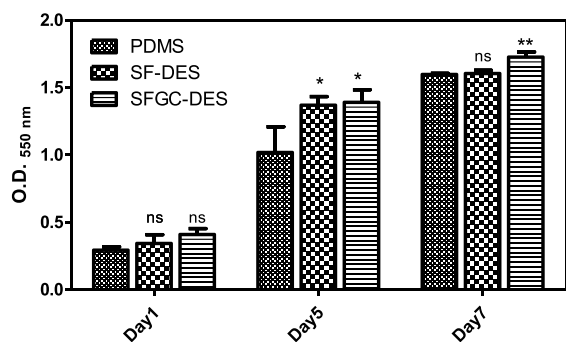
Figure 11. MTT assay using L929 cells on PDMS, SF-DES, and SFGC-DES samples for 7 days (where ns, *, and ** indicates significant differences from the control (PDMS) with $P > 0.05$, $P < 0.05$, and $P < 0.01$, respectively, and the error bars indicate the standard deviation).

thickness of coatings, and the material composition. Contrary to this observation, the surface morphology of the novel dip and electrospun PDMS strip was comparable before and after the bending test (Figure 2b and Figure 4c). The electrospun fibers exhibit regions of stress whitening (marked with white arrows) indicating that the mechanical stress exerted on the

samples is primarily taken up by the nanofibers, and thus, the damage caused to the lower dip coated layer is minimum. Also, as discussed earlier, the electrospun nanofibers are partially embedded in the dip-coated layer. It may, therefore, be hypothesized that these embedded fibers act as reinforcement and improve the cracking resistance of the coating. Self-reinforcement of polymer matrices using nano/microfibers is a classical and proven technique to improve the toughness of the material.[26,27]

A similar result has also been reported by authors Mandal et al.[28]; the authors used SF microfibers to improve the mechanical toughness of SF scaffolds. However, the use of the sequential dip and electrospinning process as a coating toughness enhancement mechanism is novel. The technique also worked perfectly after preparation of a blend of SF and GC as shown in Figure 4d.

Additionally to the bending test, we have also performed tensile tests on our samples. These tests were performed on dogbone-shaped PDMS substrates, coated with a dip and thick electrospun layer of SF. Our results indicate that, at strains of 100%, no physical damage to the SF nanofibers is observed. At higher strains of 150 and 200%, some regions with stress whitening can be observed on the nanofibers as shown in Figure 5a−c. However, no significant change in fiber

morphology was observed. We also looked at the behavior of these samples under wet conditions when the coatings have been swollen to equilibrium weight. Here, we observed that, when the strain is increased to 150% and 200%, some of the fibers showed a break as shown in Figure 5d−f. However, the damage is not significant, and the integrity of the coating is still maintained. We have also observed that the SF coatings retain their physical integrity under torsional loads (as shown in Figure S4).

Thus, our results demonstrate that a novel combination of two conventional processes of coating, dip and electrospinning, significantly enhances the performance of the coating under mechanical loading both in the dry and wet states. This performance improvement is highly desirable considering that implants are subjected to a variety of mechanical stresses both during handling and in use. The experiments on the dry SF coating simulate the forces exerted on an implant primarily during storage and handling. Post implantation the SF coating is wetted by the bodily fluids, and thus, the wet experiments demonstrate the stability of the coating during use after implantation in the body.

The PDMS surface was characterized after each processing step using a simple instantaneous contact angle measurement to confirm successful modification. The pristine PDMS polymer surface is highly inert and unreactive, and hence, it is extremely challenging to have a coating adhere onto the PDMS surface. Oxygen plasma was the method of choice for PDMS surface modification since it has been reported that this treatment results in the formation of hydrophilic OH groups on the surface and increases the wettability of the PDMS discs. As shown in Figure 6, oxygen plasma-treated PDMS discs exhibited a contact angle of $55 \pm 5°$, which was significantly lower than the contact angle of the discs before plasma treatment, i.e., $115 \pm 5°$. After SF-D coating, the contact angle was found to increase to $95 \pm 5°$. Further, SF-DES discs increased the contact angle to $128 \pm 3°$. This increase in contact angle post electrospinning can be attributed to the presence of small air pockets between the electrospun nanofibers that resist the wetting of the surface.[29] The SFGC-DES discs had a contact angle of $85 \pm 5°$, which is much lower that of the SF-DES mat. Glycolipids are hydrophilic molecules and hence improve the wettability of a surface. Thus, the change in contact angle after each processing step provides sufficient evidence to corroborate the modification of the PDMS surface and its successful coating.

The modification of the PDMS substrate after coating was also characterized using ATR-FTIR spectroscopy to gain insights into the conformation of the SF protein. The data has been summarized in Figure 7. The control samples used here were the pure PDMS substrate, SF degummed fibers, and as-synthesized GC molecule. The pristine PDMS has no signal beyond the 3000 cm^{-1} range. The symmetric and asymmetric stretching of CH$_3$ shows peaks at 2963 and 2906 cm^{-1}, along with the CH$_3$ bending vibration at 1258 cm^{-1}. The peak in the range 1200−800 cm^{-1} confirms the presence of Si−O−Si groups of PDMS.[30] G-citron shows a peak at 3063−3640 cm^{-1} corresponding to OH stretching from glucose. The asymmetric and symmetric stretching of CH$_2$ gives a peak at 2857 cm^{-1}. The presence of C=O stretching in glucose gives a peak at 1720 cm^{-1} due to the saturated aliphatic 6-membered ring of glucose. After coating PDMS with SF, a broader peak from 3300 to 3700 cm^{-1} is observed, and this corresponds to the OH groups present in the system. The random coil

conformation of silk fibroin shows a peak at 1650 and 1540 cm^{-1} for amide I and amide II, respectively.[23] The SF-coated PDMS exhibited peaks from both pure SF and the PDMS substrate below. This is anticipated since the IR beam is known to penetrate the first few microns of the surface. Since the coating is only ∼1 μm in thickness, the spectrum also shows peaks corresponding to the below PDMS substrate. The amide I stretching peak at 1623 cm^{-1} indicates that the protein has predominantly the β sheet conformation. Earlier reports suggest that SF after electrospinning displays a lower β sheet content. However, the methanol vapor post treatment results in the change in protein conformation. The IR spectrum displays a prominent amide I peak at the lower wavenumber of 1623 cm^{-1}. Correspondingly, a high β sheet content of ∼40% was also observed after deconvolution of the amide I spectra (data not shown). The SFGC-DES sample did show the peaks for PDMS and also for SF. However, the GC peaks were too weak to be discerned and quantified. However, the change in contact angle observed between the SF-DES and SFGC-DES sample can be considered to be a sufficient proof of the presence of GC in the coatings. Further, we also show that, when the SFGC-DES mat is incubated in PBS solution, the GC is released into the aqueous medium (as shown in Figure S5)

Stability of the Coatings. The aqueous stability of the SF coating was determined using UV−vis spectroscopy. Since no significant weight loss or SF release was observed after a 3 day period, the experiment was terminated after 7 days. The test was performed on the SF-DES discs before and after methanol vapor treatment. The release of SF into the PBS solution was monitored using UV−vis spectroscopy, and the data has been summarized in Figure 8. The SF protein in aqueous solutions shows an absorbance at 275 cm^{-1}, and this absorbance was used to estimate the amount of SF released from the coating.[25] The total amount of SF present on each disc can be estimated to be about 0.34 mg. The amount of silk fibroin released before annealing was around 50−60% of the total SF. The amount of SF released from the coating after the methanol vapor treatment was negligible and below the measurable limit. Thus, it may be concluded here that the methanol treatment results in a stable coating of SF for use in biomedical applications.

After completion of the mechanical and physicochemical characterization of the coatings, the coatings were further evaluated for their biological activity. As discussed earlier, one of the primary reasons for failure of implants is the formation of a bacterial biofilm. Also, growth of microorganisms in biofilms shows high resistance to antimicrobial agents. This is probably due to a decreased penetration of antibiotics and decreased growth rate or metabolism of the bacterial cells present in biofilms. Antibiotics give selective pressure to bacteria, and thus, they indeed find ways of resisting the newly developed antibiotics.[31] High doses of an antibiotic are required to be administered, which in turn affects the normal flora of the host body as well. Quorum sensing inhibition provides a promising alternative to antibiotic resistance by altering bacterial communication, without putting selective pressure on bacteria as well by inhibiting biofilm formation.[32] It is a means of communication between the bacterial cells using certain diffusible signal molecules, called autoinducers, specific to their species. These molecules aid bacteria to sense their population density and to regulate the expression of various genes in response to the density.[33] Quorum sensing

controls expression of genes for virulence, motility and biofilm formation, etc. which play crucial roles in the pathogenesis.[32] Thus, molecules, which target QS in the bacterial population, automatically also inhibit biofilm formation, the resultant of QS.

Reports suggest that plant-derived essential oils act as quorum sensing inhibitors.[34] However, this biological activity cannot be exploited fully due to their hydrophobicity. It has already been demonstrated by our earlier papers that the addition of a glucose moiety to these hydrophobic molecules improves their bioavailability.[21] GC is a molecule that has been demonstrated to exhibit antibiofilm and quorum-quenching activity.

Antiquorum Sensing Activity of SF- and GC-Coated PDMS Discs. *E. coli* pSB1142 was used to check the inhibition of quorum sensing mediated through a long-chain AHL signal molecule. The strain possesses lasR and las promoter of *P. aeruginosa* fused to the luxCDABE cassette from *Photorhabdus luminescens*, which responds to long-chain AHLs (C10−C14) to produce luminescence. This reporter strain does not synthesize AHL molecules, but exhibits luminescence in the presence of the external AHL signal molecule. In this experiment, the external signal molecule selected was *N*-(3-oxo-dodecanoyl)-L-homoserine lactone, one of the signal molecules produced by *P. aeruginosa*. A decrease in the luminescence of the cells (compared to positive controls) in the presence of coating confirms its anti-QS activity.[35] To exclude growth-dependent effects, OD measurements were recorded in order to normalize luminescence production to cell density. Using PDMS discs with and without coating, QSI activity of the released compound was checked when the 3-oxo-C12 HSL signal molecule was added externally. The active compound released from disc coatings with GC SF showed significant quorum sensing inhibition, which is more than 50% when compared to PDMS discs without coatings. See Figure 9.

Antibiofilm Activity of SF- and GC-Coated PDMS Discs. The formation of bacterial biofilms is one of the major phenomenon controlled by quorum sensing. Impeding bacteria's capacity to form biofilm is a major challenge in treating chronic infections. In this study, the antibiofilm activity of SF-DES and SFGC-DES PDMS disc was evaluated by using *P. aeruginosa* (NCIM 5029) and *Staphylococcus epidermidis* (NCIM 5270) as test organisms. The PDMS disc containing GC in the coating showed a significant antibiofilm activity when observed after 24 h. Around 85% biofilm inhibition when tested against *P. aeruginosa* was observed, whereas the same coating showed nearly 70% biofilm inhibition when tested against *S. epidermidis*. These results have been summarized in Figure 10a−c. Higher magnification scanning electron micrographs also support our observations (shown in Figure S6).

In Vitro Cell Proliferation and Cytotoxicity of SF- and GC-Coated PDMS Discs. The coated and/or uncoated PDMS discs were evaluated for cytotoxicity using in vitro cell culture studies with the mouse fibroblast cell line L929. Cell proliferations were evaluated by performing the MTT test. MTT data in Figure 11 show an increase in absorbance on day 1 in SF-DES as compares to SF-D and PDMS, which indicates a greater biocompatibility was achieved with the electrospinning technique. A higher cell viability with respect to all three groups was observed in SFGC-DES discs on day 1, confirming the noncytotoxicity of GC. A similar cell viability

trend was observed on the fifth and seventh day, which is sufficient to prove the non-cytotoxicity of the modified discs.

CONCLUSION

Surface coatings have emerged as a promising alternative to reduce implant failure due to both foreign body response and device-associated infections. Failure of coatings due to cracking, delamination, and flaking is also a concern for successful use of implants. Here, we report a process innovation, sequential dip and electrospinning process, that results in the formation of a self-reinforced coating of silk fibroin on an elastomeric substrate like polydimethylsiloxane. These new coatings have shown to be crack-resistant under mechanical deformations in tensile, bending, and torsional modes. Silk fibroin improves the biocompatibility of the PDMS substrate, thus mitigating the risk of implant failure due to foreign body response. Further, we have blended in a next-generation quorum-quenching antibiofilm molecule into the coating. This molecule not only retains its quorum sensing activity throughout the processing steps but also inhibits biofilm formation of two of the most notorious infection-causing bacteria, *P. aeruginosa* and *S. epidermidis*. All of these functions have been achieved while retaining the inherent biocompatibility of these materials. Thus, our work demonstrates an innovative solution to simultaneously resolve multiple causes for failures of implant devices, biofilm formation, foreign body response, and cracking of the coating.

ASSOCIATED CONTENT

Ⓢ Supporting Information

The Supporting Information is available free of charge on the ACS Publications website at DOI: 10.1021/acsabm.8b00515.

XPS spectrum of modified and unmodified PDMS substrates, distribution of fiber diameter obtained using image analysis, surface profiles of PDMS substrates before and after coating, SEM analysis after bending test, UV−vis spectroscopy of the released GC molecule, and biofilm inhibition before and after coating (PDF)

AUTHOR INFORMATION

Corresponding Authors
*E-mail: asmita.prabhune@gmail.com.
*E-mail: aa.nisal@ncl.res.in.

ORCID
Asmita Prabhune: 0000-0003-1839-2105
Anuya Nisal: 0000-0003-1633-7890

Author Contributions
E.J. prepared and characterized SF-D, SF-DES, and SFGC-DES with assistance from A.S. A.P. prepared and characterized G-citron and also performed the quorum sensing and antibiofilm assay of SF-DES and SFGC-DES with assistance from S.H. N.P. performed cytotoxicity studies for SF-DES and SFGC-DES. A.A.N. and A.A.P. supervised the study. E.J., A.P., S.H., N.P., A.A.N., and A.A.P. wrote the manuscript with input from other coauthors. E.J. and A.P. contributed equally.

Notes
The authors declare no competing financial interest.

ACKNOWLEDGMENTS

ABBREVIATIONS

GC, G-citron; SF, silk fibroin; SF-D, silk fibroin dip coating; SF-DES, sequential dip and electrospinning of silk fibroin; SFGC-DES, sequential dip and electrospinning of silk fibroin/ G-Citron

REFERENCES

(1) Nandakumar, V.; Chittaranjan, S.; Kurian, V. M.; Doble, M. Characteristics of Bacterial Biofilm Associated with Implant Material in Clinical Practice. *Polym. J.* **2013**, *45* (2), 137−152.

(2) Singha, P.; Locklin, J.; Handa, H. A Review of the Recent Advances in Antimicrobial Coatings for Urinary Catheters. *Acta Biomater.* **2017**, *50*, 20−40.

(3) Zander, Z. K.; Becker, M. L. Antimicrobial and Antifouling Strategies for Polymeric Medical Devices. *ACS Macro Lett.* **2018**, *7* (1), 16−25.

(4) Zhang, Z.; Qu, Y.; Li, X.; Zhang, S.; Wei, Q.; Shi, Y.; Chen, L. Electrophoretic Deposition of Tetracycline Modified Silk Fibroin Coatings for Functionalization of Titanium Surfaces. *Appl. Surf. Sci.* **2014**, *303*, 255−262.

(5) Valencia-Lazcano, A. A.; Alonso-Rasgado, T.; Bayat, A. Physico-Chemical Characteristics of Coated Silicone Textured versus Smooth Breast Implants Differentially Influence Breast-Derived Fibroblast Morphology and Behaviour. *J. Mech. Behav. Biomed. Mater.* **2014**, *40*, 140−155.

(6) Dunn, K. W.; Hall, P. N.; Khoo, C. T. K. Breast Implant Materials: Sense and Safety. *Br. J. Plast. Surg.* **1992**, *45* (4), 315−321.

(7) Amin, S.; Rajabnezhad, S.; Kohli, K. Hydrogels as Potential Drug Delivery Systems. *Sci. Res. Essay* **2009**, *3* (11), 1175−1183.

(8) Zeplin, P. H.; Maksimovikj, N. C.; Jordan, M. C.; Nickel, J.; Lang, G.; Leimer, A. H.; Römer, L.; Scheibel, T. Spider Silk Coatings as a Bioshield to Reduce Periprosthetic Fibrous Capsule Formation. *Adv. Funct. Mater.* **2014**, *24* (18), 2658−2666.

(9) Shi, S.; Liu, Y.; Wang, L. Methods and Compositions for Improved Tissue Regeneration by Suppression of Interferon-Gamma and Tumor Necrosis Factor-Alpha. U.S. PatentUS20140154220 A1, 2014.

(10) SentreHeart Recalls FindrWIRZ Guidewire System due to Coating Separation. https://www.fda.gov/MedicalDevices/Safety/ ListofRecalls/ucm530336.htm.

(11) Borkner, C. B.; Elsner, M. B.; Scheibel, T. Coatings and Films Made of Silk Proteins. *ACS Appl. Mater. Interfaces* **2014**, *6* (18), 15611−15625.

(12) Borkner, C. B.; Wohlrab, S.; Möller, E.; Lang, G.; Scheibel, T. Surface Modification of Polymeric Biomaterials Using Recombinant Spider Silk Proteins. *ACS Biomater. Sci. Eng.* **2017**, *3* (5), 767−775.

(13) Gronau, G.; Krishnaji, S. T.; Kinahan, M. E.; Giesa, T.; Wong, J. Y.; Kaplan, D. L.; Buehler, M. J. A Review of Combined Experimental and Computational Procedures for Assessing Biopolymer Structure-Process-Property Relationships. *Biomaterials* **2012**, *33*, 8240−8255.

(14) Kasoju, N.; Bora, U. Silk Fibroin in Tissue Engineering. *Adv. Healthcare Mater.* **2012**, *1* (4), 393−412.

(15) Kundu, B.; Rajkhowa, R.; Kundu, S. C.; Wang, X. Silk Fibroin Biomaterials for Tissue Regenerations. *Adv. Drug Delivery Rev.* **2013**, *65*, 457−470.

(16) Petrini, P.; Parolari, C.; Tanzi, M. C. Silk Fbroin-Polyurethane Scaffolds for Tissue Engineering. *J. Mater. Sci.: Mater. Med.* **2001**, *12*, 849−853.

(17) Arpacay, P.; Turkan, U. Development of Antibiotic-Loaded Silk Fibroin/ Hyaluronic Acid Polyelectrolyte Film Coated CoCrMo Alloy. *Biomed. Tech.* **2016**, *61* (5), 463−474.

(18) Wang, X.; Kim, H. J.; Xu, P.; Matsumoto, A.; Kaplan, D. L. Biomaterial Coatings by Stepwise Deposition of Silk Fibroin. *Langmuir* **2005**, *21* (24), 11335−11341.

(19) Gerdt, J. P.; Blackwell, H. E. Competition Studies Confirm Two Major Barriers That Can Preclude the Spread of Resistance to Quorum-Sensing Inhibitors in Bacteria. *ACS Chem. Biol.* **2014**, *9* (10), 2291−2299.

(20) Bjarnsholt, T.; Givskov, M. Quorum Sensing Inhibitory Drugs as Next Generation Antimicrobials : Worth the Effort ? *Curr. Infect. Dis. Rep.* **2008**, *10*, 22−28.

(21) Patil, A.; Joshi-Navre, K.; Mukherji, R.; Prabhune, A. Biosynthesis of Glycomonoterpenes to Attenuate Quorum Sensing Associated Virulence in Bacteria. *Appl. Biochem. Biotechnol.* **2017**, *181* (4), 1533−1548.

(22) Rockwood, D. N.; Preda, R. C.; Yücel, T.; Wang, X.; Lovett, M. L.; Kaplan, D. L. Materials Fabrication from Bombyx Mori Silk Fibroin. *Nat. Protoc.* **2011**, *6* (10), 1612−1631.

(23) Nisal, A.; Sayyad, R.; Dhavale, P.; Khude, B.; Deshpande, R.; Mapare, V.; Shukla, S.; Venugopalan, P. Silk Fibroin Micro-Particle Scaffolds with Superior Compression Modulus and Slow Bioresorption for Effective Bone Regeneration. *Sci. Rep.* **2018**, *8* (1), 7235.

(24) Flynn, P. B.; Busetti, A.; Wielogorska, E.; Chevallier, O. P.; Elliott, C. T.; Laverty, G.; Gorman, S. P.; Graham, W. G.; Gilmore, B. F. Non-Thermal Plasma Exposure Rapidly Attenuates Bacterial AHL-Dependent Quorum Sensing and Virulence. *Sci. Rep.* **2016**, *6*, 18−30.

(25) Wang, X.; Hu, X.; Daley, A.; Rabotyagova, O.; Cebe, P.; Kaplan, D. L. Nanolayer Biomaterial Coatings of Silk Fibroin for Controlled Release. *J. Controlled Release* **2007**, *121* (3), 190−199.

(26) Kmetty, Á.; Bárány, T.; Karger-Kocsis, J. Self-Reinforced Polymeric Materials: A Review. *Prog. Polym. Sci.* **2010**, *35* (10), 1288−1310.

(27) Lucchetta, M. C.; Morales Arias, J. P.; Mollo, M.; Bernal, C. R. Self-Reinforced Composites Based on Commercial PP Woven Fabrics and a Random PP Copolymer Modified with Quartz. *Polym. Adv. Technol.* **2016**, *27* (8), 1072−1081.

(28) Mandal, B. B.; Grinberg, A.; Seok Gil, E.; Panilaitis, B.; Kaplan, D. L. High-Strength Silk Protein Scaffolds for Bone Repair. *Proc. Natl. Acad. Sci. U. S. A.* **2012**, *109* (20), 7699−7704.

(29) Li, H.; Zhu, J.; Chen, S.; Jia, L.; Ma, Y. Fabrication of Aqueous-Based Dual Drug Loaded Silk Fibroin Electrospun Nanofibers Embedded with Curcumin-Loaded RSF Nanospheres for Drugs Controlled Release. *RSC Adv.* **2017**, *7* (89), 56550−56558.

(30) Zhou, J.; Khodakov, D. A.; Ellis, A. V.; Voelcker, N. H. Surface Modification for PDMS-Based Microfluidic Devices. *Electrophoresis* **2012**, *33* (1), 89−104.

(31) Marketon, M. M.; Gronquist, M. R.; Eberhard, A.; Gonzalez, J. E. Characterization of the Sinorhizobium Meliloti SinR/SinI Locus and the Production of Novel N-Acyl Homoserine Lactones. *J. Bacteriol.* **2002**, *184* (20), 5686−5695.

(32) Kalia, V. C. *Quorum Sensing vs Quorum Quenching: A Battle with No End in Sight* **2015**, 1.

(33) Williams, P. Quorum Sensing, Communication and Cross-Kingdom Signalling in the Bacterial World. *Microbiology* **2007**, *153* (12), 3923−3938.

(34) Mukherji, R.; Prabhune, A. Novel Glycolipids Synthesized Using Plant Essential Oils and Their Application in Quorum Sensing Inhibition and as Antibiofilm Agents. *Sci. World J.* **2014**, *2014*, 1−7.

(35) Saurav, K.; Costantino, V.; Venturi, V.; Steindler, L. Quorum Sensing Inhibitors from the Sea Discovered Using Bacterial N-Acyl-Homoserine Lactone-Based Biosensors. *Mar. Drugs* **2017**, *15*, 53.

LANGMUIR

Mechanism of Adhesion of Natural Polymer Coatings to Chemically Modified Siloxane Polymer

Emmanuel Joseph, Shatruhan Singh Rajput, Shivprasad Patil,* and Anuya Nisal*

Cite This: https://dx.doi.org/10.1021/acs.langmuir.1c00047

Read Online

| ACCESS | Metrics & More | Article Recommendations | Supporting Information |

ABSTRACT: Surface coatings play an important role in improving the performance of biomedical implants. Polydimethylsiloxane (PDMS) is a commonly used material for biomedical implants, and surface-coated PDMS implants frequently face problems such as delamination or cracking of the coating. In this work, we have measured the performance of nano-coatings of the biocompatible protein polymer silk fibroin (SF) on pristine as well as modified PDMS surfaces. The PDMS surfaces have been modified using oxygen plasma treatment and 3-amino-propyl-triethoxy-silane (APTES) treatment. Although these techniques of PDMS modification have been known, their effects on adhesion of SF nano-coatings have not been studied. Interestingly, testing of the coated samples using a bulk technique such as tensile and bending deformation showed that the SF nano-coating exhibits improved crack resistance when the PDMS surface has been modified using APTES treatment as compared to an oxygen plasma treatment. These results were validated at the microscopic and mesoscopic length scales through nano-scratch and nano-indentation measurements. Further, we developed a unique method using modified atomic force microscopy to measure the adhesive energy between treated PDMS surfaces and SF molecules. These measurements indicated that the adhesive strength of PDMS-APTES-SF is 10 times more compared to PDMS-O_2-SF due to the higher number of molecular linkages formed in this nanoscale contact. This lower number of molecular linkages in the PDMS-O_2 indicates that only fewer numbers of surface hydroxyl groups interact with the SF protein through secondary interactions such as hydrogen bonding. On the other hand, a larger number of amine groups present on PDMS-APTES surface hydrogen bond with the polar amino acids present on the silk fibroin protein chain, resulting in better adhesion. Thus, APTES modification to the PDMS substrate results in improved adhesion of nano-coating to the substrate and enhances the delamination and crack resistance of the nano-coatings.
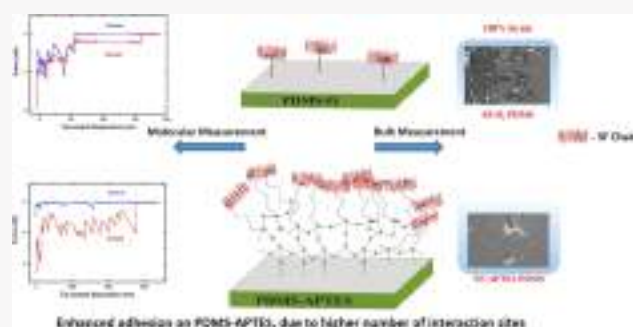
INTRODUCTION

Medical devices play a crucial role in alleviating or minimizing discomfort and pain to patients and thereby contribute toward better quality of life in various ways. Polydimethylsiloxane (PDMS) is a chemically inert silicon-based inorganic polymer that is used in various medical devices including breast implants, lenses, catheter tubing,[1,2] etc. PDMS is processed using a two-part curing process that includes the use of a cross-linker. It has tunable mechanical properties, which suit a variety of applications. PDMS also has proven biocompatibility.[3] PDMS, however, exhibits lower surface wettability and high surface energy. This hydrophobicity, with a typical contact angle greater than 90°, has been recognized as one of the reasons for the failure of PDMS implants. The hydrophobic water contact angle leads to nonspecific adsorption of proteins from the blood plasma, which triggers events such as fibrotic capsular contracture in breast implants and eventually results in its failure.[4]

To reduce the failure rate of PDMS implants, they are coated with natural polymers, and several researchers have explored this strategy.[5] However, the high surface energy of

PDMS leads to poor adhesion of coatings to the PDMS surface, and coating delamination poses multiple clinical problems and results in recall of products by regulatory bodies.[3] Thus, excellent adhesion of coating to the substrate is critical for enhancing the performance of PDMS implants.

To improve the surface wettability of PDMS, various physical and chemical treatments on the PDMS surface have been proposed.[4,6,7] The physical methods of surface modification include plasma treatments using different gases such as oxygen, argon, nitrogen, hydrogen, and helium. UV treatment and ozone treatment are other modes of physical treatments. These treatments result in the formation of hydrophilic groups such as $-OH$, $-NH_2$, $-NO_2$, and

---

ACS Publications   © XXXX American Chemical Society

A

−COOH on the PDMS surface. In addition to these physical methods, various chemical modifications of the surface to produce hydrophilic groups have also been reported. Some chemical treatments include piranha treatment, 3-amino-propyl-triethoxy-silane (APTES) treatment, and self-polymerization of dopamine. The piranha treatment produces a surface with −OH groups, while APTES provides amino functional groups. The self-polymerization of dopamine on PDMS results in stabilized stem cell adhesion, multipotency, improved hemocompatibility, and antimicrobial property.[8,9]

These treatments on the PDMS surface result in the formation of hydrophilic functional groups.[10] Presumably, these functional groups interact with the coating material through noncovalent bonds such as hydrogen bonding and electrostatic interactions. However, the adhesion of natural polymers to PDMS surfaces after these treatments has not been thoroughly investigated. In particular, the mechanical strength of these coatings and their resistance to shear stresses are poorly understood. One of the approaches to compare the interaction of different surface treatments was to quantify the amount of coating material adsorbed using fluorescent dyes on the PDMS surface after surface modification.[11]

One of the challenges in quantifying the strength of adhesion of natural polymers to the modified PDMS surface is that the PDMS is an elastomer and results in significant deformation of the bulk of the PDMS material while performing tests such as the peel test and lap shear.[12,13] The quantification of adhesive energy of the stiff material on a soft substrate is therefore a challenge. Here, we provide quantitative details of the quality of adhesion of a natural polymer, silk fibroin (SF), to the modified PDMS surface as well as the molecular-level understanding of adhesion of these coatings. Silk fibroin is a natural biocompatible protein polymer extracted from the cocoon of a *Bombyx mori* silkworm. The PDMS discs were surface-modified using oxygen plasma and the APTES treatment method to make them hydrophilic. At a macroscopic level, we compared the adhesive strength of SF coating on PDMS modified by APTES and O_2-plasma using the peel test. We used mechanical tests such as bending and tensile loading and characterized the resulting surface using microscopy. We performed nano-mechanical measurements such as nanoscratch and nano-indentation on SF coatings on PDMS. All of these tests suggest that APTES-treated PDMS is better suited for SF adhesion compared to O_2-plasma-treated PDMS. To gain insights into the molecular-level mechanism of better adhesion in the case of APTES-treated PDMS, the interaction of SF with individual functional groups of physically and chemically modified PDMS was measured using atomic force microscopy (AFM). The energy required to separate the SF-coated glass microsphere (∼20 μm) from the PDMS surface-modified to produce hydrophilic groups was also measured. To the best of our knowledge, this is the first report about characterizing the SF− PDMS interface using mechanical tests and force spectroscopic measurements, which explains the results from these macroscopic tests.

■ EXPERIMENTAL SECTION: MATERIALS AND METHODS

Preparation of PDMS Discs. Medical-grade PDMS (Sylgard 184, Dow Corning) was cast on polystyrene Petri dishes to obtain a disc with a uniform thickness of 1 mm. The prepolymer was thoroughly mixed with the curing agent for 5 min using a weight ratio of 10:1. It

was then poured into the Petri dish and degassed for 30 min. This mixture was kept in a convection oven at 40 °C for 24 h. PDMS discs of the required dimension were then cut out, and isopropyl alcohol (IPA) treatment was performed to clean the samples, which were used for further experimentation. The treatment involved 30 min sonication in an IPA bath to remove dust particles before further experimentation. This process of cleaning was followed by a drying step (60 °C for 4 h in a vacuum oven) to remove any traces of the IPA solvent.

Surface Treatments of PDMS Discs. *Oxygen Plasma Treatment.* Plasma treatment of the PDMS surface after cleaning with IPA and drying at 60 °C was performed as per the protocol already reported in the literature.[14] The plasma treatment was done on both sides of the PDMS disc using an RF plasma from Quorum Technologies (K1050X), solid-state barrel reactor. Briefly, the optimized plasma conditions of 50 W for 1 min were determined using contact angle and surface morphology of the PDMS disc after observation under an optical microscope.

3-Aminopropyl-tri-ethoxy-silane (APTES) Treatment. The chemical attachment of APTES to PDMS was performed after completing the oxygen plasma treatment as described earlier. This oxygen-plasma-treated PDMS disc was then kept in the 10% APTES solution in DI water for 20 min followed by drying for 24 h at 60 °C temperature. APTES-treated samples were stored at room temperature for further experiments.

Preparation of Silk Fibroin Solution. The SF solutions were prepared using standard protocols reported in the literature.[14] Briefly, the *B. mori* silk cocoons were boiled in a 0.5 w/v% solution of $NaHCO_3$ twice for about 30 min to remove the sericin coating. The resulting mass of fibroin fibers was then washed with water, dried, and dissolved in 9.3 M lithium bromide solutions using a ratio of 1 gm of silk fibers in 10 mL of LiBr solution. This solution was then extensively dialyzed against deionized water for 48 h at 8 °C to ensure complete removal of the salt. The solution was centrifuged at 12 000 rpm for 20 min at 4 °C, and the supernatant was collected and stored in a refrigerator for about 20 days. The solution had a concentration of ∼40 mg/mL or ∼4 wt %.

Fourier Transform Infrared (FTIR) Spectroscopy-ATR. The uncoated and coated PDMS discs, before and after methanol treatment, were characterized using an ATR-FTIR Bruker Tensor II spectrophotometer equipped with a diamond crystal probe detector. The scan was recorded from 500 to 4000 cm^{-1} with a resolution of 4 cm^{-1}.

Coating of PDMS Discs with SF Solution. Surface-treated PDMS substrates were used for coating experiments with silk fibroin. The SF solution was diluted to 4 mg/mL concentration or 0.4 (v/v)% using DI water. Surface-treated PDMS discs were dipped in the diluted SF solution for 10 min followed by a drying step.[14] The dried samples were annealed using methanol vapor treatment for 48 h to induce the formation of crystalline β-sheets. The traces of methanol vapor on the samples were removed using vacuum-drying at 60 °C for 12 h.

Contact Angle Measurement. Surface modification and surface coating on the PDMS surface were confirmed by a 4 ul sessile drop water contact angle in DI water. The equilibrium contact angle was reported as an average of four measurements done on each sample.

Scanning Electron Microscopy. The surface morphology of the SF-coated PDMS before and after mechanical deformation was characterized using a scanning electron microscope (SEM) Model − FEI Quanta 200 3D. Representative images at appropriate magnifications were recorded after sputter-coating of gold on the samples to prevent charging on samples.

Tape Test (ASTM D3359)/Cross-Hatch Test. A 5 cm × 5 cm PDMS block having a thickness of 1.5 cm was coated with SF after different physical and chemical modifications. The cross-hatch was prepared using an ASTM standard blade having sharp edges 1 mm apart. After peeling off with a scotch tape, the image was captured using a digital camera and the delaminated area was measured. The classification of the samples was done as per the ASTM standard, which states that rating 5B, 0%; 4B, <5%; 3B, 5−15%; 2B, 15−35%;
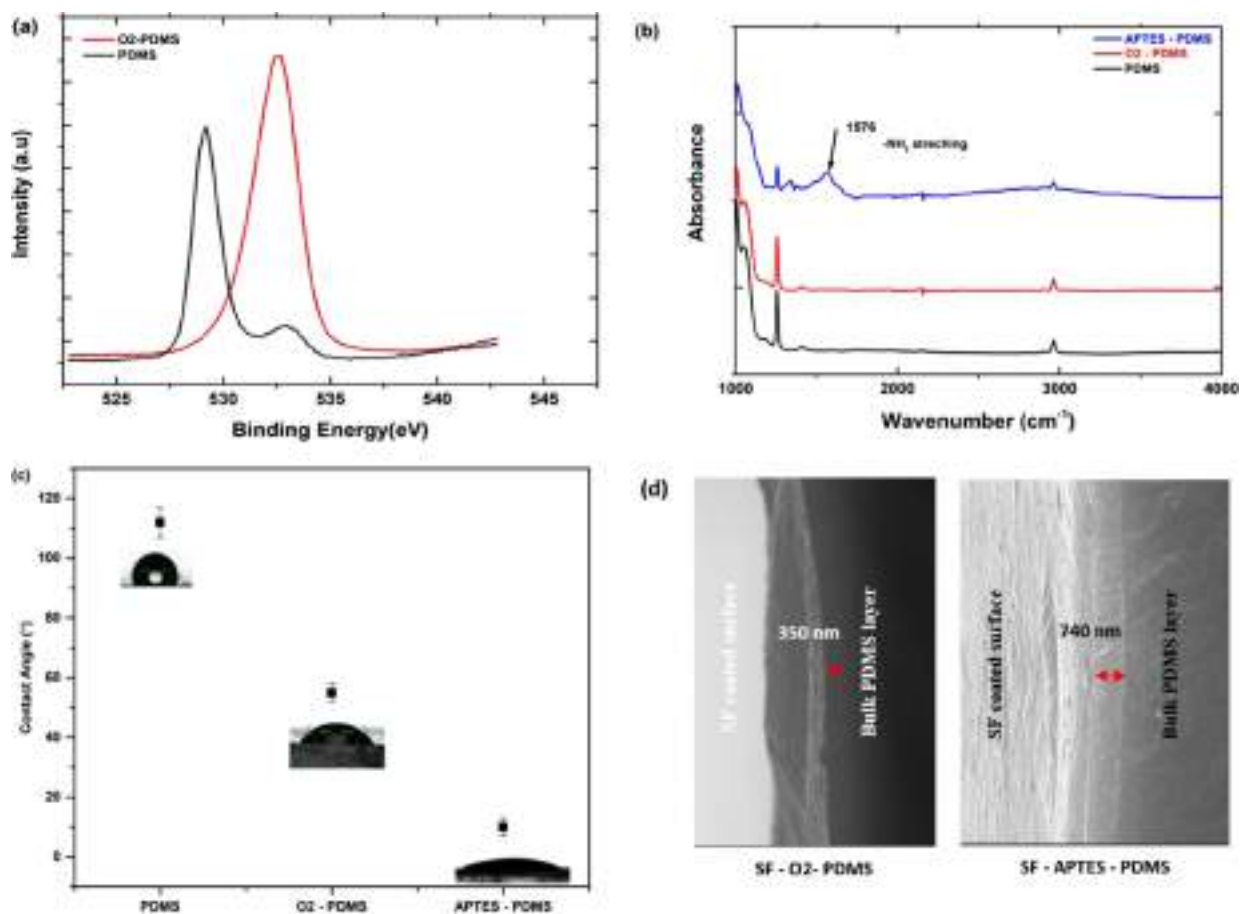
Figure 1. (a) XPS spectra of oxygen before and after oxygen plasma treatment. (b) FTIR spectroscopies of unmodified and modified PDMS. (c) Water contact angles of unmodified and modified PDMS. (d) SEM cross-sectional micrographs of SF-coated PDMS after surface modification.

and 1B, 35−65%, where the numbers denote the percentage of the area where the coating is peeled off.

Bending and Tensile Measurement. A simple bending test, followed by SEM imaging, was designed to characterize the cracking resistance of the coating on the PDMS implant. The SF-coated PDMS strip without modification was used as a control. The crack resistance of the coating was measured using a 180° bending test with a rectangular block of size 1 cm × 3 cm and 0.15 cm thickness as per the protocol described by Borkner et al.[15] The central 1 cm portion of the PDMS strip was imaged in the SEM to validate the quality of coating before subjecting the strip to any mechanical deformation. Also, 1 mm thick dumb-bell-shaped specimens were prepared from the PDMS. These specimens were stretched to 50 and 100% strains at a stretching rate of 50 mm/min using a universal tensile machine, and SEM images of the central region were recorded after the release of the strain.

Nanoscratch Test. The nanoscratch test on unmodified and modified coated PDMS discs was performed using a Rockwell C diamond, sphero-conical stylus having an initial load of 3 μN to a final load of 10 mN with a loading rate of 30 mN/min over a length of 1 mm with a speed of 3 mm/min.

Nanoindentation Test. Nanoindentation is a technique used to characterize the local elastic modulus and hardness of the surface coating. Nanoindentation of unmodified and modified SF-coated PDMS was performed using a tip with a sphero-conical head. The sample was loaded with a maximum load of 20 μN at a loading rate of 80 μN/min for 30 s.

Atomic Force Microscopy Test. A 20 μm glass bead was attached to the end of a tipless-cantilever with spring constant ∼0.8 N/m (Micromasch, Bulgaria). A superglue was used for the attachment, which made a hard contact between the cantilever and the glass bead,

which avoids the unwanted deformation of bead−cantilever contact during the measurement. The cantilever−bead assembly was brought close to the SF solution, and only the bead was carefully dipped into it for ∼60 s. A thin layer of SF got coated on the bead. The cantilever−bead assembly was pulled out of the solution and kept in methanol vapor for ∼24 h, which prevents it from redissolving into the media where measurements were performed. Coating of SF on the glass bead was confirmed by fluorescence spectroscopy. A Rhodamine-silk fibroin solution was used to confirm the formation of SF coating glass beads. When the SF-coated cantilever is pressed against the physically/chemically terminated (O_2 or APTES) substrate, bonds form between SF molecules and the surface functional groups on the substrate. Adhesion energy between the two substrates was determined by measuring the force required to pull these two surfaces apart from each other. This force was experienced by the AFM cantilever during the pulling away from the substrate.

■ RESULTS AND DISCUSSION

Polydimethylsiloxane (PDMS) is a polymeric material routinely used in a variety of biomedical implants and devices. Owing to the large surface energy and hydrophobicity, the surface of PDMS is modified using various known physical and chemical treatments.[8,16−20] All of these treatments reduce the hydrophobicity of the PDMS surface by forming −OH and −NH_2 functionalities. It has been hypothesized that these functionalities help in improving the surface energy of the PDMS surface, which helps in stable coatings that do not delaminate. In this work, PDMS discs of required sizes and
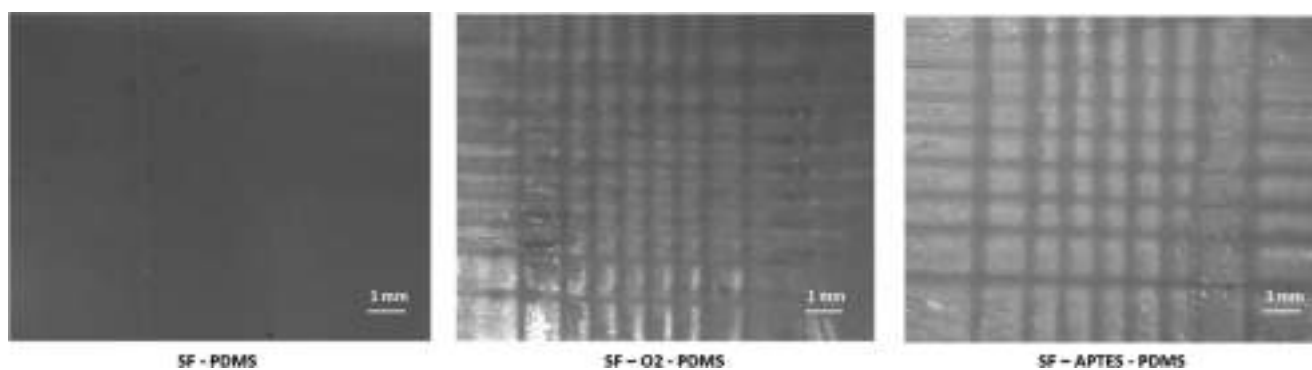
Figure 2. Processed digital images of unmodified and modified SF-coated PDMS surfaces after the cross-hatch test.

shapes were prepared and standardized protocols were used to modify their surface.

Formation and Characterization of Surface Modification. X-ray photoelectron spectroscopy (XPS) and Fourier transform infrared (FTIR) spectroscopy techniques were used as the preliminary confirmatory tests for surface modification of the PDMS surface using physical and chemical treatments. The formation of −OH groups after oxygen plasma treatment (sample abbreviation: O_2-PDMS) was confirmed by characterizing the PDMS surface using XPS. The oxygen plasma treatment was optimized by varying the RF power for plasma treatment and also the time for treatment. It was observed that increasing the RF value beyond 50 W and the exposure time beyond 1 min resulted in cracking on the PDMS surface. In the XPS spectrum, a shift in the binding energy of oxygen from 531 to 533 eV confirms the formation of −OH groups on the PDMS surface as shown in Figure 1a.[21] The oxygen plasma treatment was also corroborated by recording the change in the contact angle.

Further, the XPS spectra of APTES (sample abbreviation: APTES-PDMS) show 26% oxygen, 49% carbon, 17% silicon, and 7% nitrogen. This elemental composition from XPS analysis confirms that immobilization of APTES molecules was successfully done on the oxygen-plasma-treated PDMS discs. The XPS analyses of PDMS, PDMS-O2, and PDMS-APTES are summarized in Table S1.

Figure 1b shows the FTIR-ATR spectra for both oxygen-plasma-treated and APTES-PDMS-treated PDMS surfaces. The pristine PDMS surface shows characteristic symmetric and asymmetric stretching peaks at 2963 and 2903 cm^{-1} and vibrational bending peaks at 1253 cm^{-1} that correspond to the methyl group.[21] There are no characteristic signals present beyond the 3000 cm^{-1} range.[6] The FTIR spectrum for the O_2-PDMS sample was found to be identical to that of pure PDMS. This is because the oxygen plasma treatment is done over the first few atomic layers of the PDMS surface. Thus, the bulk PDMS signals dominate the FTIR signal. The APTES modification was validated through the absorption peak at 1576 cm^{-1} in the FTIR spectra, (Figure 1b), which is attributed to the vibrational stretching of −NH$_2$ groups.[11] The additional −NH stretching of APTES molecules on the PDMS surface confirms the formation of amino terminated silane on PDMS.

The changes in the surface wettability of unmodified and modified PDMS are summarized in Figure 1c. The contact angle decreased from $112 \pm 5°$ for the pristine PDMS surface to $55 \pm 3°$ for oxygen plasma treatment. This intermediate hydrophilicity is the optimum wettability possible with oxygen plasma treatment without any physical and visible damage to the PDMS surface. The changes in the surface wettability on the modified PDMS surface were confirmed using water contact angle. APTES-PDMS samples show complete surface wettability. This was attributed to the formation of a uniform layer of APTES with a large number of surface −NH$_2$ groups. These hydrophilic contact angles further confirm the modification of the PDMS substrate using APTES molecules.

The surface-modified PDMS discs were used for SF coating experiments. The formation of the SF nanocoatings on the PDMS substrate was also characterized using FTIR-ATR spectroscopy. The presence of amide I and amide II peaks confirms the presence of SF, which was confirmed through a sharp peak at 1623 and 1515 cm^{-1}, respectively[14] (data not included). Figure 1d shows the cross-sectional SEM image of the coated PDMS samples. As can be seen from the images, the O_2-PDMS has an SF coating of ∼350 nm thickness, while the APTES-PDMS sample exhibits a coating with a thickness that is more than double of O_2-PDMS. The surface morphology of PDMS after surface modification is also performed using AFM analysis as summarized in Figure S2. The surface roughness upon surface modification is quantified by calculating the rms roughness on both samples, proving that APTES-PDMS shows a higher surface roughness with an rms roughness of 18 nm, whereas O_2-PDMS shows a smooth textured surface with an rms roughness of 1 nm.

Further, the amount of SF on PDMS was quantified using a Bradford assay, and these results have been summarized in Figure S1. As can be seen from these results, the amount of SF adsorbed on the APTES-PDMS is the highest. The lowest amount of SF adsorbs on the unmodified PDMS, while O_2-PDMS shows an intermediate adsorption of SF.

Tape Test. The ASTM standard Tape test B (ASTM D3359) or the cross-hatch test is a qualitative measure of coating adhesion at the bulk scale and has been used to measure the adhesion between the coating and soft substrates such as PDMS, PU, etc.[22] Here, a cross-hatch of 25 squares is made on the coated surface. The cross-hatch was prepared using an ASTM standard blade having sharp edges 1 mm apart. After peeling off a scotch tape, the delaminated area was measured. Image analysis on the squares is performed to observe the amount of coating that is peeled off along with the scotch tape. The ASTM standard then specifies the classifications based on the amount of coating peeled off. The classification of the cross-hatch test is as follows: 5B, 0%; 4B, <5%; 3B, 5−15%; 2B, 15−35%; and 1B, 35−65%, where the number indicates the percentage of the coating that is peeled off. Figure 2 summarizes the delamination of SF
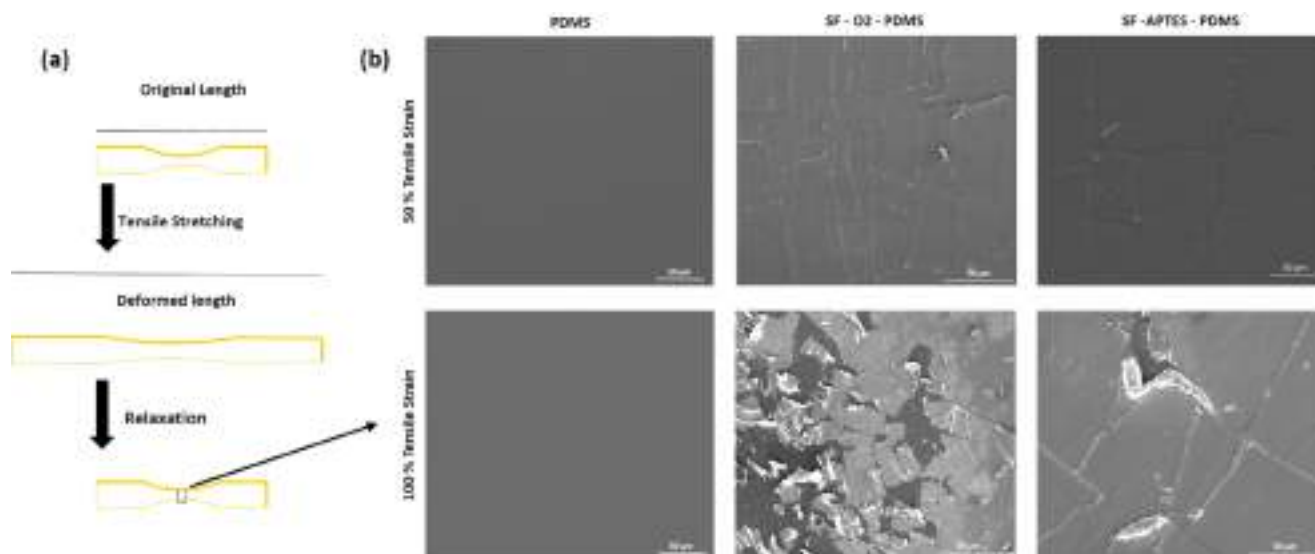
Figure 3. (a) Schematic representation of tensile deformation. (b) SEM micrographs of SF-coated PDMS after surface modification after tensile deformation.

coatings on modified and unmodified PDMS using the cross-hatch test.

The pristine PDMS shows complete delamination of the coating and hence confirms that surface modification of the PDMS is essential to coat the PDMS using SF. The oxygen plasma (SF-O_2-PDMS) and APTES (SF-APTES-PDMS) surfaces show no measurable delamination after the tape test. The qualitative measurement to compare the adhesion of coating on soft substrates is less effective due to various factors since reproducibility of test results is a challenge. We performed further quantitative tests at various length scales to determine the performance of O_2-PDMS and APTES-PDMS.

Bending and Tensile Analyses. A simple bending test, followed by SEM imaging, was designed to characterize the cracking resistance of the coating on the PDMS implant. A PDMS strip without modification was used as a control. The crack resistance of the coating was measured using a 180° bending test as per the protocol described by Borkner et al.[15] The central 1 cm portion of the PDMS strip was imaged in the SEM. The PDMS sample has a smooth surface before the bending test and does not exhibit any crack features on the uncoated PDMS surface after mechanical deformation. The surface did not exhibit any changes in surface topology after the bending test, and this confirms that development of cracks on the SF-coated PDMS is not initiated from the PDMS layer. The SF dip-coated disc also showed a uniform coating with a smooth surface on SF-O_2-PDMS and SF-APTES-PDMS samples. However, post the bending test, large visible cracks were seen on the surface of the coating on SF-O_2-PDMS discs. A similar test was conducted on recombinant spider silk coating on PDMS by Borkner et al., and they too observed cracking on the coating, although the cracking reported is not as severe as the one observed here.[23] The density of the crack formed after the 180° bending test shows a considerable difference between SF-O_2-PDMS and SF-APTES-PDMS samples. The lower crack density of SF dip-coating after the bending test confirms that the mechanical stability of surface modification under mechanical deformation is better for SF-APTES-PDMS as compared to SF-O_2-PDMS (see Figure S3 in

the Supporting Information). Since the bending deformation can also introduce subjectivity in measurement, a more controlled tensile deformation test was performed to validate these observations.

Dumb-bell-shaped specimens that were 1 mm thick were prepared from the PDMS. These specimens were stretched to 50 and 100% strains at a stretching rate of 50 mm/min using a universal tensile testing machine, and SEM images of the central region were recorded after the release of the strain. The schematic representation of tensile measurement is shown in Figure 3a.

Tensile measurements were performed on SF-O_2-PDMS and SF-APTES-PDMS. The SF-APTES-PDMS surface shows lesser crack density as compared to SF-O_2-PDMS discs, verifying the earlier data of the bending test. The SF-O_2-PDMS shows delamination of the coating at 100% strain, whereas few cracks are observed on SF-APTES-PDMS samples, which confirms that APTES shows improved mechanical stability with SF coating, as shown in Figure 3b.

From the above bulk mechanical tests, it is clear that the APTES treatment provides better delamination resistance and cracking resistance to the SF coating as compared to oxygen plasma treatment.

Nanoscratch Test. The nanoscratch test has emerged as a powerful tool to measure the adhesion of the coating to the substrate.[24] The method has been primarily used for metal/polymer coatings on hard substrates. Therefore, there is no precedent for using this method on soft substrates as the substrate here would experience large-scale elastic deformation. The cracking of coating and delamination of the coating are the two phenomena occurring simultaneously while performing nanoscratch tests. The lower load region is responsible for the tensile cracking of the coating, without the delamination of the coating from the substrate. The load at which the tensile cracking of the coating occurs is termed the first critical load (L_{c1}). The delamination of the coating will occur at higher loads corresponding to the second critical load (L_{c2}). The nanoscratch test was performed on PDMS, SF-O_2-PDMS, and SF-APTES-PDMS substrates, with a scanning load of 3 μN and a scratch of 1 mm was done. Representative optical
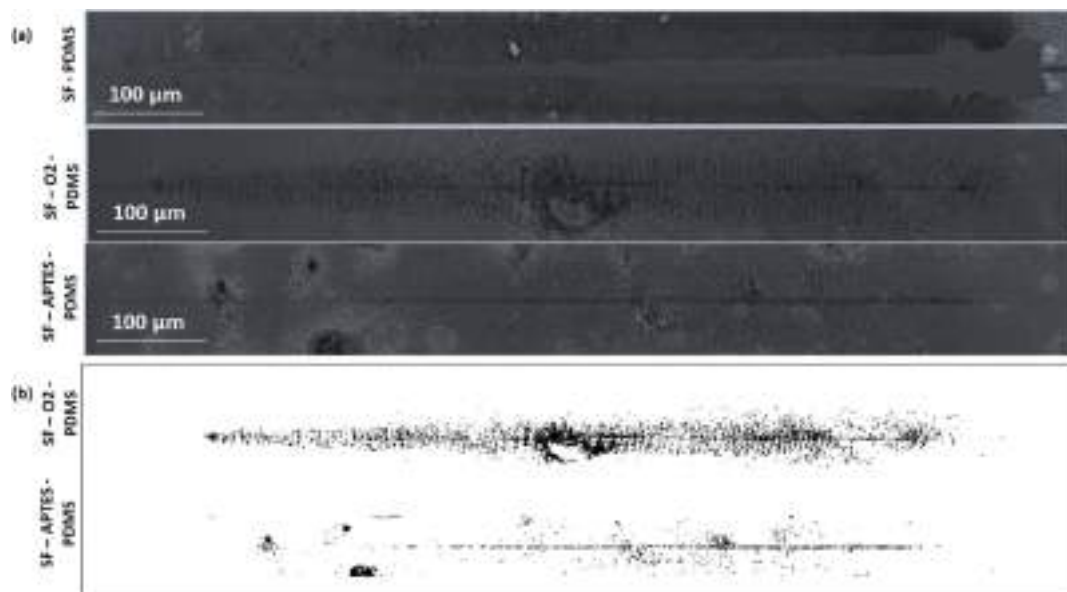
Figure 4. Optical images of unmodified and modified SF-coated PDMS substrates after the nanoscratch test showing coating delamination and cracking in the unmodified PDMS sample. (b) Processed images after the nanoscratch test showing negligible cracking in the SF-APTES-PDMS sample as compared to the SF-O$_2$-PDMS sample.

micrographs of these tests have been presented in Figure 4. For the unmodified PDMS substrate, complete delamination of SF coating was observed, while the SF-O$_2$-PDMS and SF-APTES-PDMS samples showed negligible delamination. Cracks in the coating were observed primarily for pristine PDMS and SF-O$_2$-PDMS, and these cracks intensified with an increase in the load. The cracks were observed not only on the test track but on a large area surrounding it for these samples. The PDMS showed a very low L$_{C1}$ compared to SF-APTES-PDMS and SF-O$_2$-PDMS discs. For bare PDMS, L$_{C1}$ was 0.9 mN and complete delamination occurred at 9.5 mN. The SF-APTES-PDMS and SF-O$_2$-PDMS showed comparable L$_{C1}$ values of 5.06 and 4.5 mN, respectively. However, SF-APTES-PDMS and SF-O$_2$-PDMS samples did not show any delamination of the coating from the PDMS substrate, and hence, an L$_{C2}$ value could not be calculated for these samples. The optical images of PDMS, SF-APTES-PDMS, and SF-O$_2$-PDMS are summarized in Figure 4a, and the amount of crack on the test track and surrounding regions of both modified samples was determined using Image Processing software MATLAB 2018b by converting the RGB images into pixel points. The results have been summarized in Figure 4b. It is clear from the processed images that the cracks formed on SF-APTES-PDMS are drastically less as compared to SF-O$_2$-PDMS. The processed optical images of modified PDMS samples further confirm the results obtained in the bulk mechanical measurements under different tensile strains.

Nanoindentation. Nanoindentation is a technique used to characterize the local elastic modulus and hardness of the surface coating. Carroll et al. demonstrated the adhesive strength of thermoresponsive polymer coating on nitinol wire.[25] Charitidis et al. demonstrated that nanoindentation is used to measure nanomechanical properties, creep behavior, and adhesive forces of PDMS.[17,26]

We performed the nanoindentation test using an established method where an indenter tip with a sphero-conical geometry is driven into a specific region of the material to be tested, by applying an incremental normal load. When reaching a predefined maximum load, the normal load was reduced until complete or partial relaxation occurs. This procedure was performed repeatedly, and at each stage of the experiment, the position of the indenter relative to the sample surface was precisely monitored with a differential capacitive sensor. The equipment precisely controlled the load while simultaneously measuring the penetration depth into the material and thus minimized the influence of the substrate on the resulting measurements.

Given the softness of the substrate and thickness of the top coating, the elastic modulus of the coating/modified layer by itself could not be measured. Testing the coating only would require normal loads below the capabilities of the instrument. The load−displacement curve of unmodified PDMS in Figure 5 shows a rupture at a load of ∼2 μN and a penetration depth of ∼100 nm. The SF-O$_2$-PDMS showed a slightly tougher coating with a rupture occurring at a load of 5 μN and at a penetration depth of ∼350 nm, which also matches with the overall thickness of the SF coating as shown in Figure 1d. This means that the rupture occurs at the SF−PDMS interface, indicating poor adhesion between the SF coating and the O$_2$-PDMS surface. A similar observation can also be made for the SF−PDMS sample, which has less than half of the coating thickness as compared to the SF-O$_2$-PDMS sample. The SF-APTES-PDMS did not exhibit a rupture even at loads as high as 20 μN. A mild change in slope is observed for this sample at 15 μN and a penetration depth ranging from 650 to 750 nm. Here too, it must be noted that the coating has a thickness of 750 nm, as shown in Figure 1d. These results indicate that the SF-APTES-PDMS sample has an interface that exhibits excellent adhesion between the SF-coated layer and the APTES-PDMS surface. The interface helps in efficient dissipation of the loads and prevents cracking and delamination of the nanocoating. These findings are in agreement with the higher adsorption of SF on the APTES-PDMS substrate and improved crack resistance observed in the bulk tensile measurements and the nanoscratch test results reported earlier in Figure 4. This is in agreement with the literature that the
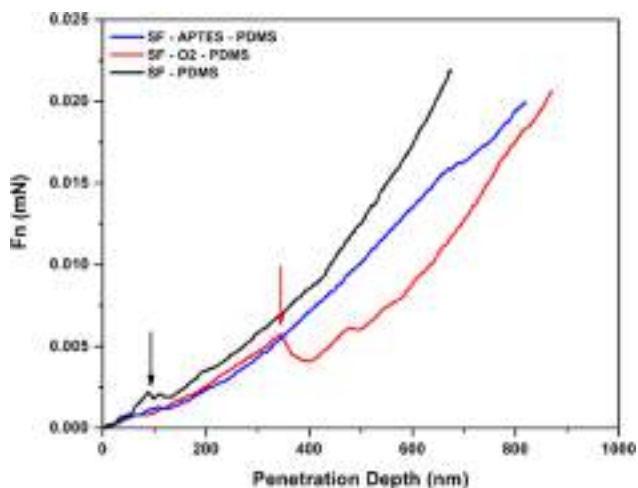
Figure 5. Force−displacement curves of the nanoindentation experiments performed on PDMS substrates coated with SF. The black curve shows the indentation curve of SF on untreated PDMS. The rupture force is ∼ 2 μN. The red curve shows the indentation curve of SF coated on O_2-PDMS. The rupture occurs at ∼5 μN. The indentation on SF coated on APTES-PDMS is shown in blue. The material does not rupture with loads of even 20 μN. It shows that the SF coated on the O_2-PDMS surface yields at higher force values compared to the SF on untreated PDMS. However, it yields at much lower forces compared to the SF coated on APTES-PDMS.

adsorption of fluorescently tagged protein molecules on APTES-treated samples shows a higher fluorescence intensity as compared to oxygen-plasma-treated PDMS samples.[27]

Atomic Force Microscopy-Force Spectroscopy. From the macroscopic as well as microscopic tests, we conclude that the SF coating on APTES-PDMS is mechanically much more robust compared to the SF coating on O_2-PDMS substrates. It yields at much higher shear and normal stresses compared to the SF coating on O_2-PDMS. In the following, we address the molecular origin of robustness of SF on APTES-PDMS compared to O_2-PDMS using force spectroscopy experiments, which are capable of measuring strengths of individual bonds in both chemistry and biology.[28] One of the challenges in using atomic force microscopy methods is that the PDMS is an elastomer and deforms easily when surfaces are made to separate from each other. By carefully separating the effects arising from this phenomenon, we were able to measure the adhesion energies required to separate the nanoscale contacts formed between the SF-coated glass surface and the APTES-PDMS substrate. The 20 μm glass beads attached to tipless AFM cantilevers were coated with SF. The glass beads were allowed to form a contact with O_2-PDMS as well as APTES-PDMS with the help of servo-control in the AFM. The beads were then pulled away, and the adhesive energy between surfaces was measured by recording the substrate movement and cantilever deflection. Figure 6a shows a typical force curve with approach and retract of the entire process. The APTES-PDMS substrate was pressed with the bead with 2 nN load, and then, it was pulled away. The binding sites of SF and APTES-PDMS bend the cantilever downward as the elastomer deforms to form a neck. The neck then relaxes, and the cantilever is almost in its zero-force equilibrium position. The further pulling of the substrate breaks these bonds sequentially, as seen in the schematic shown in the inset of Figure 6a. The process appears very similar to the unfolding of protein

domains observed using AFM. Here, the SF chains are likely getting unraveled before the bonds are broken. In this force curve, the hysteresis caused by the plastic deformation of the PDMS bulk largely dominates the measurement. The energy lost in forming the neck and its relaxation is much higher compared to the bond energies. In short, the energy required to break these bonds and separate these two surfaces is overwhelmed by the deformation of the PDMS bulk. In Figure 6b,c, we remove the approach curve and part of the retract, which is attributed to the formation and relaxation of the PDMS neck. The control experiment is performed using a bead without SF coating on it. In Figure 6b, the O_2-PDMS substrate and the SF-coated bead are pulled away from each other. The control (bead without SF) and the SF-coated bead show similar force curves, and the bond-breaking events are not significantly different. In Figure 6c, we show force curves depicting separation of the bead and APTES-PDMS. There is a striking difference between O_2-PDMS and APTES-PDMS adhesion to the SF-coated glass bead. There are multiple (∼10) bond-breaking events. These bonds cost more energy to separate the SF-coated glass bead from APTES-PDMS compared to O_2-PDMS. Figure 6d shows energies required to separate the SF-coated glass bead from APTES-PDMS and O_2-PDMS along with controls. The costs of energy for separating APTES-PDMS and O_2-PDMS from the SF-coated bead are $1.0 \pm 0.04 \times 10^{-15}$ and $4.1 \pm 0.3 \times 10^{-16}$ J, respectively. The adhesive strength of SF to APTES-treated PDMS is 10 times more compared to O_2-PDMS due to the higher number of molecular linkages formed in this nanoscale contact. Force spectroscopy experiments are also able to identify breaking of these discrete molecular bonds formed between the amine groups on APTES-PDMS and the SF on the glass beads.

In this study, we have measured the adhesion of silk fibroin nanocoatings on PDMS surfaces and have demonstrated using various techniques the mechanical and adhesive properties of these coatings. Spectroscopic measurements using infrared spectroscopy have confirmed that APTES treatment results in a surface that has amine functionalities, while the oxygen plasma produces a surface with hydroxyl groups as validated by the XPS measurement. The oxygen plasma treatment improves the hydrophilicity of the PDMS substrate only to a limited extent, reducing the contact angle to $55 \pm 3°$. Contrary to this, when a drop of water is placed on the APTES-PDMS substrate, the drop spreads completely, indicating a contact angle less than 10°. This implies that the APTES-PDMS treatment more effectively modifies the PDMS substrate and PDMS has a higher number of polar groups on the surface. These polar groups then influence the attachment of the SF protein to the substrate.

Around 70% of the SF chain is made up of a repeat sequence of amino acids: glycine−alanine−glycine−alanine−glycine−serine. The nonrepetitive sequence of the amino acid includes other hydrophilic amino acids. The SF protein interacts with the substrate during the coating process primarily through secondary interactions. These secondary interactions primarily include hydrogen bonding between the polar groups on the amino acid such as serine, tyrosine, aspartic acid, and/or glutamic acid. These amino acids hydrogen-bond with the amine groups on the APTES-PDMS substrate or the OH groups on the O2-PDMS substrate, as depicted schematically in Figure 7.
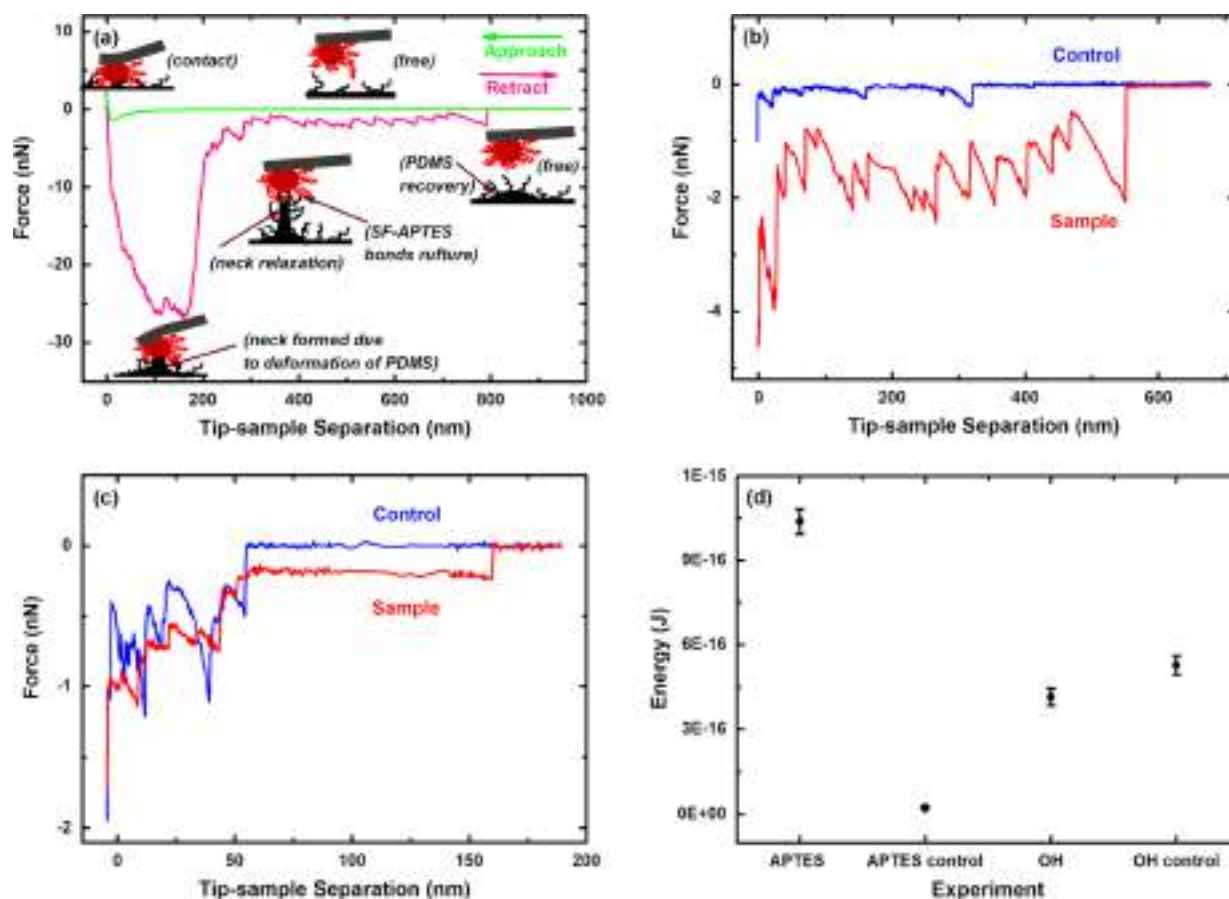
Figure 6. (a) Typical force curve showing the molecular-level interaction of SF to the PDMS surface-modified with APTES treatment. A 20 μm bead coated with SF is attached to a tipless AFM cantilever. The bead is lowered onto the APTES-PDMS substrate. The SF on the bead is shown in red, and amine groups on the APTES-PDMS are shown in black. After the contact, the substrate is loaded slightly. The SF and amine groups on the APTES-PDMS substrate form semicovalent bonds, and the bead tightly adheres to the substrate. The cantilever is then pulled away, leading to deformation in PDMS and formation of a neck. The neck is relaxed as the cantilever is pulled further away and the cantilever attains a near-equilibrium position. Finally, the individual bonds between the amine groups and SF break sequentially to produce a sawtooth-like pattern typically seen in protein-unfolding experiments. The bead leaves the PDMS surface, and the cantilever attains the zero-force equilibrium position. (b, c) We remove part of the retract curve related to the deformation caused in the bulk of PDMS and focus on molecular-level interactions of SF with O_2-PDMS and APTES-PDMS surfaces. The blue curves show control experiments wherein the glass bead is not coated with SF. The number of bonds formed between the SF-coated glass bead and O_2-PDMS does not show a significant deviation from the control (glass bead without SF coating). In the case of APTES-PDMS, there are considerably more numbers of bond-breaking events compared to the control or O_2-PDMS. These bonds between SF and amine groups require a much larger energy to separate the SF-coated surface and the APTES-PDMS substrate. (d) Energy required to separate the SF-coated surface from O_2-PDMS and APTES-PDMS substrates along with controls. The number of force curves for each case was 200. The control experiments were performed with 30 force curves. The bars represent standard error. The energy needed to separate the SF-coated surface from the APTES-PDMS surface is $1.0 \pm 0.04 \times 10^{-15}$ J, and from the O_2-PDMS surface, it is $4.1 \pm 0.3 \times 10^{-16}$ J.

Further, the amount of SF protein attached to the APTES-PDMS substrate was also found to be at least two times that observed for the O_2-PDMS substrate, resulting in a coating that is double the thickness as compared to O_2-PDMS. A bulk technique like the peel test could not differentiate between the adhesion of the SF protein to the O_2-PDMS and the APTES-PDMS treatment most likely due to the deformation of the underlying elastomeric PDMS substrate. However, when these coated surfaces were subjected to tensile and bending deformation, the SF coating on APTES-PDMS was found to be more resistant to delamination, cracking, and failure as compared to the O_2-PDMS substrate. These observations were further validated by the nanoscratch and nanoindentation measurements. The optical micrograph of the nanoscratch clearly showed increased cracking for the O_2-PDMS substrate as compared to the APTES-PDMS sample. The nano-

indentation measurement also showed a rupture at 5 μN for the O_2-PDMS substrate, whereas the APTES-PDMS substrate did not exhibit any rupture even at loads as high as 20 μN. These techniques further corroborated the findings of bulk mechanical measurements at a microscopic and a mesoscopic length scale and validated the superior performance of the APTES-PDMS substrate. At the molecular level, the atomic force microscopic technique showed that the SF protein forms a higher number of molecular linkages with the APTES-PDMS surface as compared to the O_2-PDMS surface. This improves the adhesion of the SF protein to the APTES-PDMS substrate. This is in agreement with the improved hydrophilicity and higher SF protein adsorption for the APTES-PDMS surface, as discussed earlier.

The O2-PDMS substrate has only limited hydroxyl groups available for hydrogen bonding, as is evident by the limited
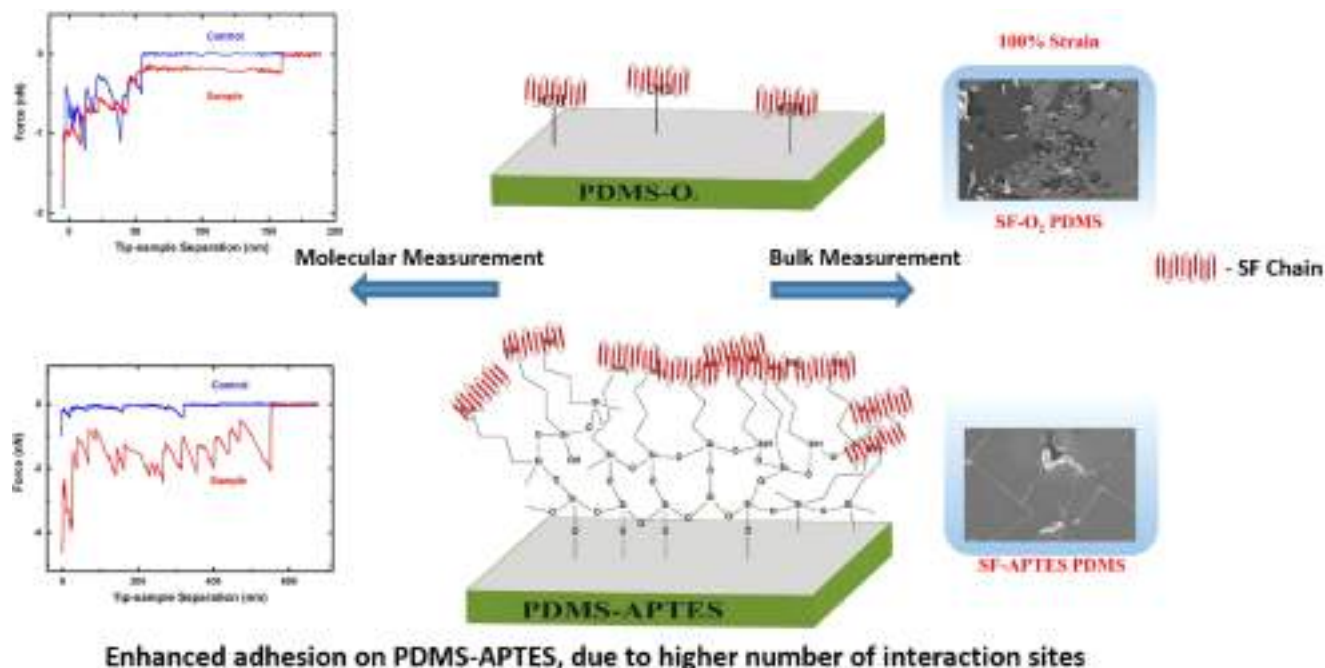
Figure 7. Schematic representation of the molecular mechanism of SF coatings on modified PDMS substrates.

hydrophilicity in the contact angle measurement. Correspondingly, only a small amount of SF protein binds to the substrate, resulting in a thinner coating. The number of bond-breaking events in O2-PDMS is also low, as seen in the modified AFM measurement.

The APTES-PDMS substrate, on the other hand, has a higher number of amine groups that are available for interaction with the SF protein. This is evident from the significantly reduced contact angle and also the higher amount of SF protein present on the APTES-PDMS surface as seen in the Bradford assay. The higher number of bond-breaking events seen in the modified AFM experiment also validates and supports this. The increased interaction between the SF protein and the APTES-PDMS substrate results in improved adhesion and enhances the delamination resistance of the protein. Improved delamination also prevents cracking of the coating when subjected to other mechanical loadings. Thus, APTES modification must be used to modify the surface for implants to improve their performance and reduce the rate of failure both during handling before surgery and also during use. This chemical modification strategy will help in the development of improved implants with reduced risks of failure.

CONCLUSIONS

Surface coating of implants using natural protein polymers has emerged as a promising strategy to reduce the failure rate of implants. Polydimethylsiloxane (PDMS) is a commonly used hydrophobic polymer for biomedical implants, and surface-coated PDMS implants frequently face problems such as delamination or cracking of the coating. In this work, we evaluated the adhesion of silk fibroin coatings on PDMS surfaces that were modified using oxygen plasma and APTES treatments. At a macroscopic length scale, using conventional tensile and bending deformation, we demonstrated that the APTES-treated PDMS surface shows enhanced crack resistance as compared to the oxygen-plasma-treated PDMS surface.

In both nanoindentation and nanoscratch tests, these observations were further validated and we showed that cracking was minimal in the nanoscratch test for the APTES-PDMS sample. In the nanoindentation measurements also, no rupture was observed for the APTES-PDMS sample up to 20 μN loads, whereas the O$_2$-PDMS sample showed a rupture at loads as low as 5 μN. This improved performance can be attributed to the higher number of molecular linkages formed between the SF protein and the APTES-PDMS substrate as was shown by the atomic force microscopy measurements. These increased molecular linkages result in better adhesion of the SF protein to the PDMS substrate, and this improved adhesion enhances the delamination and crack resistance of the nano-coatings. Therefore, this chemical modification strategy will assist in the development of coated medical devices and implants, which in turn will mitigate the risk of coating delamination and medical device failure.

ASSOCIATED CONTENT

Supporting Information

The Supporting Information is available free of charge at https://pubs.acs.org/doi/10.1021/acs.langmuir.1c00047.

XPS spectrum of the modified PDMS, FTIR spectrum of modified and unmodified PDMS, AFM images after surface modification, SEM images after surface modification, Bradford assay for the quantification of silk fibroin on modified substrates (PDF)

AUTHOR INFORMATION

Corresponding Authors

Shivprasad Patil − *Center for Energy Science, Department of Physics, Indian Institute of Science Education and Research, Pune 411008, India;* orcid.org/0000-0002-3413-4109; Email: s.patil@iiserpune.ac.in

Anuya Nisal − *Polymer Science and Engineering Division, National Chemical Laboratory, Pune 411008, India;*

*Academy of Scientific and Innovative Research (AcSIR),
Ghaziabad 201002, India;* ⊙ orcid.org/0000-0003-1633-
7890; Email: aa.nisal@ncl.res.in

Authors

Emmanuel Joseph − *Polymer Science and Engineering
Division, National Chemical Laboratory, Pune 411008,
India; Academy of Scientific and Innovative Research
(AcSIR), Ghaziabad 201002, India*

Shatruhan Singh Rajput − *Center for Energy Science,
Department of Physics, Indian Institute of Science Education
and Research, Pune 411008, India*

Complete contact information is available at:
https://pubs.acs.org/10.1021/acs.langmuir.1c00047

Author Contributions

The manuscript was written through the contributions of all
authors. All authors have given approval to the final version of
the manuscript.

Notes

The authors declare no competing financial interest.

■ ABBREVIATIONS USED

PDMS polydimethylsiloxane
APTES 3-amino(propyl)triethoxysilane

■ REFERENCES

(1) Rolfe, B.; Mooney, J.; Zhang, B.; Jahnke, S.; Le, S.-J.; Chau, Y.-
Q.; Huang, Q.; Wang, H.; Campbell, G.; Campbell, J. The Fibrotic
Response to Implanted Biomaterials: Implications for Tissue
Engineering. In *Regenerative Medicine and Tissue Engineering-Cells
and Biomaterials*, 2011.

(2) Lawrence, E. L.; Turner, I. G. Materials for Urinary Catheters: A
Review of Their History and Development in the UK. *Med. Eng. Phys.*
2005, *27*, 443−453.

(3) Gomathi, N.; Mishra, I.; Varma, S.; Neogi, S. Surface
Modification of Poly(Dimethylsiloxane) through Oxygen and Nitro-
gen Plasma Treatment to Improve Its Characteristics towards
Biomedical Applications. *Surf. Topogr. Metrol. Prop.* **2015**, *3*,
No. 35005.

(4) Kuddannaya, S.; Chuah, Y. J.; Lee, M. H. A.; Menon, N. V.;
Kang, Y.; Zhang, Y. Surface Chemical Modification of Poly-
(Dimethylsiloxane) for the Enhanced Adhesion and Proliferation of
Mesenchymal Stem Cells. *ACS Appl. Mater. Interfaces* **2013**, *5*, 9777−
9784.

(5) Zeplin, P. H.; Maksimovikj, N. C.; Jordan, M. C.; Nickel, J.;
Lang, G.; Leimer, A. H.; Römer, L.; Scheibel, T. Spider Silk Coatings
as a Bioshield to Reduce Periprosthetic Fibrous Capsule Formation.
Adv. Funct. Mater. **2014**, *24*, 2658−2666.

(6) Wang, L.; Sun, B.; Ziemer, K. S.; Barabino, G. A.; Carrier, R. L.
Chemical and Physical Modifications to Poly(Dimethylsiloxane)
Surfaces Affect Adhesion of Caco-2 Cells. *J. Biomed. Mater. Res. -
Part A* **2010**, *93*, 1260−1271.

(7) Wong, I.; Ho, C. M. C. M. Surface Molecular Property
Modifications for Poly(Dimethylsiloxane) (PDMS) Based Micro-
fluidic Devices. *Microfluid. Nanofluidics* **2009**, *7*, 291−306.

(8) Zeng, Q.; Zhu, Y.; Yu, B.; Sun, Y.; Ding, X.; Xu, C.; Wu, Y.-W.;
Tang, Z.; Xu, F.-J. Antimicrobial and Antifouling Polymeric Agents for
Surface Functionalization of Medical Implants. *Biomacromolecules*
2018, *19*, 2805−2811.

(9) Xue, P.; Li, Q.; Li, Y.; Sun, L.; Zhang, L.; Xu, Z.; Kang, Y.
Surface Modification of Poly(Dimethylsiloxane) with Polydopamine
and Hyaluronic Acid to Enhance Hemocompatibility for Potential
Applications in Medical Implants or Devices. *ACS Appl. Mater.
Interfaces* **2017**, *9*, 33632−33644.

(10) Chuah, Y. J.; Koh, Y. T.; Lim, K.; Menon, N. V.; Wu, Y.; Kang,
Y. Simple Surface Engineering of Polydimethylsiloxane with Polydop-
amine for Stabilized Mesenchymal Stem Cell Adhesion and
Multipotency. *Sci. Rep.* **2015**, *5*, No. 18162.

(11) Qian, Z.; Ross, D.; Jia, W.; Xing, Q.; Zhao, F. Bioactive
Polydimethylsiloxane Surface for Optimal Human Mesenchymal Stem
Cell Sheet Culture. *Bioact. Mater.* **2018**, *3*, 167−173.

(12) Lewis, F.; Mantovani, D. Methods to Investigate the Adhesion
of Soft Nano-Coatings on Metal Substrates - Application to Polymer-
Coated Stents. *Macromol. Mater. Eng.* **2009**, *294*, 11−19.

(13) Cha, C.; Antoniadou, E.; Lee, M.; Jeong, J. H.; Ahmed, W. W.;
Saif, T. A.; Boppart, S. A.; Kong, H. Tailoring Hydrogel Adhesion to
Polydimethylsiloxane Substrates Using Polysaccharide Glue. *Angew.
Chem., Int. Ed.* **2013**, *52*, 6949−6952.

(14) Joseph, E.; Patil, A.; Hirlekar, S.; Shete, A.; Parekh, N.;
Prabhune, A.; Nisal, A. Glycomonoterpene-Functionalized Crack-
Resistant Biocompatible Silk Fibroin Coatings for Biomedical
Implants. *ACS Appl. Bio Mater.* **2019**, *2*, 675−684.

(15) Borkner, C. B.; Elsner, M. B.; Scheibel, T. Coatings and Films
Made of Silk Proteins. *ACS Appl. Mater. Interfaces* **2014**, *6*, 15611−
15625.

(16) Shin, S.; Kim, N.; Hong, J. W. Comparison of Surface
Modification Techniques on Polydimethylsiloxane to Prevent Protein
Adsorption. *Biochip J.* **2018**, *12*, 123−127.

(17) Charitidis, C. A.; Koumoulos, E. P.; Tsikourkitoudi, V. P.;
Dragatogiannis, D. A.; Lolas, G. Influence of Accelerated Aging on
Nanomechanical Properties, Creep Behaviour and Adhesive Forces of
PDMS. *Plast. Rubber Compos.* **2012**, *41*, 94−99.

(18) Efimenko, K.; Wallace, W. E.; Genzer, J. Surface Modification
of Sylgard-184 Poly(Dimethyl Siloxane) Networks by Ultraviolet and
Ultraviolet/Ozone Treatment. *J. Colloid Interface Sci.* **2002**, *254*, 306−
315.

(19) Gao, C. Y.; Guo, Y. Y.; He, J.; Wu, M.; Liu, Y.; Chen, Z. L.; Cai,
W. S.; Yang, Y. L.; Wang, C.; Feng, X. Z. L-3,4-Dihydroxyphenyla-
lanine-Collagen Modified PDMS Surface for Controlled Cell Culture.
J. Mater. Chem. **2012**, *22*, 10763−10770.

(20) Hong, S. M.; Kim, S. H.; Kim, J. H.; Hwang, H. I. Hydrophilic
Surface Modification of PDMS Using Atmospheric RF Plasma. *J. Phys.
Conf. Ser.* **2006**, *34*, 656−661.

(21) Mata, A.; Fleischman, A. J.; Roy, S. Characterization of
Polydimethylsiloxane (PDMS) Properties for Biomedical Micro/
Nanosystems. *Biomed. Microdevices* **2005**, *7*, 281−293.

(22) Chalker, P. R.; Bull, S. J.; Rickerby, D. S. A Review of the
Methods for the Evaluation of Coating-Substrate Adhesion. *Mater. Sci.
Eng. A* **1991**, *140*, 583−592.

(23) Borkner, C. B.; Wohlrab, S.; Möller, E.; Lang, G.; Scheibel, T.
Surface Modification of Polymeric Biomaterials Using Recombinant
Spider Silk Proteins. *ACS Biomater. Sci. Eng.* **2017**, *3*, 767−775.

(24) Tomastik, J.; Ctvrtlik, R. In Nanoscratch Test-A Tool for
Evaluation of Cohesive and Adhesive Properties of Thin Films and
Coatings, *EPJ Web of Conferences*, EDP Sciences, 2013; Vol. 48, p
00027.

(25) Burke, M.; Clarke, B.; Rochev, Y.; Gorelov, A.; Carroll, W.
Estimation of the Strength of Adhesion between a Thermoresponsive

Polymer Coating and Nitinol Wire. *J. Mater. Sci. Mater. Med.* **2008**, *19*, 1971−1979.

(26) Kassavetis, S.; Logothetidis, S.; Zyganitidis, I. Nanomechanical Testing of the Barrier Thin Film Adhesion to a Flexible Polymer Substrate. *J. Adhes. Sci. Technol.* **2012**, *26*, 2393−2404.

(27) Siddique, A.; Meckel, T.; Stark, R. W.; Narayan, S. Improved Cell Adhesion under Shear Stress in PDMS Microfluidic Devices. *Colloids Surf., B* **2017**, *150*, 456−464.

(28) Hinterdorfer, P.; Dufrêne, Y. F. Detection and Localization of Single Molecular Recognition Events Using Atomic Force Microscopy. *Nat. Methods* **2006**, *3*, 347−355.